INTELLIGENT MODEL-BASED CONTROL OF COMPLEX THREE-LINK MECHANISMS

A thesis submitted to Cardiff University in the candidature for the degree of

Doctor of Philosophy

By

Haider Galil Kamil, B.Sc., M.Sc.

School of Engineering

Cardiff University

United Kingdom

April 2015

ABSTRACT

The aim of this study is to understand the complexity and control challenges of the locomotion of a three-link mechanism of a robot system. In order to do this a three-link robot gymnast (Robogymnast) has been built in Cardiff University. The Robogymnast is composed of three links (one arm, one torso, one leg) and is powered by two geared DC motors. Currently the robot has three potentiometers to measure the relative angles between adjacent links and only one tachometer to measure the relative angular position of the first link.

A mathematical model for the robot is derived using Lagrange equations. Since the model is inherently nonlinear and multivariate, it presents more challenges when modelling the Robogymnast and dealing with control motion problems. The proposed approach for dealing with the design of the control system is based on a discrete-time linear model around the upright position of the Robogymnast.

To study the swinging motion of the Robogymnast, a new technique is proposed to manipulate the frequency and the amplitude of the sinusoidal signals as a means of controlling the motors. Due to the many combinations of the frequency and amplitude, an optimisation method is required to find the optimal set. The Bees Algorithm (BA), a novel swarm-based optimisation technique, is used to enhance the performance of the swinging motion through optimisation of the manipulated parameters of the control actions. The time taken to reach the upright position at its best is 128 seconds.

Two different control methods are adopted to study the balancing/stablising of the Robogymnast in both the downward and upright configurations. The first is the optimal control algorithm using the Linear Quadratic Regulator (LQR) technique with integrators to help achieve and maintain the set of reference trajectories. The second is a combination of Local Control (LC) and LQR. Each controller is implemented via reduced order state observer to estimate the unmeasured states in terms of their relative angular velocities.

From the identified data in the relative angular positions of the upright balancing control, it is reported that the maximum amplitude of the deviation in the relative angles on average are approximately 7.5° for the first link and 18° for the second link. It is noted that the third link deviated approximately by 2.5° using only the LQR controller, and no significant deviation when using the LQR with LC.

To explore the combination between swinging and balancing motions, a switching mechanism between swinging and balancing algorithm is proposed. This is achieved by dividing the controller into three stages. The first stage is the swinging control, the next stage is the transition control which is accomplished using the Independent Joint Control (IJC) technique and finally balancing control is achieved by the LQR. The duration time of the transition controller to track the reference trajectory of the Robogymnast at its best is found to be within 0.4 seconds. An external disturbance is applied to each link of the Robogymnast separately in order to study the controller's ability to overcome the disturbance and to study the controller response.

The simulation of the Robogymnast and experimental realization of the controllers are implemented using MATLAB® software and the C++ program environment respectively.

ACKNOWLEDGEMENTS

I would like to thank my supervisors Dr.Eldaw E. Eldukhri and Dr. Michael Packianather for their supervision, help and continuous encouragement. My thanks go to them for accepting me to be one of their students in the School of Engineering at Cardiff University.

I would like to acknowledge Dr. Y Xue for his support and advice.

Further gratitude and appreciation is expressed to my country, Iraq for funding my study and giving me this opportunity.

A warm and special thanks are expressed to my parents and my wife for their endless support and patience during these four years of study.

DEDICATION

THIS THESIS IS DEDICATED TO

MY FATHER,

MY MOTHER,

MY MOTHER IN-LAW,

MY WIFE,

MY CHILDREN FATIMAH, RUQAYAH AND MUHAMMAD RIDHA,

AND MY BROTHER ALI

DECLARATION AND STATEMENTS

DECLARATION

This work has not previously been accepted in substance for any degree and is not concurrently submitted in candidature for any degree.

Signed ……..…… (Haider G. Kamil) Date…….…….

STATEMENT 1

This thesis is being submitted in partial fulfillment of the requirements for the degree of Doctor of Philosophy (PhD).

Signed ……..…… (Haider G. Kamil) Date…….…….

STATEMENT 2

This thesis is the result of my own independent work/investigation, except where otherwise stated. Other sources are acknowledged by explicit references.

Signed ……..…… (Haider G. Kamil) Date…….…….

STATEMENT 3

I hereby give consent for my thesis, if accepted, to be available for photocopying and for inter-library loan, and for the title and summary to be made available to outside organisations.

Signed ……..…… (Haider G. Kamil) Date…….…….

CONTENTS

LIST OF FIGURES

LIST OF TABLES

ABBREVIATIONS

Robogymnast	Robot gymnast
LQR	Linear Quadratic Regulator
LC	Local Control
IJC	Independent Joint Control
SG	Speed Gradient
SDRE	State Dependent Riccati Equation
DOF	Degrees of Freedom
MDFC	Multiple-prediction Delayed Feedback Control
PD	Proportional Derivative
BVP	Boundary Value Problem
TLIPs	Triple Link Inverted Pendulums
DIP	Double Inverted Pendulum
NN	Neural Network

PID	Proportional Integral Derivative
CPSO	Chaos-embedded Particle Swarm Optimisation
DLQR	Discrete-time Linear Quadratic Regulator
PSO	Particle Swarm Optimisation
QPSO	Quantum Particle Swarm Optimisation
TES	Total Energy Shaping
MOEA	Multi Objective Evolution Algorithm
BA	Bees Algorithm
ACROBOT	Acrobatic Robot
DC	Direct Current
AD/DA	Analogue to Digital/ Digital to Analogue
RC	Resistor-Capacitor
R	Resistor
PC	Personal Computer

LIST OF SYMBOLS

K	Kinetic energy
D	Dissipation energy
P	Potential energy
y	Output signal from Robogymnast to computer
u_i	Input voltage from computer to ith driving motor
θ_i	Angle of ith link from the vertical line
T_i	Generalised torque at angle θ_i
l_i	Length of the i_{th} link
I_i	Moment of inertia of ith link around its centre of gravity
m_i	Mass of the i_{th} link
C_i	Viscous friction coefficient of the i_{th} joint
G_i	Static gain of i_{th} motor/gearbox
I_{p_i}	Moment of inertia of ith motor/ gearbox reflected at the output shaft of the gearbox

C_{p_i}	Viscous friction coefficient of ith motor/gearbox reflected at the out-put shaft of the gearbox dissipation energy
T_{m_i}	Torque generated by the ith motor
a_i	Centre of gravity of ith link
g	Acceleration of gravity (9.81m/s2)
k_i	Ratio of the ith gearbox
q_i	Relative angle of ith link
$\emptyset_i$	Angle of ith sinusoidal control signal
T_s	Sampling time
α, δ	Variable values
$A_1, A_2, \eta, \Delta\alpha, \Delta\delta$	Constant values
J	Performance index
Q , R	Weight matrices
F	Gain matrix

y_r	Desired reference output signal
y_i	Actual output of ith relative angular position from Robogymnast to computer
e	Difference between the desired reference y_r and the actual relative angular position y_i
w	Integrator value
K_p	Proportional gain
K_I	Integral gain
$v(k+1)$	State observer
E	Reduced order observer dynamics
T	Transform matrix
d_i	Derivative values
K_{d_i}	Derivative gains

Chapter 1

Introduction

1.1 Introduction

A mechanical system is classified as underactuated when the number of actuators is less than the number of degrees of freedom (Liu and Yamaura 2011; Xue et al. 2011; Hara et al. 2009; Spong 1998). In recent years, interest in the study of underactuated systems has been increasing. This field of research is attractive for several reasons including: (1) Underactuated systems are commonly found in many real-life applications; (2) There is an increasing demand for reducing the number of actuators in systems in order to reduce cost and weight, and hence optimise energy usage. (3) There is a strong trend of recent developments in underactuated systems to address this demand.

1.2 Motivation

One very interesting underactuated control system is the inverted pendulum. It forms one of the most widely used groups of underactuated systems and has been extensively utilised for examining control algorithms. For example, a single inverted link mounted on a movable cart (Saberi et al. 1995; Yi et al. 2001; Rock 2001; Zhi-Hao Xu et al.

2002; Bugeja 2003; Yamada et al. 2004; Mus et al. 2006) is a good illustration of a rocket booster during lift off.

The structure of inverted pendulums has often included multiple links. This increases the number of degrees of freedom, which leads to an increase in the complexity of the system. Although the definition of an underactuated system is simple, this simplicity masks a number of complex needs and challenges. The multi-link systems are inherently nonlinear, multivariable and present challenging modelling and control problems.

Due to the dynamic structures of the complex (underactuated) multi-link systems, they provide useful testbeds for performance simulation, evaluation, optimisation, validation and comparison of different control techniques. In particular, the study of such systems will enable researchers to develop solutions aimed at addressing motion problems encountered by disabled and/or injured people experiencing limb impairment. In addition to the analysis of locomotion, the development of a walking robot (Dariush and Fujimura 2000; Hasegawa and Fukuda 2004; Tsuji and Ohnishi 2002; Stephens 2007; Vukobratovic et al. 1970; Golliday Jr and Hemami 1976; Hemami and Chen 1984) can be implemented through consideration of the robot as a multi-link system which mimics a simplified model of a human standing on two legs.

In this work, the research presents a new design for a three-link robot gymnast (Robogymnast) with two powered joints. Each of the links consists of two parallel rods which represent the symmetry of the human body (two hands and two legs). The system is mounted on a free rotating high bar. This robot should be capable of carrying out a

dynamic movement to achieve a desired motion. In this work, Robogymnast mimics the human acrobat who hangs from a high bar and tries to 'swing-up' to an upside-down position with his/her hands still on the bar. Unlike human acrobats, Robogymnast's hands are firmly attached to a freely rotating high bar which is mounted on ball bearings. Although the rotating of the high bar helps during the 'swinging-up' phase, it poses a great challenge when attempting to balance the robot in an upright position. The research investigates the development and implementation of various control strategies. Figure 1.1 represents the real Robogymnast.

1.3 Research aim and objectives

The aim of this project is to model, simulate and design a controller for an under-actuated Robogymnast system that can achieve the swing-up and balance of a triple link structure (Robogymnast), and can combine these actions into a single movement.

Throughout this project, the objectives of this work were:

- To develop a new method for the 'swinging-up' of a 3-link Robogymnast system mounted on a freely rotating high bar.

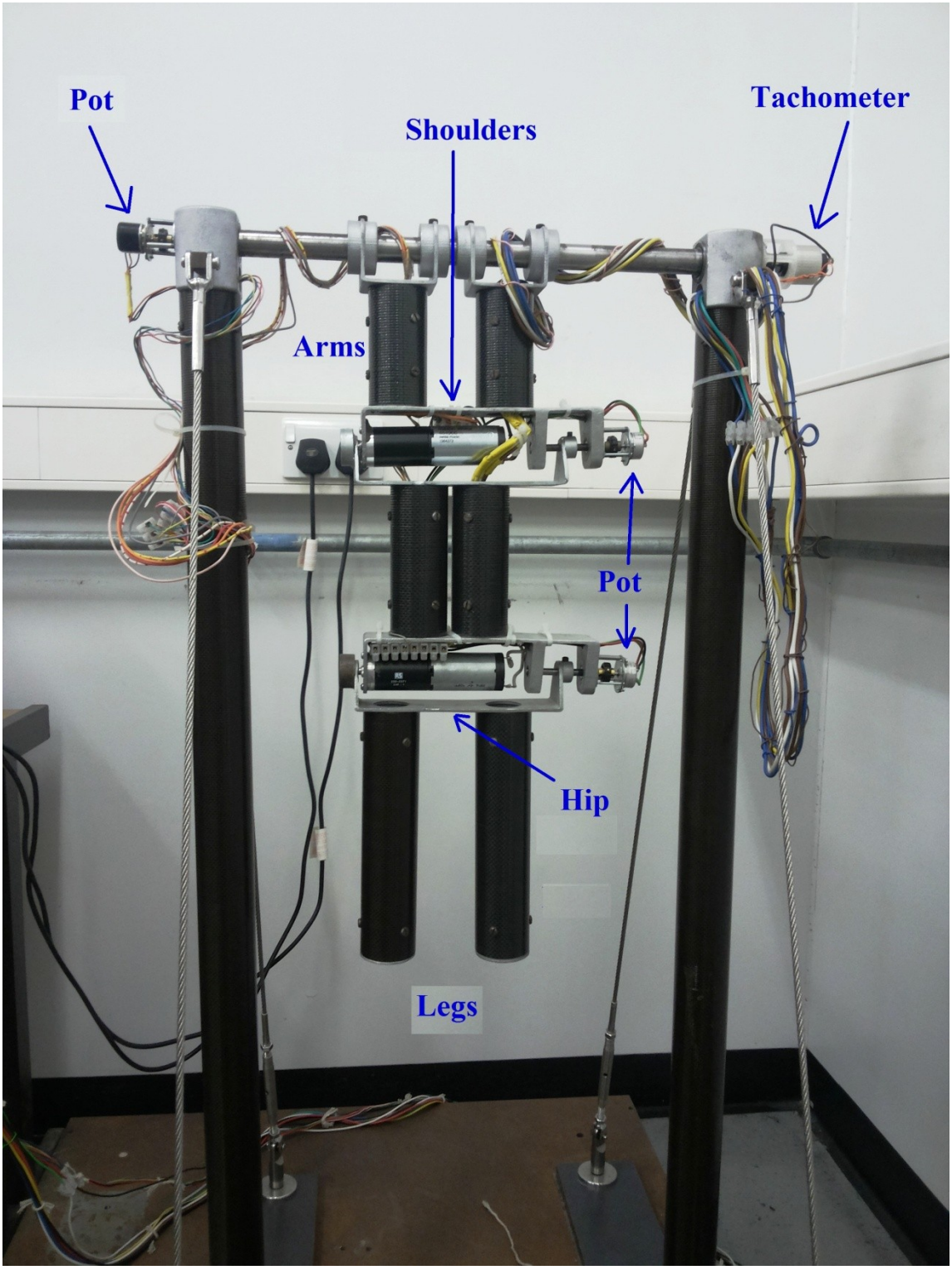

Figure 1.1: Robogymnast

- To apply a novel swarm-based optimisation technique to optimise a parameter that manipulates the control action applied simultaneously to the two motors driving the robot.

- To apply the optimised parameters for swinging-up on the real system.

- To design a different types of controllers under which the robot can be brought into any arbitrarily small neighbourhood of the downward/upright equilibrium point, where all three links of the Robogymnast stay in their desired location.

- To design a reduced order observer to estimate the unmeasured states.

- To validate and evaluate the different proposed controllers experimentally by using them to balance the Robogymnast in the downward position during the application of an external disturbance to each link separately.

- To simulate and analyse the control system for stablising the Robogymnast in the upright configuration using its mathematical model together with the proposed controllers techniques.

- To design a switching controller to enable the swing-up and balancing control systems to be combined.

- To apply a proposed transition controller to achieve the transition of the Robogymnast from the swinging to balancing locomotion.

- To assess the ability of the designed controller to overcome external disturbances, and to analyse the Robogymnast motion response.

1.4 Methodology

To achieve the above objectives, the following methodology was adopted:

- Reviewing previous works through an extensive search of the most relevant papers for each research topic, in order to identify any shortcomings in the current state of the art. This investigation focuses on identifying the potential solutions to the project objectives.

- The Euler-Lagrange approach will be used to derive a mathematical model and dynamic equations of the Robogymnast in the stable equilibrium point (downward position) and the second in the unstable position (upright).

- The simulation of the swing-up control will be achieved using the MATLAB® software and its associated toolboxes. The parameters of the swing-up control will be optimised using the BA, then implementing the findings on the real system using the C++ program environment.

- The problem of balancing/stablising the Robogymnast in the downward/upright position will be investigated. The optimal control theory and a combination of a local control with an optimal control theory will be used to satisfy the desired motions. The MATLAB® software will be used to simulate the designed controllers of balancing/stablising the Robogymnast. The implementation of the designed controller on the real system will be achieved via the C++ program environment.

- The combining of the swing-up and balancing control systems will be carried out. That will be achieved through proposing a switching control mechanism to transfer the Robogymnast from the swing-up to transition control, and then to balance control. The MATLAB® software will be utilised to simulate the behaviour of Robogymanst during all the controller phases, and to evaluate the performance of the transition controller.

- Finally the disturbance rejection and controller response of the Robogymnast will be investigated.

1.5 Thesis outline

The remainder of the thesis is organised as follows:

Chapter 2 presents a comprehensive review of the relevant literature in the field of underactuated systems. The chapter focuses on the most relevant structures which are the single, double and triple inverted link systems. The swing-up and balancing motion are highlighted with different control methods. Furthermore the combining of the swing-up and balancing motions is demonstrated.

Chapter 3 describes the design and modelling of a complex three degree of freedom Robogymnast mounted on a freely rotating high bar. The system description and the overall experimental setup are discussed. The Euler-Lagrange approach is used to depict the system dynamics through the derivation of a mathematical model of the Robogymnast in the upright and downward positions.

Chapter 4 is devoted to the analysis and design of the controller for the swing-up motion of the Robogymnast system. A new proposed technique is used to manipulate the frequency and the amplitude of the sinusoidal control signals which supply to motors. Moreover the BA is utilised to enhance the performance of the swinging motion through optimisation of the manipulated parameter of the control actions. Both experimental and simulation results are given.

Chapter 5 describes the controllers of the Robogymnast. The purpose of the work in this chapter is to design different controller methods. These methods are adopted to study the balancing/stablising of the Robogymnast in both the downward and upright configurations. The realisation performance of the Robogymnast is conducted through implementing the controller for the downward balancing problem of the Robogymnast on the real system. Each designed controller uses state feedback, which is implemented with a reduced order observer.

Chapter 6 investigates the problem of stabilising and balancing the Robogymnast system in the upright position. The simulation performance of the Robogymnast is considered. The designed controller is applied via a reduced order observer to estimate the unmeasured states (angular velocities).

Chapter 7 tackles the combining of the swing-up and balancing control systems. A switching control mechanism is suggested. A transition controller is proposed to transfer the Robogymnast from the swing-up regime to the balancing regime. Moreover, the disturbing effect on the each component of the Robogymnast is studied in this chapter.

Chapter 8 summarises the conclusions and the contributions of the research and provides suggestions for further research.

Figure 1.2 shows an outline of the thesis structure and the research questions which it addresses.

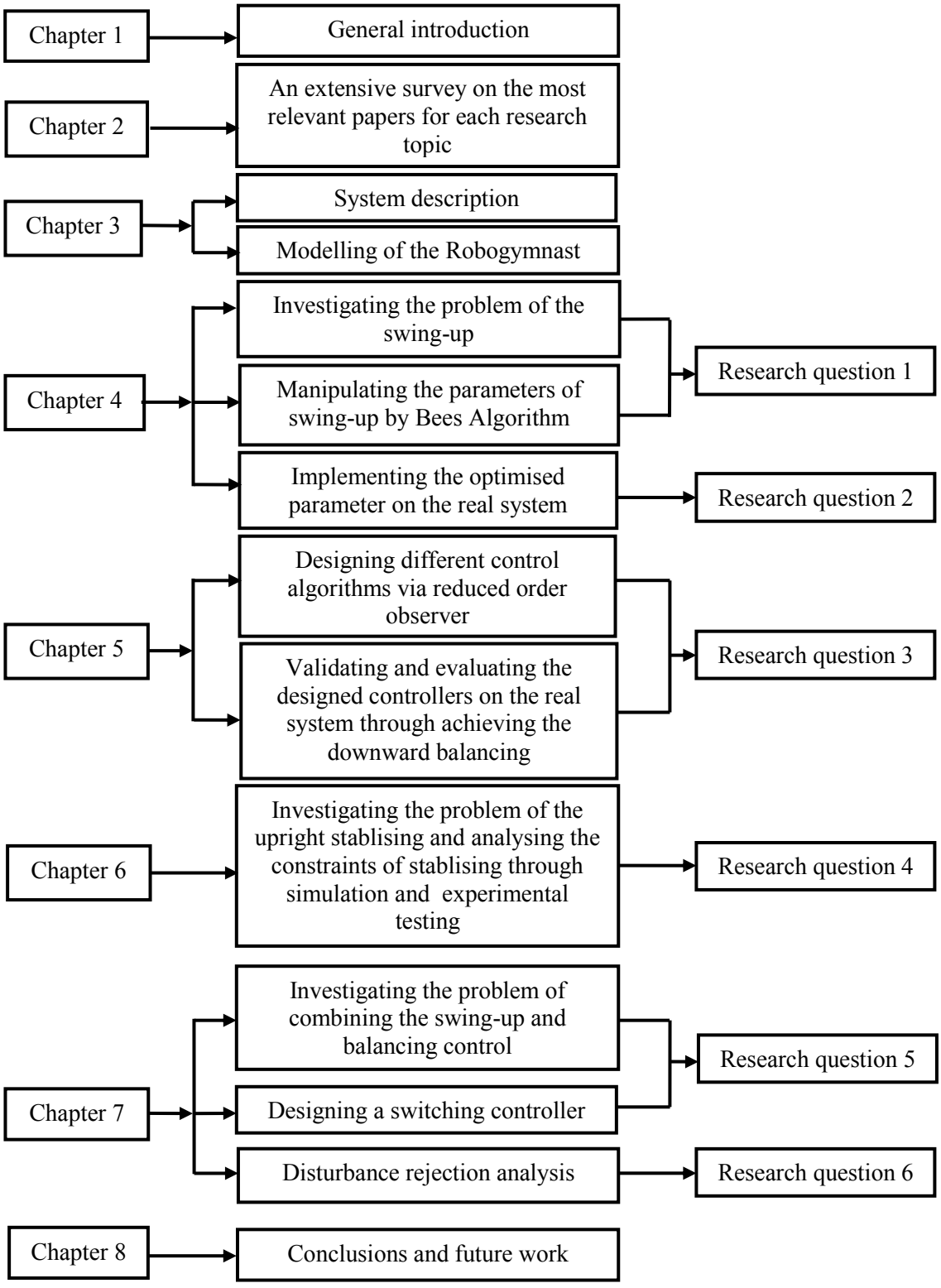

Figure 1.2: Thesis outlines and research questions

1.6 Publications

- **Journals**

Eldukhri, E.E. and **Kamil, H.G.** 2013. Optimisation of swing-up control parameters for a robot gymnast using the Bees Algorithm. *Journal of Intelligent Manufacturing*, pp. 1–9.

- **Conferences**

Kamil, H.G., Eldukhri, E.E. and Packianather, M.S. 2012. OPTIMISATION OF SWING-UP CONTROL PARAMETERS FOR A ROBOT GYMNAST USING THE BEES ALGORITHM. In*: Proceedings of 8th International Symposium on Intelligent and Manufacturing Systems (IMS 2012)*. Adrasan/Antalya/Turkey 27-28 September 2012, pp. 456–466.

Kamil, H.G., Eldukhri, E.E. and Packianather, M.S. 2014. Balancing control of Robogymnast Based on Discrete-time Linear Quadratic Regulator Technique. In: *2014 Second International Conference on Artificial Intelligence, Modelling and Simulation.* Madrid, Spain 18-20 November 2014: IEEE Computer Society, pp. 137–142.

Chapter 2

Background Review

2.1 Introduction

This chapter reviews the notation associated with underactuated control systems, and explores the basic concepts and problems of some of the most used examples. Several pieces of relevant literature describe single, double and triple link dynamic system problems. This literature is reviewed and analysed in this chapter. In addition, the theories of conventional control and trainable control have been summarised. Each previous study has focused on a different type of controller design. Some of the researchers focused on designing a control system for swinging-up, while a large volume of separate publications has focused on designing a control system for balancing in the up-right configuration. Some attempts have been made to combine the swing-up and balancing control systems.

2.2 Background

There are many volumes of published studies establishing a dynamic model of the single

inverted pendulum system (Zhai et al. 2007; Landry et al. 2005; Mus et al. 2006; Chen et al. 2007; Farmanbordar et al. 2011; Bush 2001; Medrano-Cersa 1999; Yi et al. 2001).

Several other studies have examined the double inverted pendulum (Yu et al. 2012; Jadlovska and Sarnovsky 2012; Yadav et al. 2012; Graichen et al. 2007; Yamakita et al. 1995; Medrano-Cerda et al. 1995; Brown and Passino 1997; Henmi et al. 2004; Xin and Yamasaki 2012).

One of the most important investigations for the current research is the triple inverted pendulum. A considerable amount of literature has been published on the dynamic modelling and control of triple inverted pendulums (Medrano-Cerda et al. 1995; Eltohamy and Kuo 1998; Lam and Davison 2006; Furut et al. 1984; Fer and Enns 1996; Eldukhri and Pham 2010; X Xin and Kaneda 2007; Araki et al. 2005; Awrejcewicz et al. 2008; Lingling Yang et al. 2010). A major challenge with this kind of application is the inherent nonlinearity of the system which presents a challenge in modelling and control problems. The literature review is classified based on the type of the desired motion of the system (i.e. swing-up, balancing, and a combination of swing-up and balancing). In addition, the literature explains the using of different optimisation technique to find the optimal control parameters.

2.3 Swing-up control

The problem of the swing-up of inverted pendulums with passive joints was extensively studied by many researchers (Eldukhri and Pham 2010; Fantoni et al. 2000; Bradshaw and Shao 1996; Xin Xin and Kaneda 2007; Xin et al. 2010; Furuta and Iwase 2004; Åström and Furuta 2000; Chung and Hauser 1995; Gordillo et al. 2003). Spong (1995) in particular, proposed an approach based on partial feedback linearisation (Isidori 1995) . This approach was very sensitive to the gain values of the outer loop and the switching times. Fantoni et al. (2000) discussed the swinging of the pendubot, where a pendubot is simply a double pendulum with one end connected to a motor, and an encoder attached at the elbow. The authors suggested utilising energy based approach to establish the proposed control law to move the first link to the upright position. As compared with (Spong and Block 1995), this method does not demand a high controlling gain. However, the approach appears to be inefficient to overcome the oscillation of the second link.

As noted by Yamakita et al. (1995) various methods are proposed to control the movements of the rotary inverted pendulum. Yamakita et al. (1995) proposed a designed controller which combined a feedforward controller that swings-up pendulums and a feedback controller that stabilises the pendulum in the upright position.

In an analysis of an inverted pendulum, Åström and Furuta (1996) showed which factors affected the global behaviour of the swing-up. They determined that the maximum

acceleration of the pivot enables the pendulum to achieve an upright position in one swing.

Acosta et al. (2001) compared their results with Åström and Furuta (1996), focusing on the Furuta pendulum swing-up. By way of this research, the controller design was reported using the Speed Gradient (SG) Algorithm technique (Andrievskii et al. 1996). In this exploratory investigation, the author was able to show experimentally the effectiveness of the new control law by accounting for the velocity of the arm and the reaction torques from the pendulum to the arm.

Furuta and Iwase (2004) emphasised the duration of a pendulum swing-up from the downright to the upright position. It should be noted that the State Dependent Riccati Equation (SDRE) (Mracek and Cloutier 1996) has been implemented along with the sliding mode (Lu 1999). Moreover, the parameters of the nonlinear system control and initial states have been evaluated through utilising the colour map set technique (Graichen et al. 2005; Devaney and Devaney 1989).

To study the problem of a swinging two-bar linkage and to maintain a different pattern of movements, Han et al. (2007) designed a neural controller to control the motion of the system by mimicking human arms in a harmonic swing-up movement. The authors designed a neural controller to attain the small swing and giant rotating movements. The preference of this type of methodology is that it has better control over the movement of the character. It does have the fundamental detriment that the authenticity of the

subsequent movements depends profoundly on the precision of the model and the movement controller.

(Xin et al. 2010) reconsidered the use of the energy based approach to solve the problem of the swing-up which was used previously by Fantoni et al. (2000). In this detailed analysis of the swing-up problem, Xin et al. (2010) were able to attain the control objectives by avoiding the singular points in the control law with a higher controller factor than was used in the previous work.

Another method was used to study the swing-up problem by Xin and Kaneda (2007). They considered links 2 and 3 to be a virtual composite link. They then used a coordinate transformation on the angles of the active joints 2 and 3.

Analysis of the control of a three-link gymnastic robot was carried out by Duong et al. (2009). In their analysis, the researchers proposed a neurocontrol system to implement the swing-up of the 3-DOF manipulator. The proposed controller was implemented via a neural network and a genetic algorithm.

Eldukhri and Pham (2010) suggested a new control technique to solve the problem of driving the Robogymnast from its downward position to its upright position. The basic principle of this method was to apply frequently varying sinusoidal torques to the two motors located at the hip and shoulder joints. In this method the angular positions and angular velocities are not involved in the derivation of the control signals.

An alternative method, known as Multiple-prediction Delayed Feedback Control (MDFC), was used to generate homogenous swinging by studying the characteristics of chaotic systems (Liu and Yamaura 2011). In this case the control signal was dependent on the angular positions of the joints.

Xue et al. (2011) discussed the three-link acrobat swing-up problem. They used a sensory motor schema method and divided the controller actions into multiple stages (multi stage). In some stages they used the Bang Bang method, in some the other Proportional Derivative (PD) controller, and in some a combination of the two. The simulation results were obtained using MATLAB® software, and showed that the swing-up to the upright stance had been successfully achieved.

Glück et al. (2013) experimentally achieved swing-up of a triple inverted pendulum on a cart. They suggested that the key challenge of the swing-up manoeuvre is the design of an appropriate feedforward controller. The design was based on the solution of a boundary value problem (BVP). The experimental results illustrate a successful swing-up of the system.

2.4 Upright position control

A number of researchers have studied the problem of stabilising inverted pendulums with passive joints at the upright position (Sahba 1983; Furut et al. 1984; Meier Farwig and Unbehauen 1990; Arai and Tachi 1991; Larcombe 1992; Medrano-Cerda et al. 1995; Fer and Enns 1996; Eltohamy and Kuo 1998; Lakshmi 2007; Zhai et al. 2007;

Farmanbordar et al. 2011; Wu et al. 2011; Vinodh Kumar and Jerome 2013). The problem of stabilising and controlling the attitude of a triple inverted pendulum was also studied by Furut et al. (1984). In this system, the lower link was hinged to the ground and, to support the control of the whole system, horizontal bars were fixed to the links to increase their moments of inertia.

In the same vein, the problem of stabilising control of a double inverted pendulum mounted on a single parallel bar was presented by Hauser and Murray (1990). The researchers proposed a nonlinear control method of approximate linearisation to cause the system to move along the set of inverted equilibrium positions. In the suggested design, a braking mechanism was supplied to unactuated joints to reduce the coupling between the linkages and to simplify the control problem,. The simulation results show that this strategy functioned well but required slow motion.

Arai and Tachi (1991) published a paper in which they described the method of control of two degrees of freedom systems. The constructed system consisted of an active joint with an actuator and a passive joint with a holding brake instead of an actuator. The proposed controller was based on using the coupling physical characteristics of manipulator dynamics (Arai and Tachi 1991).

Medrano-Cerda et al. (1995) designed a robust computer control system for balance and position control of double and triple link inverted pendulums (TLIPs). The controllers were based on linearised models of the pendulums and included integral actions and optimal state feedback implemented via functional observers.

In a similar study, Fer and Enns (1996) discussed the difficulty of utilising a single control input to stabilise a triple inverted pendulum on a cart which moves on a rail. The system has four degrees of freedom, so the stabilisation problem is more complicated than in some other studies (Furut et al. 1984; Meier Farwig and Unbehauen 1990). Fer and Enns (1996) used two types of controller to achieve a solution. The first was the LQR method (Anderson and Moore 1990) and the second was the multiple time-scale approximation (Bugajski and Enns 1992) with a nonlinear dynamic inversion approach.

Eltohamy and Kuo (1998) used a numerical optimisation algorithm for the controller design, which included a globally convergent numerical technique. Their designed controller was produced as an optimisation problem which accounted for the constraints of physical boundaries, system stability conditions, and the nonlinear infinite dimensional difference.

Bogdanov (2004) presented a comparison between various optimal controller algorithms for use in a Double Inverted Pendulum Controller (DIPC). In this research a feedback gain matrix was used to stabilise the system. The gain matrix manipulation was achieved via employing the LQR, State Dependent Riccati Equation (SDRE), Neural Network (NN) and NN+LQR/SDRE control schemes.

Delibasi (2007) described the stabilisation and disturbance rejection of an inverted double pendulum, which was achieved experimentally. In this research, the state feedback controller idea was dependent on the use of Proportional Integral Derivative (PID) controller technology.

Wongsathan and Sirima (2009) described how to find the optimal values of the controller to stabilise an inverted pendulum system using a genetic algorithm. There were significant simulated results obtained from the preliminary analysis of the system response with the optimised controller.

Sehgal and Tiwari (2012) used a continuous LQR optimal control system to understand the mechanisms involved in balancing a triple inverted pendulum. The simulation results showed that the controller successfully stabilised the system with good performance. In the same manner Gupta et al. (2014) utilised the LQR system to stabilise a triple link inverted pendulum on a moving cart. The presented results show that the proposed controller could achieve the balancing of a system of upside down pendulums.

Yadav (2012) investigated the stablisation of a single input and multiple outputs Double Inverted Pendulum (DIP) on a cart. They presented the LQR to maintain stabilisation about the upright equilibrium position. For the same system structure, Singh and Yadav (2012) compared the optimal LQR controller with a PID controller based on a pole placement technique.

For trajectory tracking and balancing of a single inverted pendulum on a cart, Kumar et al. (2013) proposed two ways to stablise the system by utilising traditional and optimal control techniques. The controller was introduced using a proportional-integral-derivative and optimal state variable feedback using an optimal control LQR. The reported results show that the system was swung up and was then stabilised using the

two suggested balancing controllers. The LQR controller was found to be a more robust controller than the PID controller.

Analysis of the stablisation and tracking control for a triple link structure Robogymnast (Eldukhri and Kamil 2013) was first carried out by Kamil et al. (2014). In this research the author combined a discrete-time linear quadratic regulator (DLQR) controller and an integral control action to satisfy the required performance of the control system. The simulation results showed that the overshoot of angular positions of the first, second and third links were satisfactory, and the Robogymnast could be settled in the upright position for an acceptable amount of time (Kamil et al. 2014).

2.5 Combining the swing-up and balancing control

A considerable amount of literature has been published on the swing-up of single and multiple pendulum systems, and the subsequent stablisation at the upright equilibrium point. Several control researchers have been achieving and analysing the locomotion of different frameworks of inverted pendulums through utilising various control methods (Kobayashi et al. 2002; Jian and Zushu 2003; Lakshmi 2007; Zhai et al. 2007; Wu et al. 2011; Xue et al. 2011; Park et al. 2011; Jianbao and Xinbing 2011; Saito et al. 1994).

Saito et al. (1994) discussed the challenges and strategies for swinging-up and balancing a two-link robot. In their research, the authors used a combination of the feedforward input (generated by a heuristic method) and feedback control. This enabled the

locomotion to be organised, and was represented through the generated motion and the direction of the arm to the target.

Another study focused on the combination of the swing-up and balance control for an underactuated planar revolute robot known as pendubot (Block 1996). A pendubot is a two-link pendulum with an actuator at the shoulder, but no actuator at the elbow. The researchers managed the control movement by introducing an approach for switching between the swinging-up control to the balance control. The proposed switching controller begins working when the links are within the attractive region of balancing. Partial feedback linearisation techniques were used for the swing-up control, while the optimal LQR controller was utilised for stabilisation around the desired equilibrium position.

One study by Brown and Passino (1997) utilised intelligent and classical control for swing-up and balancing of the acrobot. This was achieved by using a PD controller with inner-loop partial feedback linearisation, a state feedback, and a fuzzy controller to swing-up the acrobat from its stable equilibrium position of the inverted region. As a part of this study, Brown and Passino (1997) investigated optimisation of the performance of the designed controller by developing two genetic algorithms to tune the controller.

Zhong and Rock (2001) proposed the energy shaping method to swing-up a double inverted pendulum system and used the LQR controller to optimise the control gains for the feedback controller which balances the system. The authors reported the results

through simulation plots where the controller begins the swinging from the initial condition and then balances in the upright position.

Kobayashi and Komine (2002) demonstrated two types of control method to maintain the swing-up and then balancing of the pendulum about the upright position. Two kinds of technique were used in their study. The first technique is based on energy control. The second technique is based on linear feedback control and was prepared according to the assignment of closed system poles which make the pendant position unstable and the upright position stable. The simulation results show a good swing-up of the system and good stable balancing.

Bugeja (2003) set out to investigate the swinging of underactuated pendulum systems, and recommended the energy based method. The designed stabilisation controller was based on the state feedback method and utilised a simple pole assignment control approach.

In another major study, Jian and Zushu (2003) discussed the challenges of planning the motion of a three link horizontal bar gymnastic robot. By means of characteristic states or energy transfer processes, the swing-up and inverted equilibrium were described.

Furthermore, an extension of the conventional particle swarm optimisation (PSO) algorithm, called quantum particle swarm optimisation (QPSO) (Jun Sun et al. 2004), provided a new approach for controller modification. (Hassani and Lee 2014) deployed this controller to automatically and optimally adjust the weighting matrices of the LQR. This method was implemented to stabilise an inverted pendulum system.

Inoue et al. (2006) carried out an investigation into the control of a cart-type serial double inverted pendulum (Deng et al. 2007; Inoue 2005). The authors implemented this work on an experimental system, and the sliding mode control was adopted as a controller to manoeuvre between the first or second pendulum and the cart. This allowed the swing-up and the stabilisation of the first and the second pendulums in the upright position (Inoue et al. 2006).

Furthermore, the problem of the Swing-up and Stabilising Control of a cart with inverted pendulum was presented by (Lakshmi 2007). The research focused on using an energy control method called a total energy shaping (TES) and two swing-up controls. The stabilisation of the inverted pendulum was also considered. Additionally, the investigators designed an intermediate algorithm to transfer from the swing-up controller to the stabilising controller depending on the state variable.

Graichen et al. (2007) achieved experimentally the stabilisation and side-stepping of the triple inverted pendulum problem. The inversion based feedforward control design and optimal feedback controllers, are applied to determine trajectories for the swing-up manoeuvre and the stablising at the upright position respectively (Graichen et al. 2007). The author reported that the swing-up manoeuvre was successfully implemented and tested. The results show a good response of the system with stable balancing.

Another study proposed a new method to consider a swing-up and stabilisation problem for an inverted pendulum, through switching control (Zhai et al. 2007). The proposed

controller consists of a combination of a linear optimal regulator, a SDRE and an energy dissipative controller to stabilise the system within the linear operating region.

In the same way, the double inverted pendulum system controller was designed using a fuzzy logic control (Cheng-jun et al. 2009). The weighting coefficients of a fuzzy logic controller can be optimised by utilising the genetic algorithm optimisation technique. It is apparent that the approach can attain stronger, robust, real time and controllers, (Zhang et al. 2012) used the same approach to design the controller for a triple inverted pendulum on a cart.

Wu et al. (2011) studied the motion of the 3-link gymnast robot moving. In this investigation, the researchers considered two spaces of motion in the vertical plane. They divided the space of motion into two subspaces, one for balancing about the upright position and one for resting in the swing-up area. Consequently, in order to achieve the control motion of the gymnast robot, a different controller is considered for each subspace. The validation of this method was fulfilled through the simulated results.

Swing-up and Stablising of a rotary inverted pendulum was demonstrated experimentally by Park et al. (2011). A modified bang-bang control technique was used to swing-up the pendulum safely and quickly. Thereafter to achieve the stabilisation and balance at the upright position a LQR was used. The Experimental results illustrate that the swing-up time was generally less than 3 seconds and the system was able to recover after applying a disturbance.

In a study which set out to establish the combination of the swing-up and stabilisation of the single pendulum system, Angeli (2001) used an energy-shaping method, with smooth switching between positive and negative feedback, to obtain a globally stabilised controller. Meanwhile, Mihara and Yokoyama (2012) suggested a two step control method for single pendulum system locomotion (Mihara and Yokoyama 2012).

2.6 Optimisation algorithm

There is a large volume of published studies describing the role of evolutionary optimisation algorithms in the control system design (Ha and Kim 1997; Zhang 2007; Mobaieen et al. 2012; Qian et al. 2008). (Ha and Kim 1997) used a genetic algorithm to optimise the weights of an LQR controller for stablising a single inverted pendulum system. In the same way, the genetic algorithm can be used to find the optimised weight matrices of the linear quadratic regulator. This approach was applied on an active suspension system (Zhang 2007). Qian et al. (2008) achieved the stabilisationn of a double inverted pendulum on a cart at the upright position by constructing a sliding mode controller. The author utilised improved genetic algorithms to determine the optimal sliding controller surface in the design.

Due to their increasing popularity, swarm-based optimisation algorithms have been used by researchers to solve a diverse range of engineering and manufacturing problems. In recent studies, a PSO (Kennedy and Eberhart 1995) has been used to develop the designed controller for the inverted pendulum system. For example, Xiong and Wan

(2010) optimised the optimal controller with an improved PSO and realised the stability control of a double inverted pendulum. Chandra Debnath et al. (2013) extended the capability of the PSO algorithm to improve the Gaussian membership functions of the fuzzy model of a nonlinear problem. In this way an effective adaptive fuzzy logic controller was designed to attain the target problem for the cart with the inverted pendulum system. Fierro and Castillo (2013) employed the particle swarm optimisation metaheuristic and two of its variants to calculate the optimal membership functions of fuzzy control systems for the water tank and inverted pendulum benchmark problems. Solihin and Akmeliawati (2009) adopted the PSO optimisation technique to tune the state feedback gains and analyse the stablisation and tracking of a single inverted pendulum on a cart.

A multi-objective evolution algorithm (MOEA) was considered by Li et al. (2008) to achieve the Pareto-optimal solutions of the LQR weighting matrices. Consequently, the desired multiple performance indices were established to meet the control system. The suggested method for controller design was applied to a double inverted pendulum system.

A novel swarm-based optimisation technique called the Bees Algorithm (BA) (Pham et al. 2006) provided a new approach for controller tuning. Pham et al. (2009) used this to regulate the parameters of a fuzzy logic controller designed to balance an under-actuated two-link acrobatic robot (Spong 1995). They developed a Linear Quadratic Regulator to obtain the scaling gains needed to design the fuzzy logic controller.

In another major study, (Darwish 2009) suggested the use of fuzzy logic to design a controller to stabilise and balance an under-actuated two-link acrobatic robot (ACROBOT) in the upright position. (Darwish 2009) utilised the BA to optimise the membership functions and the scaling gains of the fuzzy system. The simulation results show a good response of the system and with stable balancing.

Eldukhri and Kamil (2013) and Kamil et al. (2012) proposed a new way to swing-up a Robogymnast consisting of three links and three joints. The process was to pump in energy and consequently swing Robogymnast until it flipped past the upright position. This was achieved by manipulating the input control signals applied to the two Direct Current (DC) motors mounted at the shoulder and hip joints. The BA was used to optimise the parameters regulating the amplitudes and frequencies of the sinusoidal control signals.

2.7 Summary

A review of different designs of single and multi link underactuated systems has been presented. This chapter gave an overview of various controller methods that have been used to satisfy different types of complex n-link robot system locomotion focusing on the literature for swing-up control, balancing control, and the combination of the swing-up control and balance control. In addition, the literature of using an optimisation technique to achieve the control performance has been presented. In the next chapter, the

description of the Robogymnast system is given and a mathematical model for the Robogymnast will be derived.

Chapter 3

System Description and Mathematical Modelling

3.1 Introduction

This chapter presents a mathematical model and system description for Robogymnast. The Robogymnast relies on a greatly coupled complex dynamical multi-joint mechanical framework. The multifaceted nature of this framework is not unusual for a mechanical structure of this complexity and a control system of this difficulty. The lack of full actuation brings challenges when setting up feasible trajectories and planning controllers. In the design, the Robogymnast had a total of three degrees of freedom, including two powered degrees of freedom.

The main fundamental problems with Robogymnast are (i) the ability to move from one place to another, (ii) determining the complex mathematical equations of motion and (iii) the analysis and control of multiple kinds of movement.

The equations of motion must be derived in order to understand the behaviour of the Robogymanst under different conditions. Moreover, these laws are used to derive appropriate feedback control laws and to simulate the Robogymnast's performance under feedback control (Hemami and Farnsworth 1977).

The Lagrangian motion methodology has been used to determine the system dynamics of a serial-chain mechanical manipulator with a rigid link (Arnold 1989; Spong et al. 2006; Craig 1985). The dynamic system model and equations of motion of the multilink system are determined mathematically using Lagrange's equation method to depict the system dynamics. This approach has been used in many previous studies (Furut et al. 1984; Medrano-Cerda et al. 1995; Eltohamy and Kuo 1998).

In this study, the Robogymnast is a planar three-link system in the vertical plane, with two actuators at the second joint (shoulder joint) and the third joint (hip joint), but no actuator at the first joint (hand joint). Lagrange's mathematical statements are used to determine the mathematical representation for the Robogymnast, in the same manner as used by Eldukhri and Pham (2010).

The Robogymnast configuration was designed to be adaptable for future adaptations or modifications. These may include: changing the actuators for more powerful ones; increasing the degrees freedom by adding extra link(s); changing the length of the shaft or the free rotating bar; adding sensors to measure the angular velocity (e.g. tachometer) of the second and third links; replacing the angular position sensors (potentiometers) with more accurate ones; disposing of the impact of the backlash in some if not all joints (e.g. hip joint) by utilising anti-backlash.

Section 3.2 presents a description of the system, including sketches and schematic diagrams of the Robogymnast. In Section 3.3, the mathematical continuous-time model of the Robogymnast at its upright position is derived. The numerical continuous-time

and discrete-time models are then presented. In Section 3.4 presents the numerical continuous-time and discrete-time models of the Robogymnast at the downward position. A summary of the chapter is given in Section 3.5.

3.2 System description

In this study, the controller is to be implemented by a PC supported by an appropriate AD/DA converter. A block diagram representation of the experimental apparatus is shown in Figure 3.1.

The ADLINK DAQ-2501 AD/DA converter has a resolution of 12 bits for analogue input and 14 bits for analogue output. The converter time is 1 microseconds and the settling time is less than 3 microseconds. The bipolar input and output range of the voltage is ±l0 V and ±12 V respectively.

The interfacing circuit between the computer and the robot comprises amplifiers and first-order filters. These filters reduce effects introduced by sampling the system's outputs, and smooth the control signals sent to the power amplifiers/motor drive units (Medrano-Cerda et al. 1995, Fadali and Visioli 2012).

The analogue feedback signals y(t) consist of two types of information. The first is the sensors readings, which are considered as a controllable disturbance. This type of disturbance is relatively low frequency. The second type is the uncontrollable disturbance, which is related to high frequency noise. This type may relate to

measurement noise, or drift in electrical pickup (Anderson and Moore 1990). Such noise signals cause problems in analogue systems, such that low-pass filtering is regularly used to permit greater control execution (Burns 2001). Therefore, the computer interface in this study contains first order anti-aliasing filters for each sensor. All the anti-aliasing filters were chosen to be first-order resistor capacitor (RC) filters with the same cut-off frequency. Additional filters were used to smooth the reconstructed continuous-time controls u(t). These were chosen to be first order and to have the same cut-off frequency.

The amplifiers are 741 series operational amplifiers. They are connected in non-inverting mode. The amplifiers for the control signals (u) have a gain of 2 for $R_i = R_f = 10k\Omega$. The amplifier for the first output signal (y_1) have a gain of 3.7 for $R_i = 1k\Omega$ and $R_f = 2.7k\Omega$. Each one of the second and third output signals (y_2 and y_3) have a gain of 2 for $R_i = R_f = 10k\Omega$. The amplifier for the fourth output signal (y_4) have a gain of 7.8 for $R_i = 1k\Omega$ and $R_f = 6.8k\Omega$. The amplifiers for the control signals (u) and the output signals (y) are biased with ±15V DC. Figure 3.2 shows the circuit diagram of a first order filter in series with the amplifiers. Before sending, the computed control signals u(k) are divided by the amplifier gain of 2. The read signals y(k) are also divided by the gain of each signal amplifier gain before being processed.

The power amplifiers are LM12 series. The LM12 is a power operational amplifier capable of driving ±25V at ±10A while operating from a $\pm 30V$ power supply. Every pair of LM12 power amplifiers is supplied from ±13.8V, ±13A peak, ±10A continuous, or regulated DC power supplies. The circuit diagram of the power amplifier is shown in

Figure 3.3. A description of LM12CL 80W Operational Amplifier of is given in Appendix A.1.

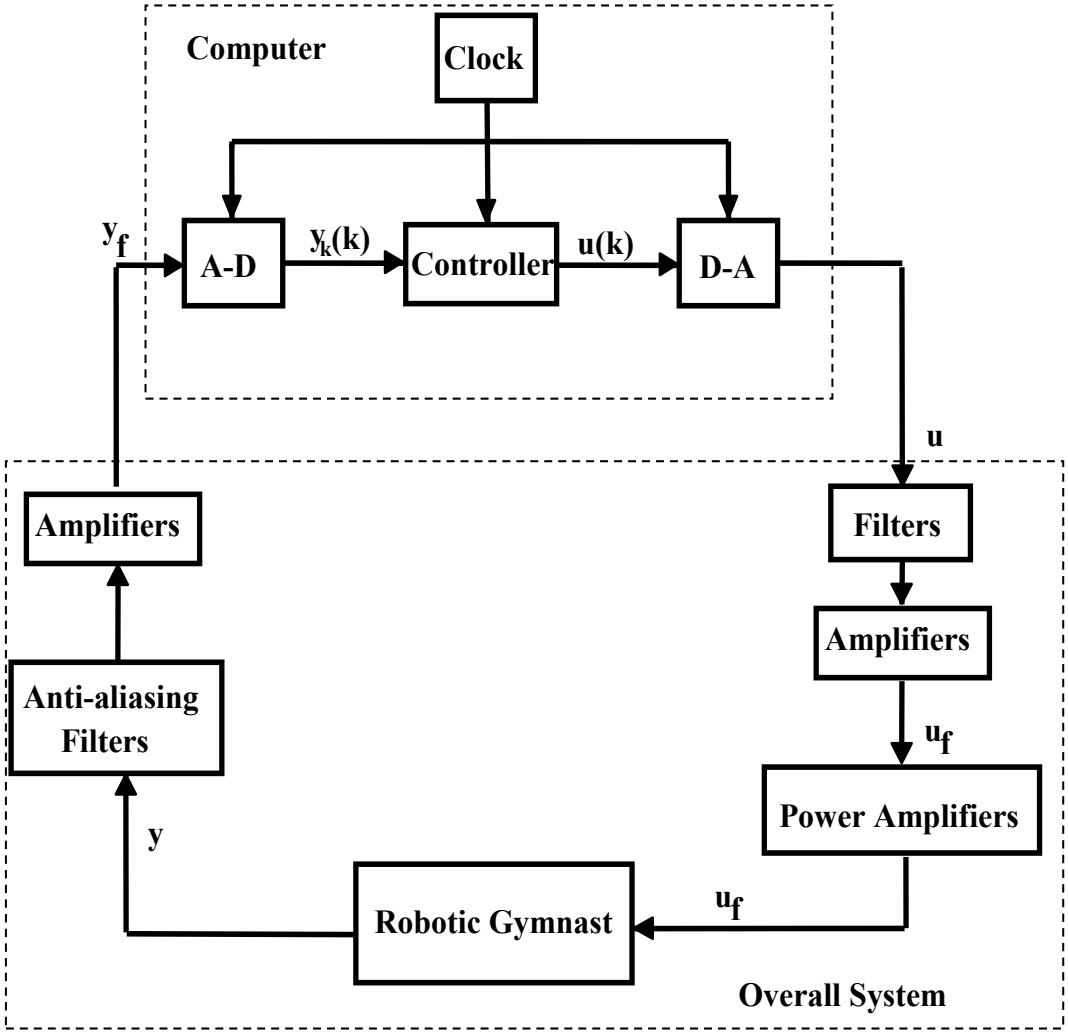

Figure 3.1: Block diagram representation of the experimental apparatus

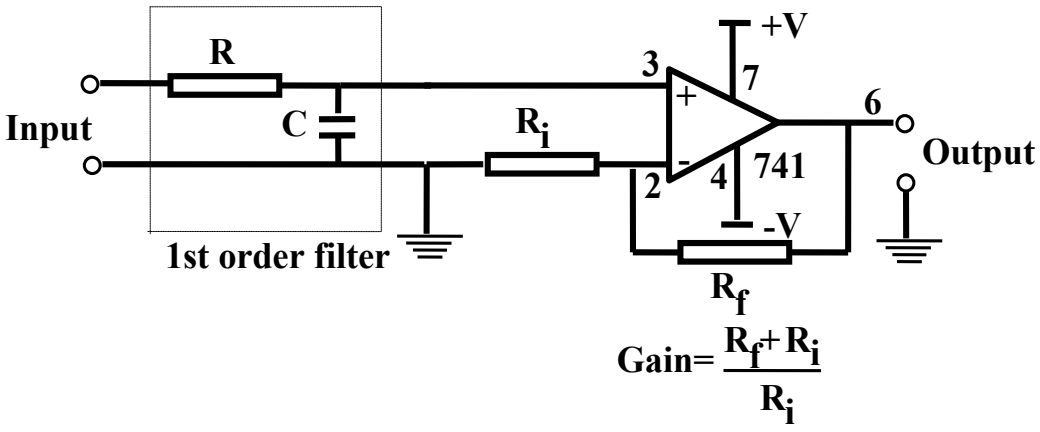

Figure 3.2: Circuit diagram of 1st order filter in series with operational amplifier

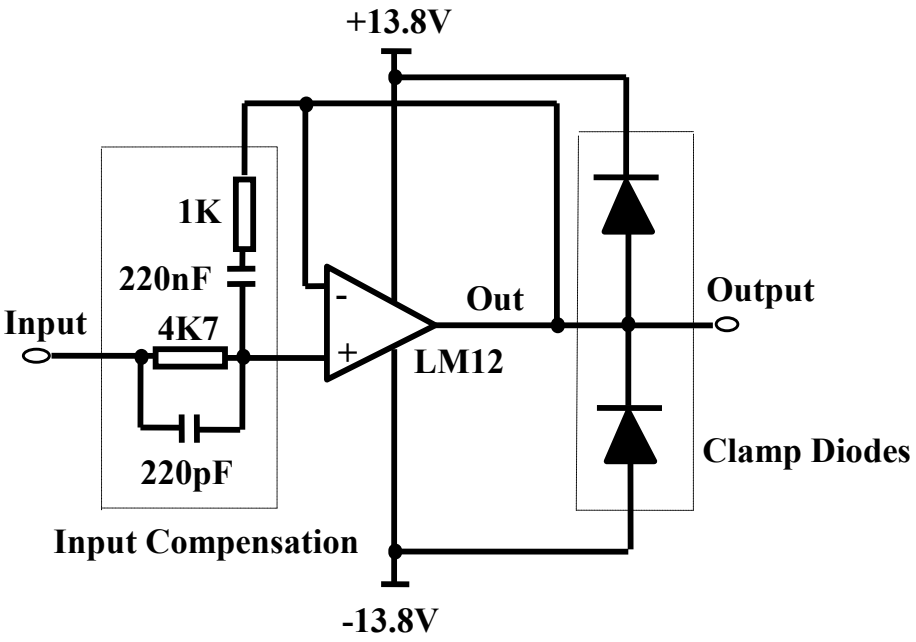

Figure 3.3: Circuit diagram of the power amplifier

C++ program environment is used to transmit the input/output commands between the Personal Computer (PC) and the Robogymnast. The program consists of a code to

record experimental data and store the information on a hard disk. The computer controller programs contain: a state feedback controller, discrete integrator, and a reduced order observer. It also contains an adjustment to the offset in the control outputs. Furthermore, the programs contain scaling factors and sensor gains to convert the input channels signals from volts to radians and to use them in the control action calculations. Figure 3.4 depicts the Robogymnast hardware components (Eldukhri and Pham, 2010). The structure of Robogymnast is modelled on a human gymnast swinging on a freely rotating high bar with his/her hands firmly fixed to the bar. Link 1 represents the arms without the elbow and wrist joints. The head, neck and torso are combined into Link 2 as a single rigid body. Link 3 represents the legs without knee and ankle joints. The main part of each link is manufactured from two rigid carbon fibre tubes, which are 50 mm in diameter. These are economical, simple to cut, and weigh just 0.213 kg/m. At both ends of each link, aluminum segments (3 mm in thickness) are appended to give structure on which to mount the sensors and actuators.

Joint 1 consists of a steel shaft mounted on ball bearings. At one end of the shaft a potentiometer is mounted to measure the angle of Link 1. At the other end of the shaft a tachometer is mounted to measure the angular velocity of Link 1. A description of E-series tachometer generators is given in Appendix A.2. Joints 2 and 3 consist of two parts. The first part comprises a DC motor/gearbox combination with its output shaft coupled to the respective link. Planetary gearboxes with a rated continuous capacity of

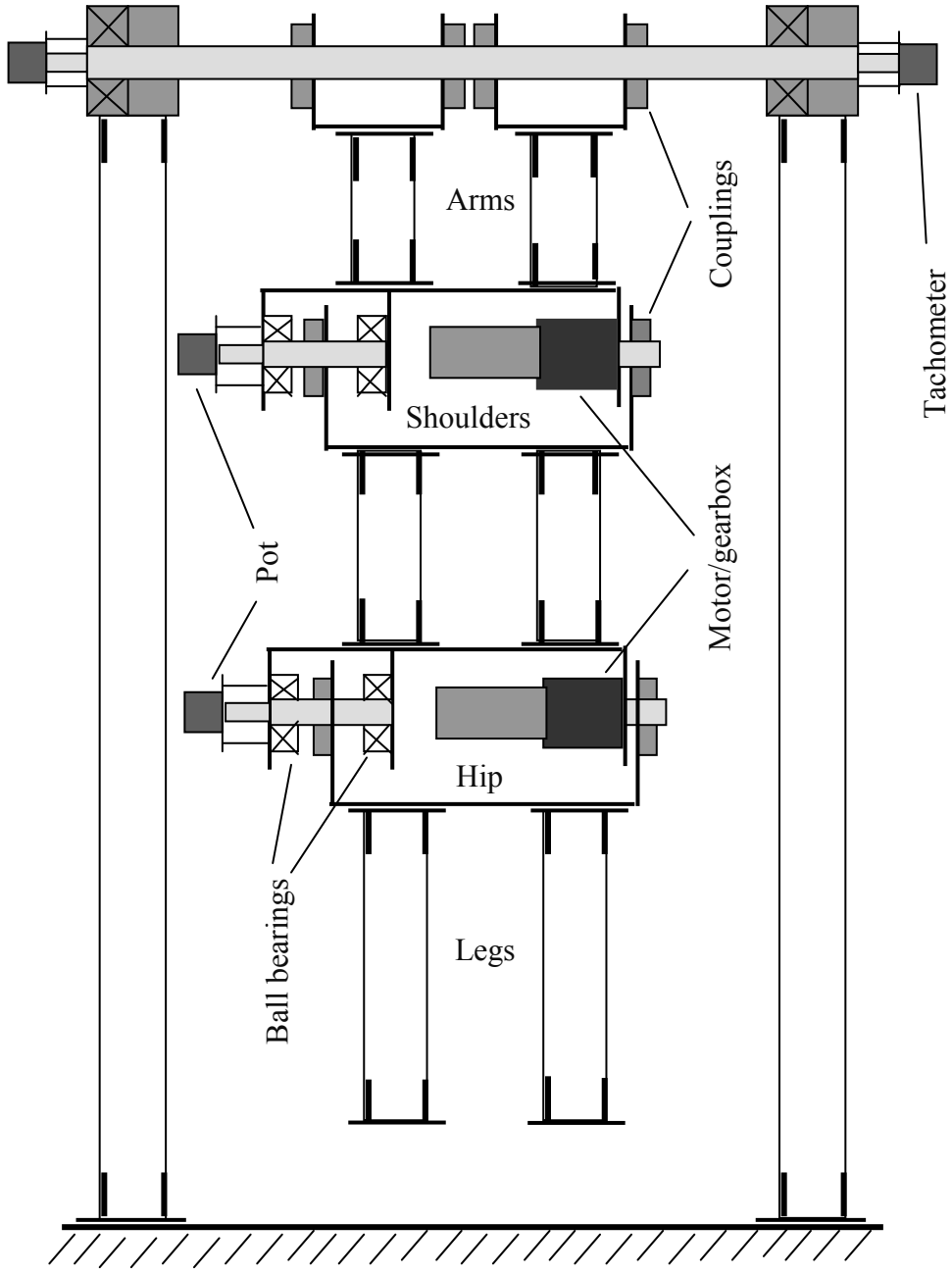

Figure 3.4: Hardware components of Robogymnast

4.5 Nm were chosen. The second part includes the potentiometer, which measures the relative angles between adjacent links. The potentiometer is attached to a short steel shaft mounted on both sides on ball bearings. One of the most important points in robot design is the selection of the actuators. Good selections give a robot more capability to achieve different types of movement. Conversely, the speed and torque of the actuator are an important characteristic in the performance of the robot, and they play a key role in the selection of actuators to maintain the required locomotion. In this study, electric actuators were selected to control the joints of the robot on the grounds that they are generally less expensive and lighter in weight than other available options. The movements of the Robogymnast are modelled mathematically as described in the following section.

3.3 Mathematical model of the Robogymnast in the upright position

The equations of motion for Robogymnast, as represented by the schematic diagram in Figure 3.5, were derived using Lagrange equations (Eldukhri and Pham 2010; Eltohamy and Kuo 1998; Furuta et al. 1984; Medrano-Cerda et al. 1995). It is considered as a triple-link pendulum in an unstable equilibrium configuration.

The mathematical model is derived using the Lagrange equation:

$$\frac{\mathrm{d}}{\mathrm{dt}}\left(\frac{\partial \mathrm{K}}{\partial \dot{\theta}_\mathrm{i}}\right) - \frac{\partial \mathrm{K}}{\partial \theta_\mathrm{i}} + \frac{\partial \mathrm{D}}{\partial \dot{\theta}_\mathrm{i}} + \frac{\partial \mathrm{P}}{\partial \theta_\mathrm{i}} = \mathrm{T_i} \qquad \mathrm{i} = 1,2,3 \ldots \tag{3.1}$$

The system Kinetic energy K, the potential energy P and the dissipation energy D are computed through Equations (3.2), (3.3) and (3.4) respectively. θ_i is defined as the absolute angle of the i_{th} link measured from the vertical line. T_i is the generalised torque at angle θ_i.

The kinetic energy in terms of robot parameters is given by:

$$K = \frac{1}{2}\sum_{i=1}^{3}\left\{\begin{matrix} I_i\dot{\theta}_i^2 + m_i\left[\frac{d}{dt}\left(\sum_{k=i-3}^{i-1} l_k \sin(\theta_k) + a_i \sin(\theta_i)\right)\right]^2 + \\ \left[\frac{d}{dt}\left(\sum_{k=i-3}^{i-1} l_k \cos(\theta_k) + a_i \cos(\theta_i)\right)\right]^2 \end{matrix}\right\}. \tag{3.2}$$

The potential energy is defined as:

$$P = \sum_{i=1}^{3} m_i g\left(a_i \cos(\theta_i) + \sum_{k=i-3}^{i-1} l_k \cos(\theta_k)\right), \tag{3.3}$$

and the dissipative energy is given by:

$$D = \frac{1}{2}\sum_{i=1}^{3}\left(C_i\left(\dot{\theta}_i - \dot{\theta}_{i-1}\right)^2\right), \tag{3.4}$$

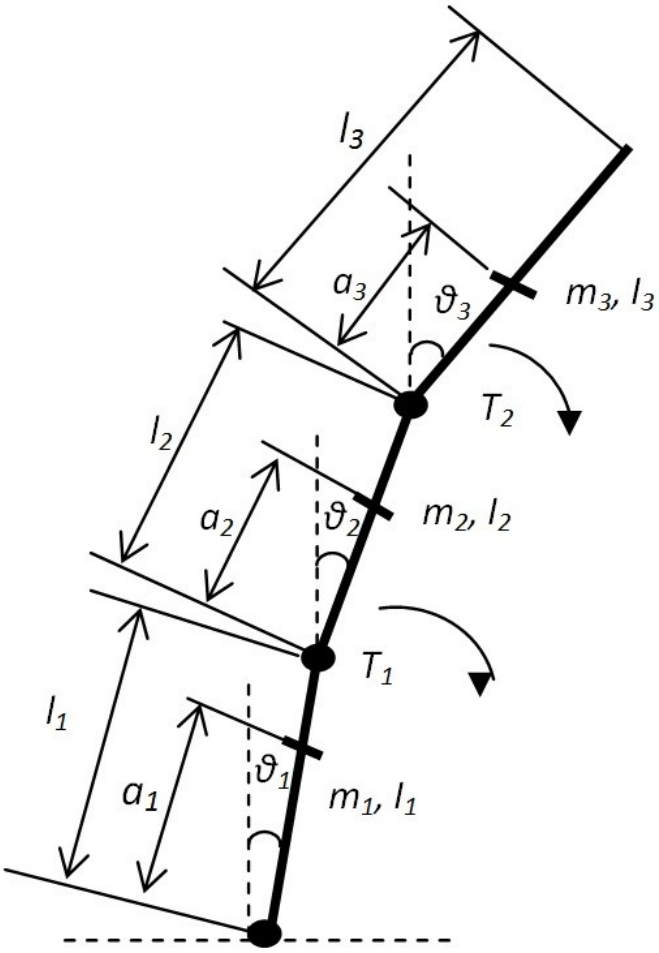

Figure 3.5: Schematic representation of Robogymnast in the upright position

l_i, m_i, I_i , a_i and C_i are defined respectively as: the length of the i_{th} link; the mass of the i_{th} link; the moment of inertia of the i_{th} link around its centre of gravity; the center of gravity of the i_{th} link, and the viscous friction coefficient of the i_{th} joint. Here, g is the acceleration due to gravity.

The Robogymnast has three joints. Since it is freely rotating on a high bar, there is no actuator at the first joint (the hands).I Its motion is manipulated by two DC motors mounted at the second joint (shoulder) and third joint (hip). Hence, the first joint is affected by the torques applied to powered joints (second joint and third joint). The torques of the two DC motors that are located at the shoulder and hip are represented as follows:

$$T_{m_1} = G_1 u_1 - I_{p_1}(\ddot{\theta_2} - \ddot{\theta}_1) - C_{p_1}(\dot{\theta}_2 - \dot{\theta}_1), \tag{3.5}$$

$$T_{m_2} = G_2 u_2 - I_{p_2}(\ddot{\theta_3} - \ddot{\theta}_2) - C_{p_2}(\dot{\theta}_3 - \dot{\theta}_2), \tag{3.6}$$

where u_1 and u_2 ($|u_1|$ and $|u_2| \leq 10V$) represent the input voltage to the DC motors. G_i, I_{p_i} and C_{p_i} are the static gain of i_{th} motor/gearbox, the moment of inertia of i_{th} motor/gearbox reflected at the output shaft of the gearbox, and the viscous friction coefficient of the i_{th} motor/gearbox reflected at the output shaft of the gearbox respectively.

The torque of the first joint of the Robogymnast is generated by the effect of the second joint DC motor torque. Hence $T_1 = -T_{m_1}$, and also $T_2 = T_{m_1} - T_{m_2}$ and $T_3 = T_{m_2}$.

The total kinetic energy of system components is expressed as follows:

$$K = \frac{1}{2}\left[I_1\dot{\theta_1}^2 + I_2\dot{\theta_2}^2 + I_3\dot{\theta_3}^2\right] + \frac{1}{2}[m_1a_1^2 + m_2l_1^2 + m_3l_1^2]\,\dot{\theta_1}^2\cos^2(\theta_1)$$

$$+ \frac{1}{2}[a_1^2 + 2l_1^2]\,\dot{\theta_1}^2\sin^2(\theta_1)$$

$$+ \frac{1}{2}[m_2a_2^2 + m_3l_2^2]\,\dot{\theta_2}^2\cos^2(\theta_2)$$

$$+ [m_2l_1a_2 + m_3l_1l_2]\,\dot{\theta_1}\dot{\theta_2}\cos(\theta_1)\cos(\theta_2)$$

$$+ \frac{1}{2}[a_2^2 + l_2^2]\,\dot{\theta_2}^2\sin^2(\theta_2) \qquad (3.7)$$

$$+ [l_1a_2 + l_1l_2]\dot{\theta_1}\dot{\theta_2}\sin(\theta_1)\sin(\theta_2)$$

$$+ \frac{1}{2}m_3a_3^2\,\dot{\theta_3}^2\cos^2(\theta_3) + \frac{1}{2}a_3^2\,\dot{\theta_3}^2\sin^2(\theta_3)$$

The total potential energy of system components is presented as follows:

$$P = g[m_1a_1 + m_2l_1 + m_3l_1]\cos(\theta_1) + g[m_2a_2 + m_3l_2]\cos(\theta_2) \qquad (3.8)$$

$$+ m_3ga_3\cos(\theta_3)$$

In addition, the total dissipation energy of system components is written as follows:

$$D = \frac{1}{2}[C_1 + C_2]\,\dot{\theta_1}^2 + \frac{1}{2}[C_2 + C_3]\,\dot{\theta_2}^2 + \frac{1}{2}C_3\,\dot{\theta_3}^2 - C_2\dot{\theta_1}\dot{\theta_2} - C_3\dot{\theta_2}\dot{\theta_3} \qquad (3.9)$$

The system equations of motion can be derived by solving Equation (3.1) for each system coordinate $[\theta_1 \ \theta_2 \ \theta_3]$ as follows:

$$\frac{d}{dt}\left(\frac{\partial K}{\partial \dot{\theta}_1}\right) - \frac{\partial K}{\partial \theta_1} + \frac{\partial D}{\partial \dot{\theta}_1} + \frac{\partial P}{\partial \theta_1} = T_1 \tag{3.10}$$

$$\frac{d}{dt}\left(\frac{\partial K}{\partial \dot{\theta}_2}\right) - \frac{\partial K}{\partial \theta_2} + \frac{\partial D}{\partial \dot{\theta}_2} + \frac{\partial P}{\partial \theta_2} = T_2 \tag{3.11}$$

$$\frac{d}{dt}\left(\frac{\partial K}{\partial \dot{\theta}_3}\right) - \frac{\partial K}{\partial \theta_3} + \frac{\partial D}{\partial \dot{\theta}_3} + \frac{\partial P}{\partial \theta_3} = T_3 \tag{3.12}$$

Substituting Equations (3.7), (3.8) and (3.9) in Equations (3.10), (3.11) and (3.12) yields three nonlinear differential equations describing the system dynamics. In order to simplify the control system analysis and design, the differential equations are linearised about the upright position ($\theta_i = 0$). System equations of motion can hence be written as follows:

$$\begin{aligned}\left[I_1 + m_1 {a_1}^2 + m_2 {l_1}^2 + m_3 {l_1}^2 + Ip_1\right]\ddot{\theta}_1 + [m_2 l_1 a_2 + m_3 l_1 l_2 - Ip_1]\ddot{\theta}_2 \\ + [m_3 l_1 a_3]\ddot{\theta}_3 + \left[C_1 + C_2 + C_{p_1}\right]\dot{\theta}_1 + [-C_2 - Cp_1]\dot{\theta}_2 \\ + [-g m_1 a_1 - g m_2 l_1 - g m_3 l_1]\theta_1 + G_1 u_1 = 0\end{aligned} \tag{3.13}$$

$$[m_2 l_1 a_2 + m_3 l_1 l_2 - Ip_1]\ddot{\theta}_1 + \left[I_2 + m_2 {a_2}^2 + m_3 {l_2}^2 + Ip_1 + Ip_2\right]\ddot{\theta}_2 + [-Ip_2 + m_3 l_2 a_3]\ddot{\theta}_3 + [-C_2 - Cp_1]\dot{\theta}_1 + [C_2 + C_3 + Cp_1 + Cp_2]\dot{\theta}_2 + [-C_3 - Cp_2]\dot{\theta}_3 + [-gm_2 a_2 - gm_3 l_2]\theta_2 - G_1 u_1 + G_2 u_2 = 0 \quad (3.14)$$

$$[I_3 + m_3 a_3^2 + Ip_2]\ddot{\theta}_3 + [m_3 l_2 a_3 - Ip_2]\ddot{\theta}_2 + [m_3 l_1 a_3]\ddot{\theta}_1 + [-Cp_2 - C_3]\dot{\theta}_2 + [C_3 + Cp_2]\dot{\theta}_3 + [-m_3 a_3 g]\theta_3 - G_2 u_2 = 0 \quad (3.15)$$

The linearised continuous model is expressed below:

$$\widetilde{M}\begin{bmatrix}\ddot{\theta_1}\\ \ddot{\theta_2}\\ \ddot{\theta_3}\end{bmatrix} + \widetilde{N}\begin{bmatrix}\dot{\theta_1}\\ \dot{\theta_2}\\ \dot{\theta_3}\end{bmatrix} + \widetilde{P}\begin{bmatrix}\theta_1\\ \theta_2\\ \theta_3\end{bmatrix} + \widetilde{G}\begin{bmatrix}u_1\\ u_2\end{bmatrix} = \begin{bmatrix}0\\ 0\\ 0\end{bmatrix} \quad (3.16)$$

where

$$\widetilde{M} = \begin{bmatrix} J_1 + I_{p_1} & l_1 M_2 - I_{P_1} & l_1 M3 \\ l_1 M_2 + I_{P_1} & J_2 + I_{p_1} + I_{p_2} & l_2 M_3 - I_{p_2} \\ l_1 M_3 & l_2 M_3 - I_{p_2} & J_3 - I_{p_2} \end{bmatrix}$$

$$\widetilde{N} = \begin{bmatrix} C_1 + C_2 + C_{p_1} & -C_2 - C_{p_1} & 0 \\ -C_2 - C_{p_1} & C_2 + C_3 + C_{p_1} + C_{p_2} & -C_3 - C_{p_2} \\ 0 & -C_3 - C_{p_2} & C_3 - C_{p_2} \end{bmatrix}$$

$$\widetilde{P}=\begin{bmatrix} -M_1 g & 0 & 0 \\ 0 & -M_2 g & 0 \\ 0 & 0 & -M_3 g \end{bmatrix}$$

$$\widetilde{G} = \begin{bmatrix} G_1 & 0 \\ -G_1 & G_2 \\ 0 & -G_2 \end{bmatrix}$$

where

$$M_1 = m_1 a_1 + m_2 l_1 + m_3 l_1$$

$$M_2 = m_2 a_2 + m_3 l_2$$

$$M_3 = a_3 m_3$$

$$J_1 = I_1 + m_1 a_1^2 + (m_2 + m_3) l_1^2$$

$$J_2 = I_2 + m_2 a_2^2 + m_3 l_2^2$$

$$J_3 = I_3 + m_3 a_3^2$$

Next the linearised continuous model can be re-written in terms of the relative angle q_i. These angles are measured by potentiometers. The relationship between the relative angle q_i and the angle θ_i is explained below:

$$W = \begin{bmatrix} 1 & 0 & 0 \\ -1 & 1 & 0 \\ 0 & -1 & 1 \end{bmatrix}, \theta = \begin{bmatrix} \theta_1 \\ \theta_2 \\ \theta_3 \end{bmatrix} \text{ and } q = \begin{bmatrix} q_1 \\ q_2 \\ q_3 \end{bmatrix}$$

then

$$q = \begin{bmatrix} q_1 \\ q_2 \\ q_3 \end{bmatrix} = \begin{bmatrix} \theta_1 \\ \theta_2 - \theta_1 \\ \theta_3 - \theta_2 \end{bmatrix} = W\theta$$

In the next step, each θ is replaced by $W^{-1}q$ in Equation (3.16). This equation can therefore be re-written as follows:

$$MW^{-1}\begin{bmatrix} \ddot{q}_1 \\ \ddot{q}_2 \\ \ddot{q}_3 \end{bmatrix} + NW^{-1}\begin{bmatrix} \dot{q}_1 \\ \dot{q}_2 \\ \dot{q}_3 \end{bmatrix} + PW^{-1}\begin{bmatrix} q_1 \\ q_2 \\ q_3 \end{bmatrix} + G\begin{bmatrix} u_1 \\ u_2 \end{bmatrix} = \begin{bmatrix} 0 \\ 0 \\ 0 \end{bmatrix} \tag{3.17}$$

and then:

$$\begin{bmatrix} \ddot{q}_1 \\ \ddot{q}_2 \\ \ddot{q}_3 \end{bmatrix} = -WM^{-1}NW^{-1}\begin{bmatrix} \dot{q}_1 \\ \dot{q}_2 \\ \dot{q}_3 \end{bmatrix} - WM^{-1}PW^{-1}\begin{bmatrix} q_1 \\ q_2 \\ q_3 \end{bmatrix} - WM^{-1}G\begin{bmatrix} u_1 \\ u_2 \end{bmatrix} \tag{3.18}$$

From Equation (3.18) the state space representation in terms of relative angle can be expressed as below:

$$\begin{gathered} \dot{x} = Ax + Bu = \begin{bmatrix} 0_3 & I_3 \\ -WM^{-1}PW^{-1} & -WM^{-1}NW^{-1} \end{bmatrix} x + \begin{bmatrix} 0_{3\times 2} \\ -WM^{-1}G \end{bmatrix} \begin{bmatrix} u_1 \\ u_2 \end{bmatrix} \\ y = Cx = [I_4 \quad 0_{4\times 2}]x \end{gathered} \tag{3.19}$$

where

$$\mathrm{I}_4 = \begin{bmatrix} 1 & 0 & 0 & 0 \\ 0 & 1 & 0 & 0 \\ 0 & 0 & 1 & 0 \\ 0 & 0 & 0 & 1 \end{bmatrix}, \qquad 0_{4\times 2} = \begin{bmatrix} 0 & 0 \\ 0 & 0 \\ 0 & 0 \\ 0 & 0 \end{bmatrix}, \qquad 0_{3\times 2} = \begin{bmatrix} 0 & 0 \\ 0 & 0 \\ 0 & 0 \end{bmatrix}$$

Here, the output vector $\mathrm{y} = \mathrm{q}$.

The numerical model of the Robogymnast is calculated by substituting the values of the parameters given in Table 3.1 and Table 3.2 into the Equation (3.19) using MATLAB®/toolboxes and additional M-files developed by the researcher.

Table 3.1: Parameters of Robogymnast

Link1	**Link2**	**Link3**
$l_1(\mathrm{m}) = 0.155$	$l_2(\mathrm{m}) = 0.180$	$l_3(\mathrm{m}) = 0.242$
$a_1(\mathrm{m}) = 0.0426$	$a_2(\mathrm{m})$=0.138	$a_3(\mathrm{m})$=0.065
$m_1(\mathrm{kg})$=2.625	$m_2(\mathrm{kg})$=0.933	$m_3(\mathrm{kg})$=0.372
$I_1(\mathrm{kgm}^2) = 0.014$	$I_2(\mathrm{kgm}^2) = 0.018$	$I_3(\mathrm{kgm}^2) = 0.002$
$C_1(\mathrm{Nms})$=0.0172	$C_2(\mathrm{Nms})$=0.0272	$C_3(\mathrm{Nms})$=0.035

Table 3.2: Motors Parameters

Motor1	**Motor2**
$I_{p_1}(kgm^2) = 0.0358$	$I_{p_2}(kgm^2) = 0.0358$
C_{p_1}(Nms)=7.73	C_{p_2}(Nms)=7.73
G_1(Nm/V)=1.333	G_2(Nm/V)=0.625
$k_1 = 246:1$	$k_2 = 110.6:1$

This gives A and B as:

$$A=\begin{bmatrix} 0_3 & I_3 \\ A_{21} & A_{22} \end{bmatrix}, \qquad 0_3 = \begin{bmatrix} 0 & 0 & 0 \\ 0 & 0 & 0 \\ 0 & 0 & 0 \end{bmatrix}, \qquad I_3 = \begin{bmatrix} 1 & 0 & 0 \\ 0 & 1 & 0 \\ 0 & 0 & 1 \end{bmatrix}$$

$$A_{21} = \begin{bmatrix} -36.42 & -0.35 & 0.21 \\ 13.10 & -22.06 & -2.23 \\ -2.14 & -1.50 & -5.68 \end{bmatrix}, A_{22} = \begin{bmatrix} -0.20 & 88.38 & 9.17 \\ 0.20 & -168.29 & 7.70 \\ 0.02 & 7.69 & -201.45 \end{bmatrix}$$

$$B=\begin{bmatrix} 0_{3\times 2} \\ -15.19 & -0.74 \\ 28.92 & -0.62 \\ -1.32 & 16.21 \end{bmatrix}$$

The eigenvalues of the continuous time model shown in Equation (3.19) at the upright position. These are:

[-166.8506 -203.1990 -5.4598 5.3762 0.1662 0.0270].

From the eigenvalues above, it appears that the system is unstable as there are three positive characteristic roots.

The discrete time model of the Robogymnast is obtained by discretising the continuous time model. The important point to find in the discrete dynamic model of the Robogymnast is the calculation of the sampling time to control the system motion perfectly. The sampling time represents the communication time required to operate the computer controller within a real system for every iteration of all the control system process. At each step the process time actually consists of the following sub-processes:

1- Initialisation of the system situation through reading sensors via the A-D conversion.
2- Load the control parameters.
3- Compute the control actions.
4- Output control to the motor by sending the control actions via the D/A convertor.

The experimental determination of the sampling time Ts relies on upon being sufficiently short, and the reproduced control signal being near to the signal that the creative analogue controller would have generated. The discrete time model of the Robogymnast is obtained by discretising the continuous time model in Equation (3.19) with a sampling time interval 25 milliseconds using MATLAB® software. The discrete time model is the sampling time

$$x(k+1) = A_d x(k) + B_d u(k)$$

$$y(k) = C_d x(k). \tag{3.20}$$

The A_d, B_d and C_d matrices can be written as:

$$A_d = \begin{bmatrix} 1.0100 & 0.0024 & 0.0002 & 0.0250 & 0.0101 & 0.0021 \\ -0.0015 & 1.0025 & 0.0003 & 0.0000 & 0.0059 & 0.0002 \\ -0.0003 & 0.0002 & 1.0006 & 0.0000 & 0.0002 & 0.0049 \\ 0.7770 & 0.2337 & 0.0241 & 1.0070 & 0.5232 & 0.0646 \\ -0.0772 & 0.1300 & 0.0143 & -0.0003 & 0.0158 & 0.0021 \\ -0.0134 & 0.0122 & 0.0286 & -0.0001 & 0.0020 & 0.0068 \end{bmatrix}$$

$$B_d = \begin{bmatrix} -0.0017 & -0.0001 \\ 0.0033 & -0.0000 \\ -0.0000 & 0.0016 \\ -0.0895 & -0.0052 \\ 0.1696 & -0.0001 \\ -0.0002 & 0.0800 \end{bmatrix}, \quad C_d = \begin{bmatrix} 1 & 0 & 0 & 0 & 0 & 0 \\ 0 & 1 & 0 & 0 & 0 & 0 \\ 0 & 0 & 1 & 0 & 0 & 0 \\ 0 & 0 & 0 & 1 & 0 & 0 \end{bmatrix}$$

The discrete time model represented in Equation (3.20) also has three unstable eigenvalues (outside the unit circle) as given below:

$$[0.0156 \;\; 0.0062 \;\; 1.1439 \;\; 0.8724 \;\; 1.0042 \;\; 1.0007].$$

3.4 Mathematical model of the Robogymnast in the downward position

In this section the Robogymnast is regarded as a triple pendulum in a stable equilibrium configuration as shown in Figure 3.6. The system mathematical model in the downward position has been described as being similar to the methodology used in Section 3.3.

For the linearised continuous-time state-space model of the Robogymnast in the downward position, the matrices A, B and C in Equations (3.19) are expressed as follows:

$$A=\begin{bmatrix} 0_3 & I_3 \\ A_{21} & A_{22} \end{bmatrix}, \qquad 0_3 = \begin{bmatrix} 0 & 0 & 0 \\ 0 & 0 & 0 \\ 0 & 0 & 0 \end{bmatrix}, \qquad I_3 = \begin{bmatrix} 1 & 0 & 0 \\ 0 & 1 & 0 \\ 0 & 0 & 1 \end{bmatrix}$$

$$A_{21} = \begin{bmatrix} 36.42 & 0.35 & -0.21 \\ -13.10 & 22.06 & 2.23 \\ -2.14 & 1.50 & 5.68 \end{bmatrix}, \; A_{22} = \begin{bmatrix} -0.20 & 88.38 & 9.17 \\ 0.20 & -168.29 & 7.70 \\ 0.02 & 7.69 & -201.45 \end{bmatrix}$$

$$B=\begin{bmatrix} 0_{3\times 2} \\ -15.19 & -0.74 \\ 28.92 & -0.62 \\ -1.32 & 16.21 \end{bmatrix}$$

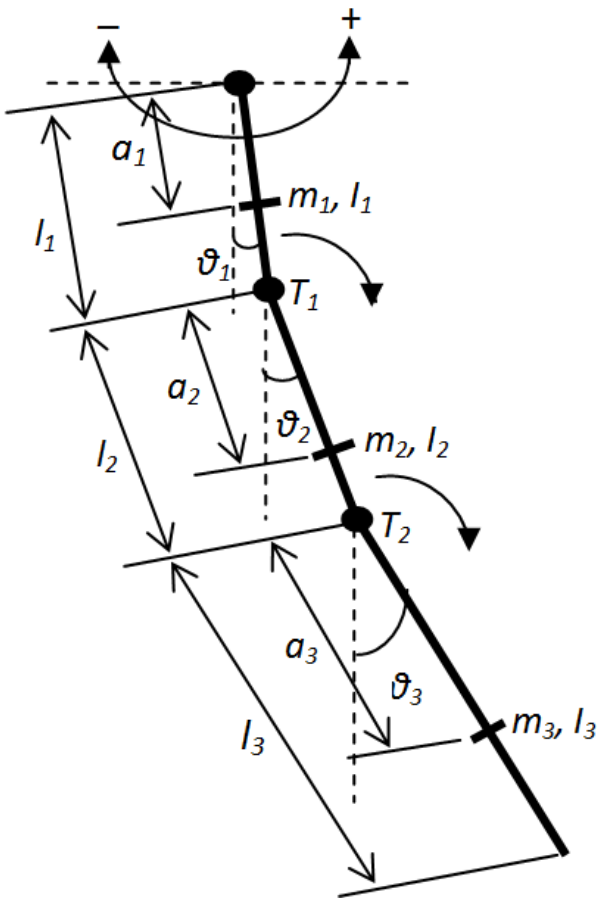

Figure 3.6: Schematic representation of Robogymnast at the downward position

The eigenvalues of the continuous time model shown in Equation (3.19) at the downward position are:

[-166.5012 -203.1428 -0.0511+5.4175i -0.0511-5.4175i -0.1665 -0.0269].

From the eigenvalues above, it can be noted that four of the eigenvalues are real and stable, while two of them are stable complex conjugates.

In the same manner applied to Equation (3.20) in Section 3.3, the A_d, B_d and C_d matrices for the downward position can be written as:

$$A_d = \begin{bmatrix} 1.0100 & 0.0024 & 0.0002 & 0.0250 & 0.0101 & 0.0021 \\ -0.0015 & 1.0025 & 0.0003 & 0.0000 & 0.0059 & 0.0002 \\ -0.0003 & 0.0002 & 1.0006 & 0.0000 & 0.0002 & 0.0049 \\ 0.7770 & 0.2337 & 0.0241 & 1.0070 & 0.5232 & 0.0646 \\ -0.0772 & 0.1300 & 0.0143 & -0.0003 & 0.0158 & 0.0021 \\ -0.0134 & 0.0122 & 0.0286 & -0.0001 & 0.0020 & 0.0068 \end{bmatrix}$$

$$B_d = \begin{bmatrix} -0.0017 & -0.0001 \\ 0.0033 & -0.0000 \\ -0.0000 & 0.0016 \\ -0.0895 & -0.0052 \\ 0.1696 & -0.0001 \\ -0.0002 & 0.0800 \end{bmatrix}, \quad C_d = \begin{bmatrix} 1 & 0 & 0 & 0 & 0 & 0 \\ 0 & 1 & 0 & 0 & 0 & 0 \\ 0 & 0 & 1 & 0 & 0 & 0 \\ 0 & 0 & 0 & 1 & 0 & 0 \end{bmatrix}$$

For the discrete time model represents in Equation (3.20) with the downward position, it can be seen all the eigenvalues are inside the unit circle and are given below.

[0.0156 0.0062 0.9896+0.1349i 0.9896-0.1349i 0.9958 0.9993].

3.5 Summary

The objective of this chapter was to design a complex three degree of freedom Robogymnast. The system description and the characteristics of the system parts have been demonstrated. Furthermore, a mathematical model of the Robogymnast has been derived based on the Euler-Lagrange approach describing the system dynamics. The linearised equations of motion and their state-space representation were then introduced. The linearised model of the system represented by the upright (unstable) and downward

(stable) positions. A linearised general model of the system is needed in order to test the Robogymnast's ability to perform different movements with various types of controllers. This will be discussed in detail in the following later chapters. In particular, chapter 4 will present the swing-up control.

Chapter 4

Swinging-up Control

4.1 Introduction

In this chapter, the swing-up problem of a nonlinear, three-link robot gymnast (Robogymnast) is discussed. Different control strategies were used to study the swing-up of such an inverted pendulum-like mechanism (Eldukhri and Pham 2010; Xin and Kaneda 2002; Spong 1995; Han et al. 2007).

With a specific end goal to enhance the system reaction and reduce the energy consumption, which are prompting more productive utilization of energy, the ideal control increases gains to be explored through utilizing optimal control parameters.

In this chapter, a novel optimization technique called the Bees Algorithm (BA) (Pham et al. 2006) provided a new approach to optimise the control system parameters. The BA is used to tune the parameters of the swing up control developed by Eldukhri and Pham (Eldukhri and Pham 2010). The BA is applied for the first time in this research to a constrained enhancement issue by means of penalty capacities and characterizing the limits of the Robogymnast system.

The remainder of the chapter is organized as follows. In Section 4.2, the swing-up control problem is investigated. Section 4.3 introduces the BA. Section 4.4 demonstrates

how the BA is used for tuning the swing-up control parameters. Section 4.5 discusses the simulation and experimental results. The summary is given in Section 4.6.

4.2 Swing-up control problem

The challenge posed by Robogymnast is how to make it swing up from the downward position (stable equilibrium posture) to upward attitude (unstable configuration). The swing-up must be achieved in a reasonable operation time without the risk of damaging any of the structure components. This requires determining of suitable input control signals to the motors located at joints 2 and 3 to obtain satisfactorily smooth sequence of oscillations. Eldukhri and Pham (2010) proposed a solution to this problem by manipulating the frequency and amplitudes of the sinusoidal input control signals applied to the two DC motors driving links 1 and 2. This enabled the two motors to pump energy into the system and consequently swing Robogymnast until it eventually flipped past the upright position. This was, in effect, achieved by causing the value of the first angle ($q_1 = \theta_1$) moves from the initial status ($q_1 = 0$) to the upright position, i.e. $q_1 = \pi$ (or $q_1 = -\pi$, depending on the direction of movement). The equations of the input control signals are given as:

$$u_1 = A_1 \alpha \sin(\emptyset_1) \tag{4.1}$$

$$u_2 = A_2 \alpha \sin(\emptyset_2) \tag{4.2}$$

Where without loss of generality, $[u_1, u_2]^T$=u(k) as described in equation (3.20) in Chapter 3. A_1 and A_2 are constants and $\emptyset_1$ and $\emptyset_2$ are dependent on δ.

During each sinusoidal cycle (multiple of sampling intervals T_s depending on the value of δ), $\emptyset_1$ and $\emptyset_2$ were varied between 0 and 2π with a step increment of η/δ applied during each sampling interval. η is constant and fractional to π. At the end of each duty cycle ($\emptyset_1$and $\emptyset_2 = 2\pi$) α, δ were increased by Δα and Δδ respectively. A_1, A_2, α, η and δ were initially set at 3, 2.5, 1, 0.3142 and 1 respectively (Eldukhri and Pham 2010). By means of exploitation of MATLAB® software and its associated toolboxes, the discrete time model (Equation (3.20) in Chapter 3) was used to simulate the dynamic behavior of Robogymnast during the swing up phase.

In Eldukhri and Pham's (2010) work, both the amplitudes and frequencies of the sinusoidal signals u_1 and u_2 were varied simultaneously using the same parameter, δ whose periodic increment Δδ was obtained manually (through trial and error process).

In this chapter, the BA was used as an optimization technique to automatically tune the values of the periodic increments Δα and Δδ to obtain acceptably smooth swinging of Robogymnast.

4.3 The Bees Algorithm

The Bees Algorithm (BA) is a population-based search algorithm that simulates the food foraging behaviour of honeybees to find the optimal solution (Kennedy et al. 2001). The

Algorithm emulates the harvesting process of the natural bees by doing a local search, till an acceptable result is found, or a pre-defined number of iterations has been reached (Otri 2011). It requires a number of parameters to be set, namely (Pham et al. 2009): number of scout bees (n), number of sites selected out of n visited sites (m), number of best sites out of m selected sites (e), number of bees recruited for best e sites (nep), number of bees recruited for the other (m-e) selected sites (nsp), initial size of patches (ngh) which includes site and its neighborhood and stopping criterion. The pseudo codes and the flowchart of the BA are described in Figure 4.1 and Figure 4.2 respectively.

The use of the algorithm to optimize the increments $\Delta\alpha$ and $\Delta\delta$ for attaining reasonably smooth swing-up control of Robogymnast will be discussed in the following section.

Generate initial population.

Evaluate fitness value of initial population.

Sort the initial population based on fitness result.

While stopping criteria not met

Select the elite patches and non-elite best patches for neighbourhood search.

    Recruit forager bees for selected sites.

Evaluate the fitness value of each patch.

    Sort the results based on their fitness.

Allocate the rest of the bees for global search to the non-best locations.

Evaluate the fitness value of non-best patches.

Sort the overall results based on their fitness.

End While if termination criteria met.

Figure 4.1: Pseudo code of the BA

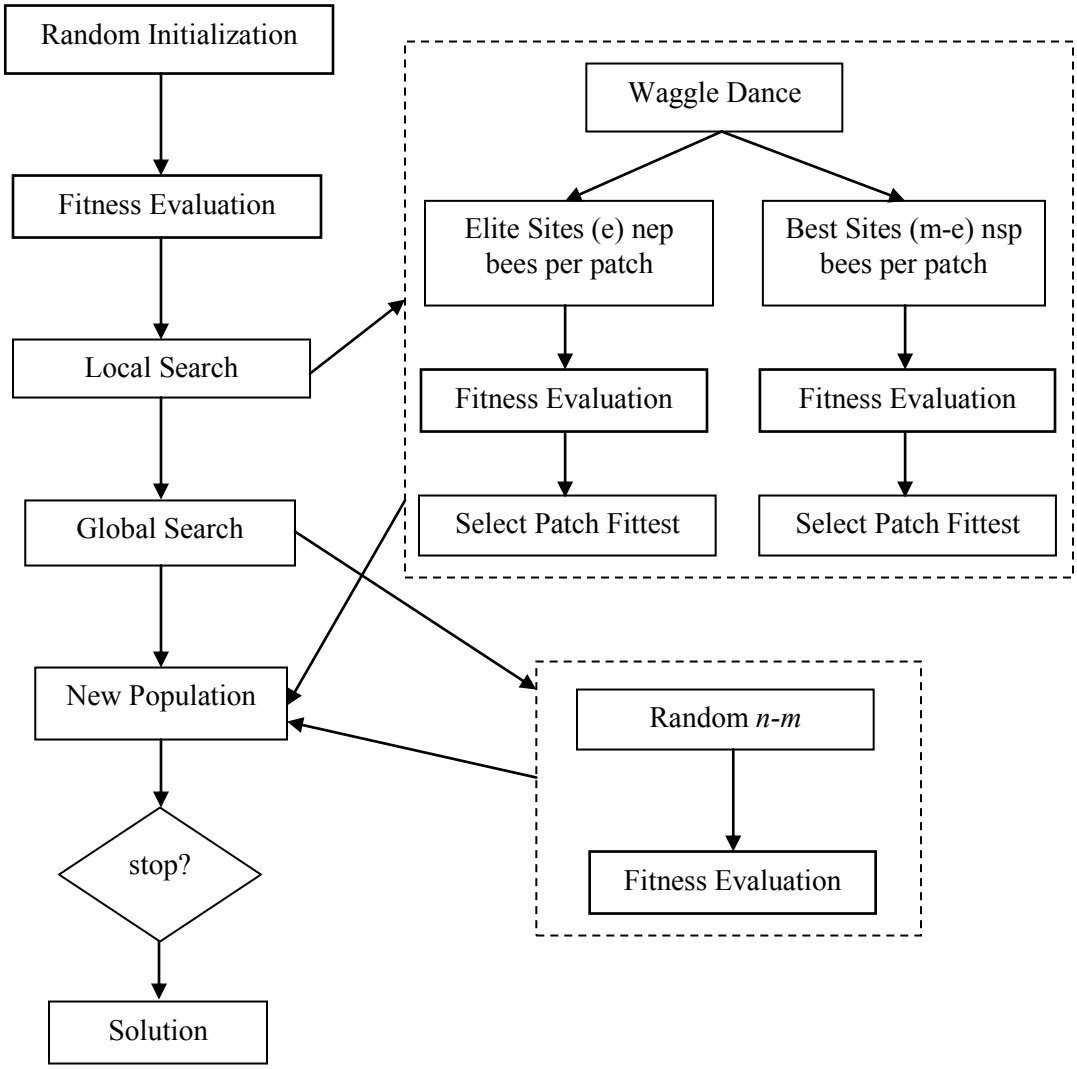

Figure 4.2: Flowchart of the BA (Fahmy et al. 2011)

Before running the BA, 20 (number of scout bees) random values of $\Delta\delta$ and $\Delta\alpha$ were selected to generate the initial population of solutions (θ_1) by simulating the Robogymnast model described in Equation (3.20) in Chapter 3 using the control signals given in Equations (4.1) and (4.2). Each of the solutions satisfy the fitness criterion θ_1=-180° within a reasonable error margin. The reason for setting the fitness criterion at θ_1=-180° is because the two control signals described in Equations (4.1) and (4.2) will tend initially to drive links 2 and 3 in the positive direction (Figure 3.6 in Chapter 3) causing link 1 to drift towards the opposite direction generating a negatively biased swing angle.

Table 4.1 shows for each selected pair of $\Delta\delta$ and $\Delta\alpha$, how long it takes to swing up Robogymnast past the upright position (θ_1~-180°). The results are ordered according to the fitness of the obtained solutions (θ_1) satisfying both the criteria for reasonable error margin (closest to 0.02°) and swing up time. The fittest solutions (m=8) are selected for smallest errors and duration time between 120 and 200 seconds. The elite (e=2) of the fittest are selected to satisfy minimum error and shortest swing up time between 120 and 160 seconds. The remaining (n−m=12) solutions are ordered accordingly. These results will be used to define the parameters for implementing the BA code (Figure 4.1). In Table 4.1, the class of each solution is determined according to the combined criteria for error margin and duration time (time to reach the upright position). The fittest solutions satisfy the criteria for smallest error and duration time between 120 and 200 seconds. The non-best solutions are the remaining solutions ordered according to their smallest error margins only.

Table 4.1: Initial population of solutions.

$\Delta\alpha$	$\Delta\delta$	Angular position θ_1 (Deg.)	Time (second) to reach the upright position	Fitness class*
0.3215	4.7493	-180.1205	145.075	Elite of fittest
0.3026	6.3464	-180.1682	158.025	Elite of fittest
0.2439	2.4221	-180.0762	181.05	fittest
0.3503	4.1570	-180.1878	128	fittest
0.2439	6.0003	-180.1951	182.125	fittest
0.3410	6.0865	-180.2341	124.1	fittest
0.2450	3.7547	-180.3446	187.075	fittest
0.3338	5.1102	-180.3703	129.3	fittest
0.6400	4.8985	-180.0022	61.9	Non-best
0.3423	4.5662	-180.0235	117.1	Non-best
0.1667	2.7247	-180.0253	252.65	Non-best
0.1297	6.5532	-180.0475	417.175	Non-best
0.2103	3.2993	-180.0731	215.5	Non-best
0.1739	3.9989	-180.0951	259.35	Non-best
0.1455	6.3434	-180.1276	355.4	Non-best
0.5681	6.2651	-180.1339	77.025	Non-best
0.3945	2.7276	-180.1730	102.925	Non-best
0.3935	2.6803	-180.2081	101.5	Non-best
0.6416	2.9092	-180.2928	62.475	Non-best
0.6668	3.3190	-180.7377	69.725	Non-best

* Elite of fittest (e)=2; fittest (m)=8; non-best (n-m)=12.

4.4 Tuning the swing-up control parameters using the BA

The BA was used to investigate the optimum values of the increments in α (Δα) and δ (Δδ) that will enable smooth swing up of the Robogymnast model (Equation (3.20) in Chapter 3) in a reasonable time. This is achieved by manipulating independently the amplitudes and the frequencies of the control signals given in Equations (4.1) and (4.2). The parameter values of the BA were set as in Table 4.2. The number of scouts (range of Δα and Δδ) was selected to be 20 (equivalent to 20 randomly selected values of Δα and Δδ) satisfying, respectively, the conditions $0.1 < \Delta\alpha < 0.7$ and $2 < \Delta\delta < 7$. The randomly selected values of Δδ and Δα vary each time the BA code is executed. Figure 4.3 demonstrating the flowchart of the swing-up control parameter optimization using the BA.

The other parameters were selected based on internally imposed conditions limiting the error boundary in the upright angle θ_1. Using the initial results of Table 4.1 and the parameters described in Table 4.2, the BA (Figure 4.1) starts to compute the fitness (i.e. the swing-up angle of Robogymnast θ_1 reaching approximately ±180°) by simulating the discrete-time model of Robogymnast (Equation (3.20) in Chapter 3) using the control signals described in Equations (4.1) and (4.2) for each of the incremented α and δ applied simultaneously. This further tuned Δα and Δδ to achieve an optimum fitness (θ_1= -180°) with small margins of error (<0.02) at which the Algorithm will stop searching. The fine-tuned results are shown in Table 4.3. Unlike the case in Table 4.1,

each of the solution classes presented in Table 4.3 were ordered according to the smallest error margin irrespective of the duration time.

Table 4.2: The parameter values of the BA.

The parameters of the BA	Values	Description
Number of scout bees(n)	20	Number of randomly chosen values of Δα and Δδ from the solution space (ranges of Δα and Δδ).
Number of recruited bees around elite selected patches (nep)	15	Number of bees (foragers) recruited to search new values of Δα and Δδ which are placed within squares of sides ngh centred on the elites of Δα and Δδ.
Number of recruited bees around best selected patches (nsp)	10	Number of bees (foragers) recruited to search new values of Δα and Δδ which are placed within a square of side ngh centered on the (m-e) locations of Δα and Δδ.
Patch radius for neighbourhood search (ngh)	0.001	The boundary of neighbourhood search for new values of Δα and Δδ by recruited bees.

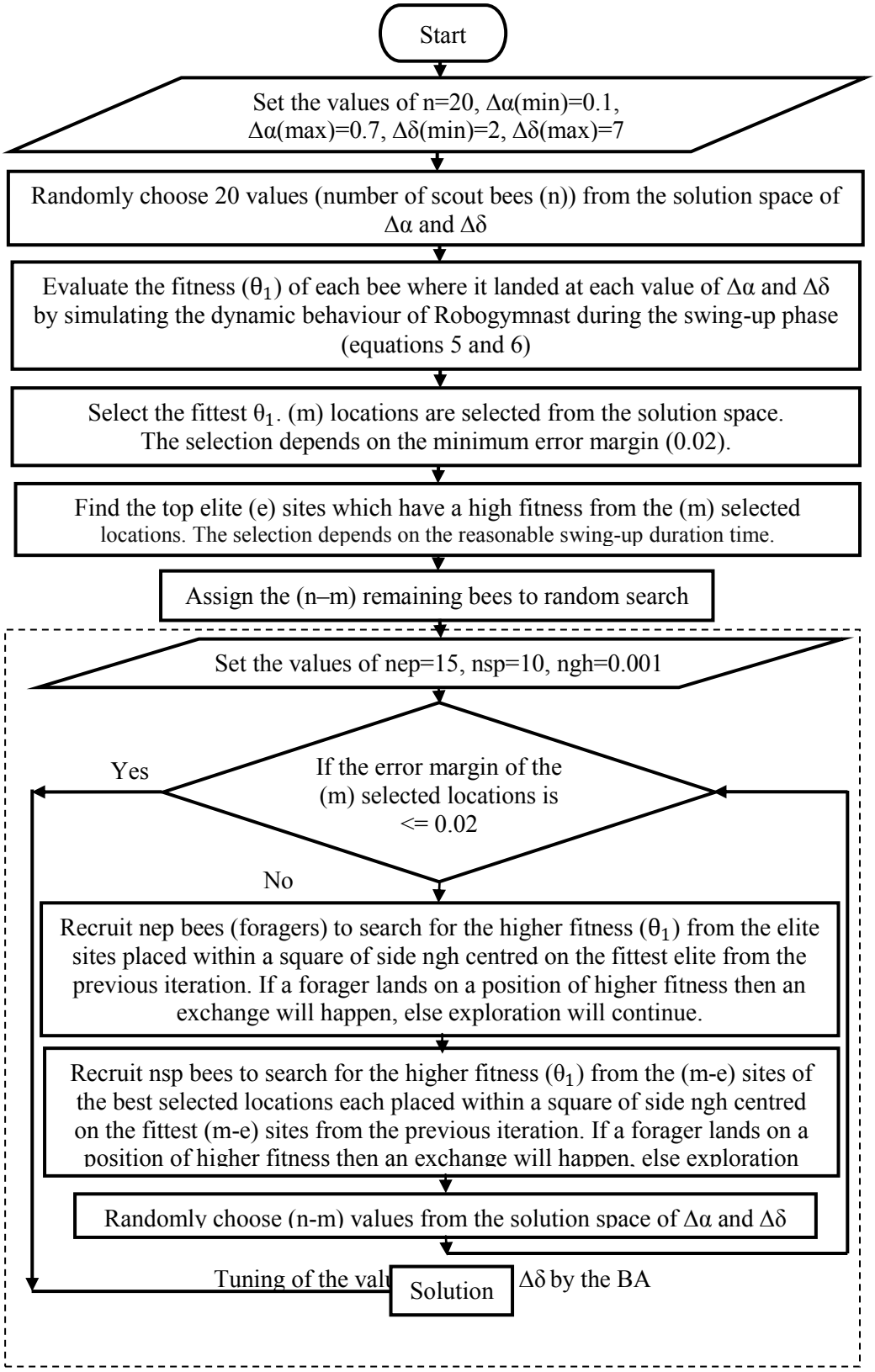

Figure 4.3: Flowchart of the swing-up control parameter optimization using the BA

4.5 Simulation and experimental results

The parameters in Table 4.2 were used to further tune Δα and Δδ by the BA to achieve an optimum fitness (θ_1= -180°) with small margins of error (<0.02) at which the Algorithm will stop searching. The fine-tuned results are shown in Table 4.3. To simulate the behaviour of Robogymnast during the swing-up phase, three values of Δα and Δδ were selected from Table 4.3. At each sampling interval, the control input signals u_1 and u_2 described in Equations (4.1) and (4.2) were recalculated and applied to the discrete-time model of Robogymnast (Equation (3.20) in Chapter 3). The first question in this study sought to determine the behavior of the relative angular position ($q_1 = \theta_1$) of the first link, where the most important point in the swing up control that reach the first link to the upright position (θ_1 reaching approximately ±180°) and then flipping regardless of the situation of the second and third link.

The system was simulated with Δα equal to 0.6400 and Δδ equal to 4.8985 as shown in Figure 4.4. The time taken to reach the upright position is short (61.9 seconds) which, from experience, may cause damage to the motor/gearbox structures. According to the above selected values of Δα and Δδ, the simulation results of the second relative angular position q_2, third relative angular position q_3, first control signal u_1 and second control signal u_2 are presented in Figure 4.5 to Figure 4.8.

Table 4.3: Results after tuning by the BA.

Δα	Δδ	Angular position θ_1 (Deg.)	Time (second) to reach the upright position	Error margin
0.3212	4.7487	-180.0100	145.075	0.0101
0.3032	6.3466	-180.0048	158.125	0.0048
0.2457	2.4230	-180.0115	181	0.0115
0.3499	4.1568	-180.0158	128	0.0158
0.2449	5.9988	-180.0035	182.05	0.0036
0.3419	6.0862	-180.0077	124.05	0.0078
0.2451	3.7569	-180.0012	187.15	0.0012
0.3103	4.9255	-180.0009	129.15	0.0010
0.6400	4.8985	-180.0022	61.9	0.0022
0.3423	4.5662	-180.0235	117.1	0.0235
0.1667	2.7247	-180.0253	252.65	0.0253
0.1297	6.5532	-180.0475	417.175	0.0475
0.2103	3.2993	-180.0731	215.5	0.0731
0.1739	3.9989	-180.0951	259.35	0.0951
0.1455	6.3434	-180.1276	355.4	0.1276
0.5681	6.2651	-180.1339	77.025	0.1339
0.3945	2.7276	-180.1730	102.925	0.1730
0.3935	2.6803	-180.2081	101.5	0.2081
0.6416	2.9092	-180.2928	62.475	0.2928
0.6668	3.3190	-180.7377	69.725	0.7377

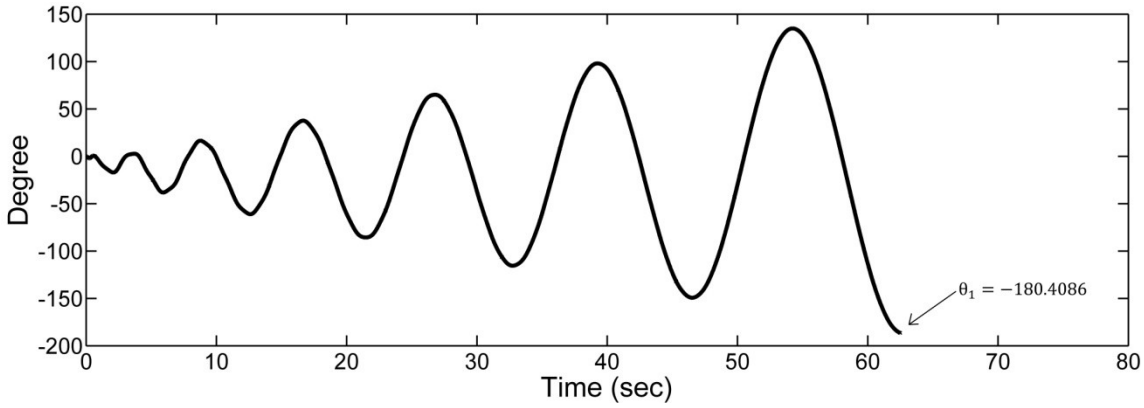

Figure 4.4: Simulated relative angular position q_1 for Δα=0.6400 and Δδ= 4.8985

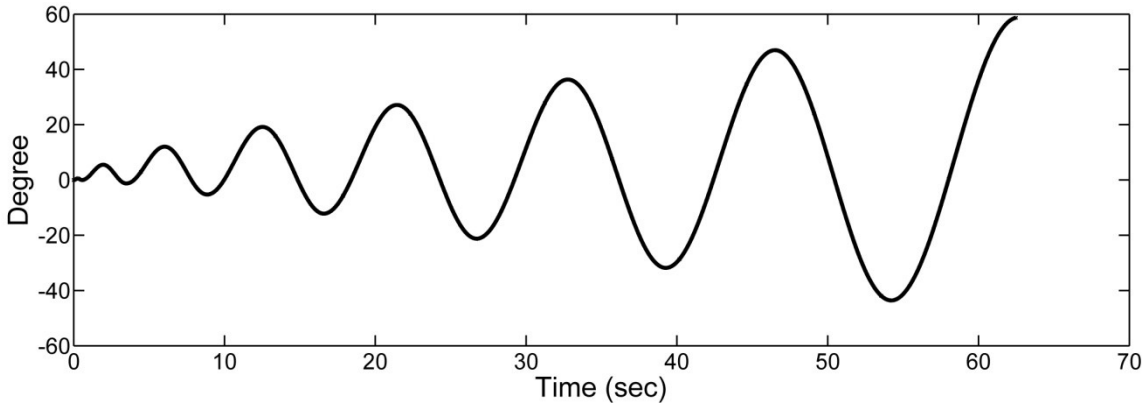

Figure 4.5: Simulated relative angular position q_2 for Δα=0.6400 and Δδ= 4.8985

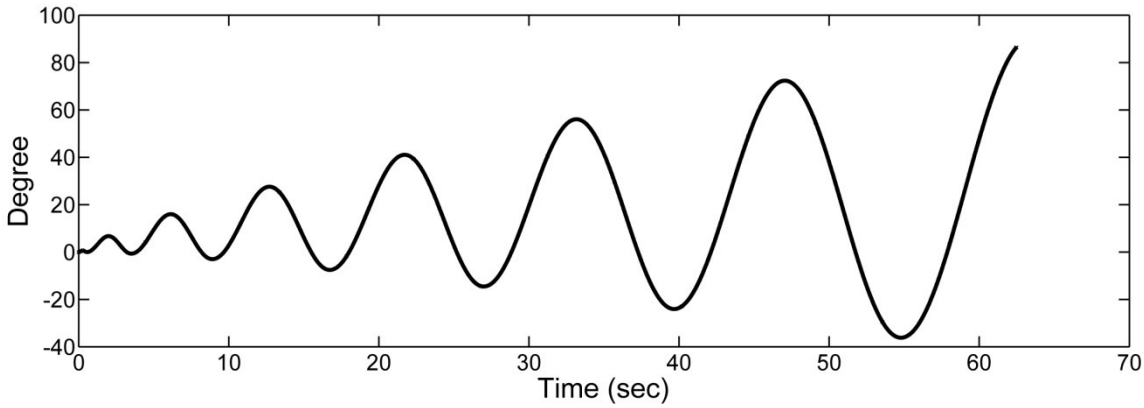

Figure 4.6: Simulated relative angular position q_3 for Δα=0.6400 and Δδ= 4.8985

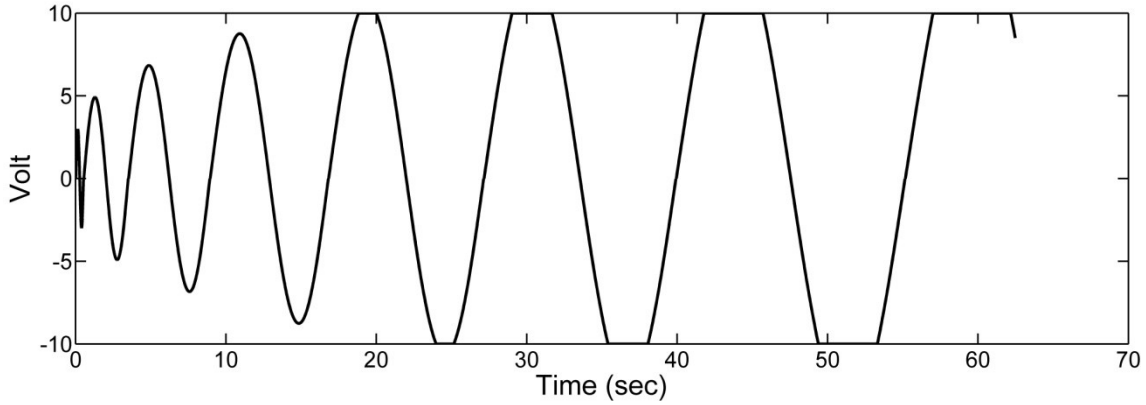

Figure 4.7: Simulated control action applied to first motor u_1 for $\Delta\alpha$=0.6400 and $\Delta\delta$= 4.8985

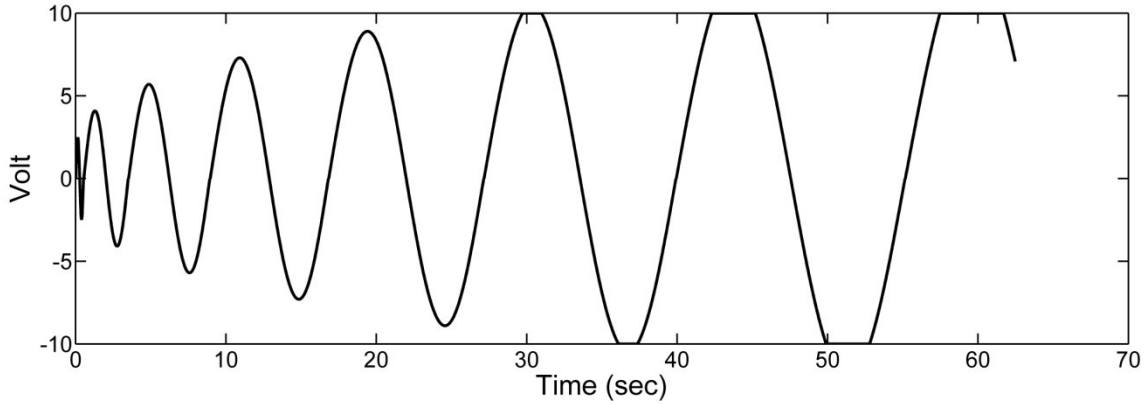

Figure 4.8: Simulated control action applied to second motor u_2 for $\Delta\alpha$=0.6400 and $\Delta\delta$= 4.8985

At $\Delta\alpha$ equal to 0.1297 and $\Delta\delta$ equal to 6.5532, the system's operation was very smooth. However, it reached the upright position in a very long time (417.175 seconds) as shown in Figure 4.9. Additionally the behavior of the second link, third link and the control signals applied to the first and second motor are shown in Figure 4.10 to Figure 4.13.

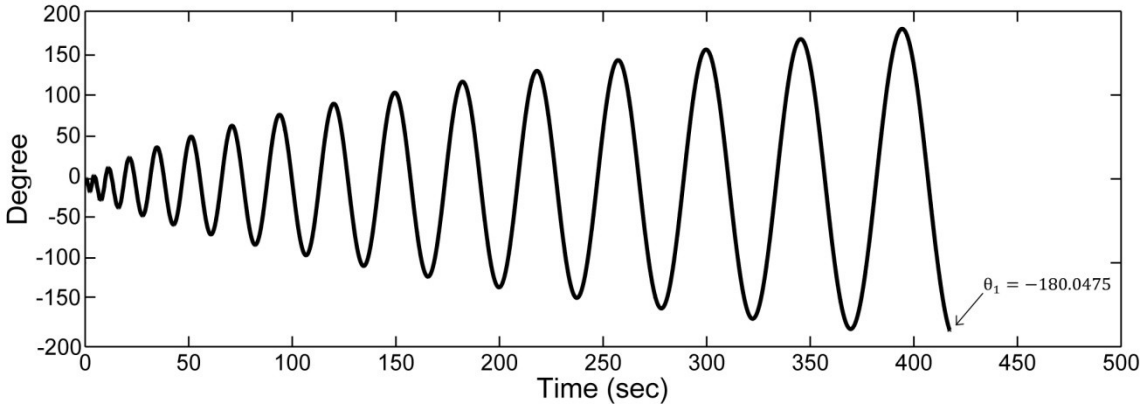

Figure 4.9: Simulated relative angular position q_1 for Δα=0.1297 and Δδ= 6.5532

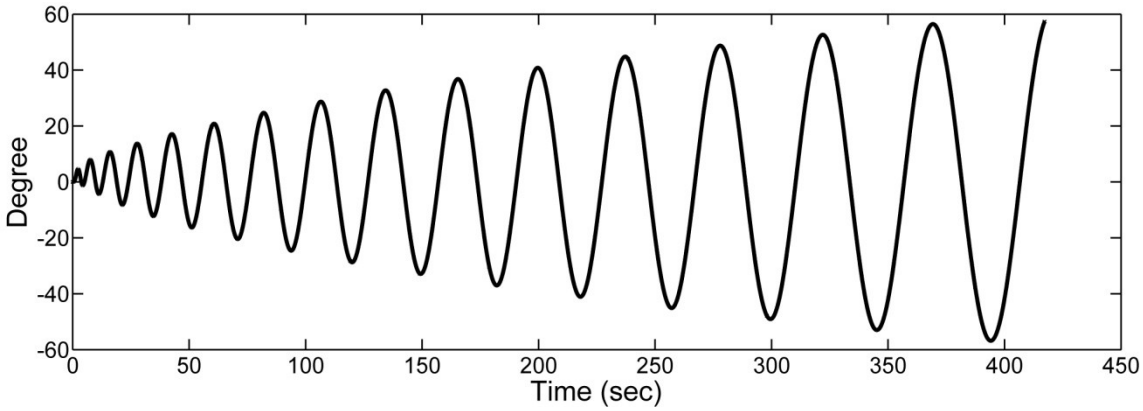

Figure 4.10: Simulated relative angular position q_2 for Δα=0.1297 and Δδ= 6.5532

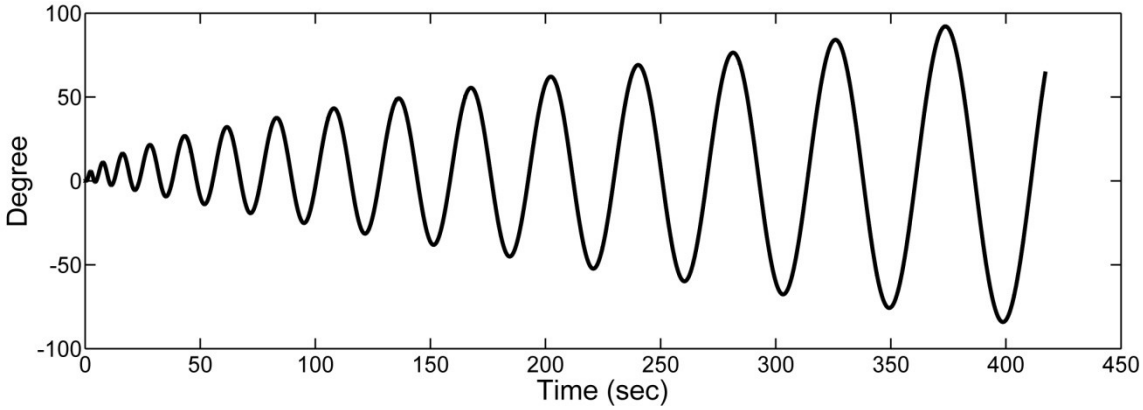

Figure 4.11: Simulated relative angular position q_3 for Δα=0.1297 and Δδ= 6.5532

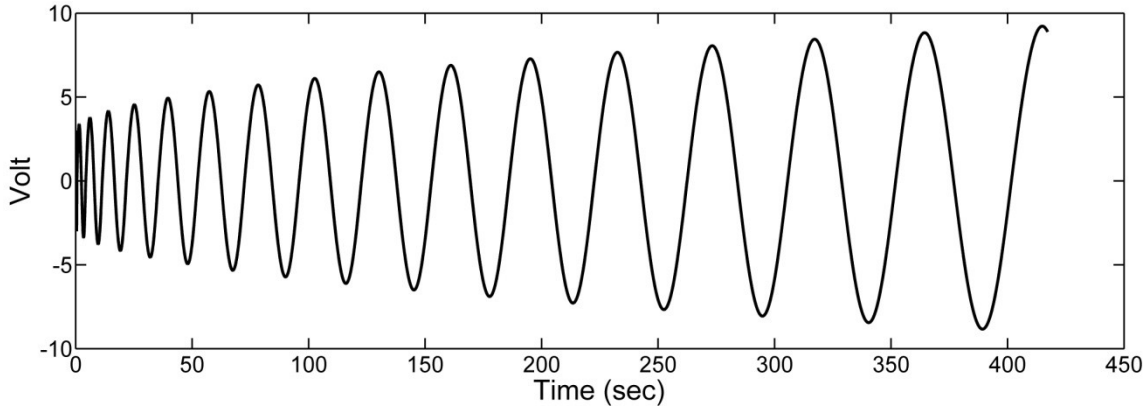

Figure 4.12: Simulated control action applied to first motor u_1 for $\Delta\alpha$=0.1297 and $\Delta\delta$= 6.5532

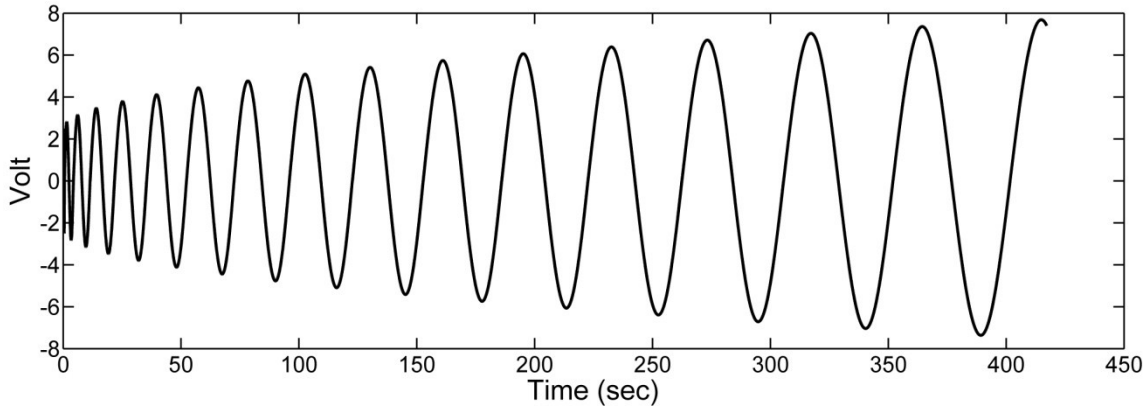

Figure 4.13: Simulated control action applied to second motor u_2 for $\Delta\alpha$=0.1297 and $\Delta\delta$= 6.5532

when $\Delta\alpha$ and $\Delta\delta$ equal to 0.3499 and 4.1568 respectively gave a satisfactory response in a reasonable duration (128 seconds) as illustrated in Figure 4.14 as comparing to the authors' previous work (Eldukhri and Pham 2010). As a part of this, it can be seen from the data in Figure 4.15 to Figure 4.18 the behavior of the second and third relative angular position as well as the applied control signals to first and second motor, which is determined by selecting best values of $\Delta\alpha$ and $\Delta\delta$ to give a reasonable response.

To implement the best-selected values on the real system and finding the experimental results, the controller is implemented using C++ program environment. The overall program includes code to capture experimental data and store them in the hard disk.

Figure 4.19 shows the experimentally measured relative angular position ($q_1 = \theta_1$) for the same value of $\Delta\alpha$ (0.3498) whereas $\Delta\delta$ was initiated at 0.041569 (1/100th of its original value) to avoid damaging the robot's motor/gearbox structures because of the inherent backlash in the gearboxes. Comparing the experimental results Figure 4.19 to those reported by (Eldukhri and Pham 2010), it is evident that in this work the swing up time is about 40 second faster. The results showing the respective relative positions of the second and third link were presented in Figure 4.20 and Figure 4.21 respectively. Furthermore, the measured control action applied to the first and second motor were shown in Figure 4.22 and Figure 4.23. Figure 4.24 demonstrating the flowchart of swing up control implementation.

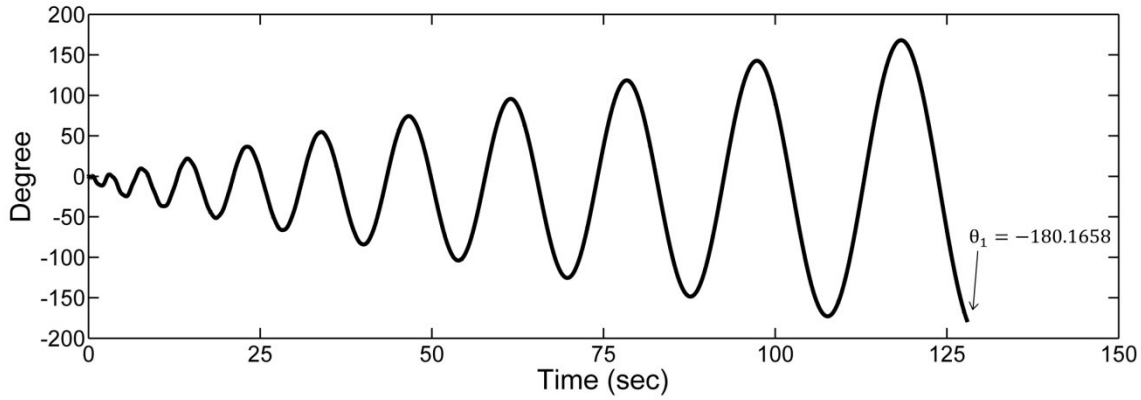

Figure 4.14: Simulated relative angular position q_1 for Δα=0.3499 and Δδ=4.1568

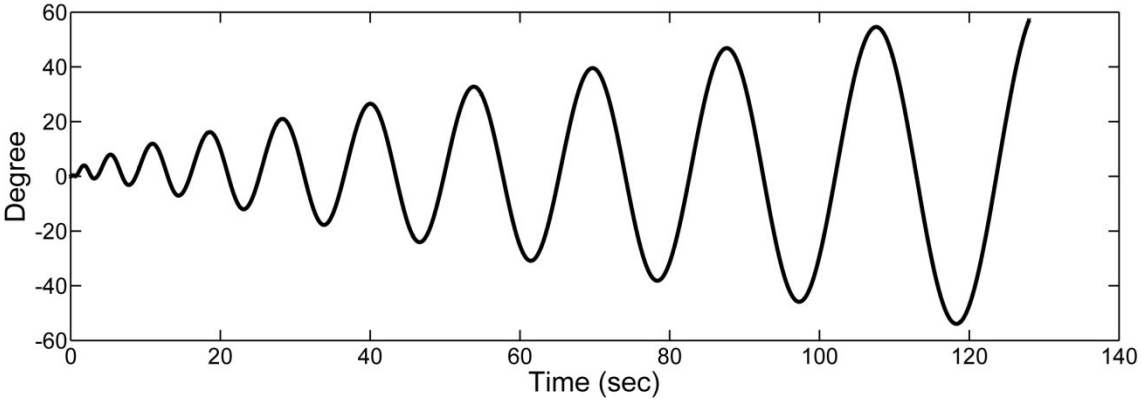

Figure 4.15: Simulated relative angular position q_2 for Δα=0.3499 and Δδ=4.1568

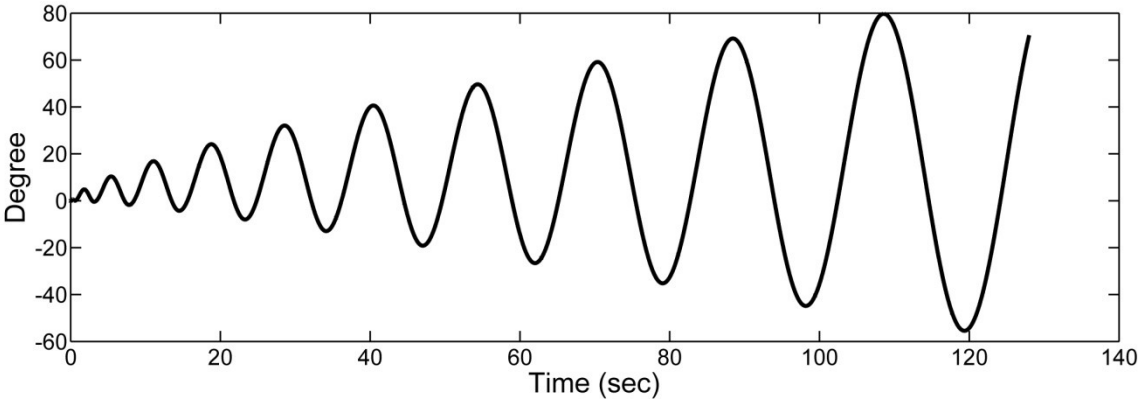

Figure 4.16: Simulated relative angular position q_3 for Δα=0.3499 and Δδ=4.1568

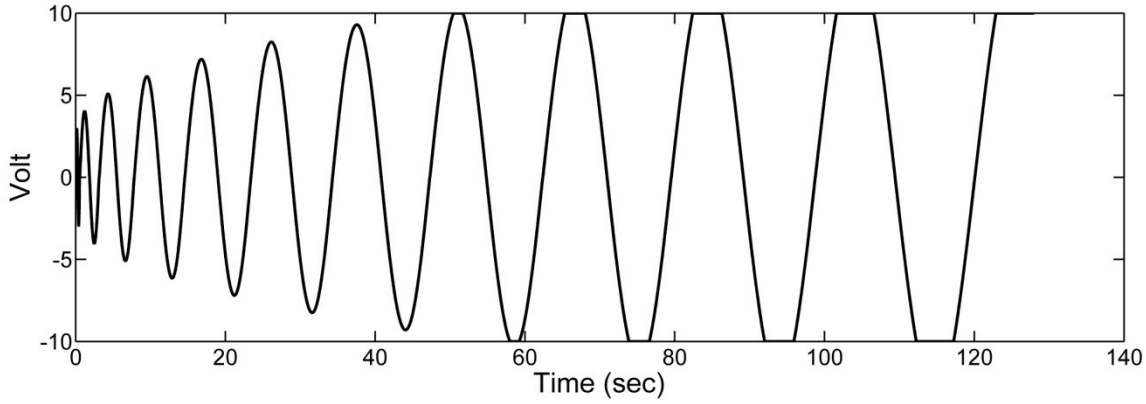

Figure 4.17: Simulated control action applied to first motor u_1 for $\Delta\alpha$=0.3499 and $\Delta\delta$=4.1568

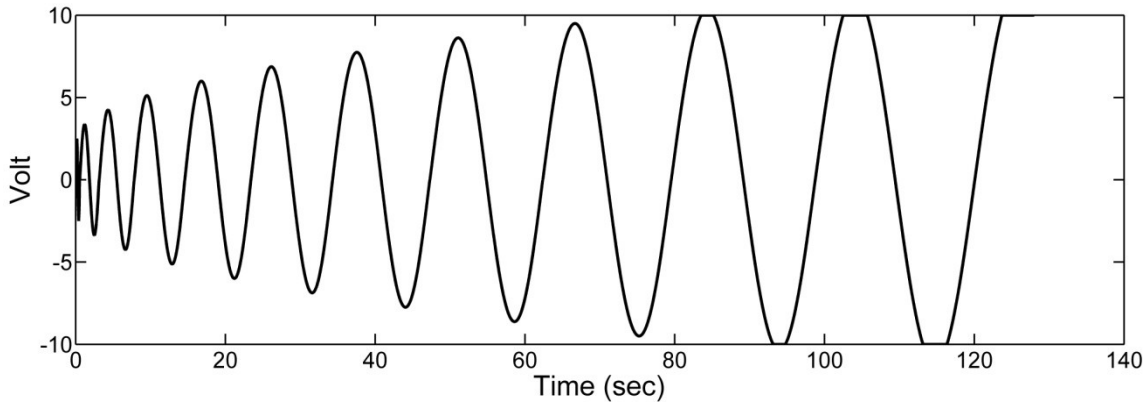

Figure 4.18: Simulated control action applied to second motor u_2 for $\Delta\alpha$=0.3499 and $\Delta\delta$=4.1568

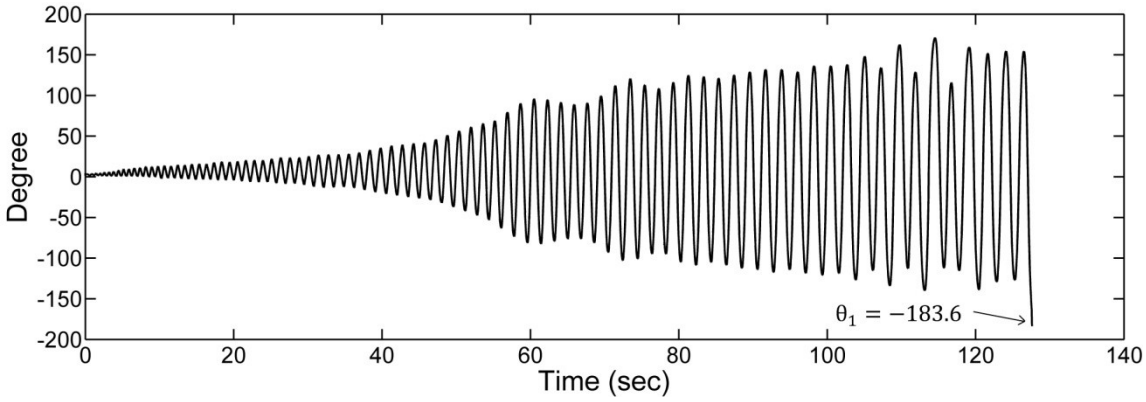

Figure 4.19: Measured relative angular position q_1 for Δα=0.3499 and Δδ=0.041568

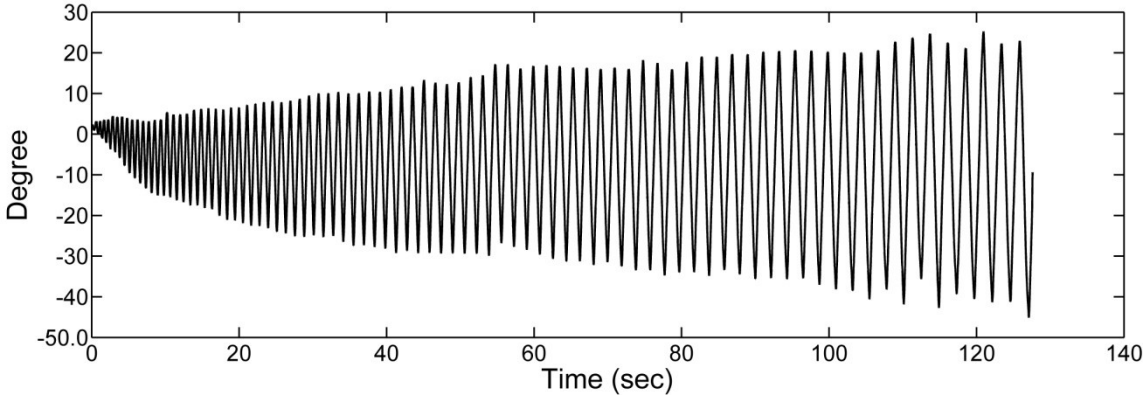

Figure 4.20: Measured relative angular position q_2 for Δα=0.3499 and Δδ=0.041568

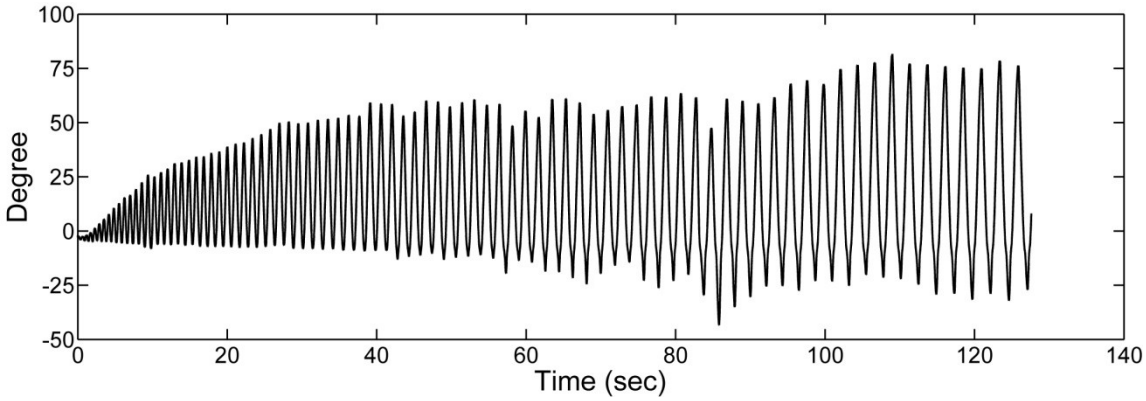

Figure 4.21: Measured relative angular position q_3 for Δα=0.3499 and Δδ=0.041568

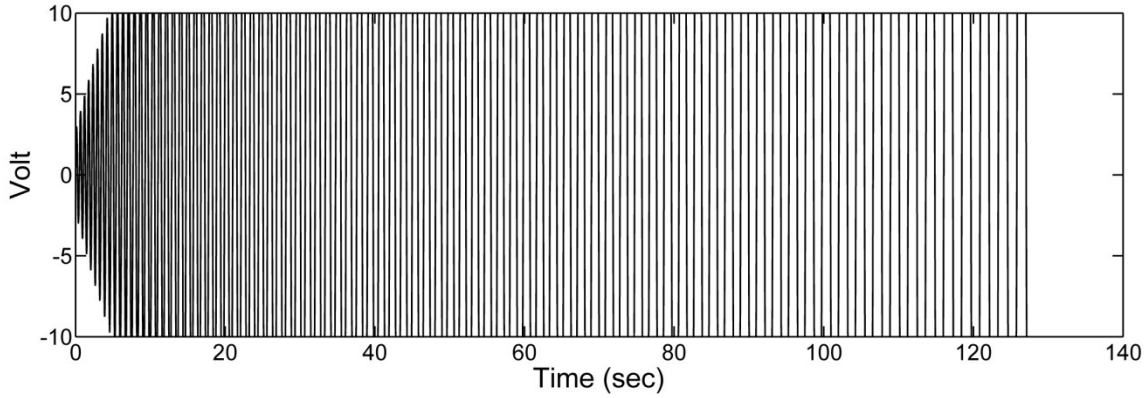

Figure 4.22: Measured control action applied to first motor u_1 for $\Delta\alpha$=0.3499 and $\Delta\delta$=0.041568

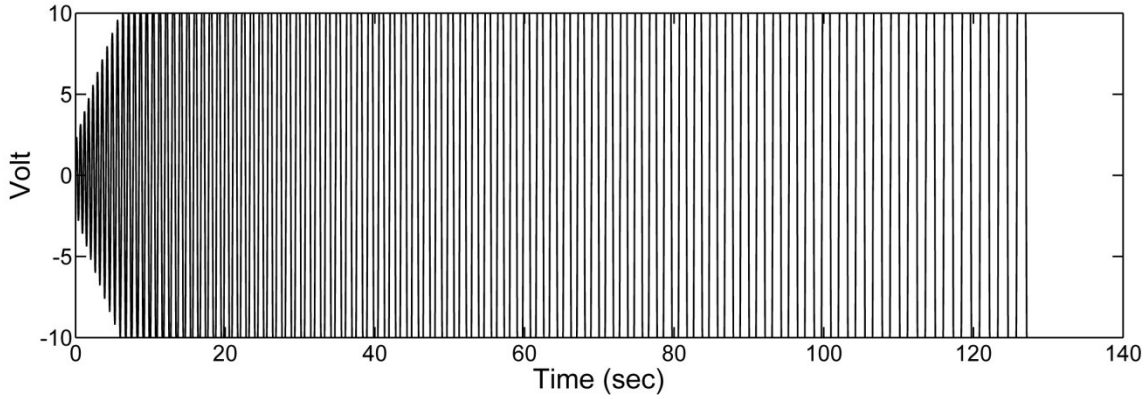

Figure 4.23: Measured control action applied to second motor u_2 for $\Delta\alpha$=0.3499 and $\Delta\delta$=0.041568

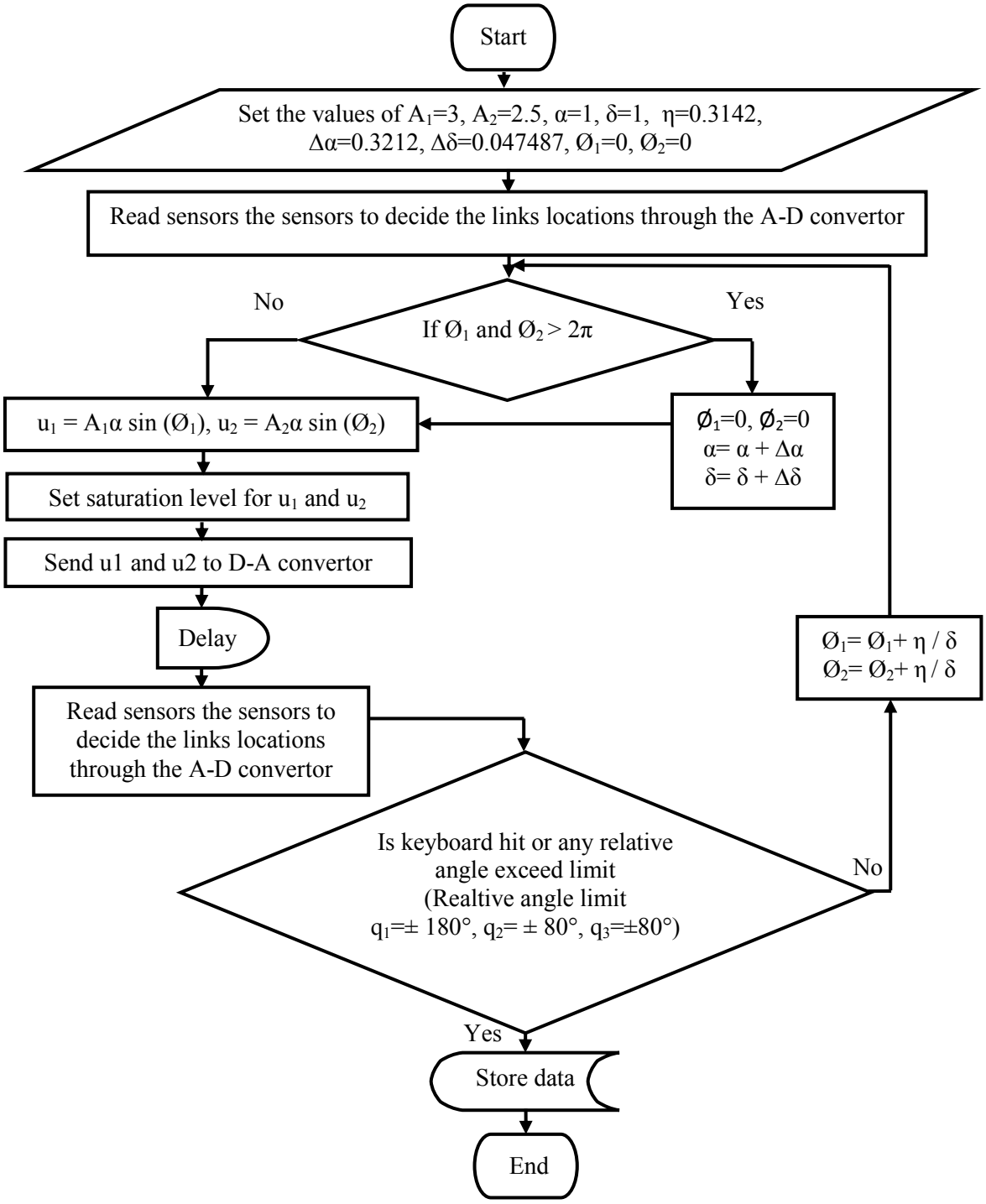

Figure 4.24: Flowchart of swing-up control implementation

4.6 Summary

This chapter focused on using the swarm-based BA to tune the parameters of a swing-up control of the Robogymnast developed by Eldukhri and Pham (Eldukhri and Pham 2010). Unlike the previous approach, the BA allowed a flexible and random selection of the parameter affecting the amplitudes and frequencies of the sinusoidal signals applied to the two DC motors driving Robogymnast. The selection of the best parameters was decided regarding to the attaining of the Robogymnast to the upright position with minimum error margin in an appropriate time. From the group of optimized parameters, the system was simulated and analyzed using MATLAB® software with three selected sets from this group. The best values of those three sets were selected to satisfy a desired system performance. In the next stage, the best values of those three sets were used to operate the real system and a satisfactory experimental result was obtained. In the following chapter, the controller design and downward balancing will be discussed.

Chapter 5

Controller Design and Downward Balancing

5.1 Introduction

The general problem of multi-link mechanical systems is one of the most widely used for control education and research. Recently, researchers have shown an increased interest in investigating different configurations of multi-link mechanical systems. A considerable amount of literature has been published on this type of system (Larcombe 1992; Eltohamy and Kuo 1997; Sehgal and Tiwari 2012).

This chapter considers the design of a robust computer control system for the Robogymnast. The aims of this chapter are to design different control strategies to control the Robogymnast locomotion and then to validate the designed controllers experimentally by accomplishing downward balancing.

The chapter is organised as follows. Section 5.2 describes the design of the system controller. The observer design is presented in Section 5.3, and Section 5.4 presents the experimental setup. The downward balancing control problem is demonstrated in Section 5.5. The experimental results of downward balancing using the LQR controller are reported in Section 5.6. Section 5.7 presents the experimental results of downward

balancing using the LQR with LC. A discussion of the results is given in Section 5.8, and a summary of this chapter is given in Section 5.9.

5.2 Controller design

This section presents descriptions and analyses of the proposed balancing and stablising controllers. To control the system and to establish the desired mechanical movement with high performance, various methods are used to solve the control problems. Each has its advantages and disadvantages, which will be explained and analysed in Section 5.8. Superior system performance can be characterised as a system with high situating precision, low tracking error, high force controlling ability and a quick appropriate response to unknown disturbances.

In order to achieve attitude control in the Robogymnast, reference signals representing the relative angular positions of the first, second and third link are generated and monitored. These are maintained through determining robust stablising control actions u(k), by means of the relative states to reach the desired reference. The control actions u(k) are computed using state feedback control. To establish feedback gain, two different control techniques are used. The first technique is the optimal control algorithm which uses the LQR. The second technique is a combination of LC and LQR. Each controller will be implemented via a reduced order state observer.

In addition to understanding the characteristics of the system, it is important to check the controllability of the system's state variables. The controllability matrix of the system is given by:

$$[\,B\ \ AB\ \ A^2B\ \ A^3B\ \ A^4B\ \ A^5B\,]$$

The rank of this controllability matrix is equal to 6. This is equal to the number of state variables belonging to the system, which means that the system is controllable.

5.2.1 Design of optimal controller using the LQR technique

The theory of optimal control is concerned with operating a dynamic system at minimum cost. Many current robot applications need to find optimal trajectories with an energy efficient movement. However, it is more important to guarantee that the system remains stable with the candidate trajectories. The LQR method is one of the more practical methods of stablising trajectories of underactuated frameworks (Zaidan et al. 2012; Sharif and Ucar 2013; Bradshaw and Shao 1996).

The LQR controller law is used to stabilise and balance a linearised model around its unstable/stable equilibrium point by finding the optimal gain matrix F. For the modelling system given in Equation (3.20) in Chapter 3, the performance function is defined as (Ramani and Atherton 1974):

$$J = \sum_{k=0}^{\infty} (x_k^T Q\, x_k + u_k^T R\, u_k)\,, \tag{5.1}$$

where Q is a real symmetric positive semi-definite matrix, and R is and a real symmetric positive definite matrix.

The feedback control law is defined as:

$$u(k) = -Fx(k) \tag{5.2}$$

A block diagram of the regulating control system is shown in Figure 5.1.

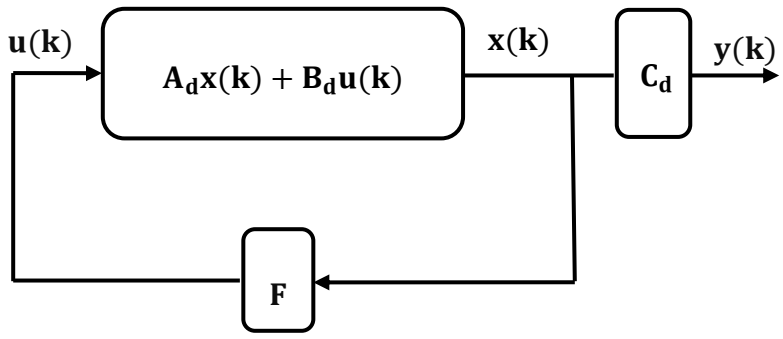

Figure 5.1: Block diagram of regulating control system

The robustness of the LQR controller depends on the selection of the weight matrices Q and R. Indeed, with just the basic character weighting matrices the framework is sufficiently rigorous to recover from huge unsettling influences in the initial conditions

while operating within actuator limits. Nevertheless, the selection of the weight matrices is very difficult and optimum results are obtained according to the designer's intuition and experience. In order to achieve the system performance requirement, an extensive computer simulation and analysis is required to find the appropriate weighing matrices that determine the feedback gain matrix.

A discrete time integrator is used to achieve the system performance requirement through improving the steady-state performance with the introduction of an additional gain parameter in the state feedback law. An integrator could then be used to obtain an integral of the error signal (e).

$$e(k) = y_r(k) - y_i(k). \tag{5.3}$$

Here

$$y_r(k) = \begin{bmatrix} y_{r_2} \\ y_{r_3} \end{bmatrix} = \begin{bmatrix} 0 \\ 0 \end{bmatrix}, \tag{5.4}$$

$$y_i(k) = \begin{bmatrix} y_{i_2} \\ y_{i_3} \end{bmatrix} = C_i\, y(k), \tag{5.5}$$

where

$$C_i = \begin{bmatrix} 0 & 1 & 0 & 0 \\ 0 & 0 & 1 & 0 \end{bmatrix}.$$

$e(k)$ is the difference between the desired reference $y_r(k)$ and the actual relative angular position $y_i(k)$ of the second and third links. The desired reference signals y_r for the second and third links are equal to zero for balancing.

The difference equation of the discrete time integrator can be written as:

$$w(k+1) = w(k) + T_s e(k), \tag{5.6}$$

where w refers to the states of the integrator. Figure 5.2 presents a block diagram of the closed loop control system with controller design using the LQR. The augmented plant model can be written as follows:

$$\begin{bmatrix} x(k+1) \\ w(k+1) \end{bmatrix} = A_{bar} \begin{bmatrix} x(k) \\ w(k) \end{bmatrix} + B_{bar}\, u(k) + \begin{bmatrix} 0_{6x1} \\ T_s y_r \end{bmatrix} \tag{5.7}$$

$$y(k) = C_{bar} \begin{bmatrix} x(k) \\ w(k) \end{bmatrix} \tag{5.8}$$

The terms A_{bar}, B_{bar} and C_{bar} have come to be used to refer to the augmented state matrix, the augmented input matrix and the augmented output matrix respectively. They can be written as:

$$A_{bar} = \begin{bmatrix} A_d & 0_{6x2} \\ -T_s C_y & I_{2x2} \end{bmatrix}, B_{bar} = \begin{bmatrix} B_d \\ 0_{2x2} \end{bmatrix}, C_{bar} = [C_d \quad 0_{4x2}],$$

where

$$0_{6x1} = \begin{bmatrix} 0 \\ 0 \\ 0 \\ 0 \\ 0 \\ 0 \end{bmatrix}, 0_{6x2} = \begin{bmatrix} 0 & 0 \\ 0 & 0 \\ 0 & 0 \\ 0 & 0 \\ 0 & 0 \\ 0 & 0 \end{bmatrix}, \ I_{2x2} = \begin{bmatrix} 1 & 0 \\ 0 & 1 \end{bmatrix}, 0_{2x2} = \begin{bmatrix} 0 & 0 \\ 0 & 0 \end{bmatrix}, 0_{4x2} = \begin{bmatrix} 0 & 0 \\ 0 & 0 \\ 0 & 0 \\ 0 & 0 \end{bmatrix}$$

The optimal state feedback for both motors was calculated using the LQR. The feedback, in terms of states and integrators, is reported as below:

$$u(k) = -F \begin{bmatrix} x(k) \\ w(k) \end{bmatrix} \tag{5.9}$$

where F is the optimal gain feedback corresponding to the state matrix A_{bar} and the input matrix B_{bar}. Q and R are selected as diagonal matrices:

$$Q = \begin{bmatrix} Q_1 & 0 & 0 & 0 & 0 & 0 & 0 & 0 \\ 0 & Q_2 & 0 & 0 & 0 & 0 & 0 & 0 \\ 0 & 0 & Q_3 & 0 & 0 & 0 & 0 & 0 \\ 0 & 0 & 0 & Q_4 & 0 & 0 & 0 & 0 \\ 0 & 0 & 0 & 0 & Q_5 & 0 & 0 & 0 \\ 0 & 0 & 0 & 0 & 0 & Q_6 & 0 & 0 \\ 0 & 0 & 0 & 0 & 0 & 0 & Q_7 & 0 \\ 0 & 0 & 0 & 0 & 0 & 0 & 0 & Q_8 \end{bmatrix}$$

$$R = \begin{bmatrix} R_1 & 0 \\ 0 & R_2 \end{bmatrix}$$

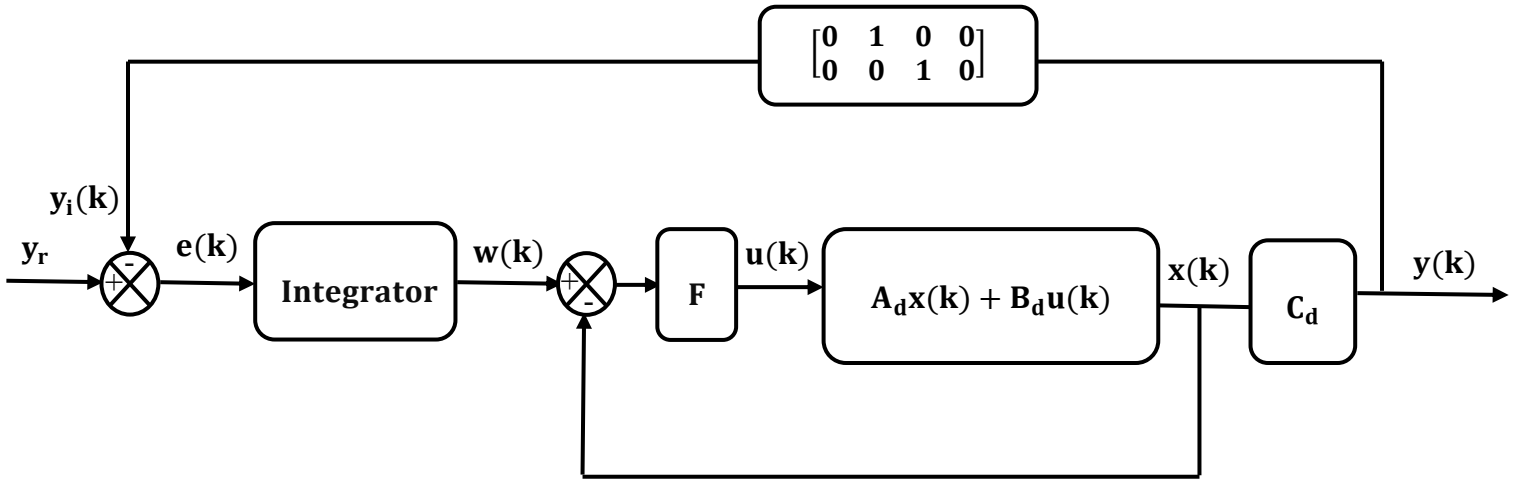

Figure 5.2: Block diagram of closed loop control system with designed controller using the LQR

5.2.2 Controller design using a combination of the LQR and LC

High positioning accuracy and low tracking error, in both position and velocity, are important performance indicators in robotics and precision motion control. The LC design can be achieved by a combination of proportional and integral position feedback, which is applied to the second motor. The combination of proportional and integral terms is important as it increases the speed of the response and reduces the steady state error. One advantage of this method is that it reduces the control action saturation of the second motor. Additionally, the LQR is used to find the optimal state feedback for the first motor.

In this case the second control signal is defined as:

$$u_2(k) = K_p e_2(k) + w_2(k) \tag{5.10}$$

$$e_2(k) = y_{r_3}(k) - y_{i_3}(k) \tag{5.11}$$

$$w_2(k+1) = w_2(k) + K_I T_s e_2(k) \tag{5.12}$$

where $e_2(k)$ is the difference between the desired reference y_{r_3} and the actual relative angular position y_{i_3} of the third link; $w_2(k)$ is the integral value of the third relative

angular position (q_3); and K_p and K_I are the proportional and integral gain respectively. In order to align link 2 with link 3, the values of K_p and K_I have been tuned extensively.

Now, the augmented plant model can be written as follows:

$$\begin{bmatrix} x(k+1) \\ w_1(k+1) \end{bmatrix} = A_{bar} \begin{bmatrix} x(k) \\ w_1(k) \end{bmatrix} + B_{bar}\ u_1(k) + \begin{bmatrix} B_{d_2} K_p \\ 0 \end{bmatrix} y_{r_3}(k) + \begin{bmatrix} B_{d_2} \\ 0 \end{bmatrix} w_2(k) + \begin{bmatrix} 0_{6x1} \\ T_s y_{r_2} \end{bmatrix} \tag{5.13}$$

$$y(k) = C_{bar} \begin{bmatrix} x(k) \\ w_1(k) \end{bmatrix} \tag{5.14}$$

The terms A_{bar}, B_{bar} and C_{bar} can now be written as:

$$A_{bar} = \begin{bmatrix} \overline{A_d} & 0_{6x1} \\ -T_s C_2 & 1 \end{bmatrix}, B_{bar} = \begin{bmatrix} B_{d_1} \\ 0 \end{bmatrix}, C_{bar} = [C_d \quad 0_{4x1}]$$

$$\overline{A_d} = A_d - B_{d_2} K_p\ C_3$$

$$C_2 = [0\ 1\ 0\ 0\ 0\ 0],\ 0_{6x1} = \begin{bmatrix} 0 \\ 0 \\ 0 \\ 0 \\ 0 \\ 0 \end{bmatrix}, 0_{4x1} = \begin{bmatrix} 0 \\ 0 \\ 0 \\ 0 \end{bmatrix}, C_3 = [0\ 0\ 1\ 0\ 0\ 0]$$

B_{d_1} and B_{d_2} represent the first and second column of B_d respectively. $w_1(k)$ is the integral value of the second relative angular position (q_2).

The state feedback controller for the first motor was obtained by using the LQR method. The feedback in this case, according to Equation 5.9, is hence:

$$u_1(k) = -F\begin{bmatrix} x(k) \\ w_1(k) \end{bmatrix} \tag{5.15}$$

where, F is the optimal gain feedback corresponding to the state matrix A_{bar} and the input matrix B_{bar}. Q and R are selected as the diagonal matrices:

$$Q = \begin{bmatrix} Q_1 & 0 & 0 & 0 & 0 & 0 & 0 \\ 0 & Q_2 & 0 & 0 & 0 & 0 & 0 \\ 0 & 0 & Q_3 & 0 & 0 & 0 & 0 \\ 0 & 0 & 0 & Q_4 & 0 & 0 & 0 \\ 0 & 0 & 0 & 0 & Q_5 & 0 & 0 \\ 0 & 0 & 0 & 0 & 0 & Q_6 & 0 \\ 0 & 0 & 0 & 0 & 0 & 0 & Q_7 \end{bmatrix}$$

$$R = [r]$$

The block diagram of a closed loop control system with controller designed using a combination of LQR and LC is shown in Figure 5.3.

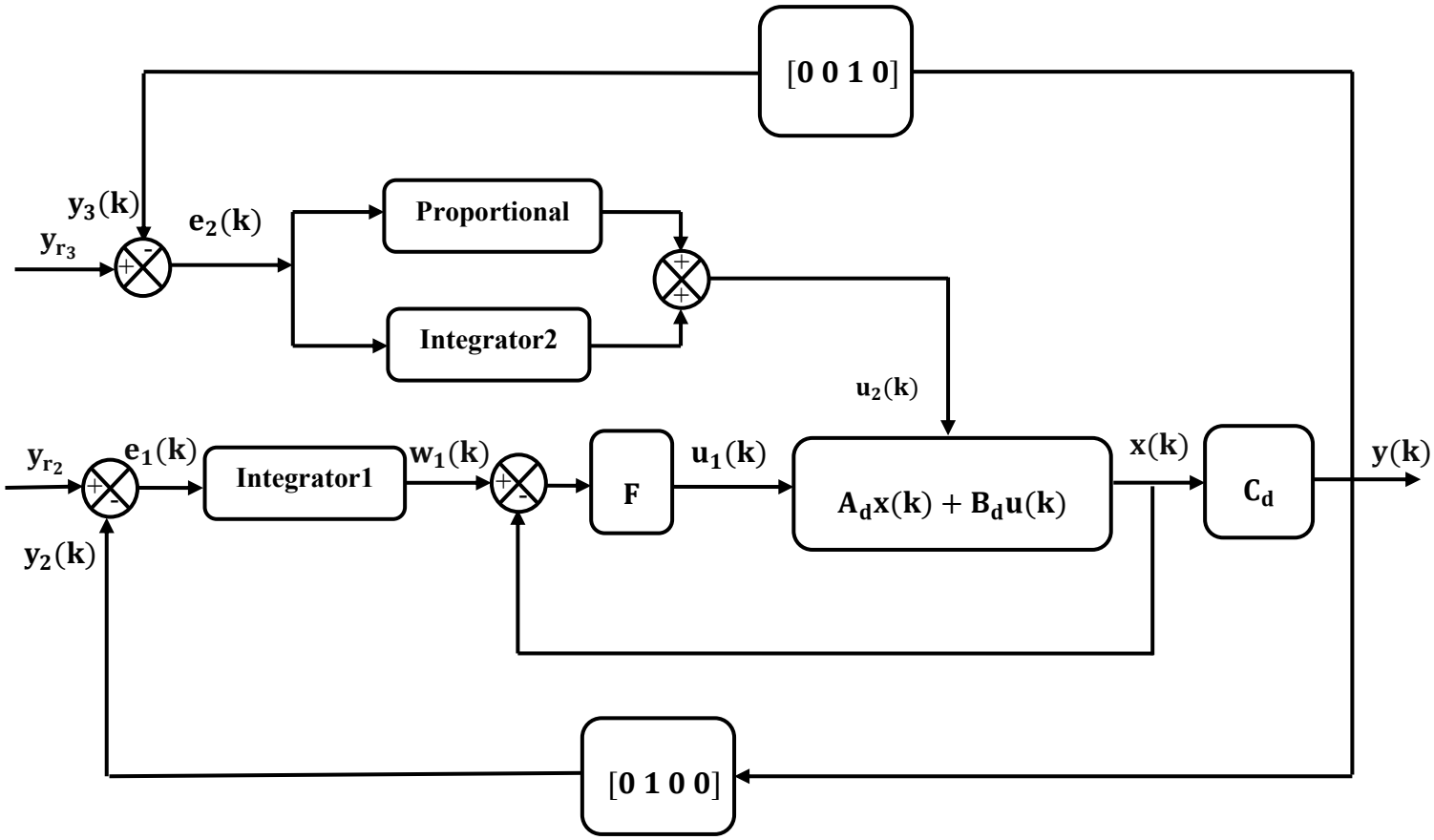

Figure 5.3: Block diagram of closed loop control system with controller designed using a combination of the LQR and LC

5.3 State observer

The control law in the previous section assumed that all state elements were available for feedback. Typically, not all state elements are measured. In fact, the Robogymnast system does not include sensors to measure the angular velocities of the second and third link. This increases the difficulty of measuring the exact state values. In order to apply the designed controller to the real system, a reduced order observer is used to estimate the unmeasured state of the system. This reconstructed state information can then be supplied to the controller. In addition to understanding the characteristics of the system, it is important to check the observability of the Robogymnast system. The observability matrix of the system is given by:

$$[\, C \;\; CA \;\; CA^2 \; CA^3 \;\; CA^4 \;\; CA^5 \,]$$

The rank of the observability matrix is equal to the number of state variables in the system, so the system is observable. The overall observer block diagram showing the estimator with full state feedback is presented in Figure 5.4.

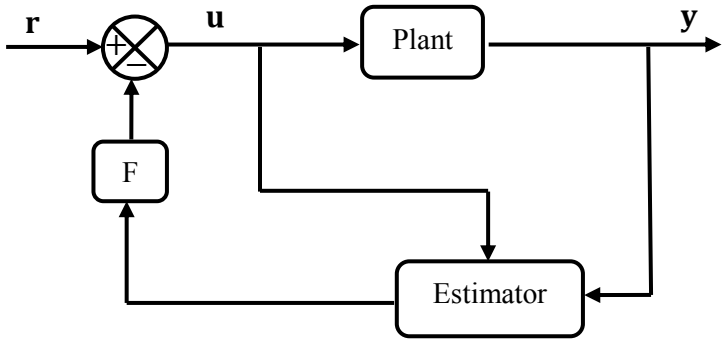

Figure 5.4: Block diagram of estimator with full state feedback

5.3.1 Design of a reduced-order state observer to estimate unmeasured states

The reduced order estimator is a dynamic system that aims to estimate the unmeasured states using the inputs and outputs of the system. In this case, only two states need to be observed.

A reduced order observer of the discrete-time model presented in Equations (5.16) and (5.17) was given by (Medrano-Cerda et al. 1995):

$$v(k+1) = Ev(k) + Hu(k) + Ky(k) \tag{5.16}$$

$$\hat{x}(k) = L_1 y(k) + L_2 v(k) \tag{5.17}$$

Where $\hat{x}(k)$ and $v(k)$ are estimates of the state $x(k)$ and the state observer respectively. E represents the reduced order observer dynamics. The values of E, H, K, L_1 and L_2 should satisfy (Medrano-Cerda et al. 1995):

$$TA - ET = KC \tag{5.18}$$

$$H = TB \tag{5.19}$$

$$[L_1 \quad L_2] = \begin{bmatrix} C \\ T \end{bmatrix}^{-1} \tag{5.20}$$

where T is a design parameter for which the inverse of Equation (5.20) is true.

The term H is a relatively new name for a B matrix which relates to the reduced observer. It is commonly referred to as the consistence number of the reduced observer states, and is definitely less than the plant states. Figure 5.5 presents the overall construction of the state feedback and reduced order observer.

In the literature (Medrano-Cerda et al. 1995; O'Reilly 1983), the term H tends to be set to zero for systems with more outputs than inputs. The reduced order observers are achieved without breaking the invertibility condition of Equation (5.20).

MATLAB® software was used to determine a set of observer designs based on rewriting Equations (5.18) and (5.19) according to the Kronecker tensor products (Wonham 1985) and according to E and H:

$$S\alpha = 0 \tag{5.21}$$

where α is a column vector constructed by sequentially arranging the rows of T and K, and taking the transpose:

$$\alpha = [t_1 \quad t_2 \quad \ldots \quad t_p \quad k_1 \quad k_2 \quad \ldots \quad k_p]^T$$

$$T = \begin{bmatrix} t_1^T & t_2^T & \ldots & t_p^T \end{bmatrix}^T$$

Matrix S then takes the form:

$$S = \begin{bmatrix} T_E \otimes A^T - E \otimes I_A & -I_E \otimes C^T \\ I_E \otimes B^T & 0 \end{bmatrix}$$

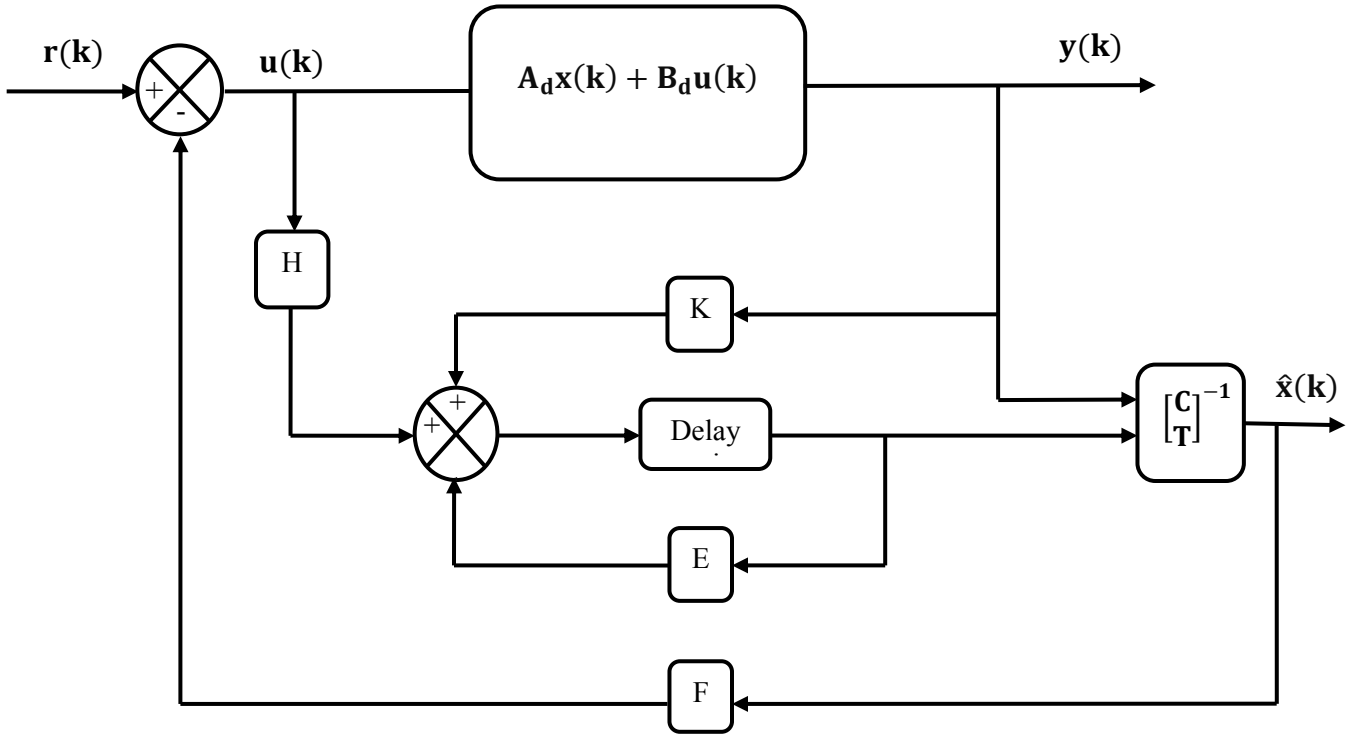

Figure 5.5: Overall construction of the state feedback and reduced order observer

where I_E and I_A refer to identity matrices the same size as E and A respectively. The set of the designed observer parameters T and K were calculated using MATLAB® software by computing an orthonormal basis for the null space of S. For each solution, the invertiblity condition of Equation (5.20) had to be checked; if it was not satisfied then it was be discarded.

More important is the determination of the dynamic response of the observer, which is related to the selection of the observer eigenvalues (E). The system is stable if all the eigenvalues lie on or within the unit circle and unstable if they are outside of this. It should be noted that the performance of the observer is associated with the location of the selected observer eigenvalues, i.e. whether or not they are located within the unit circle (Phillips and Nagle 2007; Franklin et al. 1998).

Figure 5.6 shows the exponential decay response of the system associated with positive real poles located within the unit circle. The system is oscillatory if the real poles lie on the negative real axis within the unit circle.

To obtain a response with constant magnitude, the real poles should be on the unit circle. In order to make the system oscillatory with a variable rate of decay and varying frequency of oscillations, the observer poles should be complex conjugates inside the unit circle. Moreover, in case of the complex conjugate poles on the unit circle, the response leads to oscillations which continue for an extended period or without interruption.

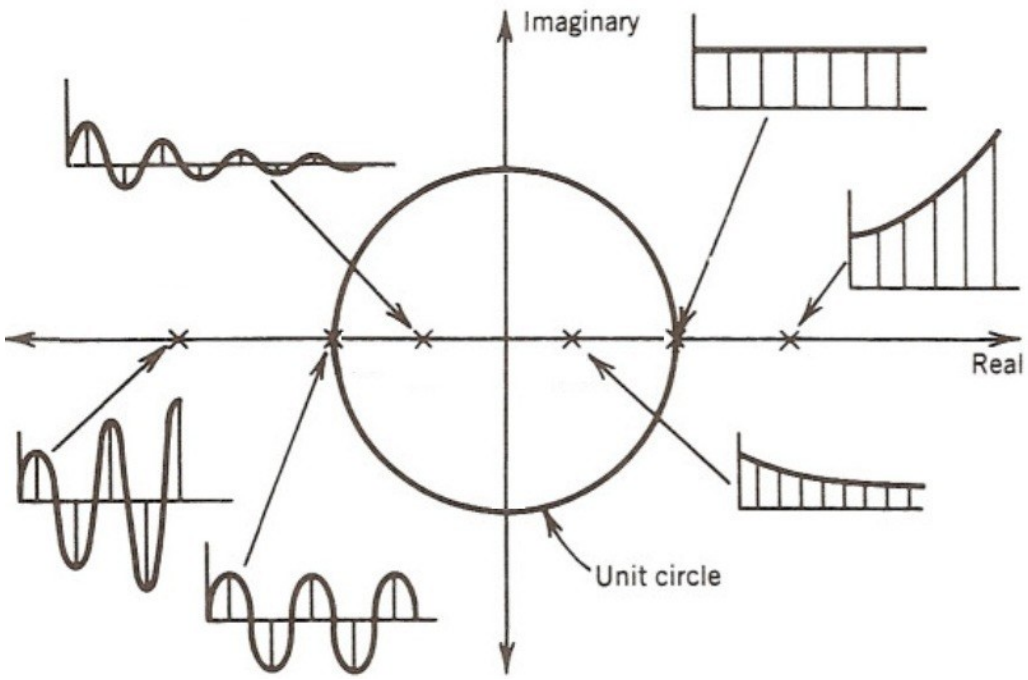

Figure 5.6: Relationship between discrete system pole locations and the system transient response

5.3.2 Controller design via reduced order observer

The overall controller (observer and integrator) is now written as:

$$\begin{bmatrix} v(k+1) \\ w(k+1) \end{bmatrix} = \begin{bmatrix} E & 0 \\ 0 & 1 \end{bmatrix} \begin{bmatrix} v(k) \\ w(k) \end{bmatrix} + \begin{bmatrix} H \\ 0 \end{bmatrix} u(k) + \begin{bmatrix} K \\ 0 \quad -T_s \quad 0 \end{bmatrix} y(k) + \begin{bmatrix} 0 \\ T_s \end{bmatrix} y_r(k) \tag{5.22}$$

$$\begin{bmatrix} \hat{x}(k) \\ w(k) \end{bmatrix} = \begin{bmatrix} L_2 & 0 \\ 0 & 1 \end{bmatrix} \begin{bmatrix} v(k) \\ w(k) \end{bmatrix} + \begin{bmatrix} L_1 \\ 0 \end{bmatrix} y(k) \tag{5.23}$$

by using the LQR to find the feedback gain matrix, the control actions in term of measured and estimated states is reported as:

$$u(k) = -F \begin{bmatrix} \hat{x}(k) \\ w(k) \end{bmatrix} \tag{5.24}$$

For the controller designed as a combination between LQR and LC, the input voltage applied to the first motor is written as:

$$u_1(k) = -F \begin{bmatrix} \hat{x}(k) \\ w_1(k) \end{bmatrix}, \tag{5.25}$$

and the control action u_2 applied to the second motor is described in Equation (5.10).

5.4 Experimental setup

For the experimental parts of this work, the control system was implemented using the C++ program environment. The programs generally include code to capture experimental data and store them on the hard disk. The controlling parameters were calculated by MATLAB® software and the data were loaded at the beginning of the C++ program.

Before applying the proposed controller, the relative angular positions and velocity sensors were calibrated to give a zero volt reading for zero relative angular positions and velocity. The sequence of the computer control algorithm at each sampling time can be divided into steps. The first step is to read in the sensor data (A/D conversion). After this, the second and third links' angular velocities are estimated. In the following stage, the control actions are calculated and checked to determine whether they are within the admissible range ($\pm$ 10V) or not. After conversion from digital to analog (by the D/A convertor) the control actions are sending to the plant. Following this, the observer and integrator states are updated. Finally, the controller waits for next sampling time and then goes back to the first step. Figure 5.7 presents a flowchart of the balance/stablisation control system implementation using LQR. The flowchart of the balance/stablisation control system implementation using the LQR with LC is given in Appendix B

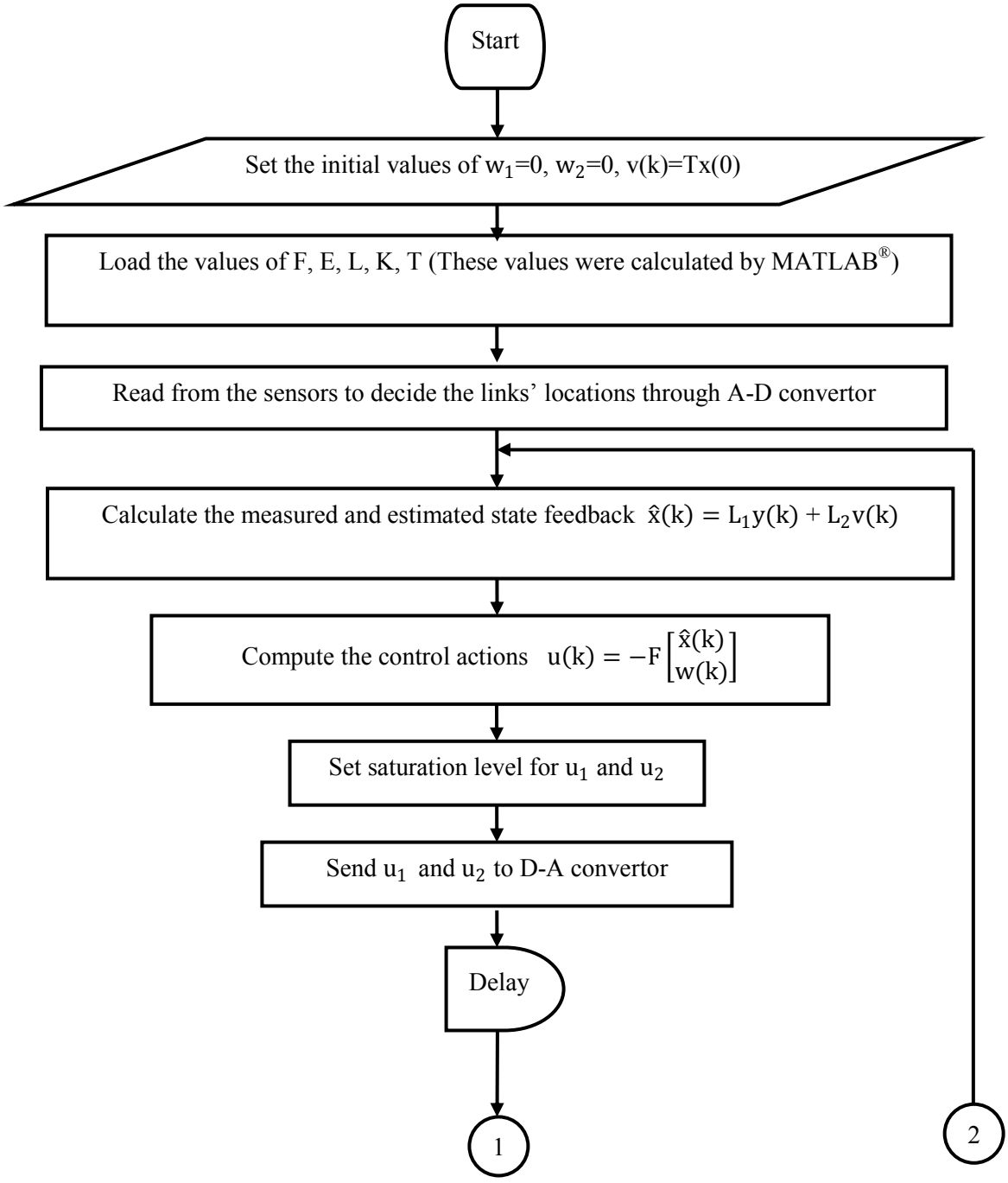
Start
Set the initial values of w_1=0, w_2=0, v(k)=Tx(0)
Load the values of F, E, L, K, T (These values were calculated by MATLAB®)
Read from the sensors to decide the links' locations through A-D convertor
Calculate the measured and estimated state feedback $\hat{x}(k) = L_1 y(k) + L_2 v(k)$
Compute the control actions $u(k) = -F\begin{bmatrix}\hat{x}(k)\\ w(k)\end{bmatrix}$
Set saturation level for u_1 and u_2
Send u_1 and u_2 to D-A convertor
Delay
1
2

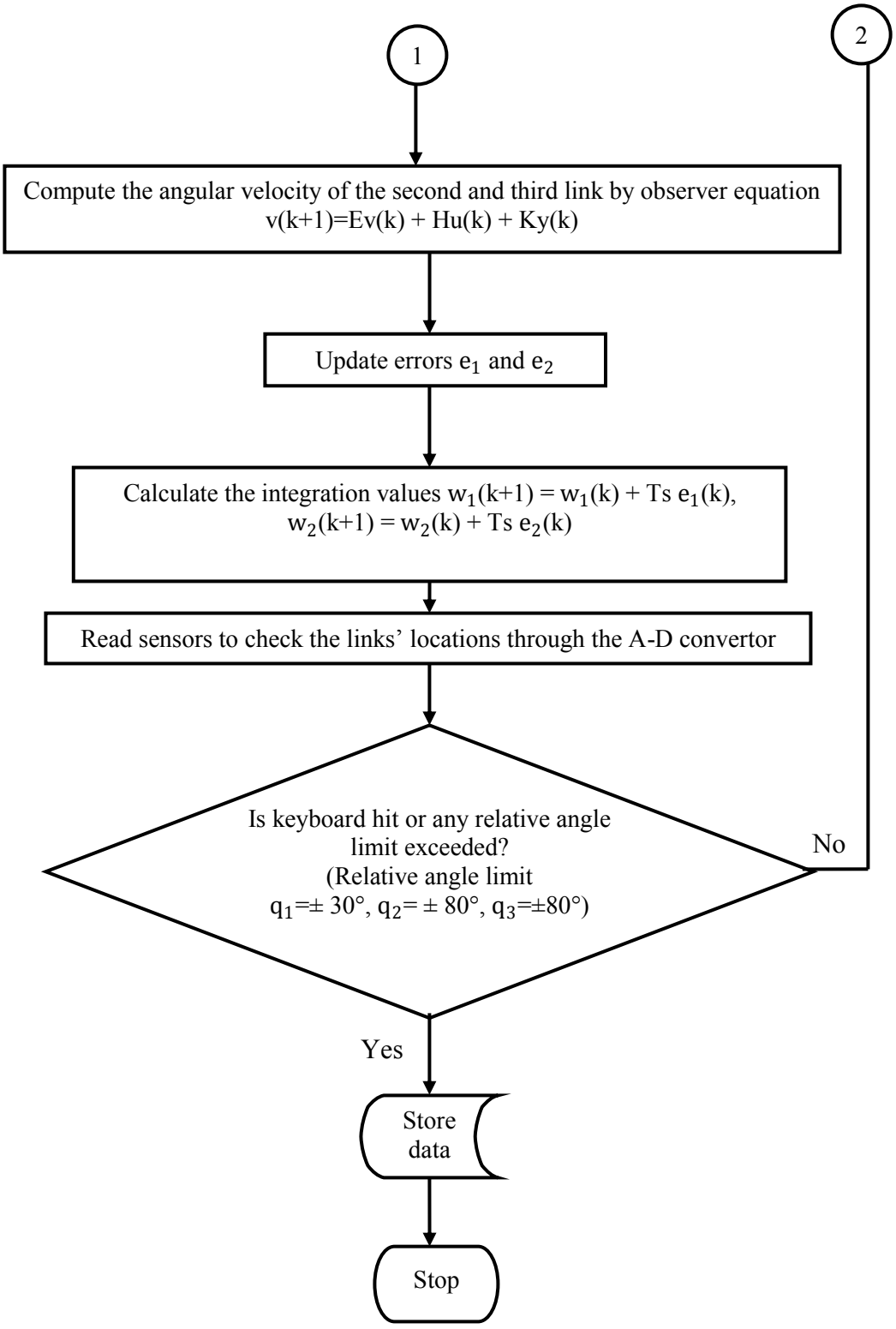

Figure 5.7: Flowchart of the balance control system implementation using the LQR

5.5 Downward balancing control problem

The main objective of this study is to validate the use of the designed controller for balancing the Robogymnast in the downward configuration. This was achieved via studying the ability of the designed controller to respond to an external disturbance. The experiments were carried out introducing small torque disturbances by gently pushing each link separately. In addition, the evaluation of the designed controller's ability to overcome the disturbance force was demonstrated through monitoring the system response and the exerted control effort.

The system performance was analysed via monitoring the control methods which were demonstrated in the designed controller Section 5.2. The mathematical model of the Robogymnast around the stable point in the downward position was presented in Section 3.4 in Chapter 3.

The response to a disturbance of the free-swinging Robogymnast in the downward position is shown in Figure 5.8 without any applied control action. It can be seen that the disturbance force caused a movement in the Robogymnast from the stable point by -30° and the system regained the steady state after 45 seconds without applying any control actions.

To implement the downward balancing control, the Robogymnast was put into the downward configuration and then of the all potentiometers were calibrated by measuring the zero offset (the difference in the voltage reading from the expected zero).

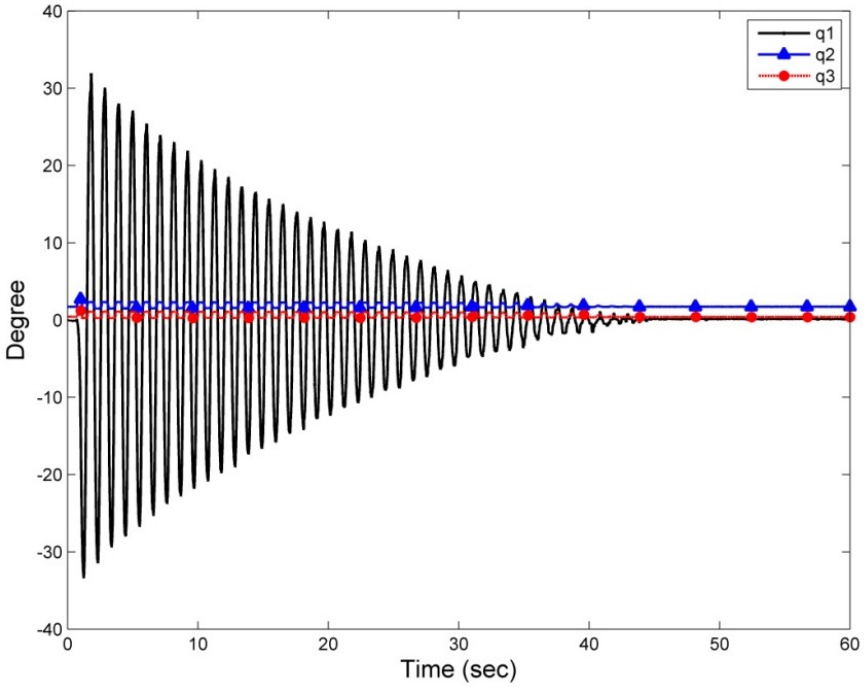

Figure 5.8: Response of free swinging Robogymnast in the downward position

5.6 Experimental results using the LQR

In this section, the reduced order observer dynamics are selected as $E = [0.5 \;\; 0.5]$, and H is set to zero. The values of T and K are hence:

$$T = \begin{bmatrix} -0.548 & -0.629 & -0.074 & 0.047 & 0.031 & 0.003 \\ 0.169 & -0.212 & -0.025 & 0.009 & 0.010 & 0.001 \end{bmatrix}$$

$$K = \begin{bmatrix} -0.304 & -0.327 & -0.040 & 0.009 \\ 0.076 & -0.01 & -0.013 & 0.008 \end{bmatrix}$$

$$L = \begin{bmatrix} 1 & 0 & 0 & 0 & 0 & 0 \\ 0 & 1 & 0 & 0 & 0 & 0 \\ 0 & 0 & 1 & 0 & 0 & 0 \\ 0 & 0 & 0 & 1 & 0 & 0 \\ -0.0017 & 0.0218 & 0.1857 & 0.3228 & -0.0016 & 0.0048 \\ 0.0001 & -0.1684 & 0.1829 & -0.0274 & 0.0001 & -0.0003 \end{bmatrix}$$

For the augmented plant model, the weight matrices Q and R were chosen through trials depending on the experience of the designer.

$$Q = \begin{bmatrix} 1090 & 0 & 0 & 0 & 0 & 0 & 0 & 0 \\ 0 & 400 & 0 & 0 & 0 & 0 & 0 & 0 \\ 0 & 0 & 50 & 0 & 0 & 0 & 0 & 0 \\ 0 & 0 & 0 & 1 & 0 & 0 & 0 & 0 \\ 0 & 0 & 0 & 0 & 0.1 & 0 & 0 & 0 \\ 0 & 0 & 0 & 0 & 0 & 0.01 & 0 & 0 \\ 0 & 0 & 0 & 0 & 0 & 0 & 5 & 0 \\ 0 & 0 & 0 & 0 & 0 & 0 & 0 & 3 \end{bmatrix}$$

$$R = \begin{bmatrix} 0.9 & 0 \\ 0 & 0.9 \end{bmatrix}$$

For this selection, the optimal gain matrix is given by:

$$F = \begin{bmatrix} -26.82 & 12.139 & -0.649 & 1.061 & 0.718 & 0.081 & -2.209 & -0.02 \\ -2.703 & -0.924 & 8.166 & -0.062 & -0.028 & 0.037 & 0.034 & -1.81 \end{bmatrix}$$

5.6.1 Applying a disturbance to the passive swinging Robogymnast

An external disturbance by gently pushing the first link was applied to cause the system to start swinging freely, without any control actions applied to the motors. The controller was then applied to balance the Robogymnast in its downward configuration. From Figure 5.9 it can be seen that the feedback control law can balance the Robogymnast

system. The steady state of the first link is achieved after 11 seconds of the control system startup. The maximum average oscillation in relative angular position of first link (q_1) and second link (q_2) are within the ranges of $\pm 6°$ and $\pm 5°$ respectively. Moreover, there is a significant oscillation in the results of the third relative angular position (q_3). The range of relative angular position for q_3 varied between approximately $-2°$ and $+28°$ to maintain the first link in the downward equilibrium point after 10 seconds. It can be noted that the first and third link re-obtained the balancing point with a 1° steady state error.

Figure 5.10 shows that the control actions were applied 2 seconds after beginning free swinging and data recording. The control effort of the second motor is greater than that of the first motor, however both of them are still within the maximum input voltage range ±10V.

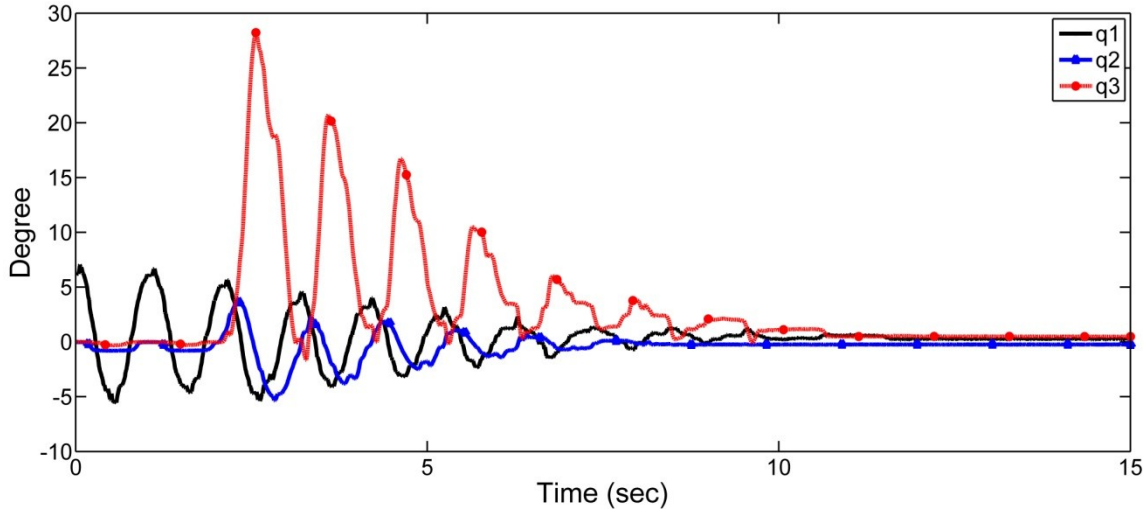

Figure 5.9: Measured relative angular positions q_1, q_2 and q_3

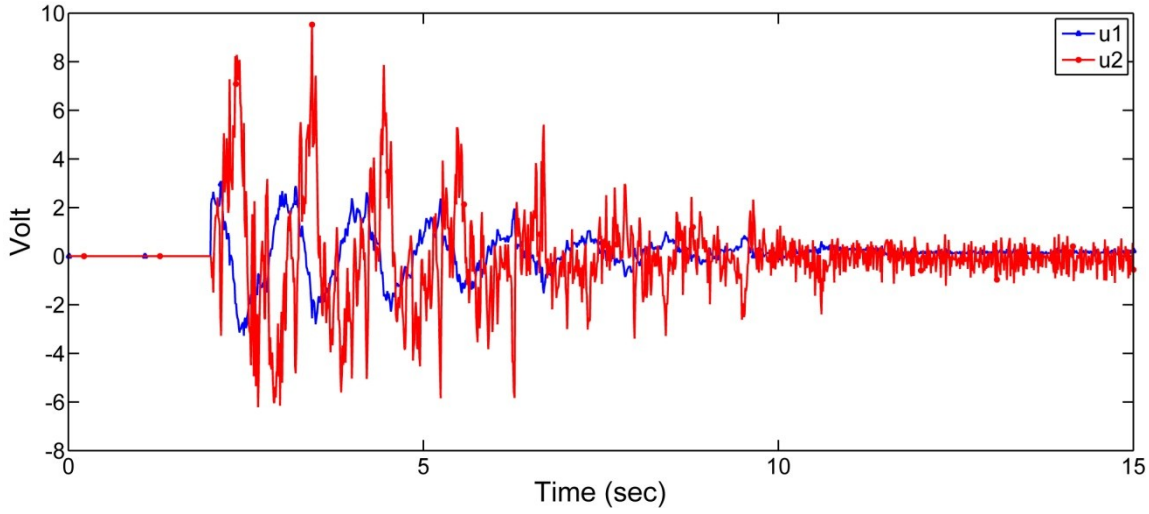

Figure 5.10: Measured control actions u_1 and u_2 applied to the motors

5.6.2 Applying a disturbance to the first link

In this case, the Robogymnast is at the downward equilibrium point and the control actions are active. A disturbance is then introduced to the first link, shifting that link from its equilibrium position. From the data shown in Figure 5.11, the magnitude of the relative angular displacement (q_1) from the equilibrium point was around $\pm 10°$ by the cause of the disturbance. It is apparent that the length of time between the disturbance and regaining of steady state was about 11 seconds. There was a significant steady state error of about 1° and 2° in the first and third links respectively. In addition, it can be seen from this figure that the third link reported significantly more movement from the balance point than the first and second links. This was required to return the first link to its downward configuration and then to track the reference signals for the second and third links. Hence, strong evidence of the effect of the third link is shown in Figure 5.12, where the control action of the second motor reached the maximum input voltage ±10V in one of the oscillation peaks. The first motor's input voltage was still in the input voltage range.

5.6.3 Applying a disturbance to the second link

In order to understand the effect of a disturbance to the second link, a disturbance was introduced to shift it from its equilibrium position. As shown in Figures 5.13 and 5.14, there are no considerable differences between the behaviour of the system in this case compared to the instance shown in Section 5.6.2.

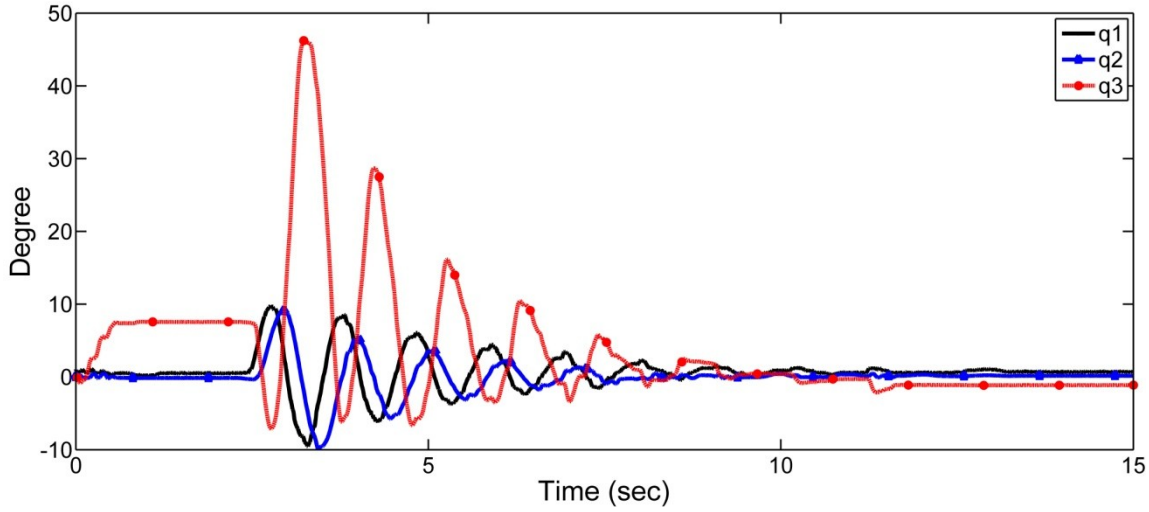

Figure 5.11: Measured relative angular positions q_1, q_2 and q_3

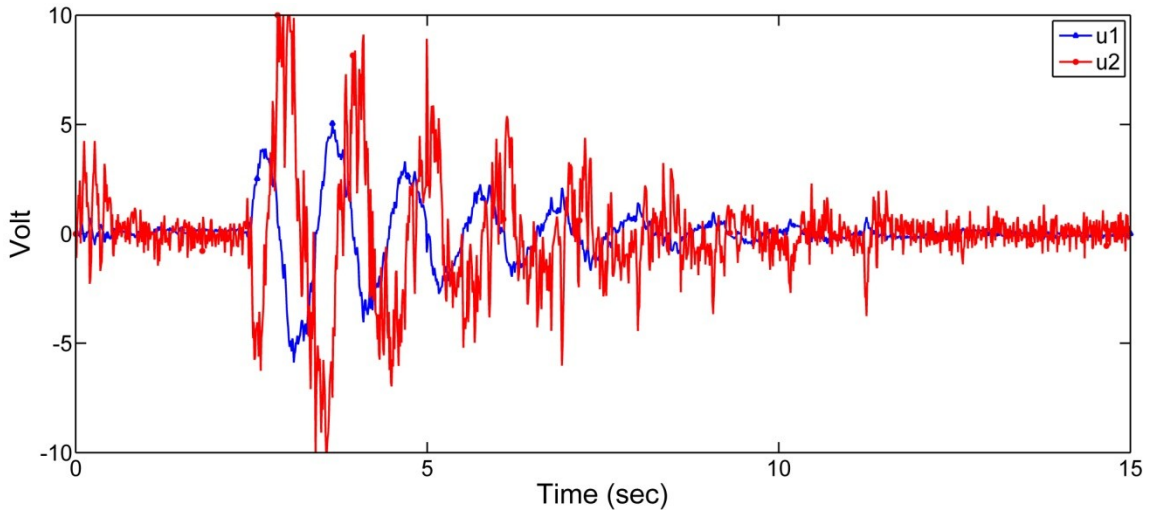

Figure 5.12: Measured control actions u_1 and u_2 applied to the motors

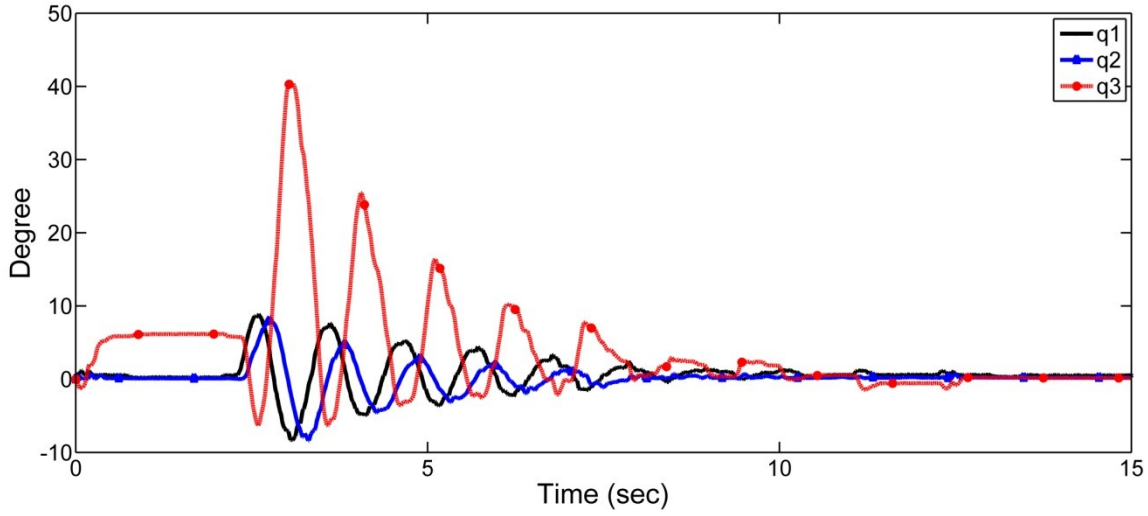

Figure 5.13: Measured relative angular positions q_1, q_2 and q_3

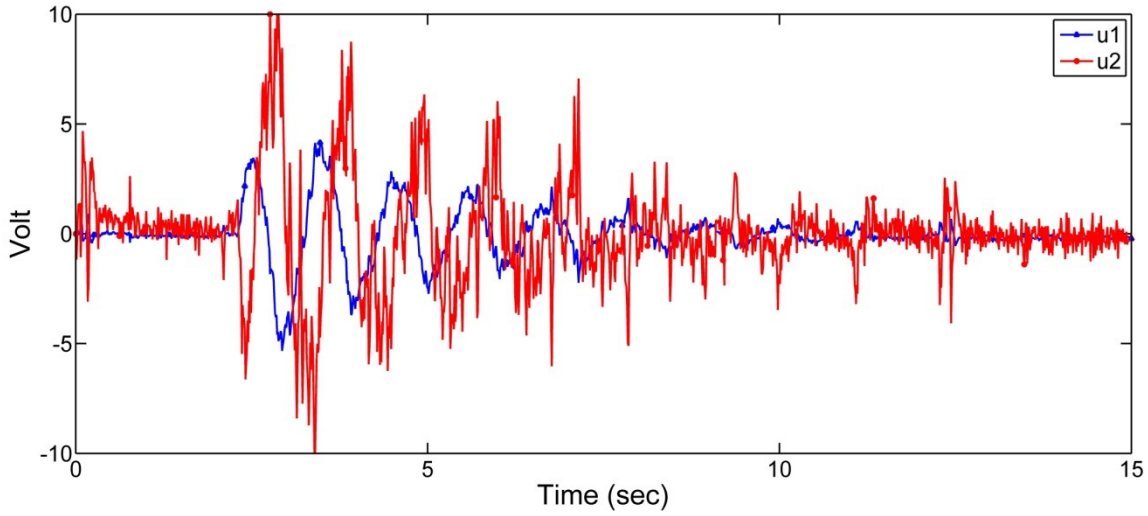

Figure 5.14: Measured control actions u_1 and u_2 applied to the motors

5.6.4 Applying a disturbance to the third link

A further instance of investigation was implemented by applying a disturbance to the third link. From the records shown in Figure 5.15, it is clear that when the disturbance was created the angle of the third link oscillated between $-11°$ and $54°$. There was also a large deviation in the relative angular position of the first link (q_1) and the second link (q_2) from the desired reference angles. The relative angular position of the first link (q_1) and the second link (q_2) oscillated within the ranges of $\pm 11°$ and $\pm 12°$ respectively. It can be seen from Figure 5.16 that the second motor requires a large amount of energy to maintain the system in a satisfactory level of performance. Consequently the control signal reached the saturation limit multiple times during the oscillation. However less power was required for the first motor. In this case, the system reaches the steady state after 11 seconds, with a significant steady state error in the third link of about -3°.

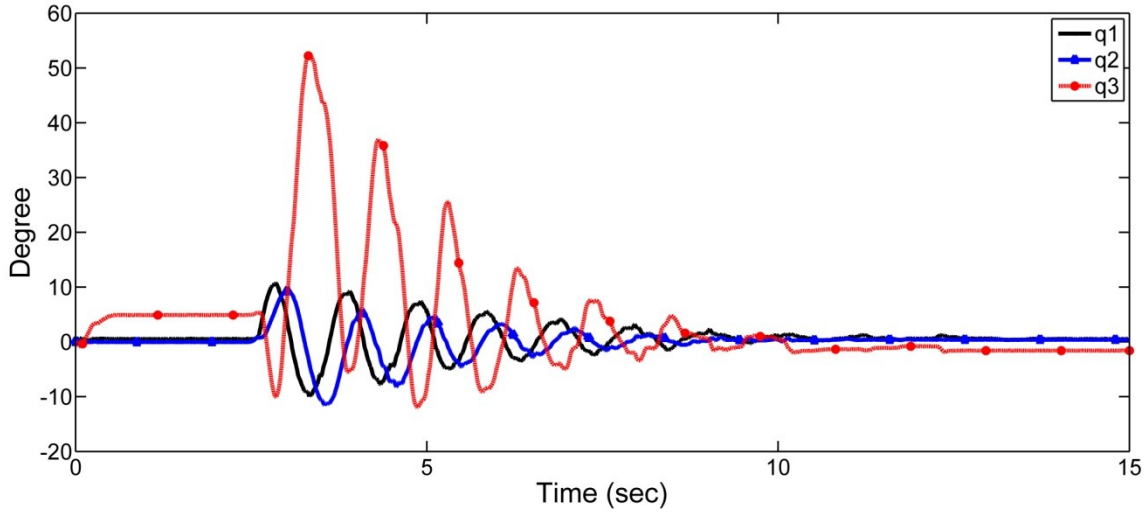

Figure 5.15: Measured relative angular positions q_1, q_2 and q_3

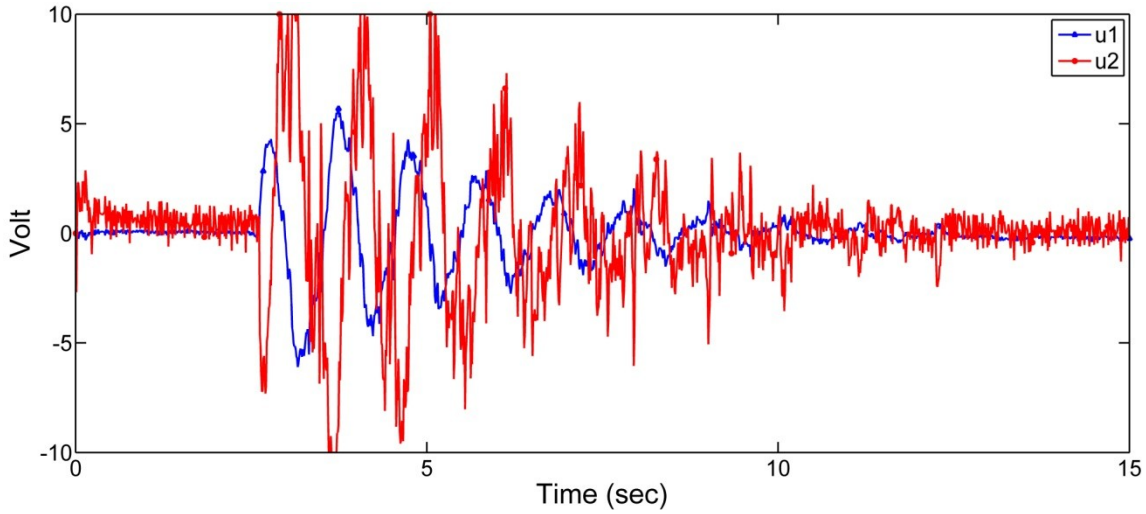

Figure 5.16: Measured control actions u_1 and u_2 applied to the motors

5.7 Experimental results using a combination of the LQR and LC

For this situation, the reduced order observer is selected as $E = [0.3\ 0.3]$ and H was set to zero. In this case the values of T, K and L become:

$$T = \begin{bmatrix} -0.397 & -0.592 & -0.071 & 0.0263 & 0.021 & 0.002 \\ 0.030 & -0.235 & -0.027 & 0.001 & 0.008 & 0.0009 \end{bmatrix}$$

$$K = \begin{bmatrix} -0.293 & -0.421 & -0.050 & 0.0082 \\ 0.207 & -0.166 & -0.019 & 0.008 \end{bmatrix}$$

$$L = \begin{bmatrix} 1 & 0 & 0 & 0 & 0 & 0 \\ 0 & 1 & 0 & 0 & 0 & 0 \\ 0 & 0 & 1 & 0 & 0 & 0 \\ 0 & 0 & 0 & 1 & 0 & 0 \\ -1223.33 & 29.306 & 0.130 & 23.002 & -1022.86 & 2702.88 \\ 10255.6 & -12.270 & 26.754 & -200.144 & 8833.99 & -22318.7 \end{bmatrix}$$

The weight matrices Q and R are chosen as follows:

$$Q = \begin{bmatrix} 1050 & 0 & 0 & 0 & 0 & 0 & 0 \\ 0 & 40 & 0 & 0 & 0 & 0 & 0 \\ 0 & 0 & 1 & 0 & 0 & 0 & 0 \\ 0 & 0 & 0 & 1 & 0 & 0 & 0 \\ 0 & 0 & 0 & 0 & 0.01 & 0 & 0 \\ 0 & 0 & 0 & 0 & 0 & 0 & 0 \\ 0 & 0 & 0 & 0 & 0 & 0 & 0.9 \end{bmatrix}$$

$$R = [0.1]$$

For this selection, the optimal gain matrix for the first motor is given by:

$$F = [-23.758 \quad 4.799 \quad -0.799 \quad 0.113 \quad 0.357 \quad 0.043 \quad -2.574]$$

Additionally, the values of K_p and K_I have been selected as 10 and 1 respectively.

5.7.1 Applying a disturbance to the passive swinging Robogymnast

The system began by swinging freely. This was initiated by applying a disturbance to the system without any control actions being applied to the motors. While the system was swinging, the control action was engaged to balance the Robogymnast in the downward configuration. The results of this study indicate that the control action began 2 seconds after the free-swinging start-up. This is shown in Figure 5.18. It can also be seen in Figure 5.17 that the first link reached a steady state after 7 seconds whilst the second link reached steady state in 10 seconds. This is too long compared with the first link's settling time. There is no significant deviation of the third link, with the relative angular position of the third link (q_3) oscillating between 0.45° and -0.35°. This is considered to be a negligible angular position variation. It can be seen in Figure 5.18 that the control action of the first motor reached the maximum peak input voltage ±10V multiple times.

5.7.2 Applying a disturbance to the first link

For this test, the Robogymnast was in the downward equilibrium position, and the control signal was applied to the motors while a disturbance was introduced to the first link. It was found that the first link oscillated between 9° and $-7°$ as shown in Figure 5.19. The second link (q_2) shows a larger movement from the desired reference angle, varying between $27°$ and $-22°$ and the settling time of the response of the second link was about 7 seconds. The first link settled to within 1° steady state error from the desired reference ($q_1 = 0$). From the plotted result in Figure 5.20, the control voltage can be

seen to be within the maximum range, though it did reach the saturation limit in the negative direction at one point.

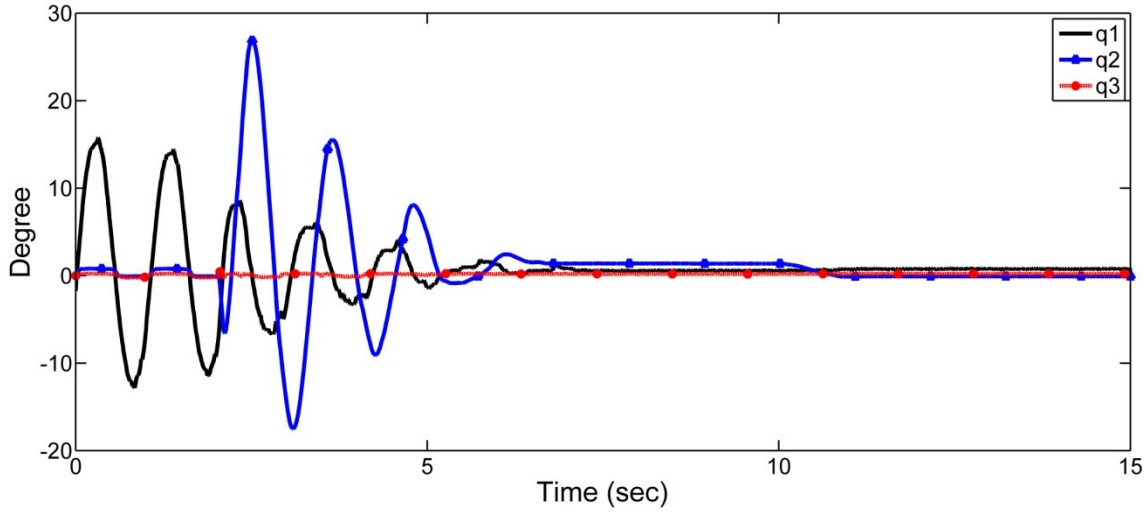

Figure 5.17: Measured relative angular positions q_1, q_2 and q_3

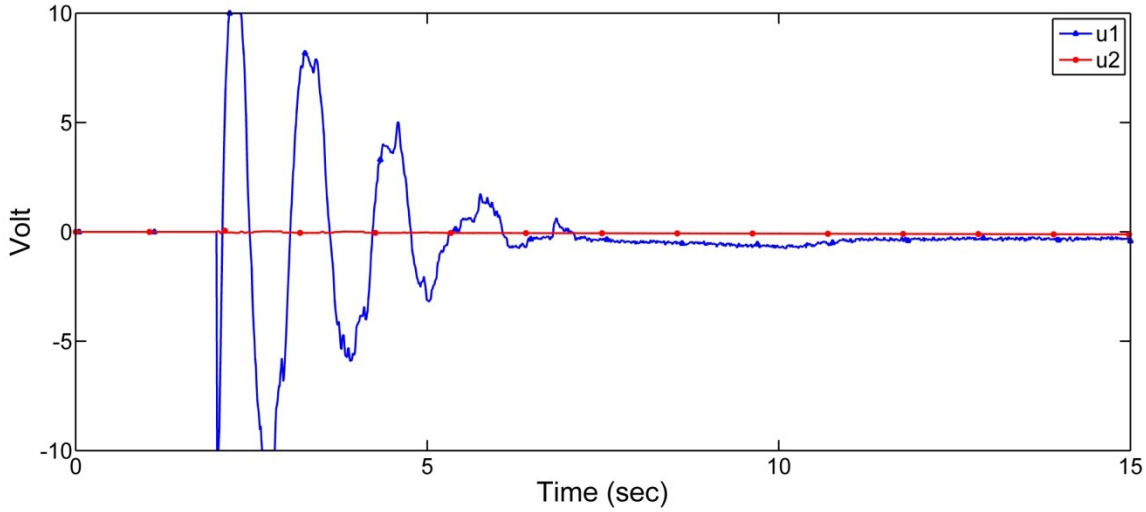

Figure 5.18: Measured control actions u_1 and u_2 applied to the motors

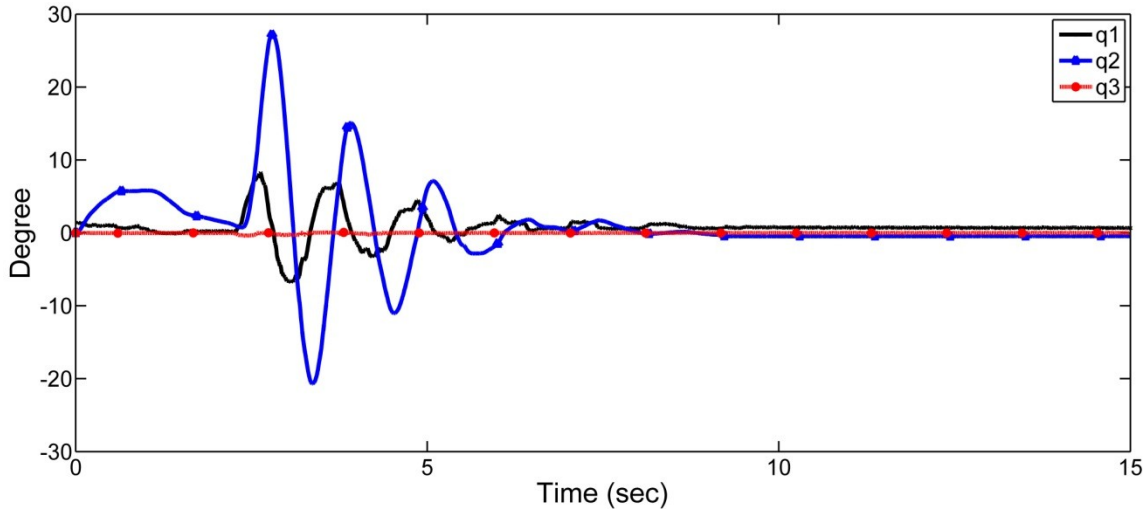

Figure 5.19: Measured relative angular positions q_1, q_2 and q_3

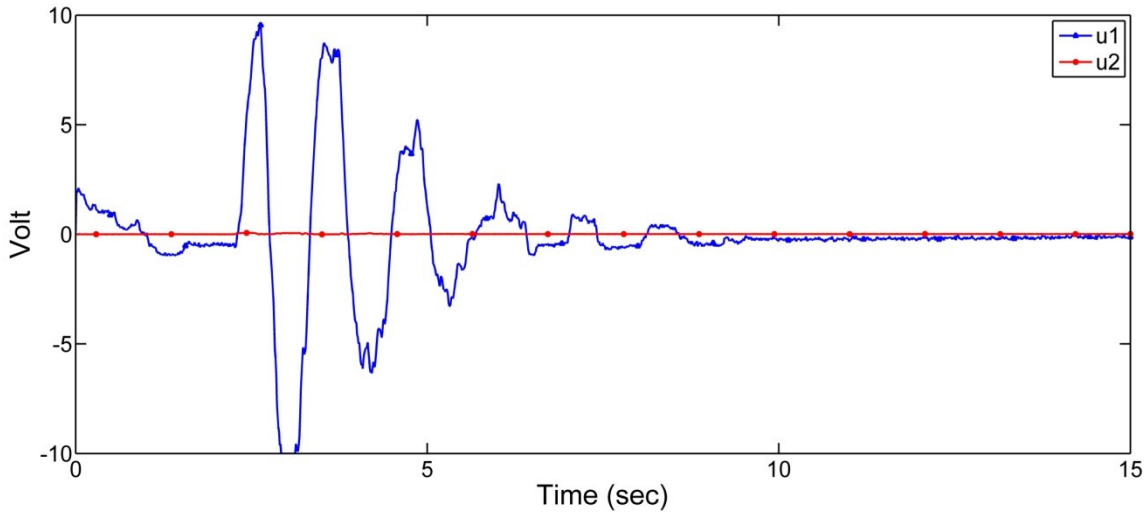

Figure 5.20: Measured control actions u_1 and u_2 applied to the motors

5.7.3 Applying a disturbance to the second link

This experiment was implemented to study the effect of introducing a disturbance to the second link while the Robogymnast was in the downward equilibrium position and the

control action was activated. It can be seen from the plotted results in Figures 5.21 and 5.22 that the results did not report significant differences with those presented in Section 5.7.2 when the disturbance applied to the first link.

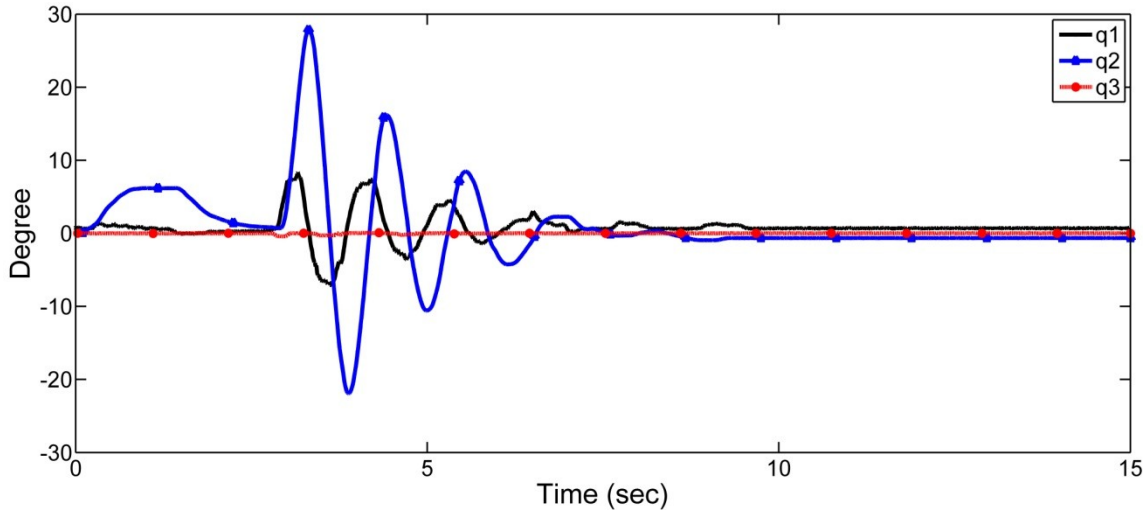

Figure 5.21: Measured relative angular positions q_1, q_2 and q_3

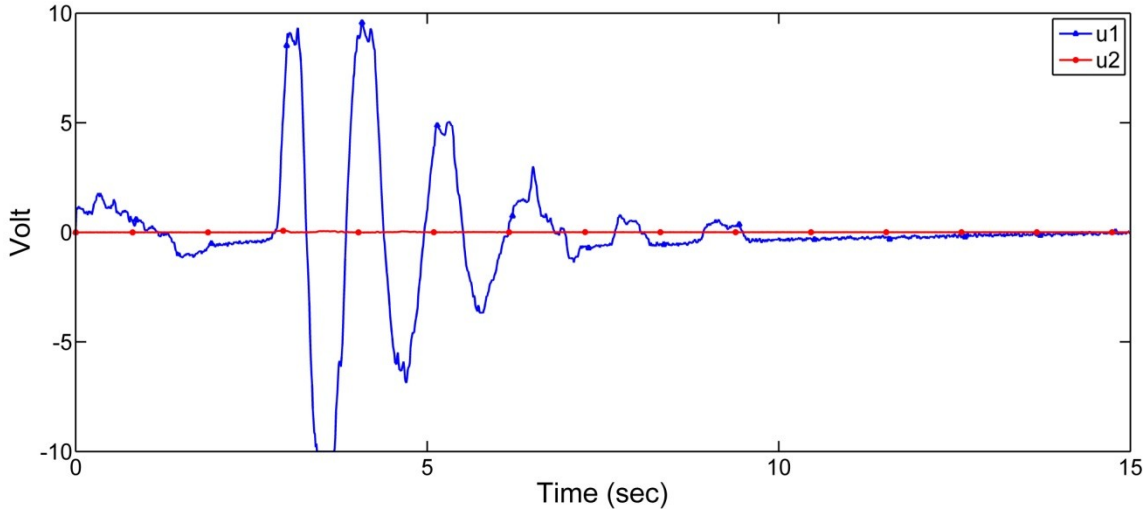

Figure 5.22: Measured control actions u_1 and u_2 applied to the motors

5.7.4 Applying a disturbance to the third link

This experiment was repeated under the same conditions as those described in Section 5.7.2 and Section 5.7.3. In this case the disturbance is applied to the third link. Figures 5.23 and 5.24 illustrate the main characteristics of the Robogymnast behaviour when the disturbance was applied to the third link. It is apparent that the control action began after 4 seconds. Furthermore, the controller was successful in rejecting the disturbance, as it was able to balance all the links around the downward equilibrium point after 7 seconds. There is a steady state error of about -2° in the relative angle of the second link while and about 1° in the relative angle of the first link. The results indicate that the required energy of the first motor is less than the energy required in previous instances. The maximum input voltage of the first motor is variable between 9V and -9V.

5.8 Discussion of results

In the case of the downward setup in the absence of an external disturbance, the system is statically stable without powering any motors. The configuration of the Robogymnast can be set physically because all joints are back drivable.

The experimental performance of the Robogymnast using the LQR controller is shown in Figure 5.9 to Figure 5.16, while the performance of the Robogymnast using the combined LQR and LC is presented in Figure 5.17 to Figure 5.24.

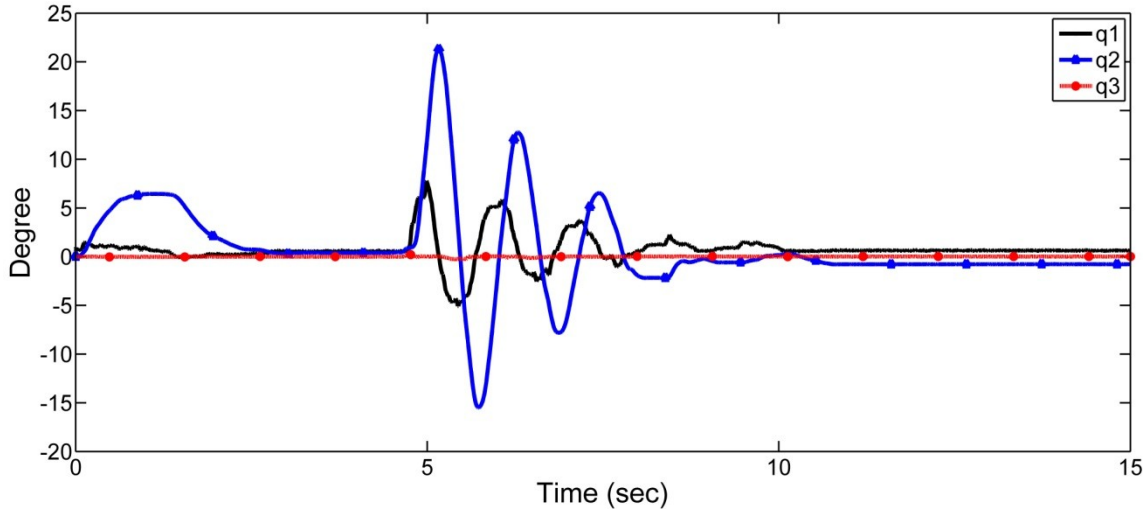

Figure 5.23: Measured relative angular positions q_1, q_2 and q_3

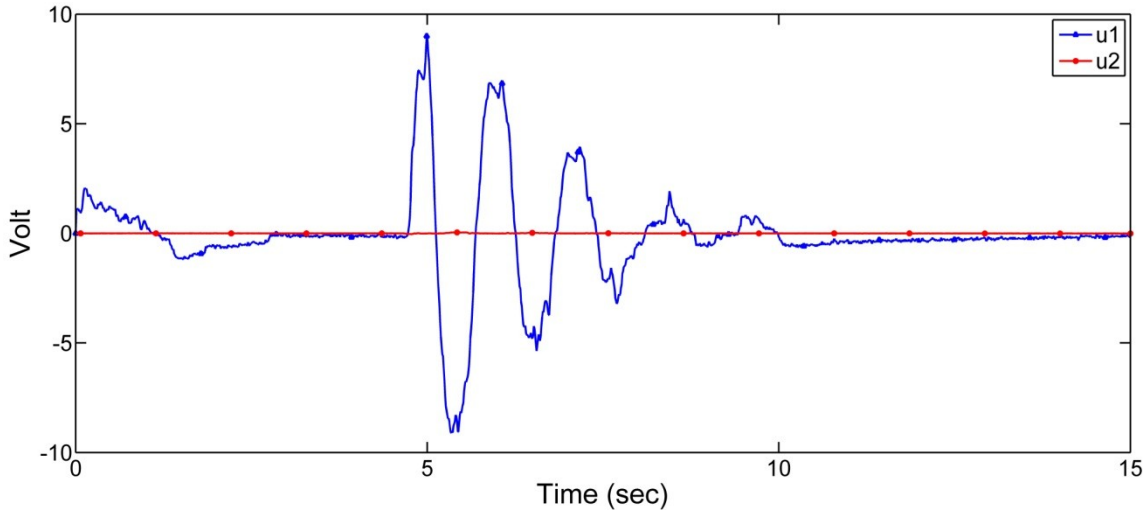

Figure 5.24: Measured control actions u_1 and u_2 applied to the motors

When rebalancing the system about the reference balancing point, the first type of controller mainly applied force to the third link, while the second type of controller mainly uses the second link to do the work. This is clearly shown by the large oscillations in the angular response of the third and second links for the first and second controllers respectively. In the current study, comparing the system response using the LQR controller with the response using the combination controller has shown that the response of the Robogymnast is faster by using the combined LQR and LC.

The most interesting finding was that the control effort of the second motor when using the LQR with LC is considerably less than the control effort of the first motor.

Despite all potentiometers being calibrated, there are unknown measurement errors in the second and third links for all the experimental cases. These errors could be related to the offsets in the potentiometer readings due to the backlash in the gearboxes during calibration. The free swinging of the Robogymnast in Figure 5.8 shows nonlinear backlash effect in the response of the second and third joints' gearboxes. In addition to this, there is a significant initial error in the reading from the second and third links, as expressed in Figures 5.9, 5.11, 5.13, 5.15, 5.17, 5.19, 5.21 and 5.23. The present results are significant in at least two major respects. The first one is the effect of the nonlinear backlash in the gearbox and the second one is the offsets in the signal measurement. This is related to the difficult calibration of the potentiometers and the measurement noise.

Nevertheless, even with the nonlinear backlash production, the unknown offsets in the sensor readings, and the power limitations, the controller was able to respond robustly to the applied disturbance and track the desired reference balancing point with a reasonable steady state error and short settling time.

5.9 Summary

The purpose of this chapter was to design different controller methods to govern the movement of the Robogymnast system. The first type of controller was an LQR controller with an integrator action. The second type was a combination between LQR and LC. A reduced order observer was also designed to estimate the unmeasured states (angular velocities). The validation of the designed controller was conducted through implementing the controller for the downward balancing problem of the Robogymnast on the real system. The first part focused on using the LQR and the application of external disturbances. Another controller was designed by using a combination between LQR and LC for balancing Robogymnast in the downward position. Downward balancing was implemented using the two types of controller, which were both able to balance the Robogymnast in the downward configuration. The next procedure which is the upright balancing will be discussed in chapter 6.

Chapter 6

Upright Balancing Control

6.1 Introduction

This chapter concerns the stabilising and balancing of the Robogymnast in its upright position. The problem of stabilising inverted pendulums with passive joints at the upright position was extensively investigated (Arai and Tachi, 1991, Furuta et al., 1991, Medrano-Cerda et al., 1995, Spong, 1995). The dynamics of the Robogymnast around the upright position are totally different from when it is in the downward position. The controller design for balancing the Robogymnast in the upright position was investigated through use of the controller methods described in Section 5.2 in Chapter 5.

A major problem with this kind of dynamic system is the balancing mechanism. In this study, control of the Robogymnast system is challenging because the Robogymnast's hands are firmly attached to a freely rotating high bar that is mounted on ball bearings.

The aim of this chapter is to investigate the problem of stabilising and balancing the Robogymnast system in the upright position through applying disturbance forces to the pendulum links of the Robogymnast while monitoring the system response and the exerted control effort.

The chapter is organised as follows. Section 6.2 demonstrates the upright balancing control problem. The experimental difficulties with upright balancing are discussed in Section 6.3. Section 6.4 shows the limitations of simulation analysis. The use of the LQR controller is presented in Section 6.5, while the use of the combined LQR and LC is reported in Section 6.6. The result is discussed in Section 6.7, and a summary of this chapter is given in Section 6.8.

6.2 Upright balancing control problem

In the case of upright balancing, it is important to keep the first link close to the upright equilibrium point, with a reasonable steady state error and minimum settling time. In the same way, the oscillation of the second and third link should stay within a realistic range. In other words, the link deviation from the upright equilibrium position should be within the range that can be controlled. Any high overshoot in the second or third link can cause the Robogymnast to fall from its vertical position.

In order to understand how to balance the real system at the specified position, it is necessary to know the dynamic model of the Robogymnast, including the parameters that affect the dynamic behavior of the system. This necessity can be satisfied through simulation analysis. The simulation study and analysis of the upright balancing is dependent on proper value selection for the weighting matrices, and proper observer dynamics. Also important is the range of the initial relative angular position of all the links when the real system starts up.

6.3 Experimental difficulties with upright balancing

Many upright balancing experiments were carried out on the real system. The startup was carried out by manually holding the links of the Robogymnast close to the vertical position. In this study the accuracy of the initial sensor values are important. The controller was designed with the assumption that all the initial relative angular positions were equal to zero for the upright balancing position. In the real physical system, it is extremely difficult to satisfy this condition. This was producing unexpected control action values applied to the first and second motors, leading to increasing probability of Robogymnast falling from its vertical position.

In these particular attempts, there are many problems which can prevent the achievement of upright balancing. The first, and most significant one is a nonlinear backlash in the second joint (shoulder joint) and third joint (hip joint) gearboxes that cause inaccurate feedback control reference signals. The second problem is the transducer offset error, which is related to the noise in the sensor measurements that affects the actual signal values. A further issue is the difficulty of sensor calibration, because the high backlash in the gearboxes can affect the error in the feedback of relative angular positions. Additionally, an aliasing filter is used to smooth and amplify the input signals, but this can generate an offset in the data. Figure 6.1 presents the flowchart of the stabilisation and balance control system implementation. Some of the unsuccessful experimental trials are given in Appendix C.

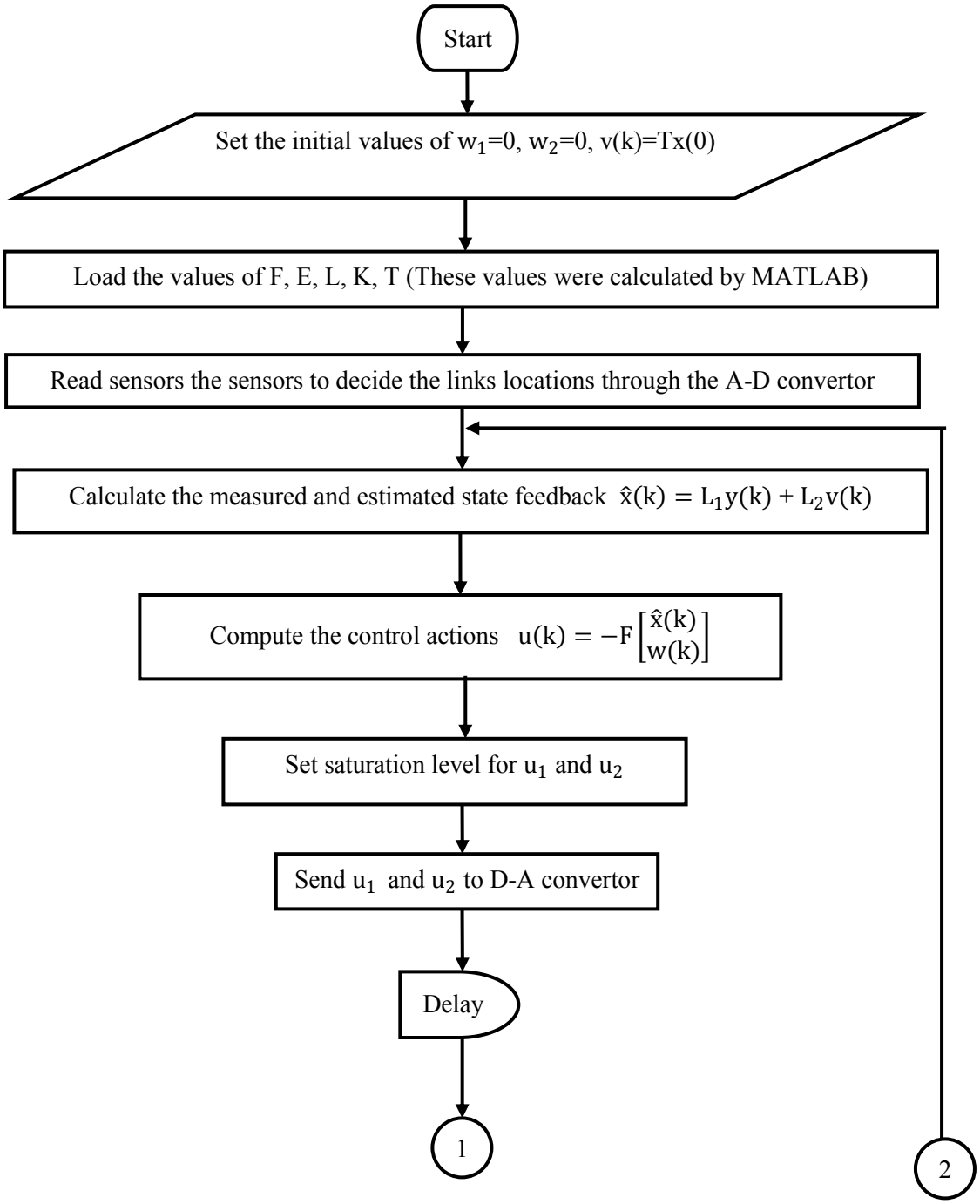
Start
Set the initial values of w_1=0, w_2=0, v(k)=Tx(0)
Load the values of F, E, L, K, T (These values were calculated by MATLAB)
Read sensors the sensors to decide the links locations through the A-D convertor
Calculate the measured and estimated state feedback $\hat{x}(k) = L_1 y(k) + L_2 v(k)$
Compute the control actions $u(k) = -F\begin{bmatrix}\hat{x}(k)\\ w(k)\end{bmatrix}$
Set saturation level for u_1 and u_2
Send u_1 and u_2 to D-A convertor
Delay
1
2

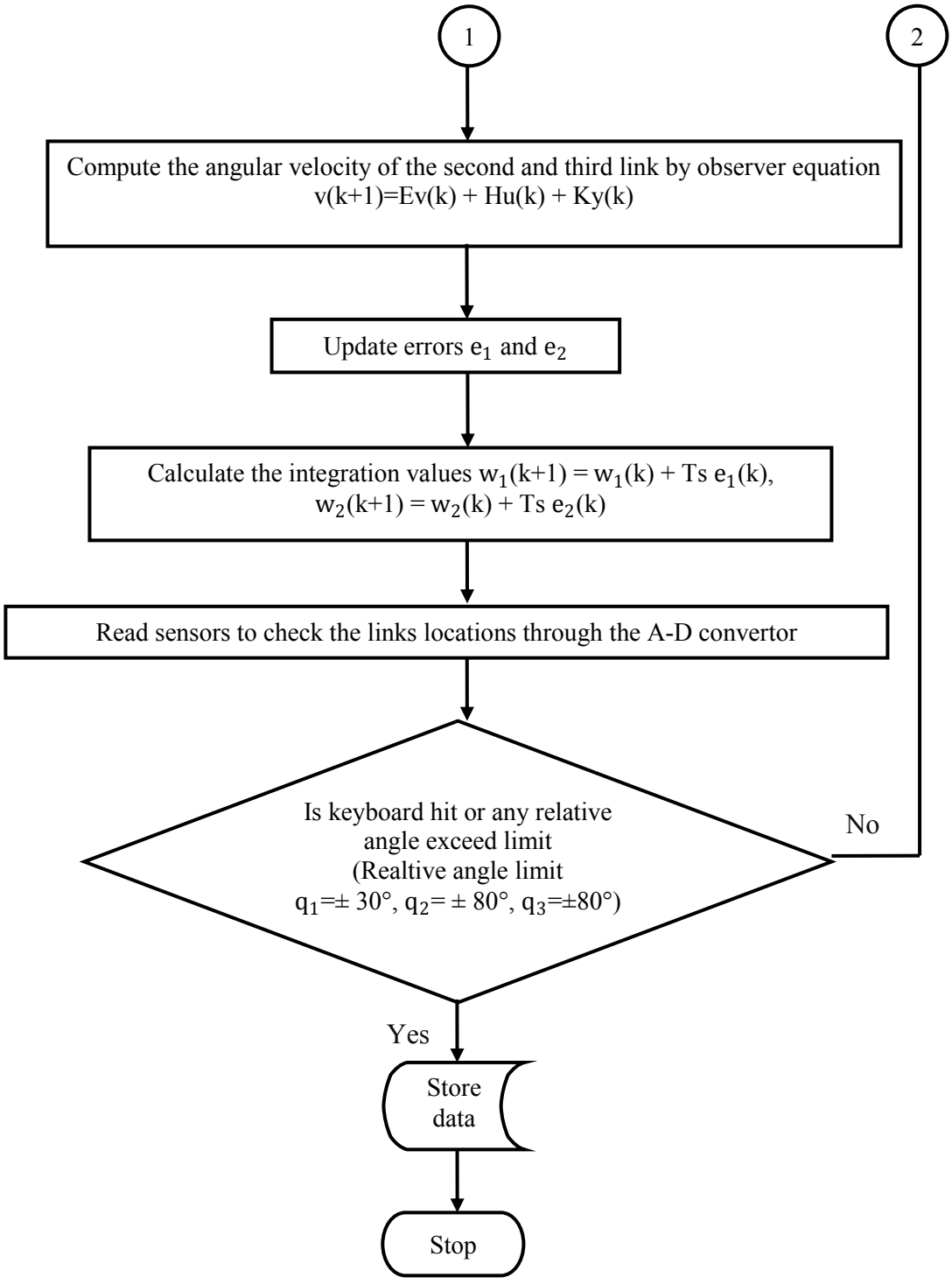

Figure 6.1: Flowchart of the stablise and balance control system implementation using the LQR

6.4 Limitations of simulation

Simulation was carried out to check the validity of the proposed controller in balancing the Robogymnast at the upright position. The simulation was conducted with the proposed designed controller. The results were presented to evaluate and assess the capability of the controller to achieve upright balancing. The selection of the weighting matrices and the reduced order dynamics were based on the gained experience from the attempts to implement the upright balancing of the real system. The upright balancing analysis was obtained by means of exploitation of MATLAB® software and its toolboxes. M-files were written by the author using the mathematical model of the Robogymnast in the upright configuration.

The main limitation of upright balancing control is how far the initial angles can be taken. For the purpose of analysing the challenges of the upright position, different initial situations have been considered to find the maximum recoverable initial angles. Consequently, the Robogymnast is kept stable around the upright position provided it does not exceed the maximum values of oscillation in each link. Three of the most probable initial configurations were utilised for analysing the balancing problem, as shown in Figure 6.2.

Simulations were conducted with multiple sets of initial conditions to describe the behavior of the system. This was conducted using the numerical model of the Robogymnast system in the upright position as described in Section 3.3 in Chapter 3.

The initial angles that will be used to test the designed controller can be listed as follows:

$$\begin{bmatrix}\theta_1\\ \theta_2\\ \theta_3\end{bmatrix} = \begin{bmatrix}1.1°\\ 0.9°\\ 0.8°\end{bmatrix} \text{ where the relative angular position } \begin{bmatrix}q_1\\ q_2\\ q_3\end{bmatrix} = \begin{bmatrix}1.1°\\ -0.2°\\ -0.1°\end{bmatrix}$$

$$\begin{bmatrix}\theta_1\\ \theta_2\\ \theta_3\end{bmatrix} = \begin{bmatrix}1.3°\\ 1.5°\\ -5°\end{bmatrix} \text{ where the relative angular position } \begin{bmatrix}q_1\\ q_2\\ q_3\end{bmatrix} = \begin{bmatrix}1.3°\\ 0.2°\\ -6.5°\end{bmatrix}$$

$$\begin{bmatrix}\theta_1\\ \theta_2\\ \theta_3\end{bmatrix} = \begin{bmatrix}1°\\ 1.1°\\ 1.2°\end{bmatrix} \text{ where the relative angular position } \begin{bmatrix}q_1\\ q_2\\ q_3\end{bmatrix} = \begin{bmatrix}1°\\ 0.1°\\ 0.1°\end{bmatrix}$$

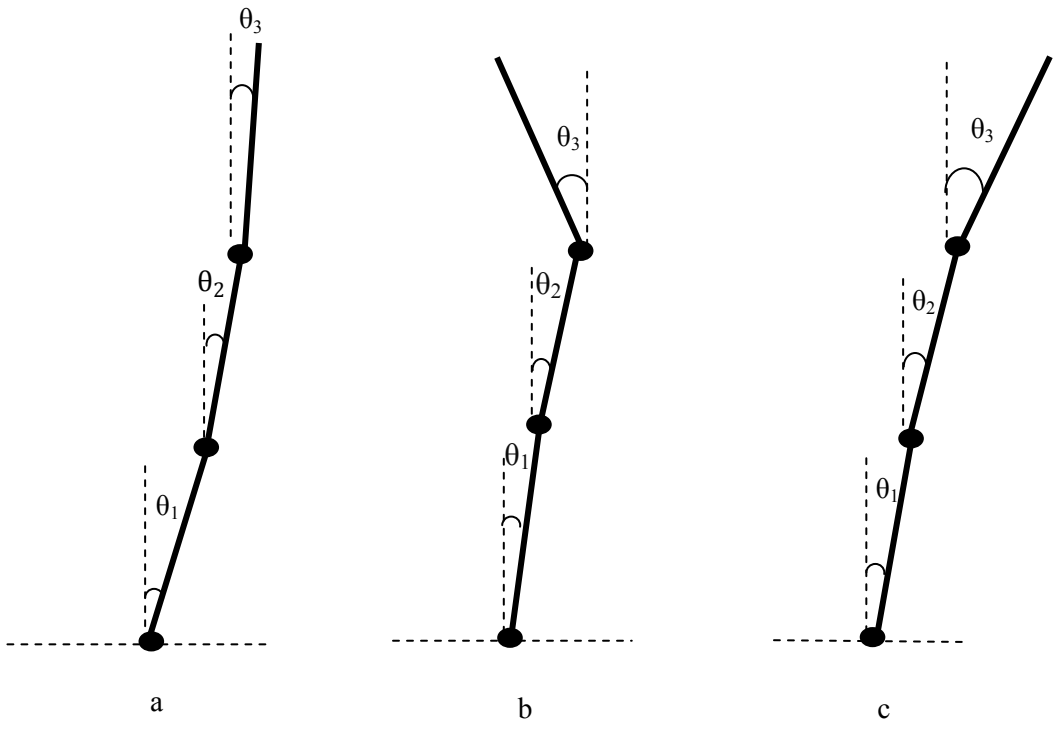

Figure 6.2: Different initial situations in the upright position

6.5 Simulation results using the LQR

In order to validate the designed controller's ability to attain upright balancing with the best selected values of the LQR weighting matrices and proper observer dynamics, the Robogymnast simulation was run with three sets of initial conditions.

In this investigation the reduced order observer dynamics were selected as $E = [0.5\ 0.5]$ and H was set zero. Apart from this, the best selected values of T, K and L are calculated as follows:

$$T = \begin{bmatrix} 0.316 & -0.344 & -0.041 & 0.013 & 0.017 & 0.002 \\ 0.655 & 0.394 & 0.048 & -0.035 & -0.019 & -0.002 \end{bmatrix}$$

$$K = \begin{bmatrix} 0.171 & -0.167 & -0.020 & 0.014 \\ 0.308 & 0.189 & 0.023 & -0.001 \end{bmatrix}$$

$$L = \begin{bmatrix} 1 & 0 & 0 & 0 & 0 & 0 \\ 0 & 1 & 0 & 0 & 0 & 0 \\ 0 & 0 & 1 & 0 & 0 & 0 \\ 0 & 0 & 0 & 1 & 0 & 0 \\ -1730.33 & 18.306 & 0.130 & 32.002 & 1979.86 & 1682.88 \\ 14222.6 & 17.270 & 22.754 & -275.144 & 15956.99 & -13979.7 \end{bmatrix}$$

To achieve the system performance requirements, the weighting matrices Q and R for the augmented plant model were chosen depending on the experience of the designer. The weight matrices Q and R are hence chosen as follows:

$$Q = \begin{bmatrix} 50 & 0 & 0 & 0 & 0 & 0 & 0 & 0 \\ 0 & 425 & 0 & 0 & 0 & 0 & 0 & 0 \\ 0 & 0 & 125 & 0 & 0 & 0 & 0 & 0 \\ 0 & 0 & 0 & 10 & 0 & 0 & 0 & 0 \\ 0 & 0 & 0 & 0 & 0.1 & 0 & 0 & 0 \\ 0 & 0 & 0 & 0 & 0 & 1 & 0 & 0 \\ 0 & 0 & 0 & 0 & 0 & 0 & 10 & 0 \\ 0 & 0 & 0 & 0 & 0 & 0 & 0 & 6 \end{bmatrix}$$

$$R = \begin{bmatrix} 0.7 & 0 \\ 0 & 0.5 \end{bmatrix}$$

According to the selected weighting matrices, the optimal feedback gain matrix F is given by:

$$\begin{bmatrix} -949.493 & -410.994 & -47.034 & -173.730 & -91.288 & -11.326 & 2.832 & 0.702 \\ -167.788 & -76.920 & 10.024 & -30.673 & -16.139 & -1.909 & 1.141 & -3.252 \end{bmatrix}$$

<u>Test 1:</u> Simulation results with initial relative angles of [1.1° -0.2° -0.1°]

At this stage of the investigation it was prescribed that the Robogymnast in the upright position had initial relative angular positions equal to [1.1° -0.2° -0.1°]. Figure 6.3 illustrates the controlled system response. It is clear that the designed controller was able to stabilise the system and converged to the set values. The control efforts of the first motor and the second motor of the system are illustrated in Figure 6.4 and Figure 6.5 respectively. It can be seen that the first link displacement had a stable response with acceptable overshoot, and a negative peak in relative angle of about -6.5°.

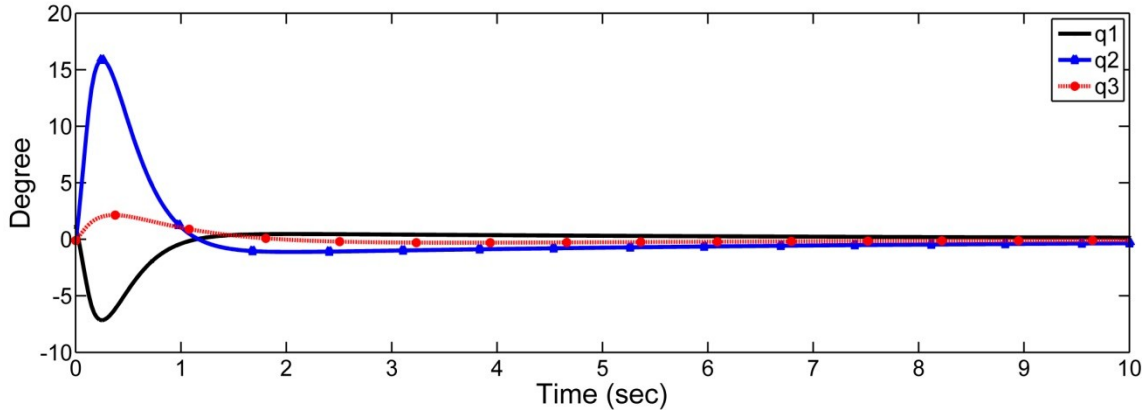

Figure 6.3: Simulated relative angular positions with initial q_1 =1.1°, q_2 = -0.2°, q_3 = -0.1°

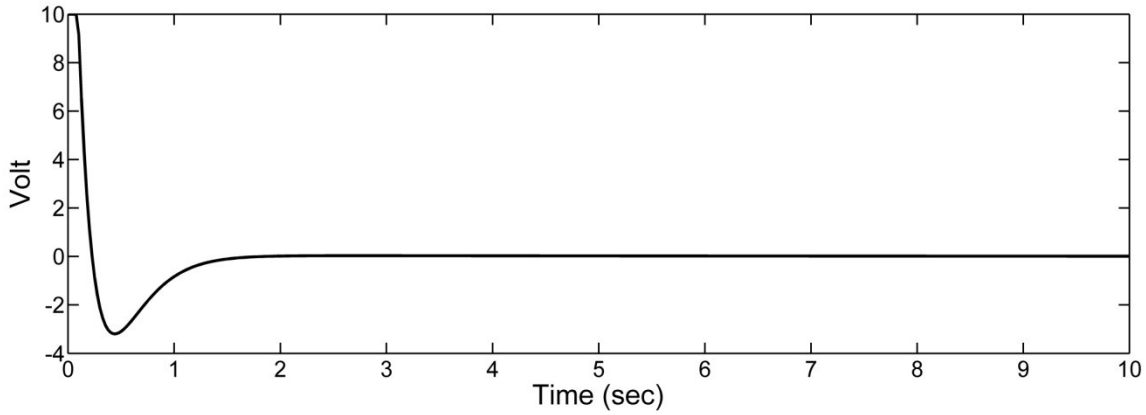

Figure 6.4: Simulated first control action with initial q_1 =1.1°, q_2 = -0.2°, q_3 = -0.1°

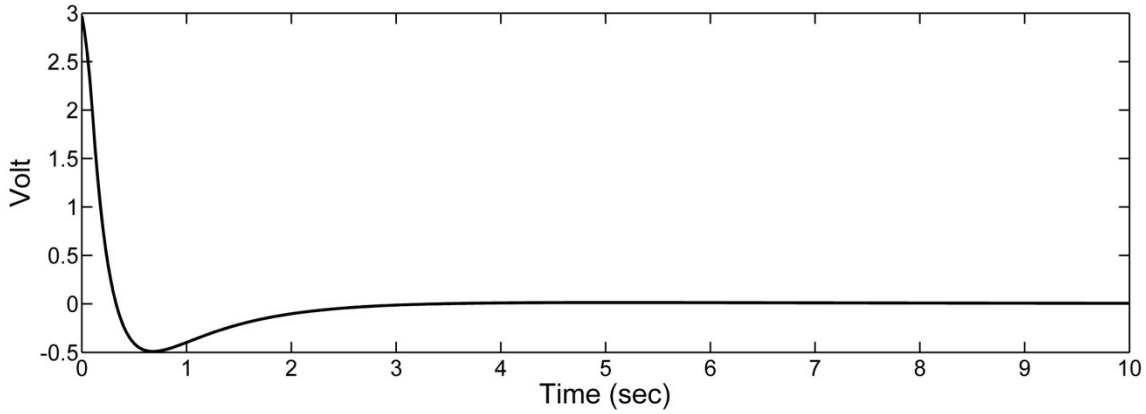

Figure 6.5: Simulated second control action with initial q_1 =1.1°, q_2 = -0.2°, q_3 = -0.1°

Additionally, it reached the settling point after approximately 10 seconds. In spite of the high deviation of the second link (about 15.5°) the controller was able to stabilise and balance the Robogymnast in the upright position.

Test 2: Simulation results with initial relative angles of [1.3° 0.2° -6.5°]

The transient and steady state response results are presented in Figure 6.6 with the assignment of initial relative angular positions equal to [1.3° 0.2° -6.5°]. In this case, the relative angular position of the first link overshoots to about -7.5° and the deviation in the second link's relative angle reaches about 17.5°.There is no significant overshot in the transient response of the third link. With these assumed values of the initial relative angles, it can be seen that the first and third links reached the steady state within 3.5 seconds, while the second link took 10 seconds. Figure 6.7 illustrates the first motor control effort used to stabilise the system. It is clear that the control effort begins at the saturation level. While the maximum control effort of the second motor is approximately 3.1 V as shown in Figure 6.8.

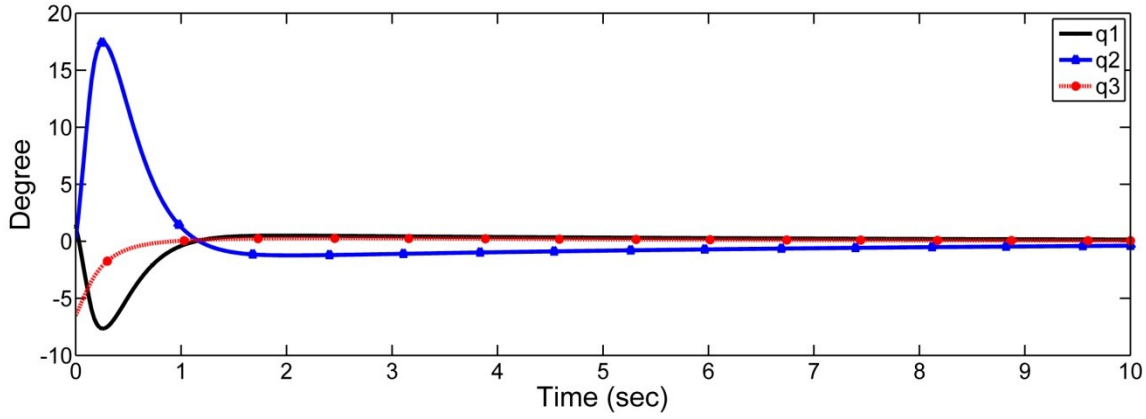

Figure 6.6: Simulated relative angular positions with initial q_1 =1.3°, q_2 = 0.2°, q_3 = 6.5°

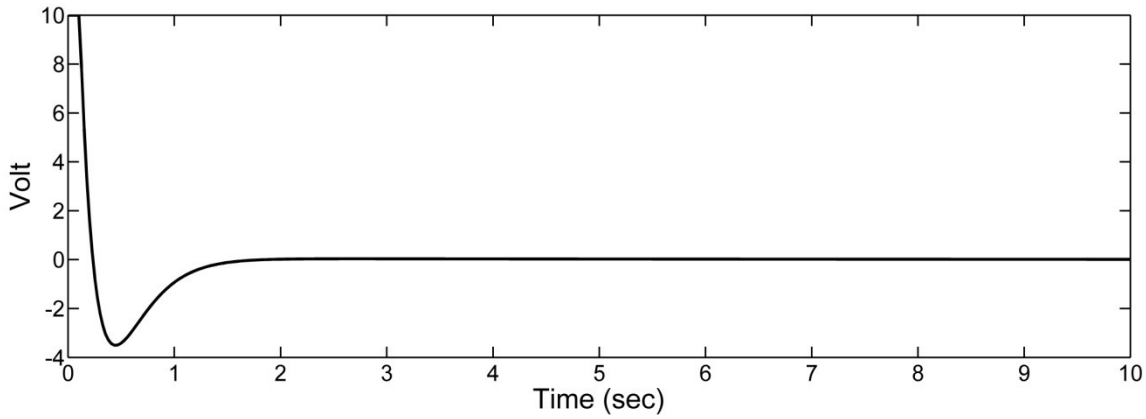

Figure 6.7: Simulated first control action with initial q_1 =1.3°, q_2 = 0.2°, q_3 = 6.5°

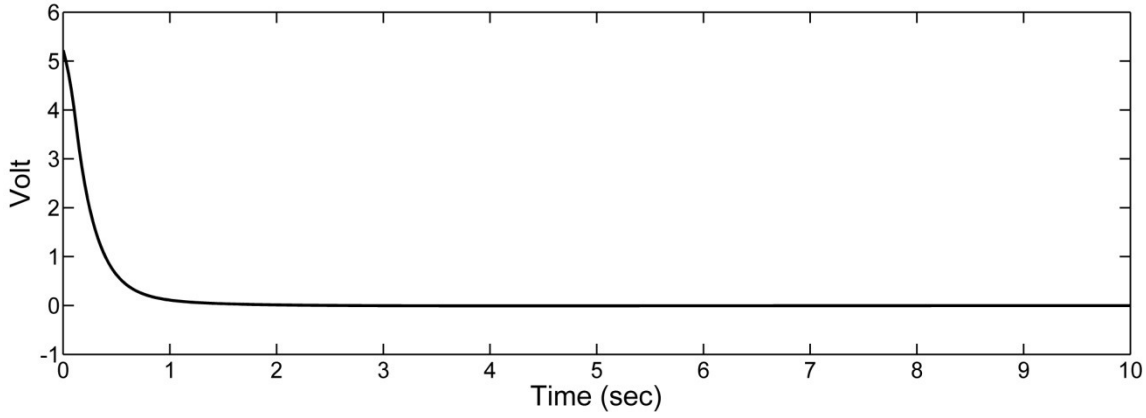

Figure 6.8: Simulated second control action with initial q_1 =1.3°, q_2 = 0.2°, q_3 = 6.5°

<u>Test 3:</u> Simulation results with initial relative angles of [1° 0.1° 0.1°]

In this stage of the study, the test was conducted according to the procedure used in the previous instances in Test 1 and Test 2. It should be noted from Figure 6.10 that the control action of the first motor initially reached the saturation value of 10V. From the data in Figure 6.11, it is apparent that the control action of the second motor was within the supply voltage limitation, with a maximum voltage of about 2.7V. The corresponding simulation transient and steady state results of the Robogymnast's links are presented in Figure 6.9. Further analysis showed that the Robogymnast returned to the full vertical balance point after approximately 9 seconds.

6.6 Simulation results using a combination of the LQR and LC

In this control strategy, as was mentioned in Section 5.3.2 in Chapter 5, the first motor and second motor will be controlled through the LQR and PI controllers respectively.

For this study, the observer dynamics were selected as $E = [0.3\ 0.3]$ and H was set to zero. In addition, the values of T, K and L are determined as follows:

$$T = \begin{bmatrix} 0.699 & 0.425 & 0.052 & -0.026 & -0.015 & -0.001 \\ -0.068 & 0.057 & 0.006 & -0.0004 & -0.002 & -0.0002 \end{bmatrix}$$

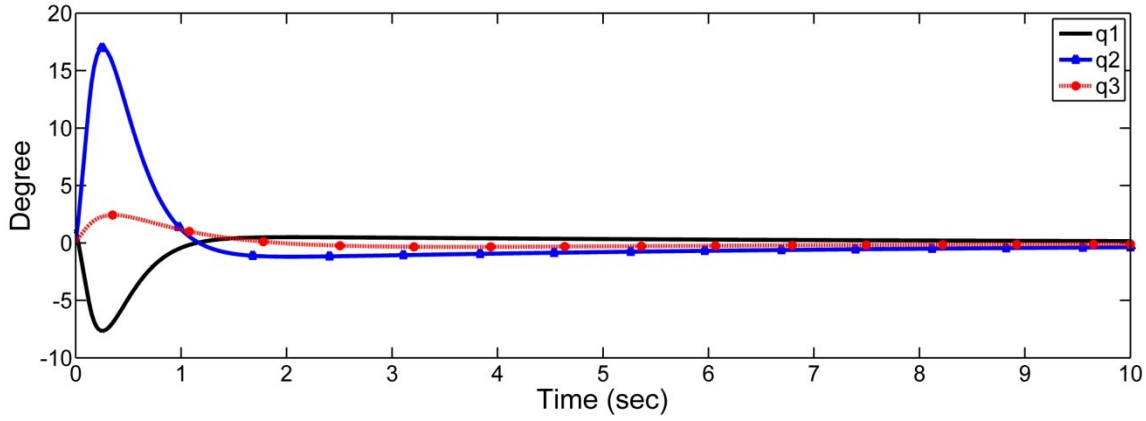

Figure 6.9: Simulated relative angular positions with initial $q_1 = 1°$, $q_2 = 0.1°$, $q_3 = 0.1°$

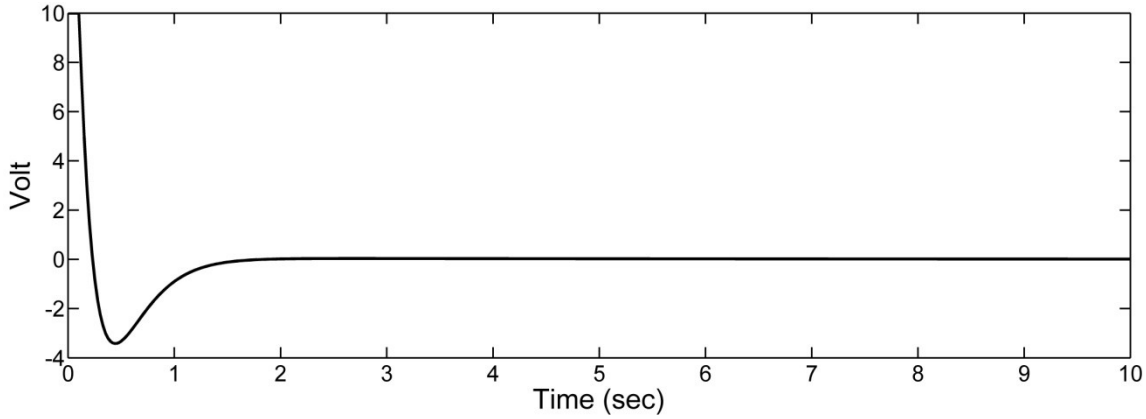

Figure 6.10: Simulated first control action with initial $q_1 = 1°$, $q_2 = 0.1°$, $q_3 = 0.1°$

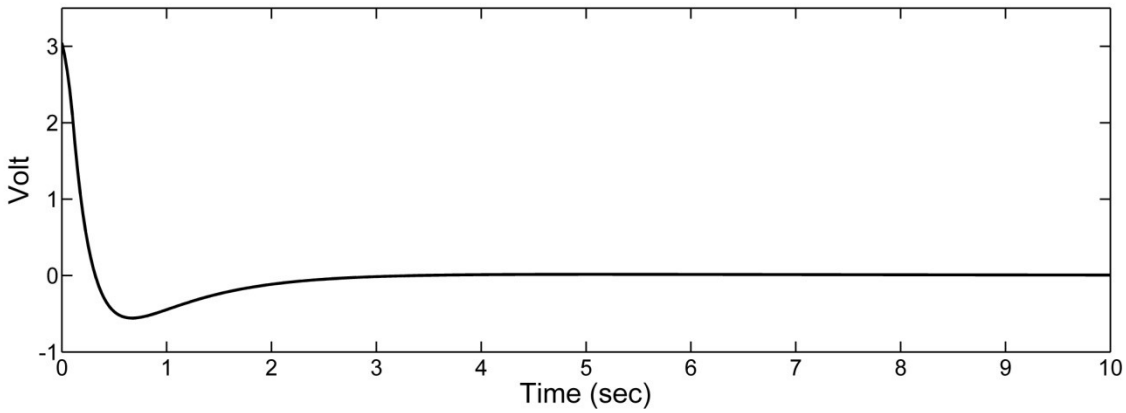

Figure 6.11: Simulated second control action with initial $q_1 = 1°$, $q_2 = 0.1°$, $q_3 = 0.1$

$$K = \begin{bmatrix} 0.476 & 0.292 & 0.036 & -0.001 \\ -0.048 & 0.039 & 0.004 & -0.002 \end{bmatrix}$$

$$L = \begin{bmatrix} 1 & 0 & 0 & 0 & 0 & 0 \\ 0 & 1 & 0 & 0 & 0 & 0 \\ 0 & 0 & 1 & 0 & 0 & 0 \\ 0 & 0 & 0 & 1 & 0 & 0 \\ -1234.927 & 26.695 & -0.130 & 23.027 & 995.186 & -7866.606 \\ 10360.701 & 12.250 & 29.243 & -200.416 & -8583.245 & 63609.954 \end{bmatrix}$$

The weight matrices Q and R were chosen through extensive trials, designer's intuition and experience. They are chosen as follows:

$$Q = \begin{bmatrix} 70 & 0 & 0 & 0 & 0 & 0 & 0 \\ 0 & 600 & 0 & 0 & 0 & 0 & 0 \\ 0 & 0 & 1 & 0 & 0 & 0 & 0 \\ 0 & 0 & 0 & 1 & 0 & 0 & 0 \\ 0 & 0 & 0 & 0 & 0.1 & 0 & 0 \\ 0 & 0 & 0 & 0 & 0 & 1 & 0 \\ 0 & 0 & 0 & 0 & 0 & 0 & 5 \end{bmatrix}$$

$$R = [0.5]$$

For this selection, the optimal gain matrix for the first motor is given by:

$$F = [-1128.683 \quad -493.795 \quad -54.451 \quad -206.494 \quad -108.541 \quad -13.455 \quad 2.536]$$

Moreover, the values of K_p and K_I have been selected as 12 and 2 respectively.

Test 1: Simulation results with initial relative angles of [1.1° -0.2° -0.1°]

It can be seen from Figure 6.12 that the first and second links reached the steady state after approximately 1.5 seconds, while there was no significant deviation in the third link from the vertical position. The angle of the first and second link from the vertical line had maxima of about -7.5° and 17° respectively. As shown in Figure 6.13, a lot of energy was used in the first motor to keep the system upright. Additionally, from this figure, it is clear that there was a high power demand at the start of the balancing operation where the control action began with the saturation level of 10 V. On the contrary, there is no considerable amount of energy expenditure in the second motor as shown in Figure 6.14.

Test 2: Simulation results with initial relative angles of [1.3° 0.2° -6.5°]

A further examination of balancing the Robogymnast is considered in this section with initial relative angular positions equal to [1.3° 0.2° -6.5°]. As noted in Figure 6.15, the maximum peak in oscillation of the first link was increased because of the initial value increment. The maximum relative angular deviation of the first and second links was about -8.5° and 19° respectively. Consequently, the settling time is increased, with the settling time of the second and third links being about 8 seconds, and the first link settled

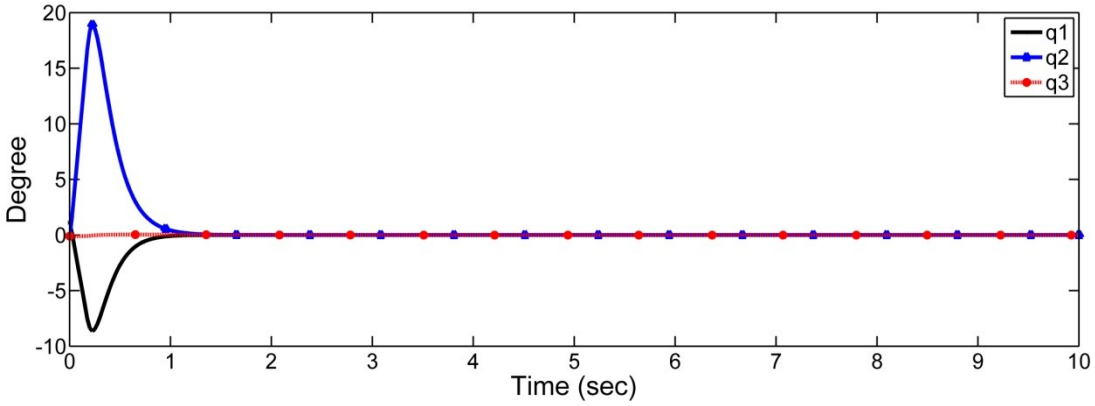

Figure 6.12: Simulated relative angular positions with initial q_1 =1.1°, q_2 = -0.2°, q_3 = -0.1°

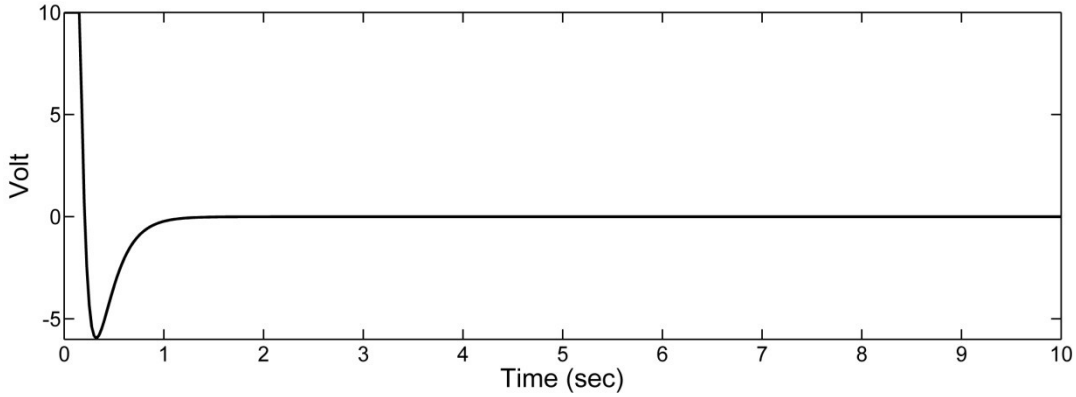

Figure 6.13: Simulated first control action with initial q_1 =1.1°, q_2 = -0.2°, q_3 = -0.1°

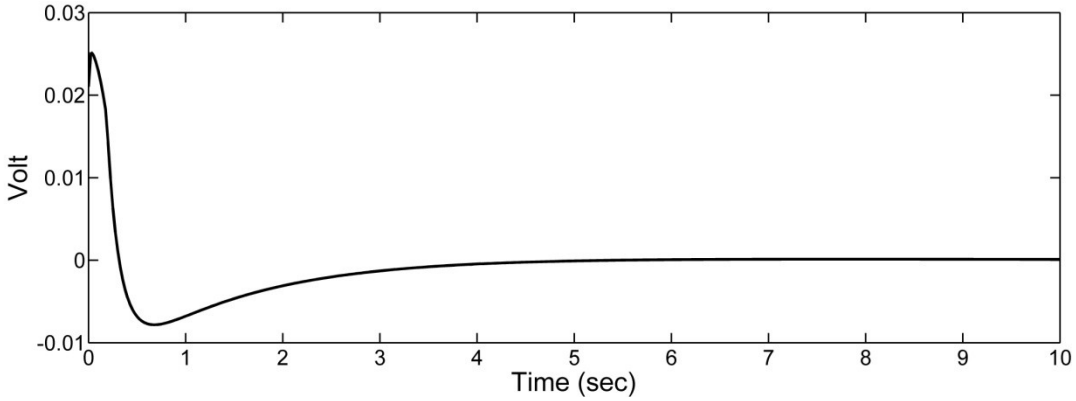

Figure 6.14: Simulated second control action with initial q_1 =1.1°, q_2 = -0.2°, q_3 = -0.1°

in about 10 seconds. On the other hand, a significant increase was noted in the control effort exerted by the first motor as shown in Figure 6.17. The control effort began with the maximum input voltage +10V. In order to keep the third link in line with the second link, more power is required from the second motor. Furthermore, the reason for increasing the initial control effort of the second motor, as presented in Figure 6.16, is due to the increments in the initial value of the third link.

Test 3: Simulation results with initial relative angles of [1° 0.1° 0.1°]

Further testing was conducted to determine the effect of initially starting all links of the Robogymnast system with positive relative angular positions. This was expected to produce a decrease in the upper limit of the initial value of the first link because all the system links slope in one direction, leading to an increases probability of falling under the effect of the gravity. Figure 6.18 illustrates the controlled system response. The overall Robogymnast's performance is similar to the response in Figure 6.12, with an increase in the maximum peak of the second relative angular position (19°). Movements in the third link were negligible. However, the controller was able to stabilise the system in the desired position within 1.5 seconds, with a maximum divergence of about -7.5° from the balance point in the first relative angular position. Figure 6.19 and Figure 6.20 provide the simulated control action applied to the motors. Figure 6.20 shows that no significant power was required from the second motor.

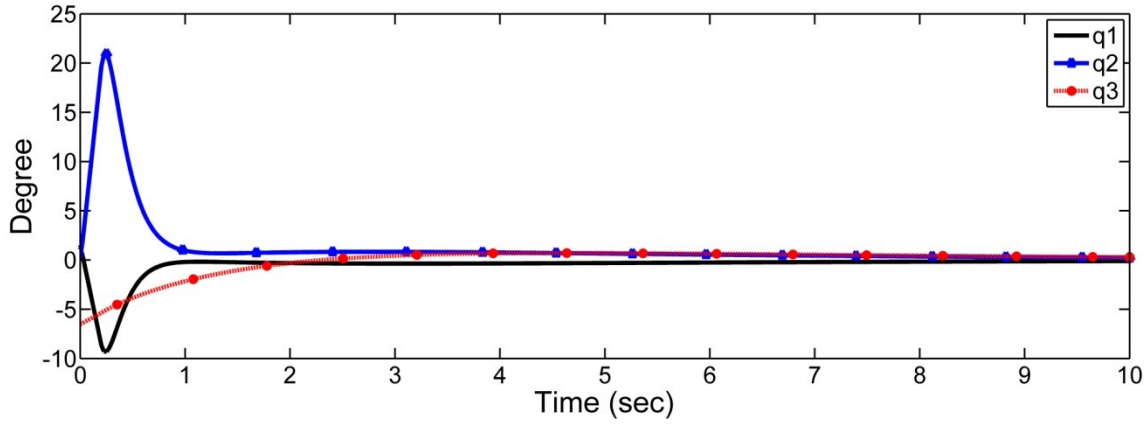

Figure 6.15: Simulated relative angular positions with initial q_1 =1.3°, q_2 = 0.2°, q_3 = -6.5°

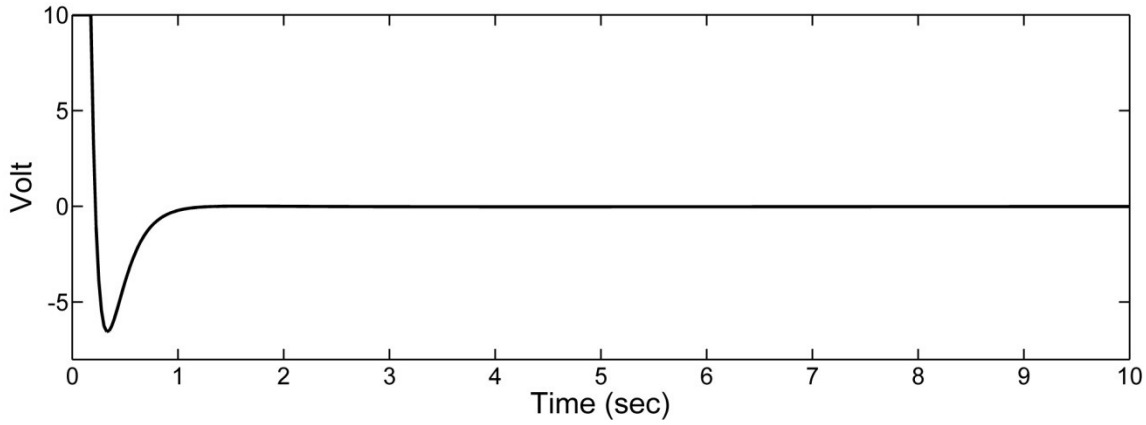

Figure 6.16: Simulated first control action with initial q_1 =1.3°, q_2 = 0.2°, q_3 = -6.5°

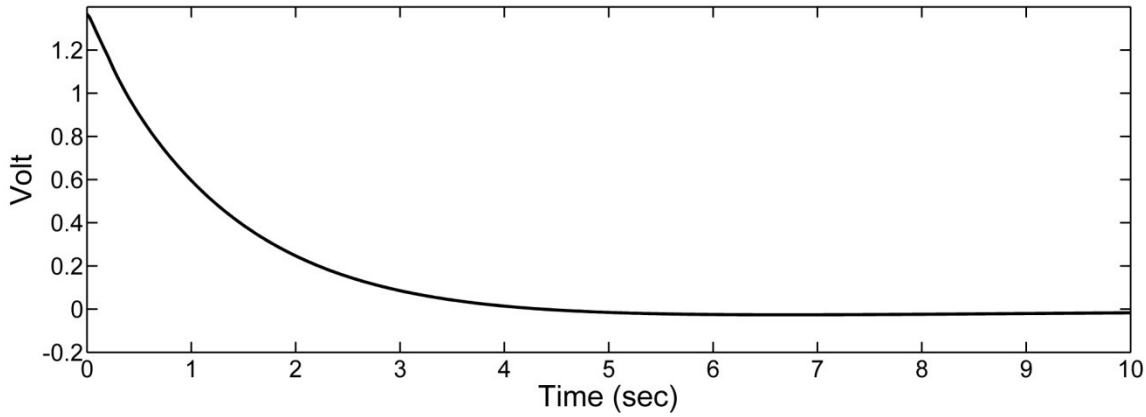

Figure 6.17: Simulated second control action with initial q_1 =1.3°, q_2 = 0.2°, q_3= -6.5°

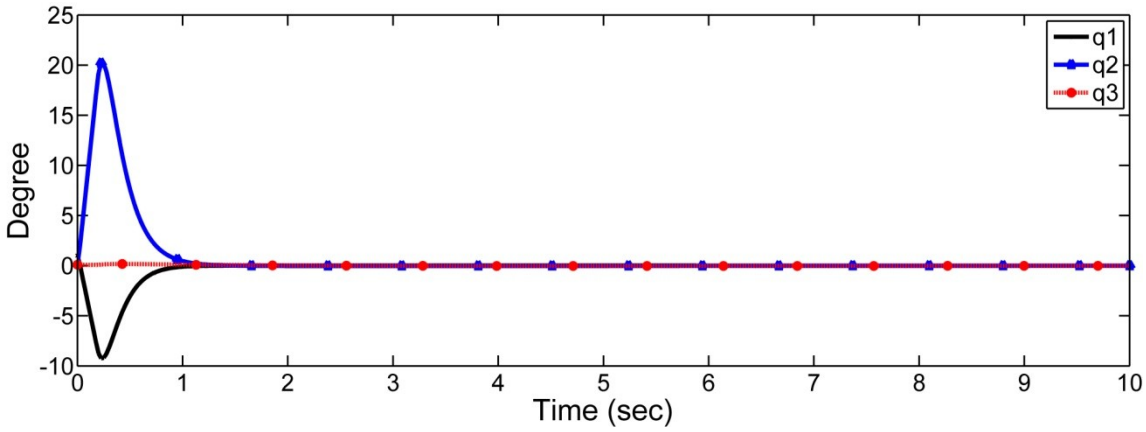

Figure 6.18: Simulated relative angular positions with initial $q_1 = 1°$, $q_2 = 0.1°$, $q_3 = 0.1°$

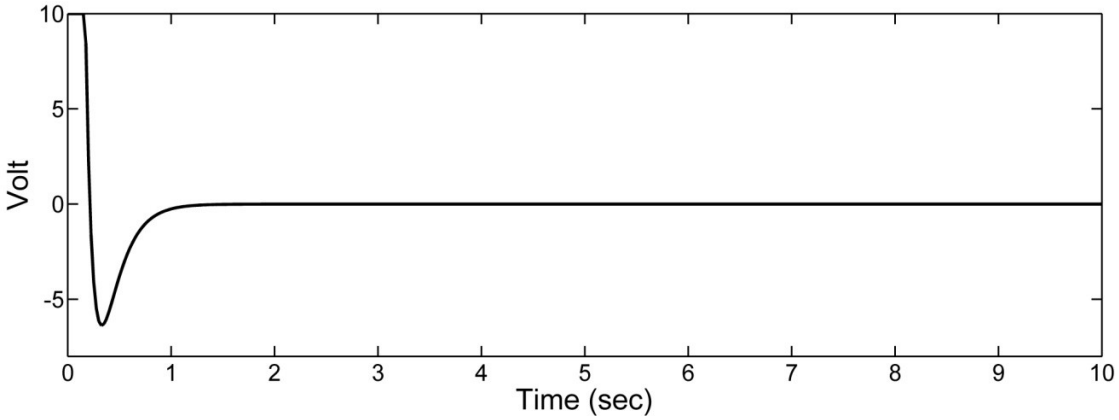

Figure 6.19: Simulated first control action with initial $q_1 = 1°$, $q_2 = 0.1°$, $q_3 = 0.1°$

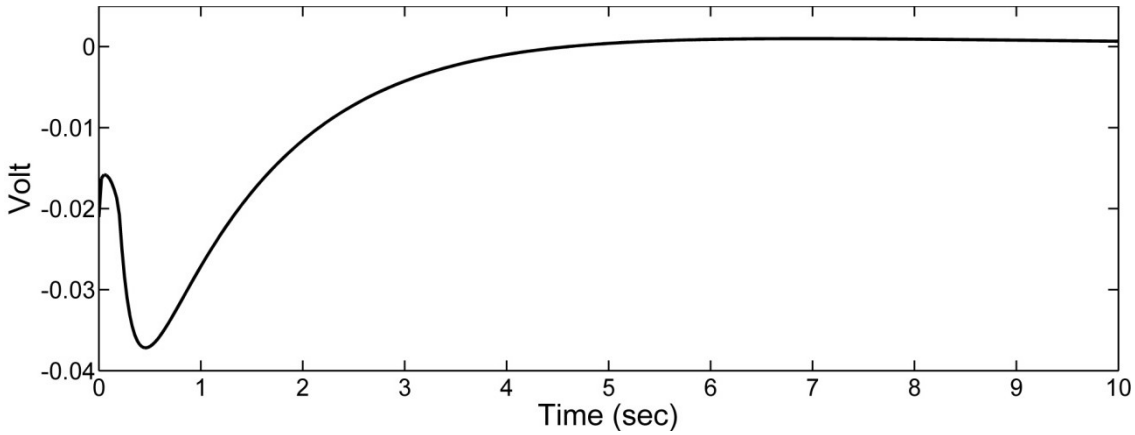

Figure 6.20: Simulated second control action with initial $q_1 = 1°$, $q_2 = 0.1°$, $q_3 = 0.1°$

6.7 Discussion of results

Based on feedback control theory, the offset error is generally seen as a factor strongly related to the upright balancing of the real system. Errors in the readings of the feedback signal will lead to a significantly incorrect value in the control action applied to the actuators. This control action could lead the Robogymnast to drift away from the desired upright balancing point.

Another type of controllable constant offset error was caused by the power amplifiers that were used to drive the Robogymnast. This error is treated by adding or subtracting a constant value from the control action signals before sending them to the A-D convertors and then to the motors.

More importantly, the power limitation of the Robogymnast's actuators cannot be disregarded. Difficulties arise when an attempt is made to implement the upright balancing. Practically the power limitation is not sufficient to enable the control system to maintain upright balancing. The limitations of the input control signals u(k) are due to the power limitation of the actuators (motors). Hence, the result of the response speed was affected by the power limitation.

Due to the linearisation of the system at the upright equilibrium point, there is an acceptable limit range for the relative angular positions. Therefore, the simulation study and analysis were focused on the upright balancing with different initial conditions (this practically represents the sensors' measurement errors). Hence, the simulation results

present the validation of the designed controller's ability to stabilise and balance the Robogymnast in the upright position within limited initial values of the links' deviation from vertical.

For the various (small) initial relative angles of the Robogymnast, it appears from Figures 6.3, 6.6, 6.9, 6.12, 6.15 and 6.18 that both designed controllers were able to stabilise the Robogymnast around the upright equilibrium point. Despite small initial relative angular positions, a large overshot appeared in the relative angular positions of the first and second links. From the identified data in the relative angular positions plot, it is reported that the maximum amplitude of the relative angle was approximately 7.5° for the first link, and 18° for the second links.

Comparison between the use of the LQR and the combination LQR and LC shows that the simulated upright balancing task is consistent with the practical findings of the downward balancing task in Chapter 5. From the system response, it can be seen that the system is ensured a much faster time to balance at the desired reference point when using the combination LQR and LC.

It is clear that at the start of each test the first motor demanded the maximum 10 V supply, regardless of which controller was used. This is despite the participating of the second motor. However, the control effort of the second motor is considerably less than the control effort for the first motor when using the second type of designed controller (LQR + LC).

6.8 Summary

The purpose of this chapter was to investigate the problem of balancing the Robogymnast in the upright position. There have been many attempts to implement the practical balancing. Here, the stabilising and balancing problem of the Robogymnast in the upward configuration was simulated. The first section focused on using the LQR to achieve the upright balancing, and the second section used LQR combined with an LC. The designed controller was applied via a reduced order observer to estimate the unmeasured states (angular velocities). According to the simulations, the Robogymnast is able to recover its balance from initial unbalanced configuration and balance itself in the vertical plane (upright configuration). A hybrid method is proposed by combining swing-up and balancing control in the next chapter.

Chapter 7

Combining Swinging-up and Balancing Control

7.1 Introduction

The aim of this chapter is to study the combination of the swing up of the Robogymnast from the pending position to balance in the upright position. Several studies investigating the problem of swinging, then balancing of an n-link underactuated robot have been carried out in the literature (Brown and Passino 1997; Spong 1995; Aoustin et al. 2011). In this study, a switching mechanism between a swinging and balancing algorithm was proposed. This can be achieved by dividing the controller into three stages. The first stage was a swinging controller and the next stage was implemented through designing a transition controller, which was implemented using independent PID joint control. Finally, the balancing controller was implemented utilising the proposed controller in Section 5.3.2 in Chapter 5. The simulations were carried out to mimic real life gymnasts and compared with the results of different Robogymnast situations. This chapter also presents the robustness of the designed controller and the ability to deal with unknown external disturbance.

The organisation of this chapter is as follows. In Section 7.2, the problem of combining the swinging and balancing control is discussed. Section 7.3 demonstrates the independent joint control idea. In Section 7.4, the proposed controller is described. The

movement from one place to another “Locomotion” of the Robogymnast is presented in Section 7.5. In Section 7.6, simulation results and discussion are presented. In Section 7.7, the robustness analysis through analysing disturbance force is studied. The summary of the chapter is given in Section 7.8.

7.2 Swing-up and balancing control combination problem

The main purpose of the swing up control is to drive the Robogymnast away from a point of stable equilibrium toward an inverted configuration and, to force the Robogymnast to enter the transition control region (transformed states region) with minimal speed to empower the balancing controller to hold it and maintain it steadily in the upwards position.

The main challenge posed by the Robogymnast is when the first link of the system reaches the upright position $q_1 = \pi$ (or $q_1 = -\pi$, depending on the direction of movement). The relative angular positions for the second and third link are diverted from the equilibrium point as shown in Figure 4.15 and Figure 4.16. The relative angular position of the second link was equal to 58° as presented in Figure 4.15, while the third relative angular position was equal to 70° as shown in Figure 4.16. In this case, it is extremely important to bring the second and the third link to the acceptable initial relative angles to start applying the adjusting balancing controller. Therefore, a transition controller using independent PID joint control was proposed to make the Robogymnast track the desired relative angular positions to start the balancing process. Therefore, a

switching algorithm was used to automatically switch between swinging control, then transition control and finally balancing control. The movement trajectories of the Robogymnast: Swing up, transition and balancing stages is presented in Figure 7.1.

Furthermore, there is another challenge which is determining suitable input control signals to motors located at joints 2 and 3 to obtain satisfactory tracking with a reasonable operating time without causing a falling of the Robogymnast from the upright position. The switching between the role of swinging and balancing should be performed smoothly.

In this chapter, the controller algorithm consists of three types of controller: the swinging controller (as described in Chapter 4), the upright balancing controller (as described in Chapter 6) and the transition controller (independent PID joint control). This design is presented in the next section. Through the use of MATLAB® software, the discrete time model Equation (3.20) was used to validate and evaluate the designed controller via the dynamic behaviour of all Robogymnast phases.

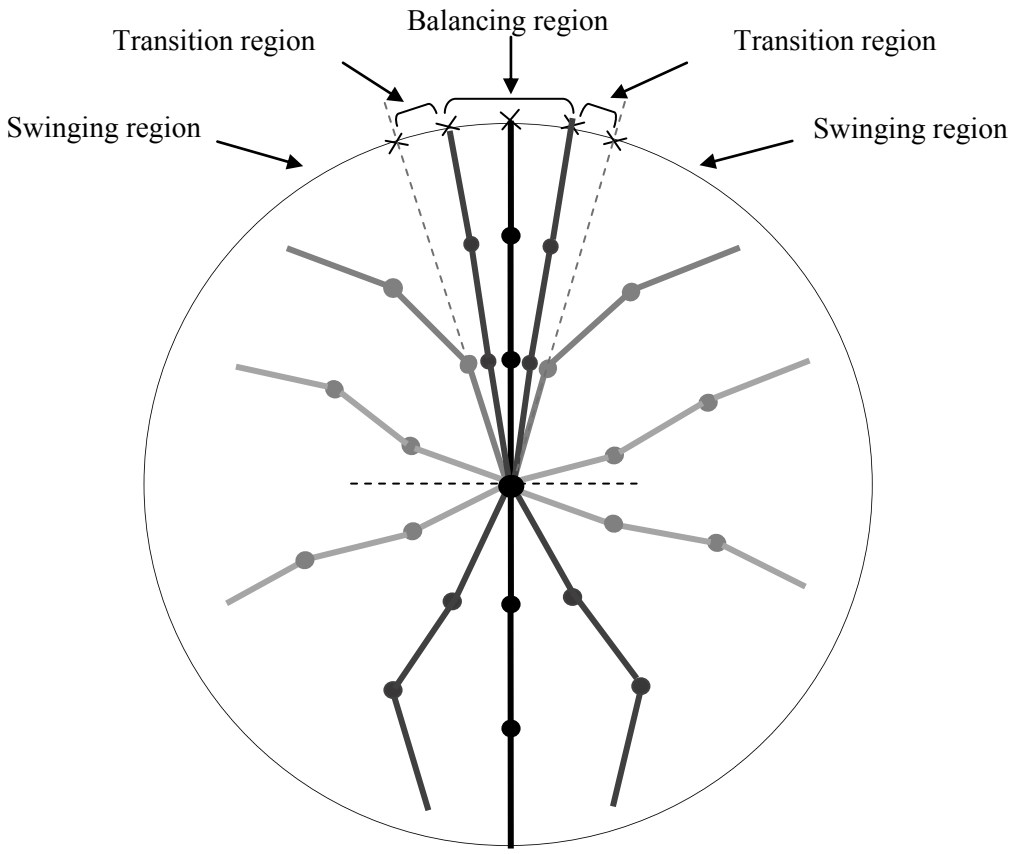

Figure 7.1: Movement trajectories of the Robogymnast : Swing up, transition and balancing

7.3 Independent Joint Control technique

The independent joint control (IJC) technique is one of the more practical ways to control the motion of the robot manipulator independently (Spong et al. 2006). The basic idea of the IJC is dealing with the robot actuators as a set of independent actuators. In other words, the control inputs of each actuator depend on the measured displacement and velocity of the corresponding joint. In this type of controller, the reaction and interaction with other joints is considered as a disturbance.

In this study, to achieve the transition controller, the PID controller was introduced as an independent joint controller (IJC) technique. The PID controller was used to satisfy the trajectory tracking path through transfer of the controlled joints from an initial position to the final position. The final position for each motor was set out using an independent PID joint control, which represents the initial angular positions of the second and third link in order to switch to start the balance control.

The strongest advantage of PID control is its straightforwardness and simplicity. This sort of controller is best in most procedures for the control of mechanical robot arms, if the execution improved by utilising complex control does not stand in different levels (Choi and Chung 2004). Design of the independent PID joint control involves deciding appropriate values of proportional, integral, and derivative gains to satisfy the design requirements.

7.4 Controller design

The control problem is how to combine swinging and balancing movements. Three proposed combined controller candidates for swinging, transition and balancing control were studied. The switching control scheme of the Robogymnast is shown in Figure 7.2. For the swinging control, the best selected result that was used to simulate the swing-up in Chapter 4 will be utilised in this chapter to drive the Robogymnast to the balancing area. For this study the equations of the input control signals are given as:

$$u_1 = A_1 \alpha \sin(\emptyset_1) \tag{7.1}$$

$$u_2 = A_2 \alpha \sin(\emptyset_2) \tag{7.2}$$

Where the values of A_1, A_2, α, η and δ were previously given in Section 4.2 in Chapter 4. As developed before, in the swinging part, $\emptyset_1$ and $\emptyset_2$ are dependent on δ. For the duration of each sinusoidal cycle (multiple sampling intervals T_s depending on the value of δ), $\emptyset_1$ and $\emptyset_2$ were varied between 0 and 2π with a step increment of η/δ applied during each sampling interval. η is constant and fractional to π. At the end of each duty cycle ($\emptyset_1$ and $\emptyset_2 = 2\pi$) α, δ were increased by $\Delta\alpha$ and $\Delta\delta$ respectively. By selecting the values of $\Delta\alpha$ and $\Delta\delta$ equal to 0.3499 and 4.1568 respectively, the first link gave a satisfactory response in a reasonable duration (128 seconds) as illustrated Figure 4.14 and the response of second and third link were presented in Figure 4.15 and Figure 4.16 respectively.

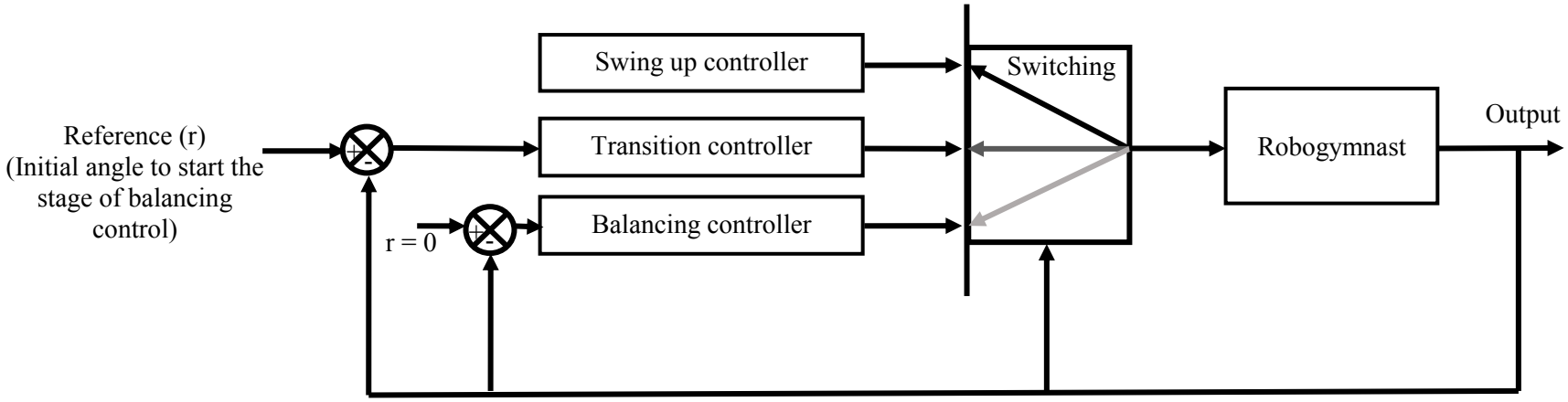

Figure 7.2: Switching control scheme of the Robogymnast

It is more important to focus on what is a realistic time to switch to the transition controller. However, if the transition controller waiting until the first link angle (q_1) reaches 0° (or $q_1 = \pm 180°$ depending on the initial angle of the swing up), this will cause the system to fall because the controller cannot compel the Robogymnast to stablise in the upright equilibrium point. Thus, it is very important to switch to transition control when the Robogymnast enters the upright balancing area. Consequently, switching from the swinging controller to the transition controller will start when the first relative angular position reaches 10°. The aim of switching is to make the second and the third relative angular positions in the acceptable range of the initial angle to start the stage of the balancing controller. The passive joint (first joint) is indirectly controlled by the motion of the active joints (second and third joints). The main problem, to satisfy movement or the ability to move from one place to another, is the selection of suitable reference trajectories for the control system which was developed in Section 6.4 in Chapter 6. Such trajectories should be periodic signals and allow smooth switching between the role of swinging and balancing which is achieved using an IJC technique for the second and third joints. To control the position of the Robogymnast at the upright position, the IJC is utilised to bring the second and third links from the last swinging states to the desired state to start the balancing (which is representing the desired initial values to start the balancing control). To use IJC, the first step is to define the desired references of the second and third links to start the balancing, and the actual states. y_{r_2} and y_{r_3} represent desired references of the second and third link respectively (desired initial relative angular positions to start the balancing). y_{i_2} and y_{i_3} represent the actual

relative angular position of the second and third link respectively. In this study, this represents the final actual values of the relative angular positions of the swinging stage. In this step, the equations of the input control signals for the transition controller using the Independent PID Joint Control are presented as:

$$u_1(k) = K_{p_1} e_1(k) + w_1(k) + d_1(k) \tag{7.3}$$

$$u_2(k) = K_{p_2} e_2(k) + w_2(k) + d_2(k) \tag{7.4}$$

where

$$e_1(k) = y_{r_2}(k) - y_{i_2}(k) \tag{7.5}$$

$$e_2(k) = y_{r_3}(k) - y_{i_3}(k) \tag{7.6}$$

K_{p_1} and K_{p_2} are the proportional gain of the first and second control input signals. The variables $e_2(k)$ and $e_2(k)$ represent the tracking errors, the difference between the desired reference y_{r_2} and y_{r_3} and the actual relative angular position y_{i_2} and y_{i_3} respectively.

$w_1(k+1)$ and $w_2(k+1)$ are defined as:

$$w_1(k+1) = w_1(k) + K_{I_1} T_s \; e_1(k) \tag{7.7}$$

$$w_2(k+1) = w_2(k) + K_{I_2} T_s \; e_2(k) \tag{7.8}$$

$w_1(k)$ and $w_2(k)$ are the integral values of the first and second error signals. K_{I_1} and K_{I_2} are the integral gain of the first and second control input signals. Ts is the sampling time.

Furthermore, $d_1(k)$ and $d_2(k)$ are given as:

$$d_1(k) = K_{d_1} \frac{e_1(k) - e_1(k-1)}{T_s} \tag{7.9}$$

$$d_2(k) = K_{d_2} \frac{e_2(k) - e_2(k-1)}{T_s} \tag{7.10}$$

$d_1(k)$ and $d_2(k)$ are the derivative values of the first and second error signals. K_{d_1} and K_{d_2} are the derivative gains of the first and second control input signals.

After the second and third relative angular positions of the Robogymnast are at the balancing desired initial values, the balancing controller is applied. For the balancing control, the LQR was considered in this study. The controller design is similar to the methodology used for the upright balancing in Section 5.3.2 in Chapter 5 with some insignificant modifications. These modifications include different values of the observer dynamics.

As presented before, the control signals applied to the Robogymnast for the balancing control are given by

$$u(k) = -F \begin{bmatrix} \hat{x}(k) \\ w(k) \end{bmatrix} \tag{7.11}$$

7.5 Locomotion

A controller algorithm which was designed to switch from a swing-up controller to a stabilizing controller is explained in three stages as follows:

- **Swinging Stage**

In this investigation, the swinging of the Robogymnast was simulated with $\Delta\alpha$ equal to 0.3499 and $\Delta\delta$ equal to 4.1568. According to the selected values of $\Delta\alpha$ and $\Delta\delta$, the Robogymnast reached the upright position $q_1 = \theta_1 = 0°$ (the swing-up starts with $q_1 = 180°$) within reasonable time duration (128 seconds). Whilst, the switching to transition should be started before the first relative angle (q_1) attains the 0° to avoid the collapse of the Robogymnast. Consequently, switching from the swinging to transition controller was started at $q_1 = 10°$.

- **Transition control stage**

When the first relative angular position becomes equal or more than 10°, the transition controller was activated. An independent PID joint controller was used to drive the second and third links to make them in line with the first and second links respectively. For independent PID joint control design, it is more important to find the best values of the PID gains ($K_{p_1}, K_{I_1}, K_{D_1}, K_{p_2}, K_{I_2}, K_{D_2}$).

It should be noted that it is very difficult to find accurate values of K_{p_1},K_{I_1} and K_{D_1} also K_{p_2}, K_{I_2} and K_{D_2} because they depend on each other. Thus, heuristically adjusted robust PID controller gains were investigated to satisfy desired performance through finding fast rise time, minimum overshoot and no steady-state error in the transient relative angular positions. The tracking references on the second and third relative angular positions are equal to 0.1° and 0.1° respectively, whereas they are representing the initial values to start switching to the balancing controller.

At this stage of verification, the control parameters were tuned heuristically with the gains in Table 7.1. The second part moves on to describe in detail the balancing control.

Table 7.1: PID controller gains

PID gains						**Duration time (second) of Transition controller**
First motor			**Second motor**			
K_{p_1}	K_{I_1}	K_{D_1}	K_{p_2}	K_{I_2}	K_{D_2}	
1	1.6	2	0.1	0.1	0.02	5.725
1	0.45	0.1	0.1	0.25	5	5
0.52	0.2	0.0001	1	0.3	0.0002	0.4

- **Balancing control stage**

As was mentioned in Section 5.2 in Chapter 5, there were two proposed designs for the controller to balance and stablise the Robogymnast in the upright position. In this study, the LQR was considered to balance the Robogymnast after the transition controller forces the second and third link to reach the initial relative angular positions to start the balancing. It is very important to note that the first relative angular position is affected by the control on the second and third joints. Consequently, the initial first relative angular position started with a value less than 1°. This value is various, this is depending indirectly on PID controller gains and how much the reaction forces from the second and third links influence on the first link motion. In this analysis, the reduced order observer dynamics were selected as $E = [0.1\ 0.1]$ and H was set to zero. In this case the values of T, K and L become:

$$T = \begin{bmatrix} -0.2302 & 0.2850 & 0.031 & 0.000 & -0.007 & 0.000 \\ 0.6349 & 0.1283 & 0.0181 & -0.01428 & -0.0035 & 0.000 \end{bmatrix}$$

$$K = \begin{bmatrix} -0.2093 & 0.2556 & 0.0279 & -0.0057 \\ 0.5668 & 0.1354 & 0.0160 & -0.0029 \end{bmatrix}$$

$$L = \begin{bmatrix} 1 & 0 & 0 & 0 & 0 & 0 \\ 0 & 1 & 0 & 0 & 0 & 0 \\ 0 & 0 & 1 & 0 & 0 & 0 \\ 0 & 0 & 0 & 1 & 0 & 0 \\ -739.57 & 35.244 & -0.075 & 13.739 & -556.977 & 962.706 \\ 6499.121 & 7.686 & 36.783 & -125.724 & 3937.257 & -8807.104 \end{bmatrix}$$

To achieve the system performance requirements, the weight matrices Q and R were chosen as follows:

$$Q = \begin{bmatrix} 50 & 0 & 0 & 0 & 0 & 0 & 0 & 0 \\ 0 & 425 & 0 & 0 & 0 & 0 & 0 & 0 \\ 0 & 0 & 125 & 0 & 0 & 0 & 0 & 0 \\ 0 & 0 & 0 & 10 & 0 & 0 & 0 & 0 \\ 0 & 0 & 0 & 0 & 0.1 & 0 & 0 & 0 \\ 0 & 0 & 0 & 0 & 0 & 1 & 0 & 0 \\ 0 & 0 & 0 & 0 & 0 & 0 & 10 & 0 \\ 0 & 0 & 0 & 0 & 0 & 0 & 0 & 6 \end{bmatrix}$$

$$R = \begin{bmatrix} 0.7 & 0 \\ 0 & 0.5 \end{bmatrix}$$

According to the selected weight matrices, the optimal feedback gain matrix F was given by:

$$\begin{bmatrix} -949.493 & -410.994 & -47.034 & -173.730 & -91.288 & -11.326 & 2.832 & 0.702 \\ -167.7886 & -76.9209 & 10.0244 & -30.6737 & -16.1395 & -1.9091 & 1.1418 & -3.2524 \end{bmatrix}$$

7.6 Simulation results

The controller was implemented using MATLAB® software. The overall program codes are to capture simulation parameters of $\Delta\alpha$ and $\Delta\delta$ of the swinging part, and PID gain values for the transition control. Additionally, the feedback gain matrices and the observer parameters were used to balance the control. When starting the swinging stage, the initial conditions of the first, second and third relative angular positions were 180°, 0° and 0° respectively. The transition control, however, started when the first relative angular position was equal to 10° or less, as well as the initial values to start the balance control when the transition control makes the relative angular positions of the second and third links equal to 0.1° and 0.1° respectively.

In order to understand how to find the best values of the transition control parameters, three different cases were performed. In other words, the parameters of the independent PID joint control were tuned to satisfy the desired performance. The conditions of the desired performance are limited to two constraints. The first one was the time duration to switch from the swinging stage to the transition stage until switching from the transition stage to the balancing stage. Secondly, the maximum overshoot in the first, second and third links.

From Figure 7.3 to Figure 7.8, the plots of the simulated relative angular positions of all links for the three cases of the designed controller are presented. The relative angle of the first link of the system was simulated while considering the parameters of all cases in Table 7.1 as shown in Figure 7.3. The time taken to reach 10° was 107 seconds and is equal for all cases because the same parameter was used to swing-up the Robogymnast. The more important parts of this analysis were depicted in Figure 7.4, which presents a zooming portion of transition control of Figure 7.3. It can be noted that the time duration of the transition control for the first case was 5.725 seconds as well as the first relative angular position (q_1) which oscillated with average relative angles equal to ±2° in the transition control period. Furthermore, it was diverted from the equilibrium point about $-4°$ in the balancing stage. For the second case, the time duration of the transition control equalled 5 seconds and the maximum average oscillation of the relative angular position of first link (q_1) was within the range of ±2°. For the third case, the first link transited from swinging to balancing in a very short time of 0.4 seconds with negligible oscillation.

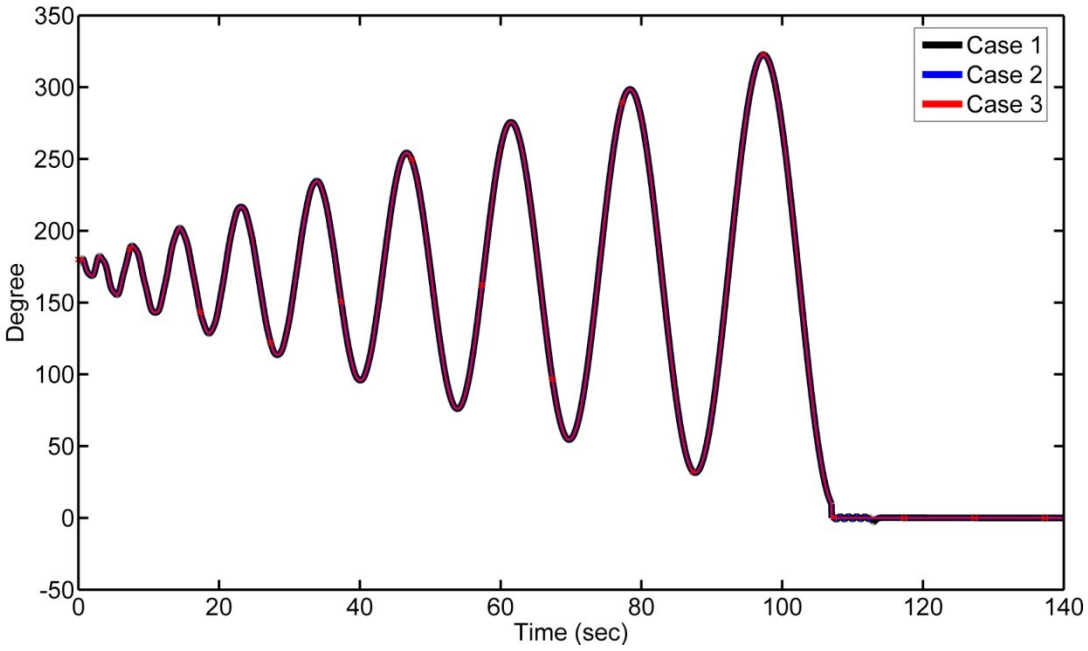

Figure 7.3: Simulated first relative angular position q_1

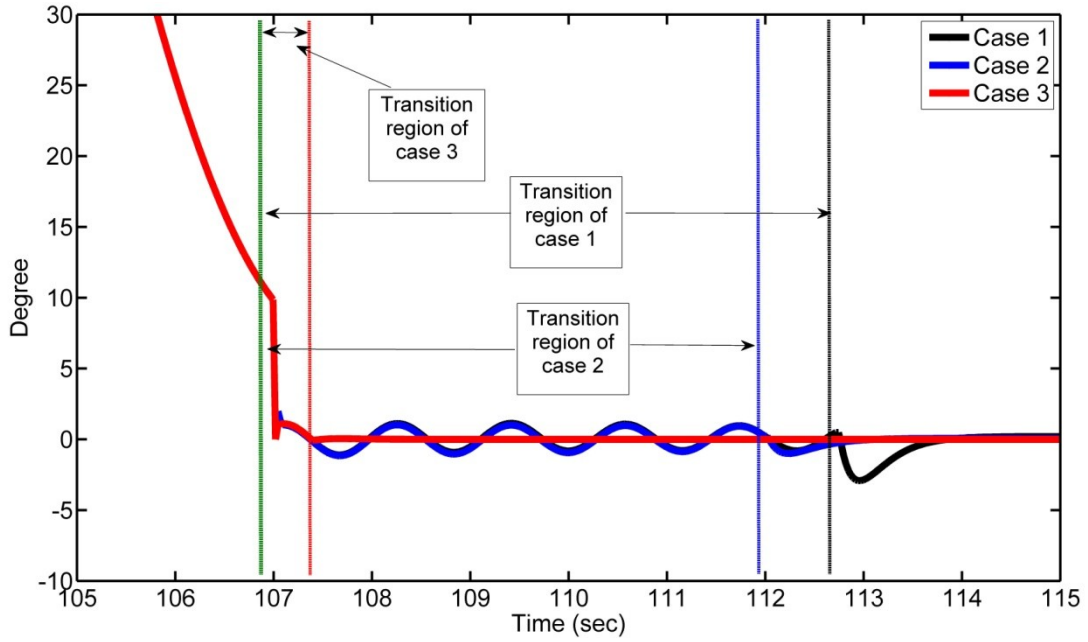

Figure 7.4: Zoomed view of simulated transition control part of first relative angular position q_1

Figure 7.5 and Figure 7.6 show the simulation response of the second relative angular position (q_2) with the three cases reported in Table 7.1. The time duration of the transition control of the second relative angular position was likely a result of the time duration of the first relative angular position (q_1). What is interesting in this data is that the second link diverted by 8° and 2° by considering the parameters in case 1 and case 2 respectively. On the other hand, by tuning the PID controller gains more to explore the best performance, case 3 reported significantly more enhancements in the behaviour of the second relative angular position. Hence, it can be seen from this figure that there is no significant movement reported in the second link and it tracks the reference trajectory of the second link in a very short time of 0.4 seconds. In the same way, in all cases, it can be seen from the information reported in Figure 7.7 and Figure 7.8 that there were no considerable movements reported in the third link with different transition control parameters. Interestingly, there were not any considerable diversions from the equilibrium point during the transition control or through the balancing stage.

Figure 7.9 to Figure 7.12 represent the simulated control signals in volt applied to the motors mounted at the respective joints. As can be seen from these controls signal plots that the first motor demanded more voltage than the second motor. The voltage required by the first motor to switch from the swinging control to transition control was equal to the saturation range of ±10V. In contrast, the required voltage of the second motor was very small compared to the first motor. Furthermore, the responses of the two motors appeared in the switching between the transition control stage and the balancing control

stage. Figure 7.13 presents the flowchart of switching control mechanism implementation.

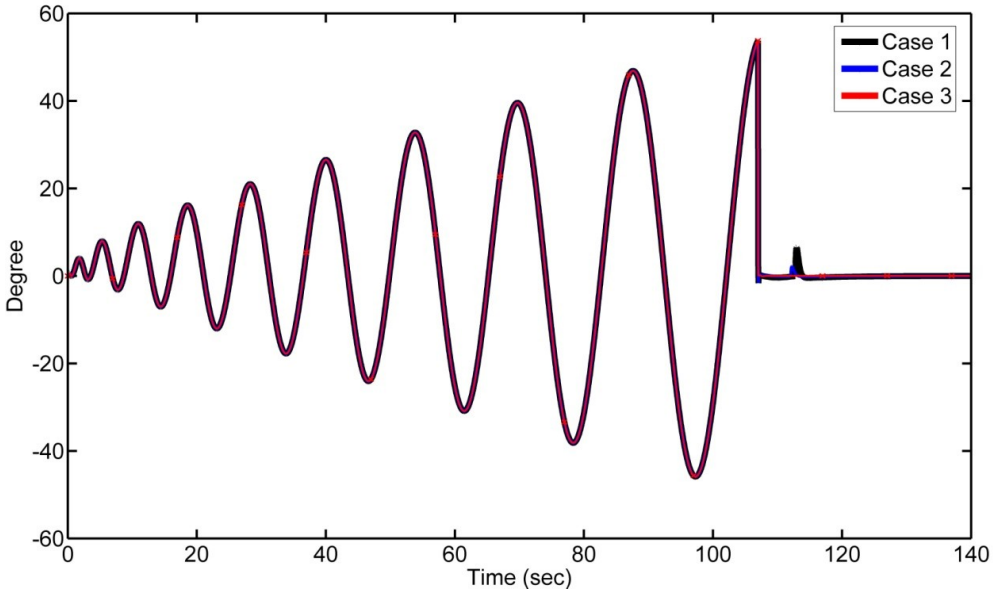

Figure 7.5: Simulated of second relative angular position q_2

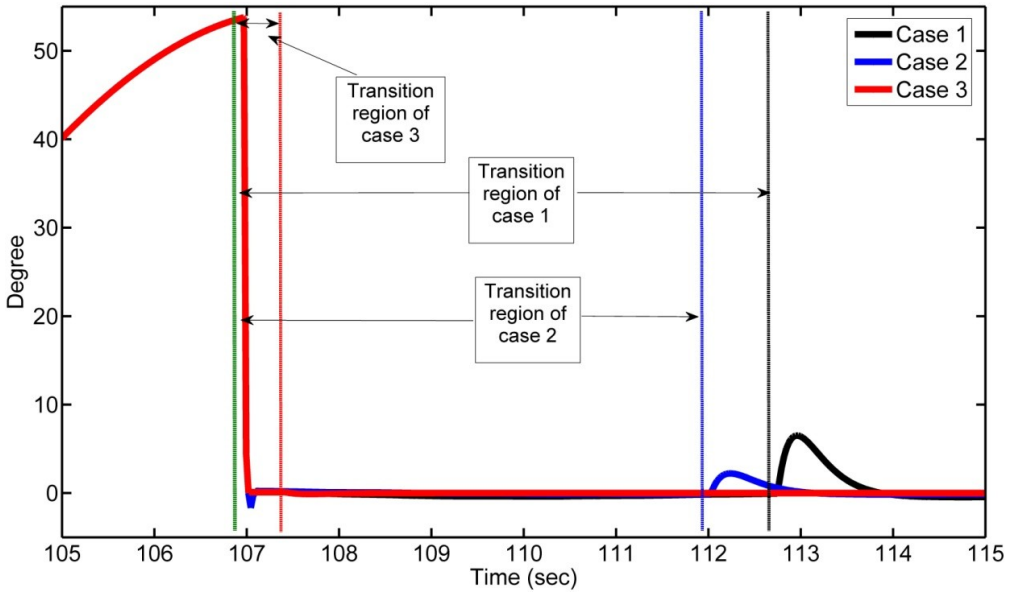

Figure 7.6: Zoomed view of simulated transition control part of first relative angular position q_2

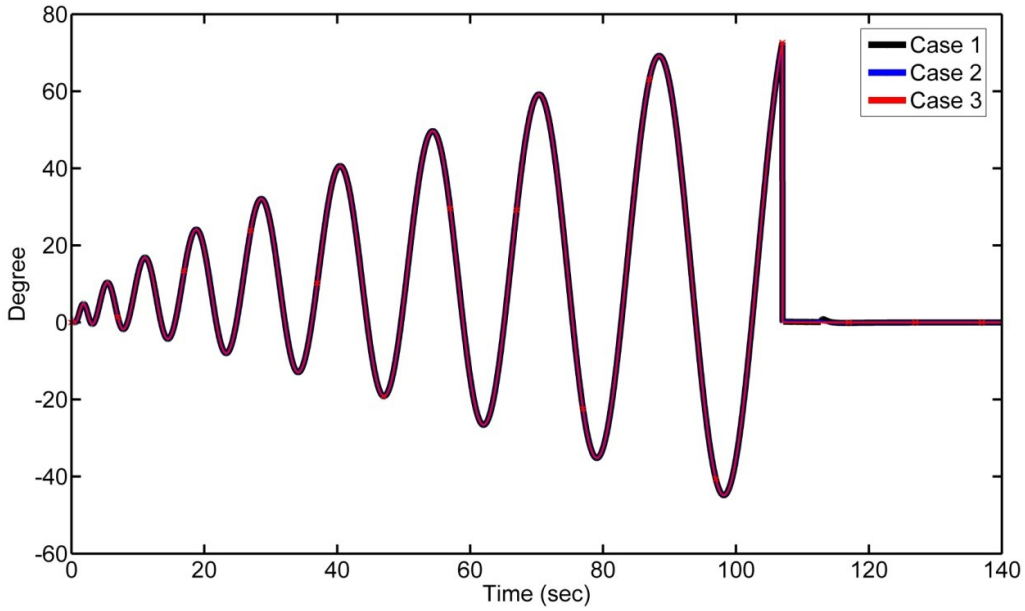

Figure 7.7: Simulated of second relative angular position q_3

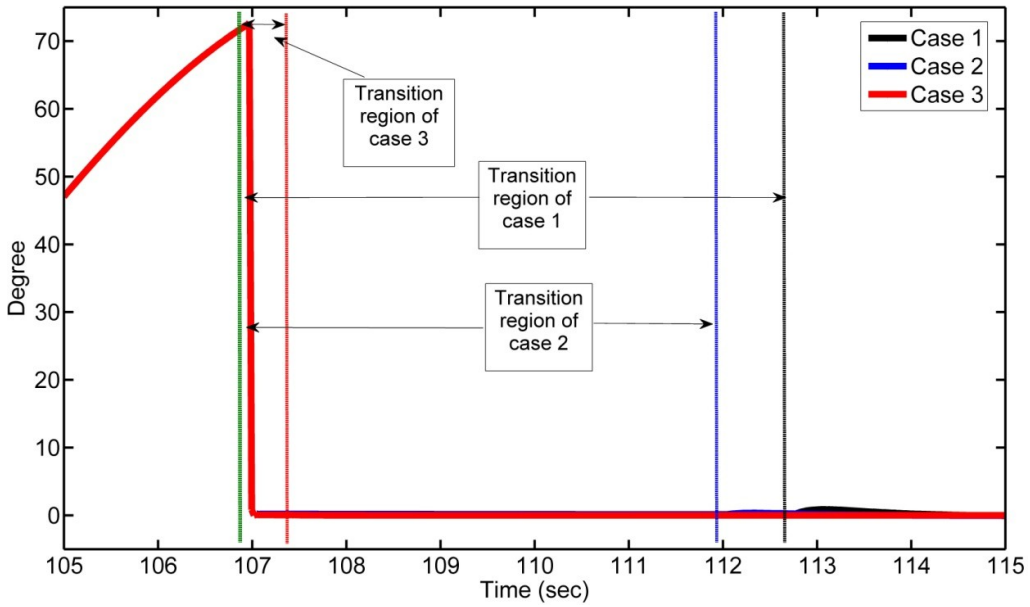

Figure 7.8: Zoomed view of simulated transition control part of first relative angular position q_3

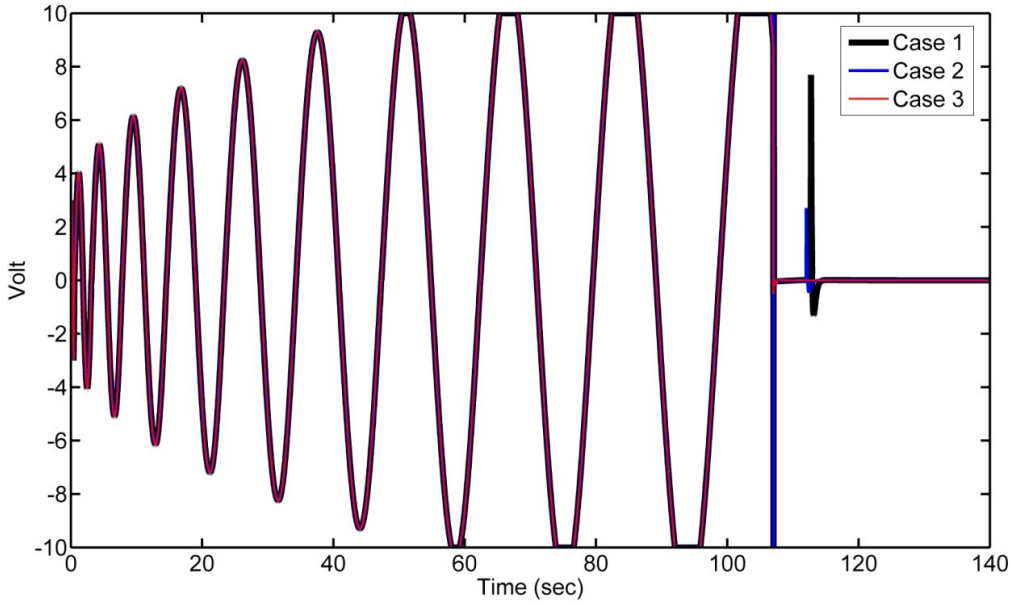

Figure 7.9: Simulated control action applied to first motor u_1

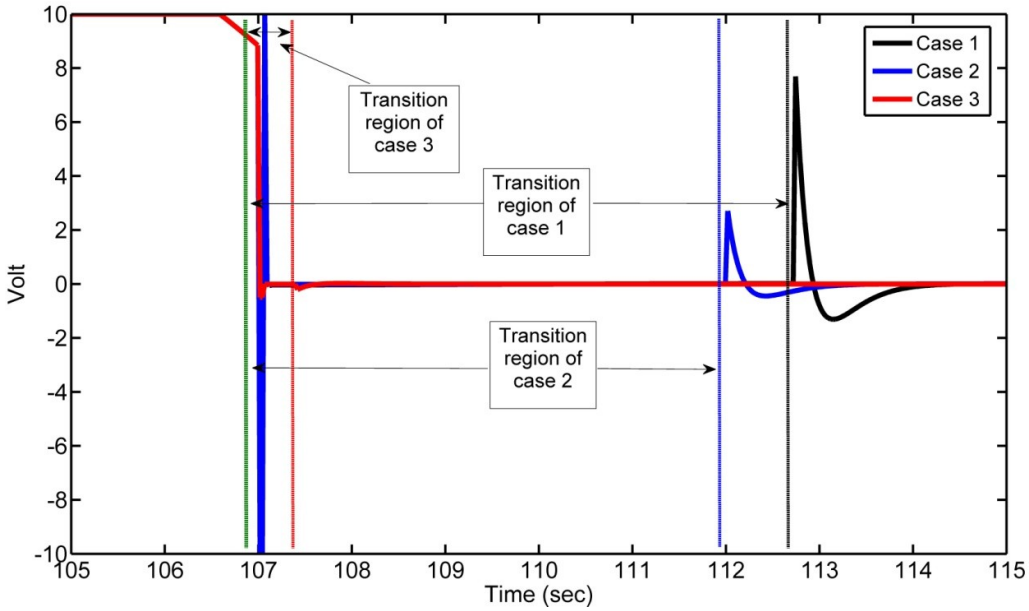

Figure 7.10: Zoomed view of simulated transition control part of control action applied to first motor u_1

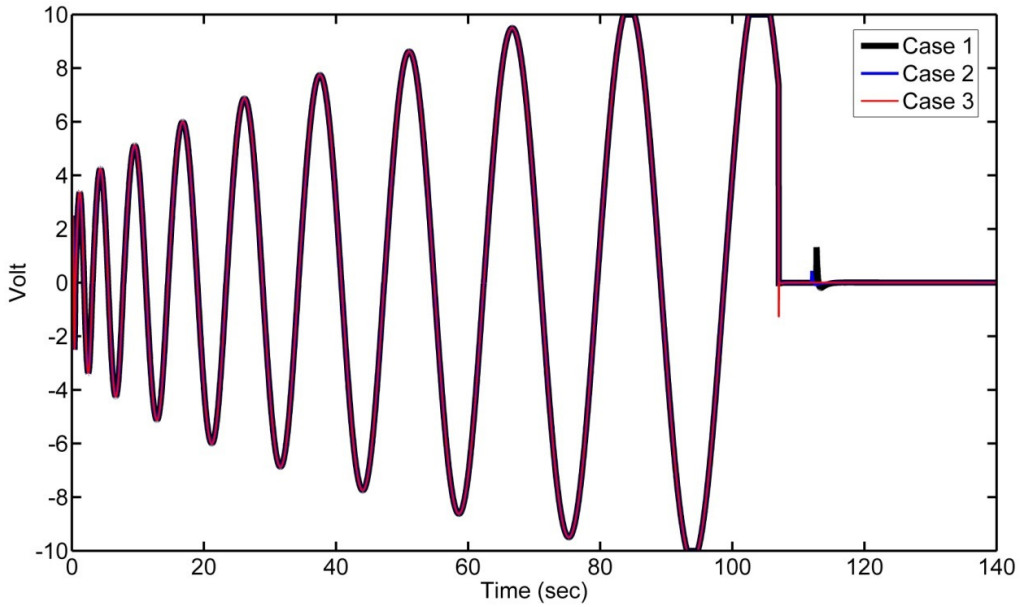

Figure 7.11: Simulated control action applied to first motor u_2

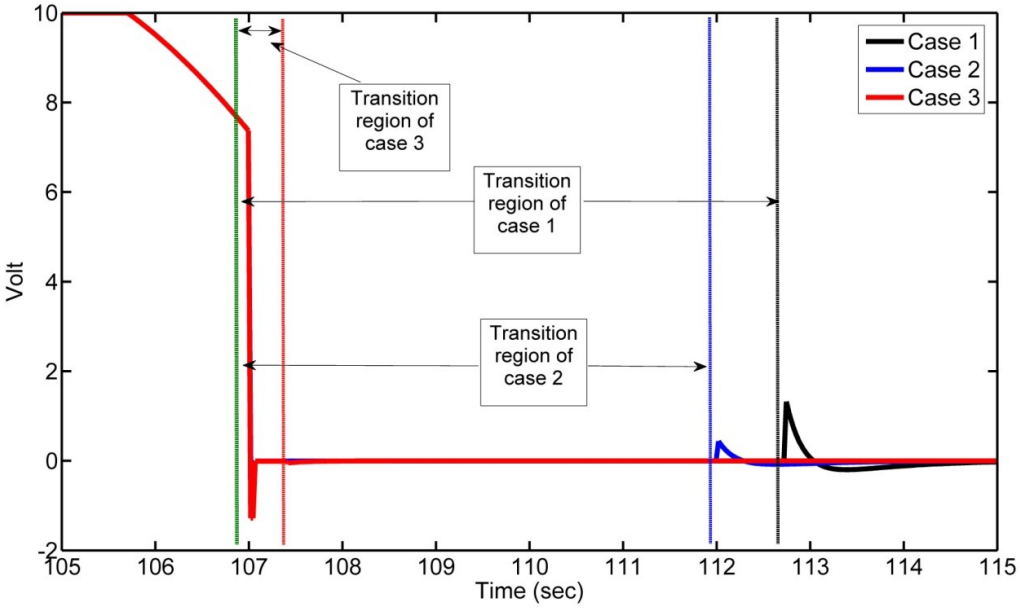

Figure 7.12: Zoomed view of simulated transition control part of control action applied to first motor u_2

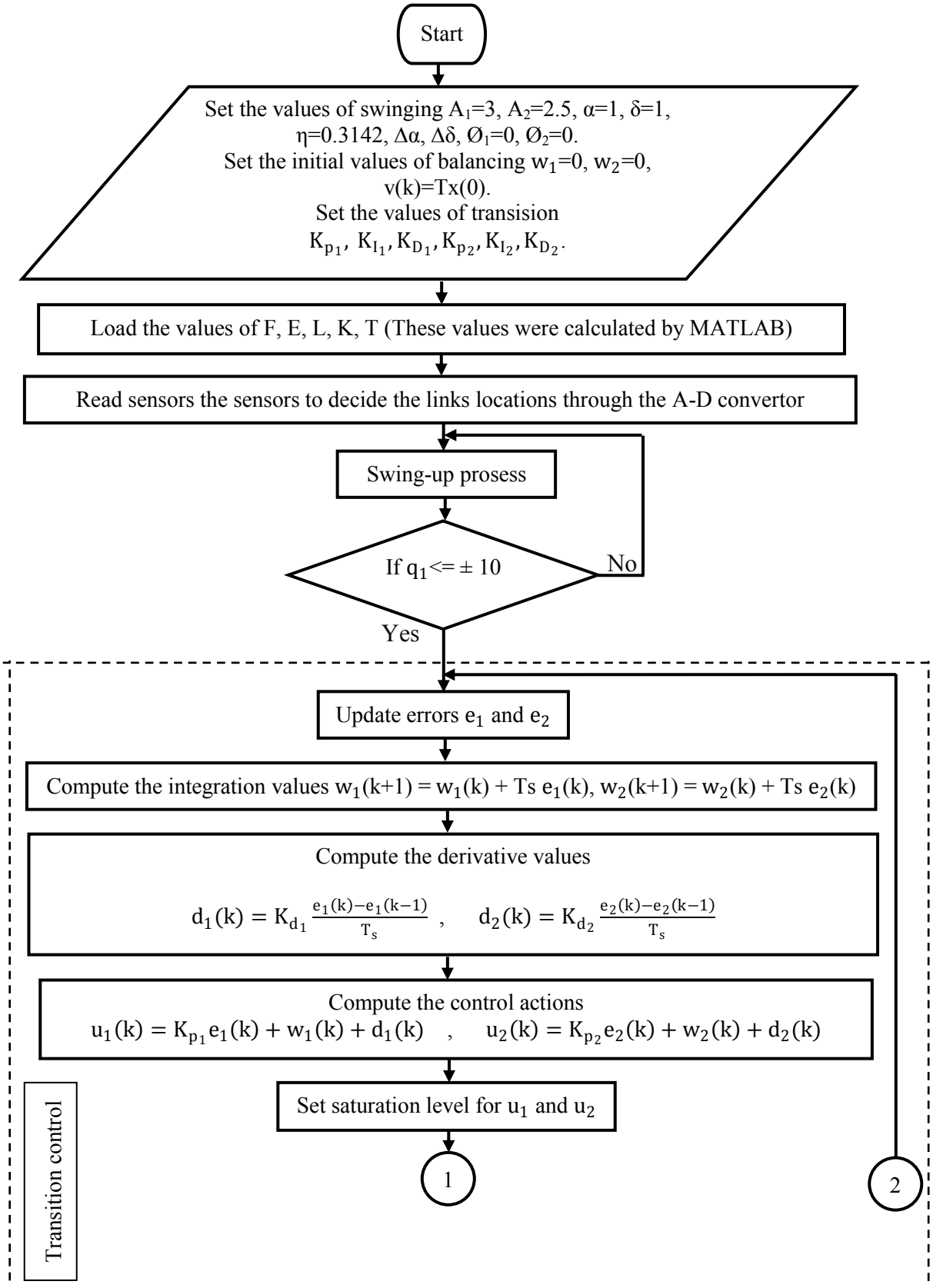
Start
Set the values of swinging A_1=3, A_2=2.5, α=1, δ=1,
η=0.3142, Δα, Δδ, $Ø_1$=0, $Ø_2$=0.
Set the initial values of balancing w_1=0, w_2=0,
v(k)=Tx(0).
Set the values of transision
$K_{p_1}, K_{I_1}, K_{D_1}, K_{p_2}, K_{I_2}, K_{D_2}$.
Load the values of F, E, L, K, T (These values were calculated by MATLAB)
Read sensors the sensors to decide the links locations through the A-D convertor
Swing-up prosess
If q_1<= ± 10
No
Yes
Update errors e_1 and e_2
Compute the integration values $w_1(k+1) = w_1(k) + Ts\ e_1(k)$, $w_2(k+1) = w_2(k) + Ts\ e_2(k)$
Compute the derivative values
$d_1(k) = K_{d_1} \frac{e_1(k)-e_1(k-1)}{T_s}$, $d_2(k) = K_{d_2} \frac{e_2(k)-e_2(k-1)}{T_s}$
Compute the control actions
$u_1(k) = K_{p_1} e_1(k) + w_1(k) + d_1(k)$, $u_2(k) = K_{p_2} e_2(k) + w_2(k) + d_2(k)$
Set saturation level for u_1 and u_2
1
2
Transition control

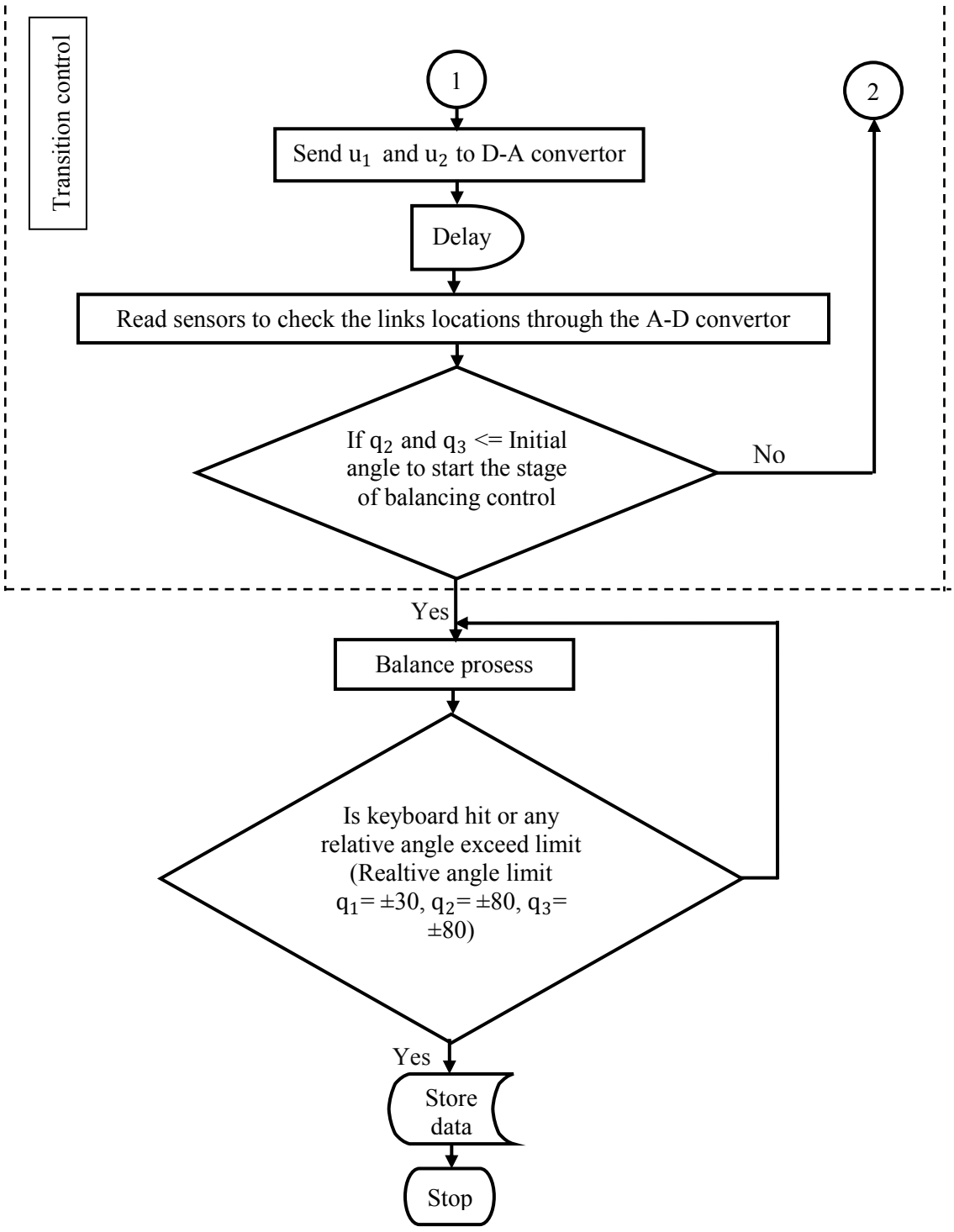

Figure 7.13: Flowchart of switching control mechanisim

7.7 Control system response under disturbance

In this section, the robustness of the designed controller to stablise the Robogymnast at upright balancing is discussed through studying the ability of the designed controller to deal with unknown external disturbance (Almeshal et al. 2013; Brown and Passino 1997). After the swing-up phase of the Robogymnast and then stablising in the upright position, disturbance was introduced on each link of the system separately, which led to three cases being analysed. The disturbance was applied after 138.75 seconds from the startup of the swinging for each case. To determine the greatest magnitude of disturbance which could be applied to each link, an extensive search was done through repeating the process several times. For the purpose of analysis, the behaviour of the Robogymnast was plotted and discussed through showing instant response for all links for each case. In addition, the effect of the introduced disturbance on the control actions was discussed. The corresponding control loop including disturbance is shown in Figure 7.14.

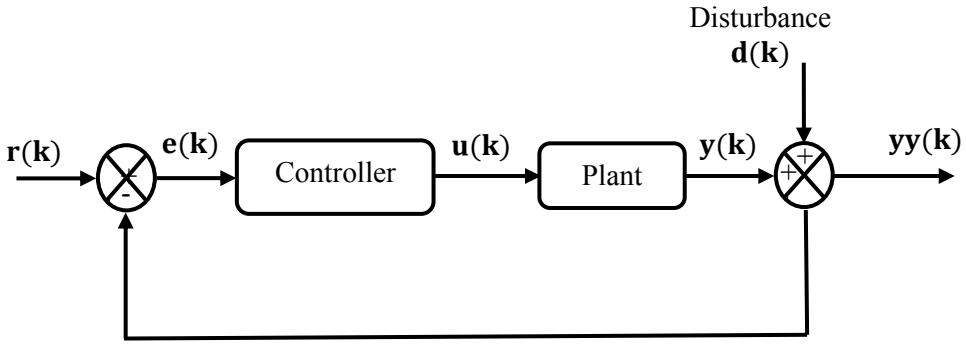

Figure 7.14: Block diagram of closed loop system including disturbance

The output of the closed loop system in terms of the disturbance is reported as below:

$$yy(k) = y(k) + d(k) \tag{7.12}$$

where d(k) represents the disturbance acting on the system outputs.

7.7.1 Applying a disturbance to the first link

In order to validate the ability of the designed controller to keep the Robogymnast in the upright position, a disturbance force was applied to the first link of the Robogymnast. It was found that the controller could stablise the system with an applied disturbance that tilted the first link by 0.4°. All the movement stages of the Robogymnast (swinging, transition, balancing and applying disturbance) are shown in Figure 7.15, which presents the simulated relative angular positions with applied disturbance on the first link. From the zoomed view of simulated relative angular positions with disturbance applied on the first link in Figure 7.16, it can be seen that the disturbance produced negative and then positive peaks at the displacement of the first link with values equal to -2° and 7.5° respectively. On the other hand, a significant deviation occurred in the second link which was between 5° and -17°. There is no big movement in the third link from the upright equilibrium point. The designed controller was capable of stabilising the Robogymnast at the trajectory reference point within an average time of approximately 5 seconds. It can be seen from Figure 7.17 and Figure 7.18 that there is a large amount of consumed energy from the first motor to maintain the system in a satisfactory level of performance. Consequently, when the disturbance was introduced, the first control

signal reached the saturation limits. Conversely, a large amount of energy was not consumed from the second motor.

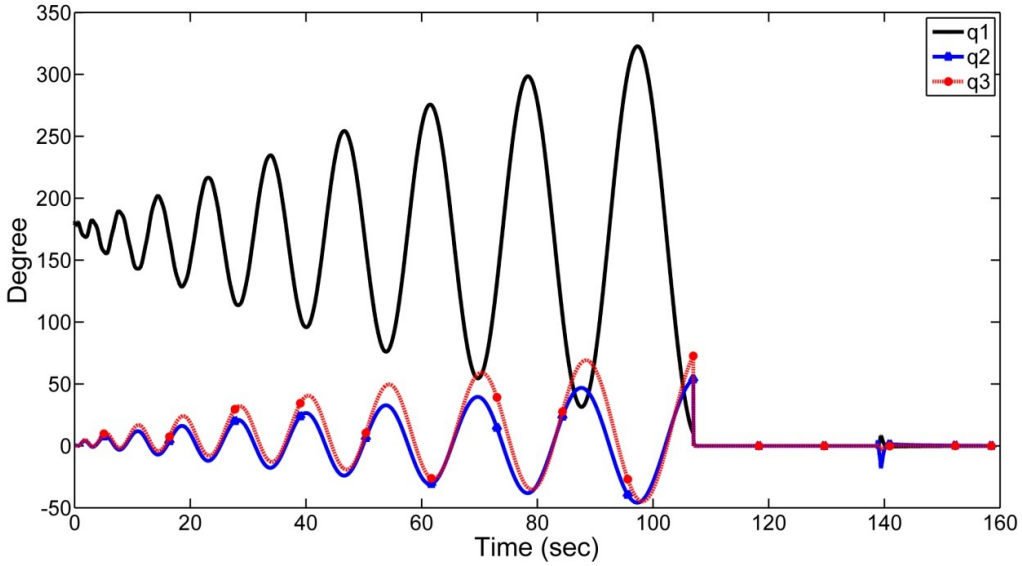

Figure 7.15: Simulated relative angular positions with applied disturbance to the first link

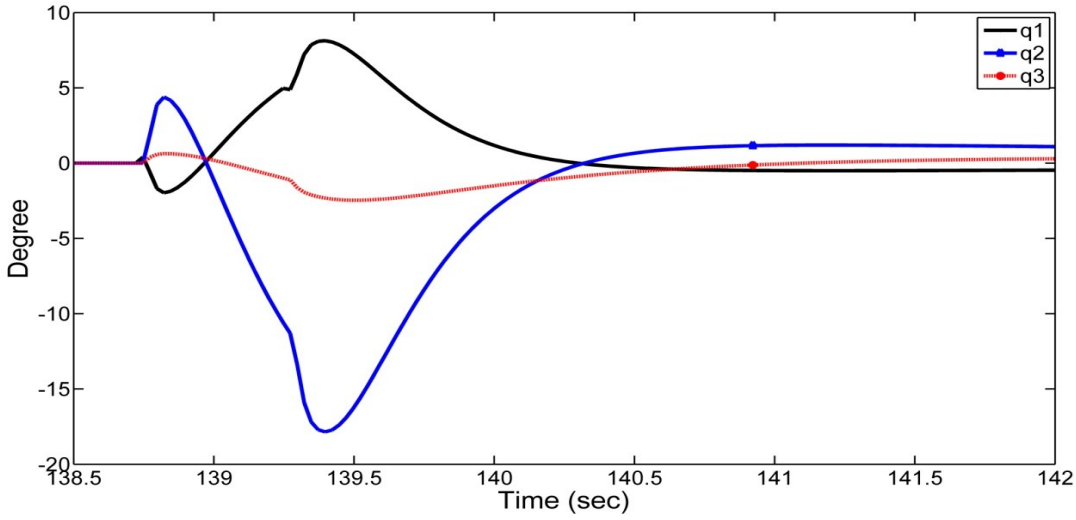

Figure 7.16: Zoomed view of simulated relative angular positions with applied disturbance to the first link

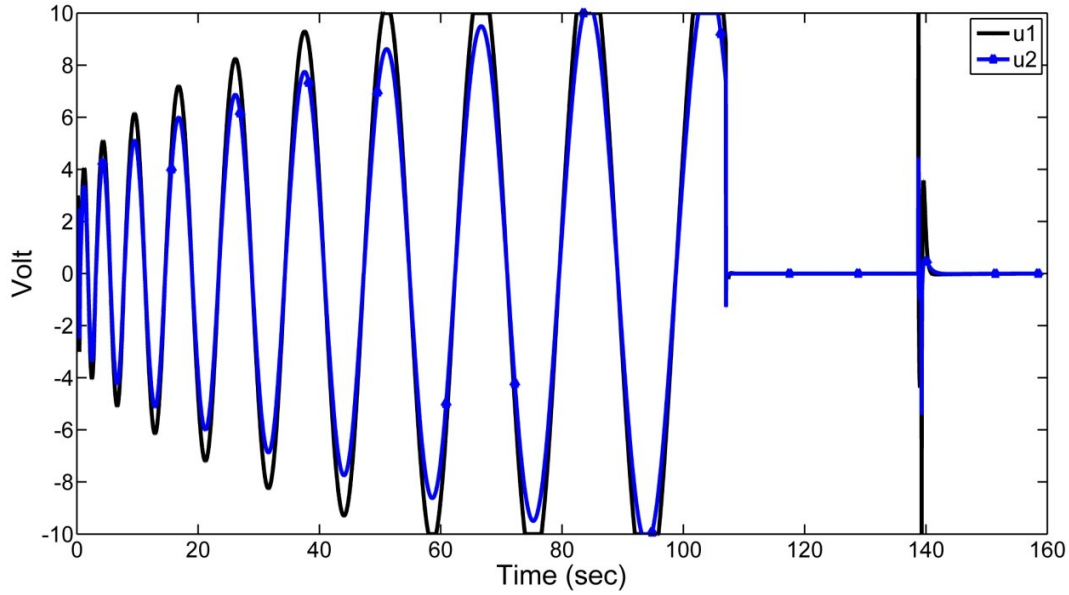

Figure 7.17: Simulated control action applied to the motors with applied disturbance to the first link

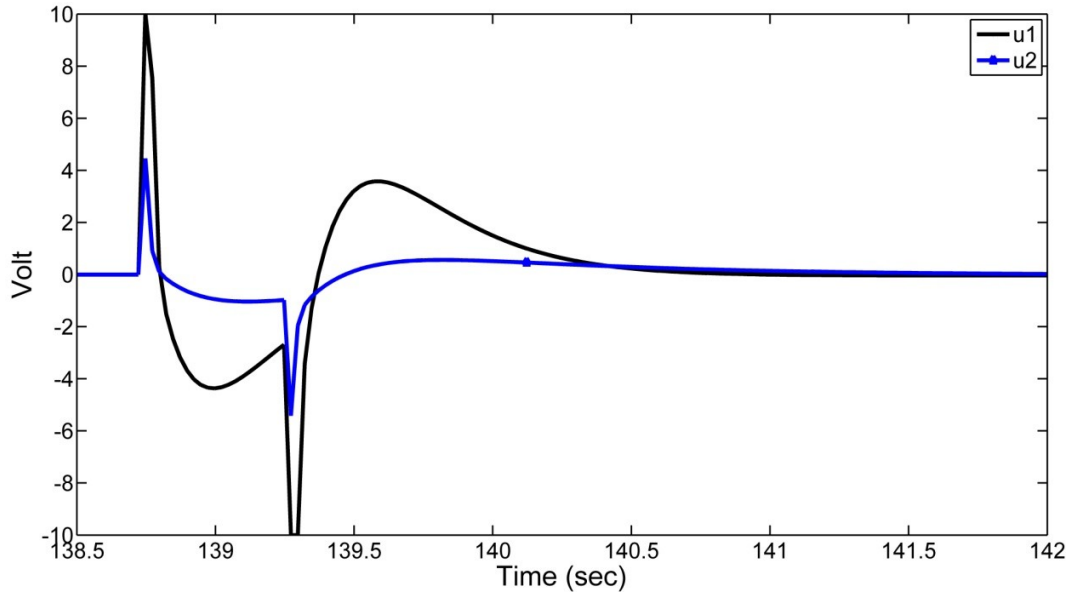

Figure 7.18: Zoomed view of simulated control action applied to the motors with applied disturbance to the first link

7.7.2 Applying a disturbance to the second link

In this case, after the Robogymnast reached the upright balancing position, a disturbance was introduced to the second link. From an extensive search, it is apparent that the controller could stablise the system with an applied disturbance that tilted the second link by 0.9°. The response of the Robogymnast undergoing a disturbance force applied to the second link and the zoomed view of the response of all the relative angular positions are presented in Figure 7.19 and Figure 7.20 respectively. As a result of this examination, the response of the Robogymnast undergoing disturbance applied to the second link was closely analogous to the Robogymnast's response in Figure 7.15 and Figure 7.16. As a consequence of introducing disturbance to the second link, it appears from Figure 7.21 and Figure 7.22 that the second motor spent more voltage to stabilize the Robogymnast around desired trajectories compared to the study of applying a disturbance to the first link as explained in Section 7.7.1. Hence, it can be seen from Figure 7.22 that the control action reported a significant increase in the demand energy of the second motor. Thus, the saturation limit was reached simultaneously with the applied disturbance. Furthermore, the control action applied to the first motor started with a maximum input voltage of +10 V.

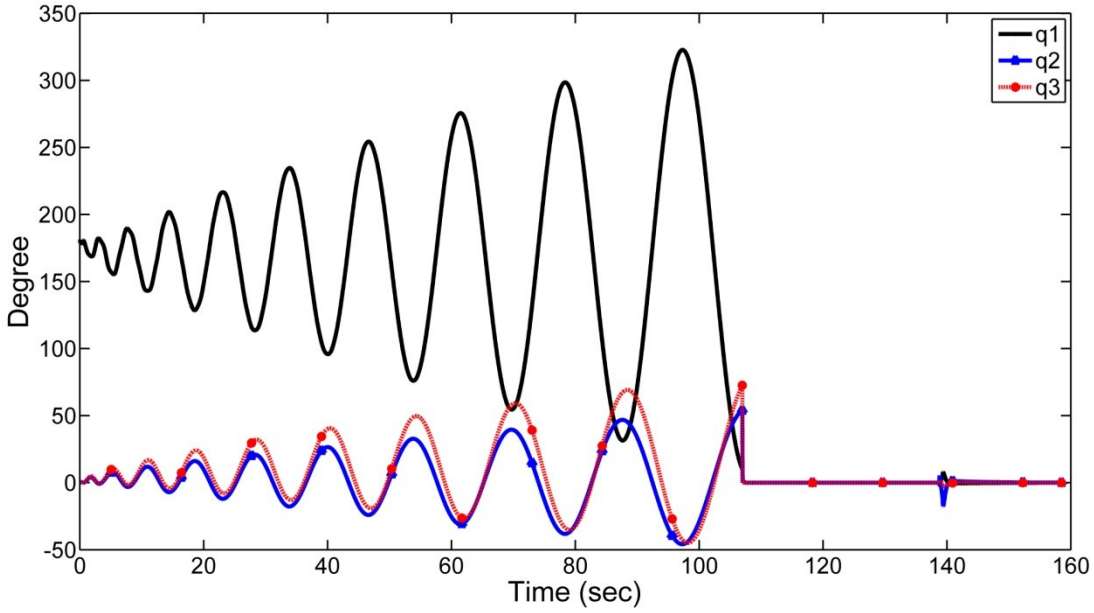

Figure 7.19: Simulated relative angular positions with applied disturbance to the second link

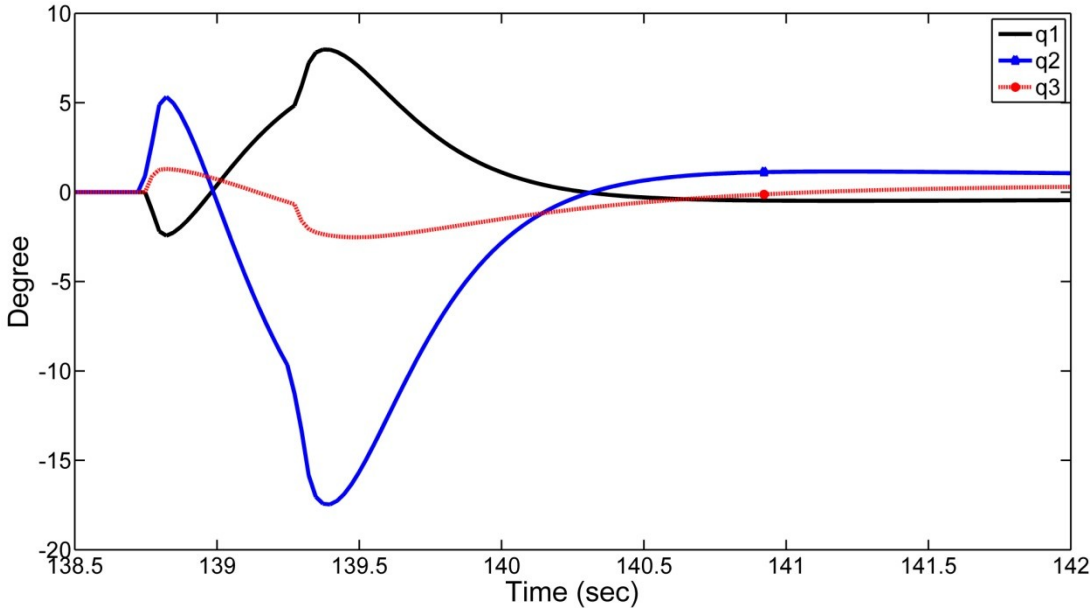

Figure 7.20: Zoomed view of simulated relative angular positions with applied disturbance to the second link

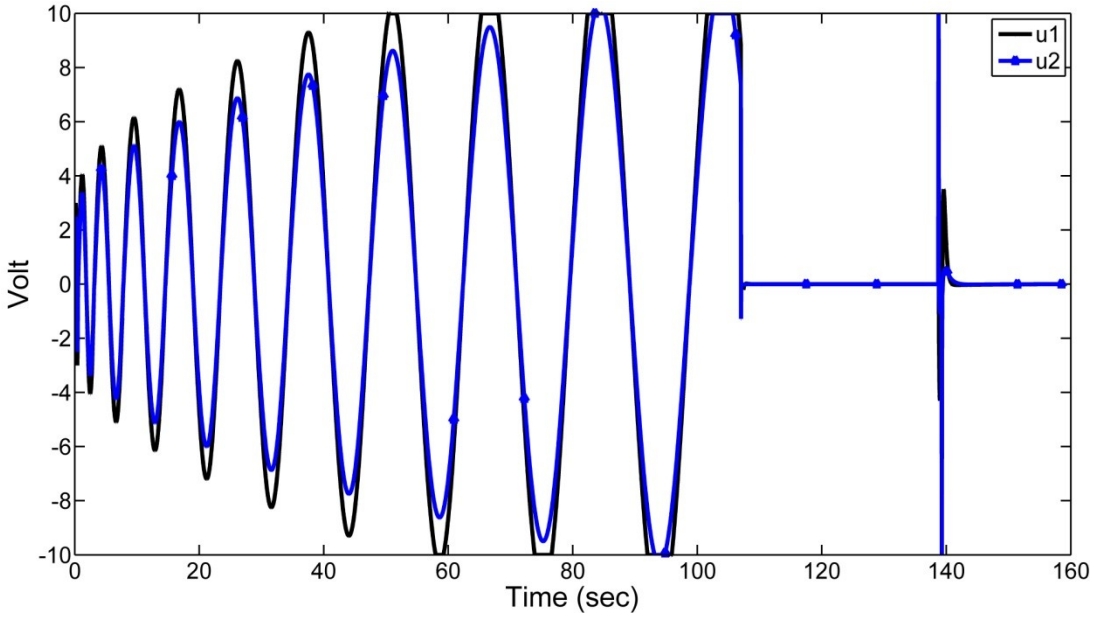

Figure 7.21: Simulated control action applied to the motors with applied disturbance to the second link

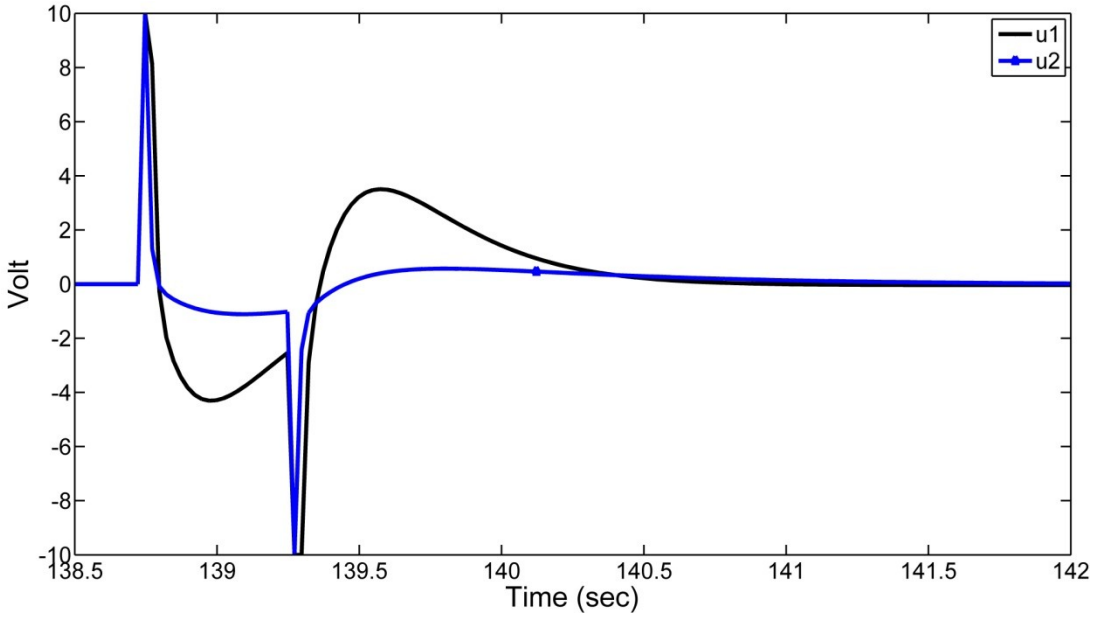

Figure 7.22: Zoomed view of simulated control action applied to the motors with applied disturbance to the second link

7.7.3 Applying a disturbance to the third link

A further assessment was implemented to examine the ability of the designed controller to stablise the system through introducing a disturbance on the third link. For the purpose of analysis, as was done in the first and second cases, it is important to know the maximum value of the disturbance that could be applied to the third link and that was done through repeating the process several times. The tests showed that the controller could stablise the system with applying a disturbance on the third link that was tilted by 8° from its upright position. Referring to the Figure 7.23 and Figure 7.24, the effect of applying disturbance to the third link can be noted. From the zoomed view of relative angular positions responses, it can be seen that the applying of the disturbance on the third link resulted in oscillations between 8° and -7° in the third link. Moreover, the performances of the first and second links were similar to the performances when the disturbance was applied to the first or second link. It can be seen from Figure 7.25 and Figure 7.26 that a large amount of energy was demanded from the first motor to maintain a satisfactory level of system performance. Consequently, the control signal reached the saturation limit at ±10 V. From the results, the control voltage of the second motor reached the saturation limit in the negative direction at one point in order to bring the third link to the equilibrium point.

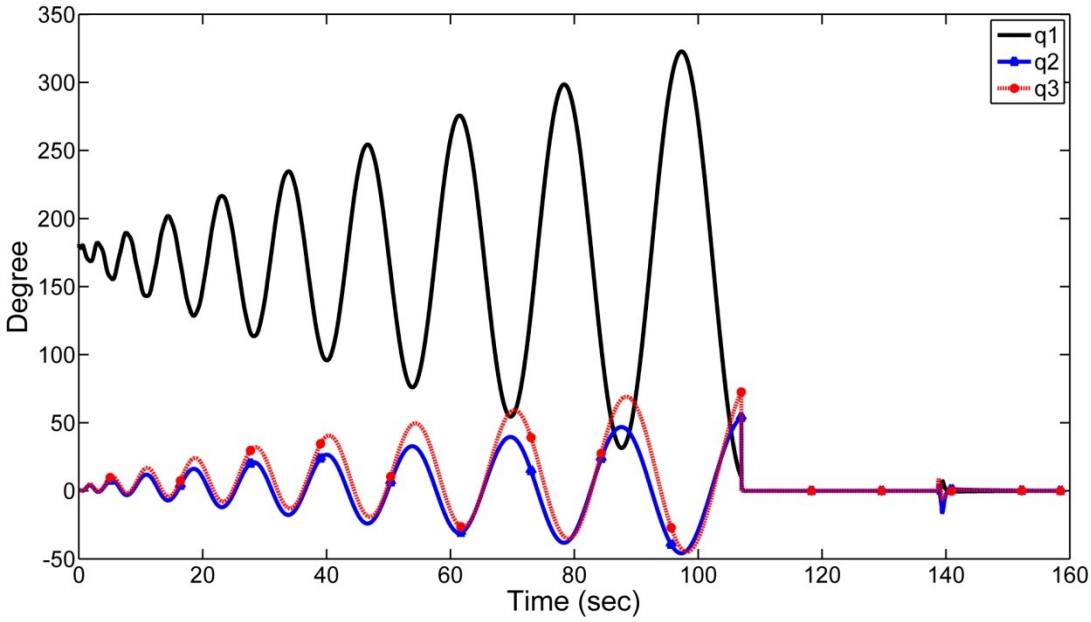

Figure 7.23: Simulated relative angular positions with applied disturbance to the third link

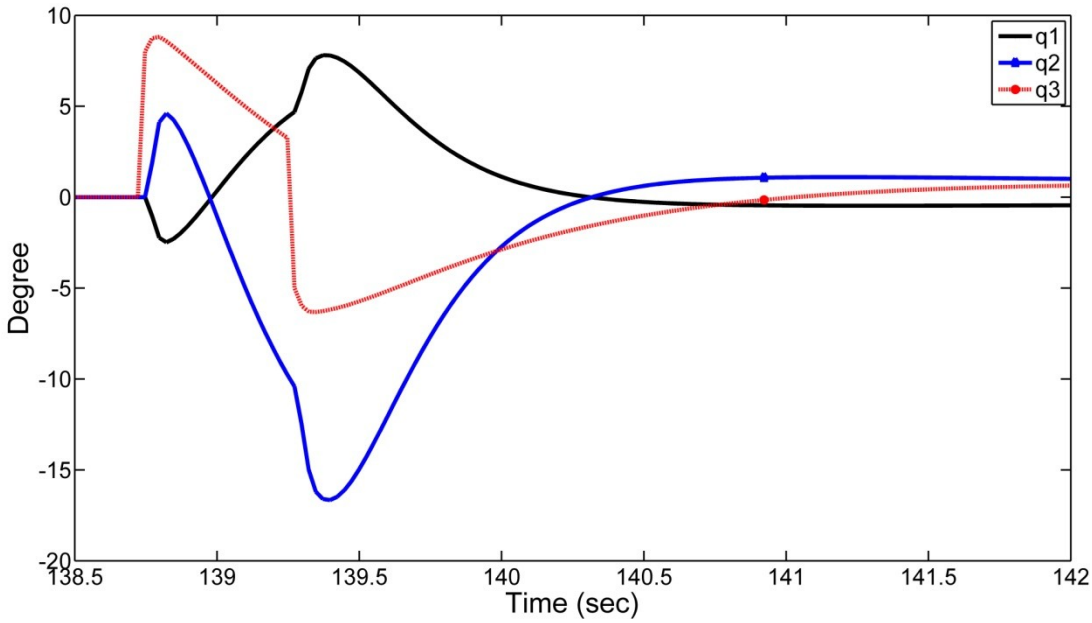

Figure 7.24: Zoomed view of simulated relative angular positions with applied disturbance to the third link

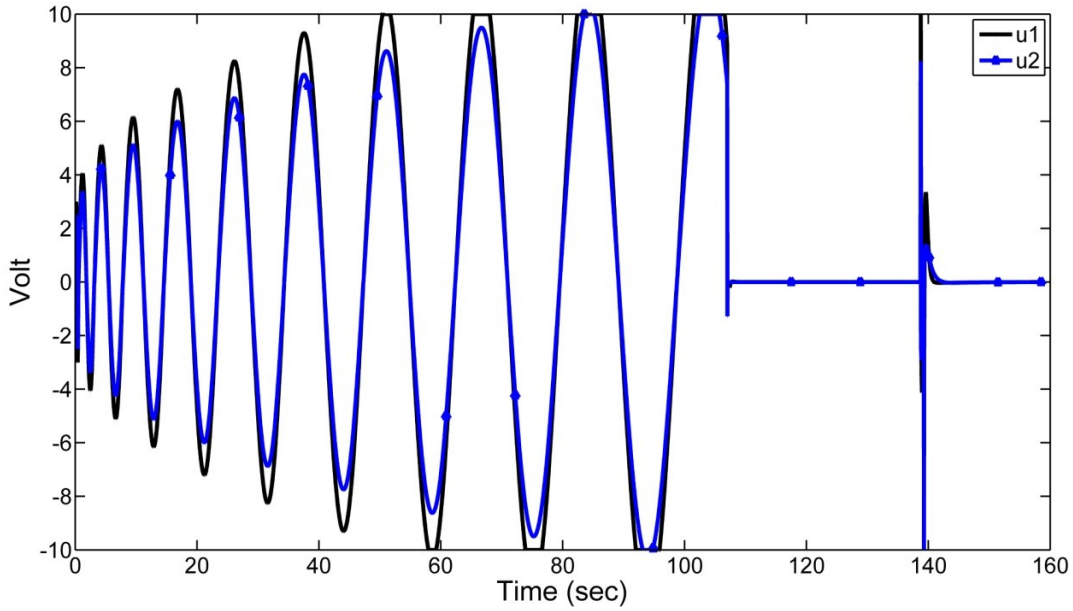

Figure 7.25: Simulated control action applied to the motors with applied disturbance to the third link

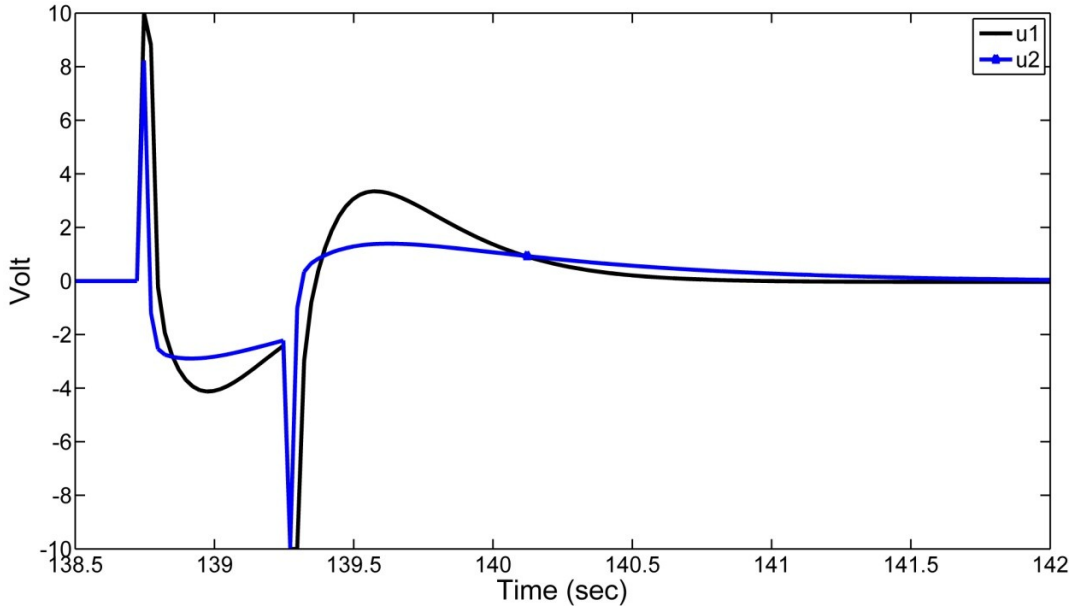

Figure 7.26: Zoomed view of simulated control action applied to the motors with applied disturbance to the third link

7.8 Summary

This chapter has been divided into two parts. The first part deals with the implementation of combining the swing up and balancing control of the Robogymnast. In this part, a switching mechanism between a swinging and balancing algorithm was suggested. A transition controller was proposed to establish the switching between swinging and balancing. A PID controller was designed as a transition controller. The results of this study illustrated that the controller and the ability of the controller to reject the applied disturbance. The performance and robustness of the system outputs were assessed through applying a disturbance to each link of the Robogymnast separately. Through it, the limitations of disturbance that could be controller was able to stabilise the Robogymnast in a satisfactory manner. The second part deals with the assessment of robustness of the designed applied to the system have been decided with a specific disturbance time duration. The simulation results showed that the controller was able to re-balance the Robogymnast around the upright equilibrium point.

Chapter 8

Conclusion, Contribution and Future Work

8.1 Conclusions

The purpose of this study was to understand and control the locomotion a of 3-DOF robot (Robogymnast). The Robogymnast is very complex and a highly nonlinear dynamical system. Furthermore, to satisfy different types of motion, it is important to take into account the dynamics of the entire system and to determine suitable control actions. One problem with this type of dynamic system is that it is difficult to model its nonlinear nature.

Due to the nonlinearity and complexity of the governing, dynamics has been simplified by considering linear approach to derive a mathematical model and dynamic equations. A continuous time model of the proposed structure of the Robogymnast was derived mathematically using the Euler-Lagrange approach and was then linearised in two different configurations (models). The first configuration was when the robot was at the stable equilibrium point (downward position) and the second was when it was at the unstable position (upright). These models were then discretised using a sampling time interval of 25 milliseconds.

In this work, the Robogymnast has been successfully controlled to satisfy different types of motion. The first motion is the swing-up control which was achieved by forcing the Robogymnast to move from the downward stable equilibrium point to the unstable inverted equilibrium point. A new method has been suggested for the swing-up control whereby the amplitudes and frequencies used as inputs to the control signals were intelligently manipulated. Two parameters have been proposed for the manipulation, one to tune the frequency and the second to tune the amplitude of the first and second control signals applied to the first and second motors respectively. A newly developed optimisation technique (BA) has been used to tune the parameters of a swing-up controller for the Robogymnast. The simulation and analysis of the designed controllers were implemented on MATLAB® software. The BA allowed a flexible and random selection of the parameters affecting the amplitudes and frequencies of the sinusoidal control signals. The simulation and experimental results of swing-up using the optimised parameters show that the controller can swing-up a Robogymnast from the lower position to the upper position in a reasonable duration (128 seconds). The simulations and experimental results demonstrated considerable improvements in the Robogymnast response with 40 seconds reduction in the swing-up time compared to that reported by Eldukhri and Pham (2010). The experimental swinging was implemented on the real system using C++ program environment. The controller was implemented on a PC supported by an appropriate AD/DA converter.

The second desired motion was the stablising and balancing of the Robogymnast in the upright position. In order to achieve this, two different controllers were designed. These

are the LQR and a combination of LC with the LQR. The first controller dealt with the Robogymnast as a triple inverted pendulum whilst the second as double inverted links by treating the second and third links as a rigid body. In the first case, both motors contribute to the balancing control, whilst in the second approach there is no contribution by the second motor, other than to keep the second and third links in alignment as a single rigid body.

The Robogymnast has three potentiometers that were used to measure the relative angular positions between the adjacent links, and one tachometer to measure the relative angular velocity of the first link. Based on this, a reduced order observer was designed to estimate the velocity of the second and third links. The two types of controllers were used for the design of a feedback control system to stabilise and balance the Robogymnast via the reduced order observer.

The integral action was used to eliminate the error between the reference trajectory signal and the actual instantaneous signal. The effect of this is to keep the Robogymnast links in line during downward balancing, and to help it to overcome gravity during upright stablising.

The performance of the control algorithm has been validated via the experimental results of the downward balancing. This was achieved through studying the ability of the designed controller to respond to an external disturbance. The key problems in downward balancing control are the calculation of the feedback controller gain, and reaching equilibrium between the system response speed and the level of oscillation

around the balancing point. This was achieved via suitable selection of the observer dynamics.

Analysis of the upright balancing was also considered, and was implemented through studying the system response with different initial configuration. The analysis based on the performance quality was determined based on the oscillation range of each link, the settling time, and the steady state error. The Robogymnast was able to stabilise and balance from various initial conditions by calculating a proper state feedback gain and selecting realistic dynamics for the reduced order observer. This ability was expressed and proven via simulation results. The analysis was explored using MATLAB® software and the discrete mathematical model for the upright configuration.

The third desired motion of the Robogymnast was a combination of swinging-up and balancing in the upright configuration. For this purpose, a transition controller was designed to achieve this transfer. The IJC mechanism was proposed to implement the transition control. The transition control was represented as a local PID controller which was used to compel the second and third links to be in line with first link. This would bring the second and third links to be within the attractive area for commencing balancing control. The validation of the designed switching mechanism has been demonstrated and proven via simulation results. The objective of the design has hence been achieved and demonstrated.

Further investigations were conducted to evaluate the robustness of the control system through analysis of its response to the application of an unknown external disturbance on

each link separately. The simulation results showed that the proposed control law can successfully overcome the applied disturbance with different allowed ranges of deviation for each link.

8.2 Contributions

The novel contributions made in this study are:

1. Investigating the problem of swinging-up of a 3-links Robogymnast through introducing a new method to manipulate the amplitudes and the frequencies of the sinusoidal control input signals. This was achieved by assigning one parameter to manipulate the control signal amplitudes, and another for manipulating the frequencies. **(Chapter 4)**
2. Employing a novel optimisation technique (Bees Algorithm) to calculate the optimal values of the manipulating control signal parameters to satisfy a desired system performance. **(Chapter 4)**
3. Implementing the optimised parameters of the proposed method on the real system. **(Chapter 4)**
4. Designing new type of controllers to obtain different motions for the new Robogymnast system. The designed controller was implemented via a reduced order observer. **(Chapter 5)**

5. Validating and evaluating the designed controller on the real system through realising downward balancing under the influence of external disturbances. **(Chapter 5)**
6. Balancing the Robogymnast in the up-right configuration using its mathematical model together with the designed control techniques, and attempting to implement the designed controller on the real system. **(Chapter 6)**
7. Designing a switching control mechanism (transition controller) to maintain the combination of the swing-up and balancing control systems. **(Chapter 7)**
8. Studying the ability of the designed controller to overcome on an external disturbance. **(Chapter 7)**

8.3 Limitations

The main limitation of motion control is the accuracy of the initial sensors' values. The controller was designed with the assumption that all the initial relative angular positions were equal to zero for the upright balancing position. In the real physical system, it is particularly difficult to satisfy this condition. This produced unexpected control action values applied to the first and second motors, leading to increasing the probability of Robogymnast to be far away from its desired position.

8.4 Future work

Future work on this topic should involve:

1. Introducing different scenarios for tuning multiple parameters which affect the control signals' amplitudes and frequencies independently, and validating their effects on the real system
2. Using the BA to optimise and manipulate the findings of point 1, and then implementing the results on the real system.
3. Replacing the actuators of the second joint (shoulder joint) and third joint (hip joint) with more powerful ones, and reducing the backlash as much as possible. These amendments would allow faster motion of the links and a reduction in the range of motion. Hence the balancing control could enable faster recovery from a deviation of the links.
4. Replacing the potentiometers of all the links with more accurate ones which are easy to adjust. This is particularly important when it is related to the offset in potentiometer readings due to calibration difficulties because of the backlash in the gearboxes or the difficult adjustment of the potentiometers.
5. Carrying out more trials to examine upright balancing on the real system after considering the modifications mentioned in point 3 and 4.
6. Using the BA to design and tune the controller for balancing Robogymnast at the upright position. This could be achieved through finding the optimum values of the optimal control weighting matrices.

7. Checking the effect of filter dynamics, which were not included in the present controller.
8. Adding extra mass on the third link in order to increase the moment of inertia and ease the control balancing problem of the real system.
9. Investigating the adaptation of the designed controller with respect to varying the external disturbance durations. This would be an extension to the proposed controller, as it already manages the upright balancing successfully.
10. Carrying out more investigations on different control algorithms for upright balancing, and applying these to the real system.

APPENDIX

Appendix A

A.1. LM12CL 80W Operational Amplifier

The LM12 is a power op amp capable of driving ±25V at ±10A while operating from ±30V supplies. The monolithic IC can deliver 80W of sine wave power into a 4Ω load with 0.01% distortion. Power bandwidth is 60 kHz. Further, a peak dissipation capability of 800W allows it to handle reactive loads such as transducers, actuators or small motors without derating. Important features include:

The IC delivers ±10A output current at any output voltage yet is completely protected against overloads, including shorts to the supplies. The dynamic safe area protection is provided by instantaneous peak- temperature limiting within the power transistor array.

The turn-on characteristics are controlled by keeping the output open-circuited until the total supply voltage reaches 14V. The output is also opened as the case temperature exceeds 150° C or as the supply voltage approaches the BV of the output transistors. The IC withstands over voltages to 80V.

This monolithic op amp is compensated for unity-gain feedback, with a small-signal bandwidth of 700 kHz. Slew rate is 9V/μseconds, even as a follower. Distortion and capacitive-load stability rival that of the best designs using complementary output

transistors. Further, the IC withstands large differential input voltages and is well behaved should the common-mode range be exceeded.

The LM12 establishes that monolithic ICs can deliver considerable output power without resorting to complex switching schemes. Devices can be paralleled or bridged for even greater output capability. Applications include operational power supplies, high-voltage regulators, high-quality audio amplifiers, tape-head petitioners, x-y plotters or other servo-control systems.

The LM12 is supplied in a four-lead, TO-220 package with V− on the case. A gold-eutectic die-attach to a molybdenum interface is used to avoid thermal fatigue problems. The LM12 is specified for either military or commercial temperature range.

The LM12 is prone to low-amplitude oscillation bursts coming out of saturation if the high-frequency loop gain is near unity. The voltage follower connection is most susceptible. This glitching can be eliminated at the expense of small-signal bandwidth using input compensation.

When a push-pull amplifier goes into power limit while driving an inductive load, the stored energy in the load inductance can drive the output outside the supplies. Although the LM12 has internal clamp diodes that can handle several amperes for a few milliseconds, extreme conditions can cause destruction of the IC. The internal clamp diodes are imperfect in that about half the clamp current flows into the supply to which

the output is clamped while the other half flows across the supplies. Therefore, the use of external diodes to clamp the output to the power supplies is strongly recommended.

A.2. E-Series Tachometer Generators

The E-Series (Subminiature) 3 volts/1000 RPM DC tachometer generator is the smallest tach generator among those offering similar technical characteristics. Many outstanding features make it particularly suitable for use in all types of servo systems. Although the diameter is only 0.760” the E-Series provides up to 3 V/1000 RPM output.

Almost any Servo-Tek DC tachometer generator can be manufactured with special configurations, various electrical specs and shaft modifications such as flats, pinions, holes, etc.

Appendix B

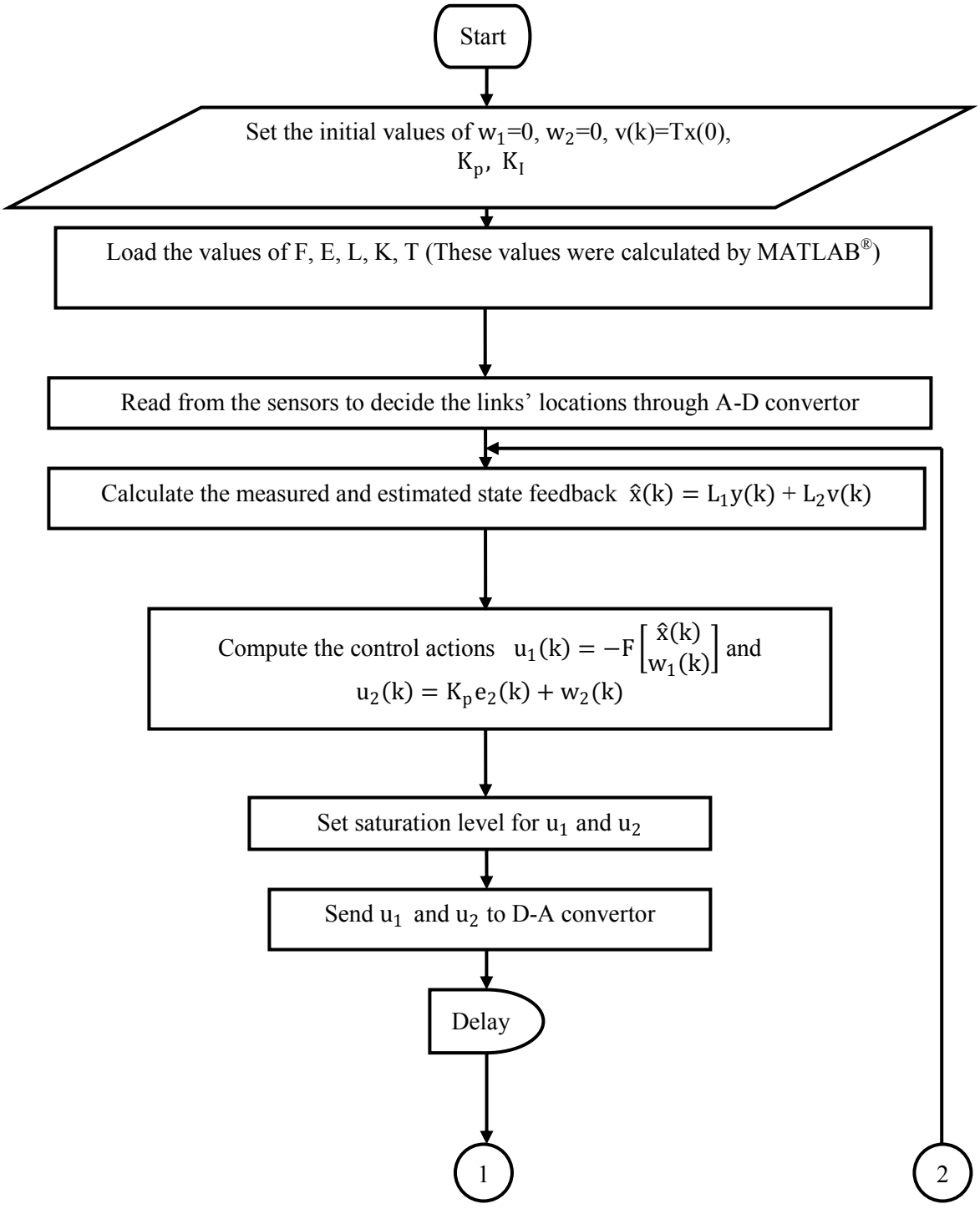
Start
Set the initial values of w_1=0, w_2=0, v(k)=Tx(0), K_p, K_I
Load the values of F, E, L, K, T (These values were calculated by MATLAB®)
Read from the sensors to decide the links' locations through A-D convertor
Calculate the measured and estimated state feedback $\hat{x}(k) = L_1 y(k) + L_2 v(k)$
Compute the control actions $u_1(k) = -F\begin{bmatrix}\hat{x}(k)\\ w_1(k)\end{bmatrix}$ and $u_2(k) = K_p e_2(k) + w_2(k)$
Set saturation level for u_1 and u_2
Send u_1 and u_2 to D-A convertor
Delay
1
2

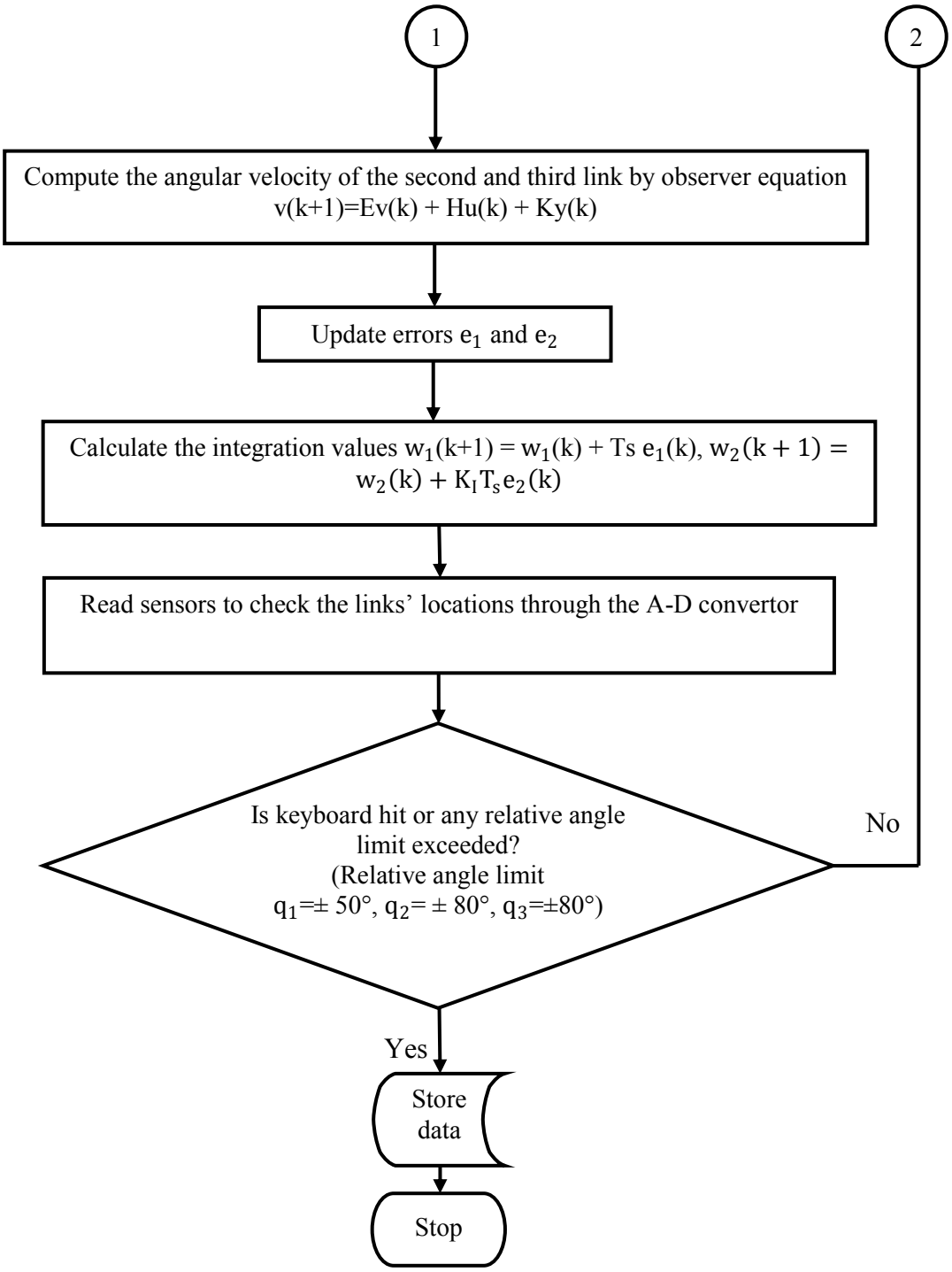

Figure B: Flowchart of the balance control system implementation using the LQR with LC

Appendix C

C.1. Upright balancing results using the LQR

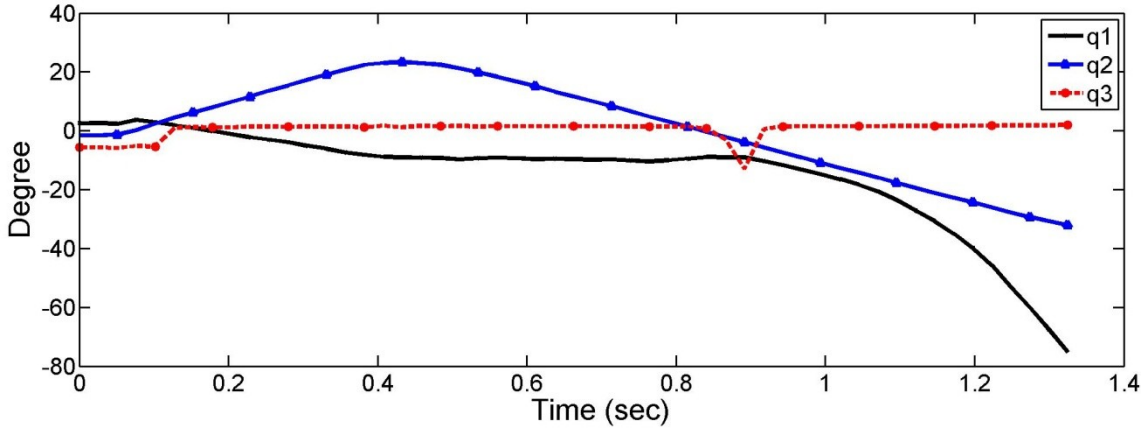

Figure C.1.1: Measured relative angular positions q_1, q_2 and q_3

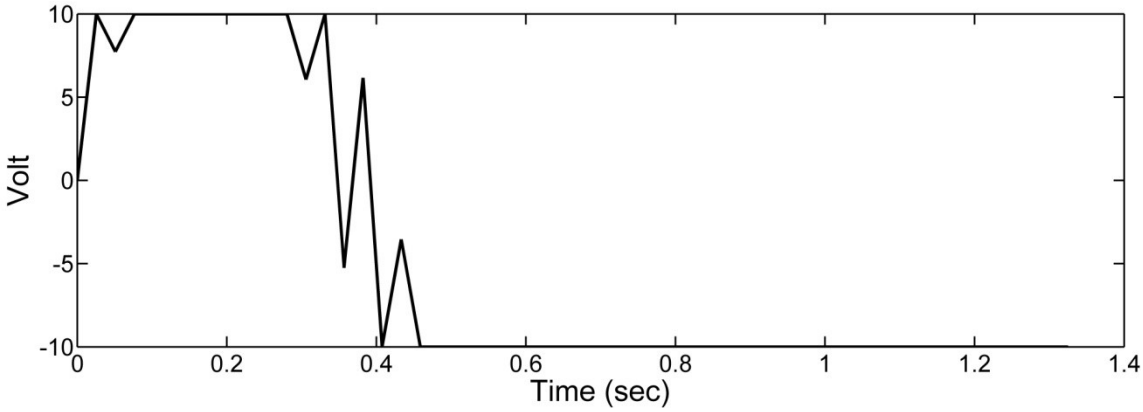

Figure C.1.2: Measured control action u_1 applied to the first motor

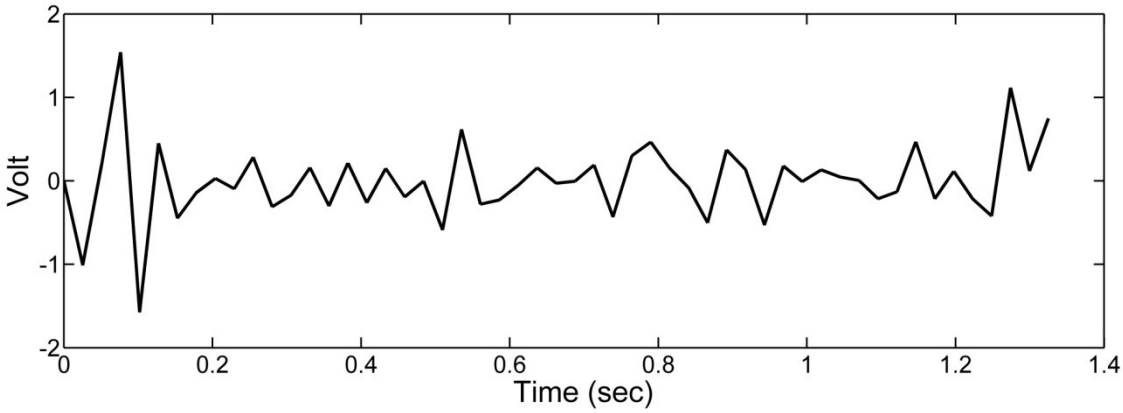

Figure C.1.3: Measured control action u_2 applied to the second motor

C.1. Upright balancing results using the LQR with LC

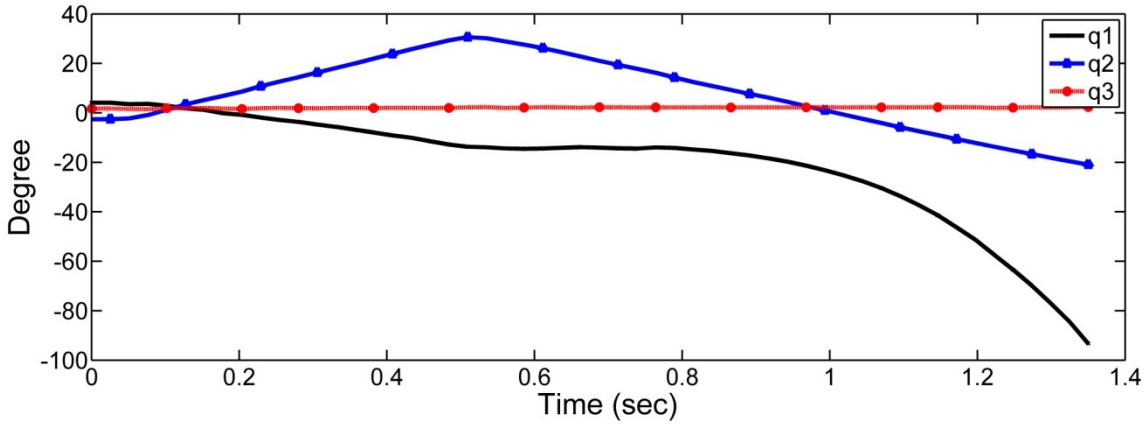

Figure C.2.1: Measured relative angular positions q_1, q_2 and q_3

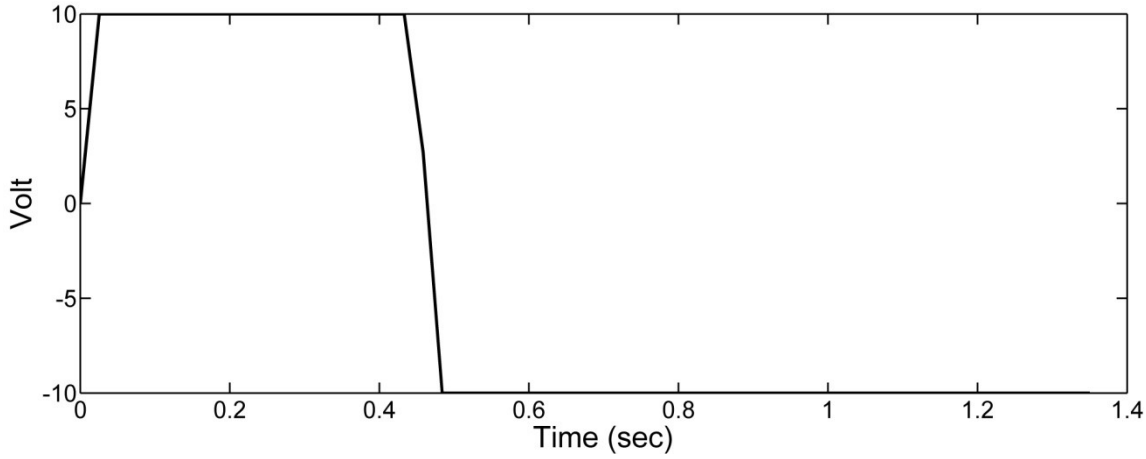

Figure C.2.2: Measured control action u_1 applied to the first motor

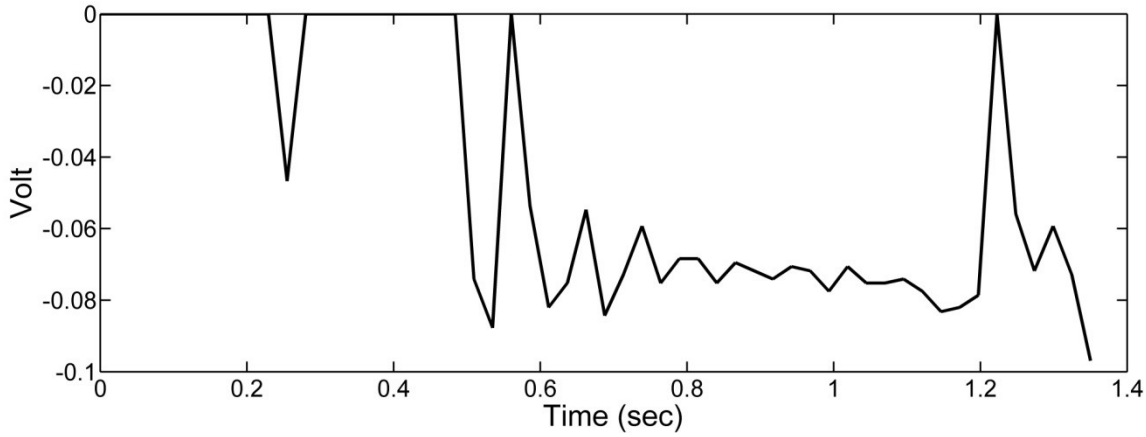

Figure C.2.3: Measured control action u_2 applied to the second motor

REFERENCES

Almeshal, a. M., Goher, K.M. and Tokhi, M.O. 2013. Dynamic modelling and stabilization of a new configuration of two-wheeled machines. *Robotics and Autonomous Systems* 61(5), pp. 443–472.

Anderson, B. and Moore, J. 1990. *Optimal control: linear quadratic methods*. Prentice-Hall Inc., London, UK.

Andrievskii, B.R., Guzenko, P. and Fradkov, A.A. 1996. Control of nonlinear vibrations of mechanical systems via the method of velocity gradient. *Automation and remote control* 57(4), pp. 456–467.

Angeli, D. 2001. Almost global stabilization of the inverted pendulum via continuous state feedback. *Automatica* 37(7), pp. 1103–1108.

Aoustin, Y., Formal'skii, A. and Martynenko, Y. 2011. Pendubot: combining of energy and intuitive approaches to swing up, stabilization in erected pose. *Multibody System Dynamics* 25(1), pp. 65–80.

Arai, H. and Tachi, S. 1991. Position control of manipulator with passive joints using dynamic coupling. *IEEE Transactions on Robotics and Automation* 7(4), pp. 528–534.

Araki, N., Okada, M., Konishi, Y. and Ishigaki, H. 2005. Parameter Identification and Swing-up Control of an Acrobot System. In: *2005 IEEE International Conference on Industrial Technology*. Hong Kong: IEEE, pp. 1040–1045.

Arnold, V.I. 1989. *Mathematical Methods of Classical Mechanics*. New York, NY: Springer New York.

Åström, K. and Furuta, K. 2000. Swinging up a pendulum by energy control. *Automatica* 36(2), pp. 287–295.

Åström, K.J. and Furuta, K. 1996. Swinging up a pendulum by energy control. *IFAC , San Francisco, 13* E, pp. 37–42.

Awrejcewicz, J., Supeł, B., Lamarque, C.-H., Kudra, G., Wasilewski, G. and Olejnik, P. 2008. NUMERICAL AND EXPERIMENTAL STUDY OF REGULAR AND CHAOTIC MOTION OF TRIPLE PHYSICAL PENDULUM. *International Journal of Bifurcation and Chaos* 18(10), pp. 2883–2915.

Block, D.J. 1996. Mechanical design and control of the pendubot. Master Thesis, University Illinois, Urbana-Champaign.

Bogdanov, A. 2004. Optimal control of a double inverted pendulum on a cart. *Oregon Health and Science University, Tech. Rep. CSE-04-006, OGI School of Science and Engineering, Beaverton, OR*.

Bradshaw, A. and Shao, J. 1996. Swing-up control of inverted pendulum systems. *robotica* 14, pp. 397–405.

Brown, S.C. and Passino, K.K.M. 1997. Intelligent control for an acrobot. *Journal of Intelligent and Robotic Systems* 18(3), pp. 209–248.

Bugajski, D.J. and Enns, D.F. 1992. Nonlinear control law with application to high angle-of-attack flight. *Journal of Guidance, Control, and Dynamics* 15(3), pp. 761–767.

Bugeja, M. 2003. Non-linear swing-up and stabilizing control of an inverted pendulum system. In: *EUROCON 2003. Computer as a Tool. The IEEE Region 8*. pp. 437–441.

Burns, R. 2001. *Advanced Control Engineering*. Elsevier.

Bush, L. 2001. Fuzzy logic controller for the inverted pendulum problem. *Computer Science Department, Rensselaer Polytechnic Institute, Troy, New York (2001)*.

Chen, X., Zhou, H., Ma, R., Zuo, F., Zhai, G. and Gong, M. 2007. Linear Motor Driven Inverted Pendulum and LQR Controller Design. In: *2007 IEEE International Conference on Automation and Logistics*. Jinan: IEEE, pp. 1750–1754.

Cheng-jun, D., Ping, D., Ming-lu, Z. and Yan-fang, Z. 2009. Double inverted pendulum system control strategy based on fuzzy genetic algorithm. In: *Automation and Logistics, 2009. ICAL'09. IEEE International Conference on*. pp. 1318–1323.

Choi, Y. and Chung, W.K. 2004. *PID trajectory tracking control for mechanical systems*. Springer Science & Business Media.

Chung, C.C. and Hauser, J. 1995. Nonlinear control of a swinging pendulum. *Automatica* 31(6), pp. 851–862.

Craig, J.J. 1985. *Introduction to robotics*. Pearson Education, Inc.

Dariush, B. and Fujimura, K. 2000. *Fuzzy Logic Based Control Model of Human Postural Dynamics*. (No. 2000-01-2178). SAE Technical Paper.

Darwish, A.H. 2009. Enhanced Bees Algorithm with fuzzy logic and Kalman filtering. Cardiff University.

Debnath, S.B.C., Chandra Shill, P. and Murase, K. 2013. Particle Swarm Optimization Based Adaptive Strategy for Tuning of Fuzzy Logic Controller. *International Journal of Artificial Intelligence & Applications* 4(1), pp. 37–50.

Delibasi, A., Kucukdemiral, I.B. and Cansever, G. 2007. A robust PID like state-feedback control via LMI approach: An application on a Double Inverted Pendulum System. In: *2007 International Symposium on Computational Intelligence in Robotics and Automation*. IEEE, pp. 374–379.

Deng, M., Inoue, A., Kosugi, M. and Henmi, T. 2007. Swing-up control of a cart-type single inverted pendulum with parasitic dynamics. *International Journal of Innovative Computing, Information and Control* 3(6), pp. 1501–1510.

Devaney, R.L. and Devaney, L. 1989. *An introduction to chaotic dynamical systems*. Addison-Wesley Reading.

Duong, S.C., Kinjo, H., Uezato, E. and Yamamoto, T. 2009. Intelligent control of a three-DOF planar underactuated manipulator. *Artificial Life and Robotics* 14(2), pp. 284–288.

Eldukhri, E.E. and Kamil, H.G. 2013. Optimisation of swing-up control parameters for a robot gymnast using the Bees Algorithm. *Journal of Intelligent Manufacturing*, pp. 1–9.

Eldukhri, E.E. and Pham, D.T. 2010. Autonomous swing-up control of a three-link robot gymnast. *Journal of Systems and Control Engineering* 224(7), pp. 825–832.

Eltohamy, K.G. and Kuo, C.Y. 1997. Real time stabilisation of a triple link inverted pendulum using single control input. *IEE Proceedings - Control Theory and Applications* 144(5), pp. 498–504.

Eltohamy, K.G. and Kuo, C.-Y. 1998. Nonlinear optimal control of a triple link inverted pendulum with single control input. *International Journal of Control* 69(2), pp. 239–256.

Fahmy, a. a., Kalyoncu, M. and Castellani, M. 2011. Automatic design of control systems for robot manipulators using the bees algorithm. *Proceedings of the Institution of Mechanical Engineers, Part I: Journal of Systems and Control Engineering* 226(4), pp. 497–508.

Fantoni, I., Lozano, R. and Spong, M.W. 2000. Energy based control of the Pendubot. *IEEE Transactions on Automatic Control* 45(4), pp. 725–729.

Farmanbordar, A., Zaeri, N. and Rahimi, S. 2011. Stabilizing a Driven Pendulum Using DLQR Control. *Modelling Symposium (AMS), 2011 Fifth Asia. IEEE, 2011.*, pp. 123–126.

Fer, H. and Enns, D. 1996. An application of dynamic inversion to stabilization of a triple inverted pendulum on a cart. *Proceedings of the 1996 IEEE International Conference on Control Applications*.

Fierro, R., Castillo, O., Valdez, F. and Melin, P. 2013. Optimization of Membership Functions for the Fuzzy Controllers of the Water Tank and Inverted Pendulum with Differents PSO Variants. *TELKOMNIKA (Telecommunication Computing Electronics and Control)* 11(4), pp. 699–714.

Franklin, G.F., Powell, J.D. and Workman, M.L. 1998. *Digital control of dynamic systems*. Addison-wesley Menlo Park.

Furut, K., Ochiai, T. and Ono, N. 1984. Attitude control of a triple inverted pendulum. *International Journal of Control* 39(6), pp. 1351–1365.

Furuta, K. and Iwase, M. 2004. Swing-up time analysis of pendulum. *Bulletin of the Polish Academy of Sciences: Technical Sciences* 52(3), pp. 153–163.

Glück, T., Eder, A. and Kugi, A. 2013. Swing-up control of a triple pendulum on a cart with experimental validation. *Automatica* 49(3), pp. 801–808.

Golliday Jr, C. and Hemami, H. 1976. Postural stability of the two-degree-of-freedom biped by general linear feedback. *Automatic Control, IEEE Transactions on* 21(1), pp. 74–79.

Gordillo, F., Acosta, J.A. and Aracil, J. 2003. A new swing-up law for the Furuta pendulum. *International Journal of Control* 76(8), pp. 836–844. Available at: http://www.tandfonline.com/doi/abs/10.1080/0020717031000116506 [Accessed: 16 April 2015].

Graichen, K., Treuer, M. and Zeitz, M. 2005. Fast Side-Stepping of the Triple Inverted Pendulum via Constrained Nonlinear Feedforward Control Design. *Proceedings of the 44th IEEE Conference on Decision and Control*, pp. 1096–1101.

Graichen, K., Treuer, M. and Zeitz, M. 2007. Swing-up of the double pendulum on a cart by feedforward and feedback control with experimental validation. *Automatica* 43(1), pp. 63–71.

Gupta, M.K., Bansal, K. and Singh, A.K. 2014. Stabilization of triple link inverted pendulum system based on LQR control technique. *International Conference on Recent Advances and Innovations in Engineering (ICRAIE-2014)*, pp. 1–5.

Ha, K.-J. and Kim, H.-M. 1997. A genetic approach to the attitude control of an inverted pendulum system. In: *Tools with Artificial Intelligence, 1997. Proceedings., Ninth IEEE International Conference on*. pp. 268–269.

Han, Q., Qin, Z., Yang, X. and Wen, B. 2007. Rhythmic swing motions of a two-link robot with a neural controller. *International Journal of Innovative Computing, Information and Control* 3(2), pp. 335–342.

Hara, M., Kawabe, N., Sakai, N., Huang, J., Bleuler, H. and Yabuta, T. 2009. Consideration on robotic giant-swing motion generated by reinforcement learning. In: *IROS*. IEEE, pp. 4206–4211.

Hasegawa, Y. and Fukuda, T. 2004. Passive dynamic autonomous control of bipedal walking. In: *Micro-Nanomechatronics and Human Science, 2004 and The Fourth Symposium Micro-Nanomechatronics for Information-Based Society, 2004.* IEEE, pp. 1–6.

Hassani, K. and Lee, W. 2014. Optimal Tuning of Linear Quadratic Regulators Using Quantum Particle Swarm Optimization. *avestia.com* (59), pp. 1–8.

Hauser, J. and Murray, R.R.M. 1990. Nonlinear controllers for non-integrable systems: the Acrobot example. *American Control Conference, 1990* (1), pp. 669–671.

Hemami, H. and Chen, B.-R. 1984. Stability analysis and input design of a two-link planar biped. *The International Journal of Robotics Research* 3(2), pp. 93–100.

Hemami, H. and Farnsworth, R. 1977. Postural and gait stability of a planar five link biped by simulation. *Automatic Control, IEEE Transactions on* 22(3), pp. 452–458.

Henmi, T., Wada, T., Deng, M., Inoue, A., Ueki, N. and Hirashima, Y. 2004. Swing-up control of an Acrobot having a limited range of joint angle of two links. In: *Control Conference, 2004. 5th Asian*. Melbourne, Victoria, Australia, pp. 1071–1076.

Inoue, A. 2005. Practical swing-up controller design for a cart-type single inverted pendulum having a serial second. In: Zítek, P. ed. *Preprints of IFAC 16th World Congress*. Czech Republic, pp. 1306–1306.

Inoue, A., Deng, M. and Tanabe, T. 2006. Practical Swing-up Control System Design of Cart-type Double Inverted Pendulum. In: *2006 Chinese Control Conference*. Harbin: IEEE, pp. 2141–2146.

Isidori, A. 1995. *Nonlinear control systems*. Springer Science & Business Media.

Jadlovska, S. and Sarnovsky, J. 2012. Classical double inverted pendulum — A complex overview of a system. In: *2012 IEEE 10th International Symposium on Applied Machine Intelligence and Informatics (SAMI)*. Herl'any: IEEE, pp. 103–108.

Jian, X. and Zushu, L. 2003. Dynamic model and motion control analysis of three-link gymnastic robot on horizontal bar. *system* 2(2), pp. 83–87.

Jianbao, H. and Xinbing, H. 2011. Mechanism design and dynamics analyses for an under-actuated three-joint acrobot. In: *2011 International Conference on Consumer Electronics, Communications and Networks (CECNet)*. XianNing: IEEE, pp. 5042–5045.

Jun Sun, Bin Feng and Wenbo Xu 2004. Particle swarm optimization with particles having quantum behavior. In: *Proceedings of the 2004 Congress on Evolutionary Computation (IEEE Cat. No.04TH8753)*. IEEE, pp. 325–331.

Kamil, H.G., Eldukhri, E.E. and Packianather, M.S. 2014. Balancing control of Robogymnast Based on Discrete-time Linear Quadratic Regulator Technique. In: *2014 Second International Conference on Artificial Intelligence, Modelling and Simulation*. Madrid, Spain 18-20 November 2014: IEEE Computer Society, pp. 137–142.

Kamil, H.G., Eldukhri, E.E. and Packianather, M.S. 2012. OPTIMISATION OF SWING-UP CONTROL PARAMETERS FOR A ROBOT GYMNAST USING THE BEES ALGORITHM. In: *Proceedings of 8th International Symposium on Intelligent and Manufacturing Systems (IMS 2012)*. Adrasan/Antalya/Turkey 27-28 September 2012, pp. 456–466.

Kennedy, J. and Eberhart, R. 1995. Particle swarm optimization. In: *Proceedings of ICNN'95 - International Conference on Neural Networks*. Perth, WA: IEEE, pp. 1942–1948.

Kobayashi, T., Komine, T., Suzuki, S., Iwase, M. and Furuta, K. 2002. Swing-up and balancing control of acrobot. In: *Proceedings of the 41st SICE Annual Conference. SICE 2002.* Soc. Instrument & Control Eng. (SICE), pp. 3072–3075.

Kumar, P., Mehrotra, O. and Mahto, J. 2013. Tuning of PID, SVFB and LQ Controllers Using Genetic Algorithms. *International Journal of Engineering Inventions* 2(7), pp. 68–73.

Lakshmi, K. 2007. DESIGN OF ROBUST ENERGY CONTROL FOR CART-INVERTED PENDULUM. *International Journal of Engineering and Technology* 4(1), pp. 66–76.

Lam, S. and Davison, E.J. 2006. The real stabilizability radius of the multi-link inverted pendulum. In: *2006 American Control Conference*. Minneapolis, MN: IEEE, pp. 1814–1819.

Landry, M., Campbell, S., Morris, K. and Aguilar, C. 2005. Dynamics of an inverted pendulum with delayed feedback control. *SIAM J. APPLIED DYNAMICAL SYSTEMS* 4(2), pp. 333–351.

Larcombe, P.J. 1992. On the control of a two-dimensional multi-link inverted pendulum: the form of the dynamic equations from choice of co-ordinate system. *International journal of systems science* 23(12), pp. 2265–2289.

Li, Y., Liu, J. and Wang, Y. 2008. Design approach of weighting matrices for LQR based on multi-objective evolution algorithm. In: *2008 International Conference on Information and Automation*. Changsha: IEEE, pp. 1188–1192.

Lingling Yang, Yun Zhang and Zhenfeng Chen 2010. Bilinear control for the triple inverted pendulum based on model bias separation. In: *2010 The 2nd International Conference on Computer and Automation Engineering (ICCAE)*. Singapore: IEEE, pp. 436–440.

Liu, D. and Yamaura, H. 2011. Giant Swing Motion Control of 3-link Gymnastic Robot with Friction around an Underactuated Joint. *Journal of System Design and Dynamics* 5(5), pp. 925–936.

Lu, X.-Y. 1999. Control of nonlinear non-minimum phase systems using dynamic sliding mode. *International journal of systems science* 30(2), pp. 183–198.

Medrano-Cerda, G.A., Eldukhri, E.E. and Cetin, M. 1995. Balancing and attitude control of double and triple inverted pendulums. *Transactions of the Institute of Measurement and Control* 17(3), pp. 143–154.

Medrano-Cersa, G.A. 1999. Robust computer control of an inverted pendulum. *Control Systems, IEEE* 19(3), pp. 58–67.

Meier Farwig, H.Z. and Unbehauen, H. 1990. Discrete computer control of a triple-inverted pendulum. *Optimal Control Applications and Methods* 11(2), pp. 157–171.

Mihara, K. and Yokoyama, J. 2012. Swing-up and stabilizing control of an inverted pendulum by two step control method. *Proceedings of the 2012 International Conference on Advanced Mechatronic Systems, Tokyo, Japan*, pp. 323–328.

Mobaieen, S., Mohamady, B., Ghorbani, H. and Rabii, A. 2012. Optimal Control Design Using Evolutionary Algorithms with Application to an Aircraft Landing System. *Journal of Basic and Applied Scientific Research* 2(2), pp. 1876–1882.

Mracek, C.P. and Cloutier, J.R. 1996. A preliminary control design for the nonlinear benchmark problem. In: *Control Applications, 1996., Proceedings of the 1996 IEEE International Conference on*. pp. 265–272.

Mus, N., Tovornik, B. and Muskinja, N. 2006. Swinging up and stabilization of a real inverted pendulum. *Industrial Electronics, IEEE Transactions on* 53(2), pp. 631–639.

O'Reilly, J. 1983. *Observers for linear systems*. Academic Press.

Park, M., Kim, Y.-J. and Lee, J.-J. 2011. Swing-up and LQR stabilization of a rotary inverted pendulum. *Artificial Life and Robotics* 16(1), pp. 94–97.

Pham, D.T., Ghanbarzadeh, A., Koc, E., Otri, S., Rahim, S. and Zaidi, M. 2006. The bees algorithm-a novel tool for complex optimisation problems. In: *Proceedings of the 2nd virtual international conference on intelligent production machines and systems (IPROMS 2006)*. pp. 454–459.

Phillips, C.L. and Nagle, H.T. 2007. *Digital control system analysis and design*. Prentice Hall Press.

Qian, Q., Qiang, H., Qiaoli, H., Yixin, Z., Lin, X. and others 2008. Optimization of sliding mode controller for double inverted pendulum based on genetic algorithm. In: *Systems and Control in Aerospace and Astronautics, 2008. ISSCAA 2008. 2nd International Symposium on*. pp. 1–5.

Ramani, N. and Atherton, D. 1974. Design of regulators using time-multiplied quadratic performance indices. *Automatic Control, IEEE Transactions on* 19(1), pp. 65–67.

Rock, H. 2001. Energy and passivity based control of the double inverted pendulum on a cart. In: *Proceedings of the 2001 IEEE International Conference on Control Applications (CCA'01) (Cat. No.01CH37204)*. Mexico City: IEEE, pp. 896–901.

Saberi, A., Gutmann, M. and Shamash, Y. 1995. Linear controller for an inverted pendulum having restricted travel-a high-and-low gain approach. In: *Proceedings of 1995 American Control Conference - ACC'95*. Seattle, WA: American Autom Control Council, pp. 2980–2984.

Sahba, M. 1983. Computer-aided design of feedback controllers for nonlinear systems with applications to control of a double-inverted pendulum. *Control Theory and Applications, IEE Proceedings D* 130(6), pp. 350–358.

Saito, F., Fukuda, T. and Arai, F. 1994. Swing and locomotion control for two-link brachiation robot. In: *[1993] Proceedings IEEE International Conference on Robotics and Automation*. Atlanta, GA: IEEE Comput. Soc. Press, pp. 719–724.

Sehgal, S. and Tiwari, S. 2012. LQR control for stabilizing triple link inverted pendulum system. In: *2012 2nd International Conference on Power, Control and Embedded Systems*. Allahabad: IEEE, pp. 1–5.

Sharif, B.A. and Ucar, A. 2013. State feedback and LQR controllers for an inverted pendulum system. In: *2013 The International Conference on Technological Advances in Electrical, Electronics and Computer Engineering (TAEECE)*. Konya: IEEE, pp. 298–303.

Solihin, M.I. and Akmeliawati, R. 2009. Self-erecting inverted pendulum employing PSO for stabilizing and tracking controller. In: *2009 5th International Colloquium on Signal Processing & Its Applications*. Kuala Lumpur: IEEE, pp. 63–68.

Spong, M.W. 1995. The swing up control problem for the Acrobot. *IEEE Control Systems Magazine* 15(1), pp. 49–55.

Spong, M.W. 1998. Underactuated mechanical systems. In: *Control Problems in Robotics and Automation*. Springer, pp. 135–150.

Spong, M.W. and Block, D.J. 1995. The pendubot: A mechatronic system for control research and education. In: *Decision and Control, 1995., Proceedings of the 34th IEEE Conference on*. New Orleans, LA, pp. 555–556.

Spong, M.W., Hutchinson, S. and Vidyasagar, M. 2006. *Robot Modeling and Control*. New York: Wiley.

Stephens, B. 2007. Integral control of humanoid balance. In: *2007 IEEE/RSJ International Conference on Intelligent Robots and Systems*. San Diego, CA: IEEE, pp. 4020–4027.

Tsuji, T. and Ohnishi, K. 2002. A control of biped robot which applies inverted pendulum mode with virtual supporting point. In: *7th International Workshop on Advanced Motion Control.* IEEE, pp. 478–483.

Vinodh Kumar, E. and Jerome, J. 2013. Robust LQR Controller Design for Stabilizing and Trajectory Tracking of Inverted Pendulum. *Procedia Engineering* 64, pp. 169–178.

Vukobratovic, M., Frank, A.A. and Juricic, D. 1970. On the stability of biped locomotion. *Biomedical Engineering, IEEE Transactions on* (1), pp. 25–36.

Wongsathan, C. and Sirima, C. 2009. Application of GA to design LQR controller for an Inverted Pendulum System. In: *2008 IEEE International Conference on Robotics and Biomimetics*. Bangkok: IEEE, pp. 951–954.

Wonham, W.M. 1985. *Linear Multivariable Control*. New York, NY: Springer New York.

Wu, M., Lai, X., She, J. and Zhang, A. 2011. Motion control of underactuated three-link gymnast robot based on combination of energy and posture. *IET Control Theory & Applications* 5(13), pp. 1484–1493.

Xin, X and Kaneda, M. 2007. Design and analysis of swing-up control for a 3-link gymnastic robot with passive first joint. In: *Proceedings of the IEEE Conference on Decision and Control*. Department of Communication Engineering, Faculty of Computer Science and System Engineering, Okayama Prefectoral University, 111 Kuboki, Soja, Okayama 719-1197, Japan, pp. 1923–1928.

Xin, Xin and Kaneda, M. 2007. Swing-Up Control for a 3-DOF Gymnastic Robot With Passive First Joint: Design and Analysis. *IEEE Transactions on Robotics* 23(6), pp. 1277–1285.

Xin, X. and Kaneda, M. 2002. The swing up control for the Acrobot based on energy control approach. In: *Proceedings of the 41st IEEE Conference on Decision and Control, 2002.* IEEE, pp. 3261–3266.

Xin, X., Tanaka, S., She, J.-H. and Yamasaki, T. 2010. Revisiting energy-based swing-up control for the Pendubot. In: *Proceedings of the IEEE International Conference on Control Applications*. Faculty of Computer Science and System Engineering, Okayama Prefectural University, 111 Kuboki, Soja, Okayama 719-1197, Japan, pp. 1576–1581.

Xin, X. and Yamasaki, T. 2012. Energy-Based Swing-Up Control for a Remotely Driven Acrobot: Theoretical and Experimental Results. *IEEE Transactions on Control Systems Technology* 20(4), pp. 1048–1056.

Xiong, X. and Wan, Z. 2010. The simulation of double inverted pendulum control based on particle swarm optimization LQR algorithm. In: *2010 IEEE International Conference on Software Engineering and Service Sciences*. Beijing: IEEE, pp. 253–256.

Xue, F., Hou, Z., Hu, Y. and Liu, C. 2011. Human simulated intelligence motion control for a three-link acrobot. In: *2011 9th World Congress on Intelligent Control and Automation*. Taipei: IEEE, pp. 844–848.

Yadav, S., Sharma, S. and Singh, M. 2012. Optimal Control of double inverted pendulum using LQR controller. *International Journal of Advanced Research in Computer Science and Software Engineering* 2(2), pp. 189–192.

Yamada, A., Yamakawa, S. and Fujimoto, H. 2004. Switching control for inverted pendulum system based on energy modification. In: *SICE 2004 Annual Conference*. Sapporo: IEEE, pp. 2316–2321 vol. 3.

Yamakita, M., Iwashiro, M., Sugahara, Y. and Furuta, K. 1995. Robust swing up control of double pendulum. In: *Proceedings of 1995 American Control Conference - ACC'95*. Seattle, WA: American Autom Control Council, pp. 290–295.

Yi, J., Yubazaki, N. and Hirota, K. 2001. Upswing and stabilization control of inverted pendulum system based on the SIRMs dynamically connected fuzzy inference model. *Fuzzy Sets and Systems* 122(1), pp. 139–152.

Yu, J., Huang, L. and Zhou, S. 2012. Fuzzy Control of Linear Flexible Double Inverted Pendulum System. In: *2012 International Conference on Control Engineering and Communication Technology*. Liaoning: IEEE, pp. 342–345.

Zaidan, A., Nouri, B. and Alsayid, B. 2012. Swing Up a Pendulum by Energy Control. *International Journal of Engineering and Technology* 2(3), pp. 528–534.

Zhai, G., Okuno, S., Imae, J. and Kobayashi, T. 2007. Swinging up and Stabilizing an Inverted Pendulum by Switching Control. In: *2007 International Conference on Mechatronics and Automation*. Harbin: IEEE, pp. 521–526.

Zhang, C.J., Bai, C.Y., Ding, Y.. Y. and Zhang, Q. 2012. LQR optimal control of triple inverted pendulum based on fuzzy quotient space theory. In: *2012 IEEE International Conference on Granular Computing*. Hangzhou, China: IEEE, pp. 633–638.

Zhang, G. 2007. GALQR Optimal Control Method and Applying in the Active Suspension System. In: *Proceedings on Intelligent Systems and Knowledge Engineering (ISKE2007)*. Paris, France: Atlantis Press, pp. 1–6.

Zhi-Hao Xu, Dong-Ming Jin and Zhi-Jian Li 2002. Using learning samples to construct fuzzy logic systems with the application to inverted pendulum control. In: *Proceedings. International Conference on Machine Learning and Cybernetics*. IEEE, pp. 1085–1088.